The effect of the galaxy environment on the size and structure of galaxies

David T. Maltby, M.Sci

The University of Nottingham

Thesis submitted to the University of Nottingham
for the degree of Doctor of Philosophy

July 2013

"*Equipped with his five senses, man explores the universe around him and calls the adventure Science.*"

– Edwin Hubble (1889–1953)

Supervisors:	Prof. Alfonso Aragón-Salamanca	
	Dr. Meghan E. Gray	
Examiners:	Dr. Michele Cappellari	(University of Oxford)
	Dr. Steven P. Bamford	(University of Nottingham)
Submitted:	6 July 2012	
Examined:	18 September 2012	
Final version:	9 November 2012	

Contents

List of Figures

List of Tables

Abstract

In this thesis, we explore the effect of the galaxy environment on the physical size and structure of the stellar distribution for relatively local galaxies ($z < 0.3$) using *Hubble Space Telescope*/Advanced Camera for Surveys imaging and data from the Space Telescope A901/2 galaxy evolution survey (STAGES).

We determine the effect of the environment on the size of the stellar distribution (i.e. galaxy sizes) by comparing the stellar-mass–size relations in the field and cluster environments for different Hubble-type morphologies. For elliptical, lenticular, and high-mass ($M_* > 10^{10}\,\mathrm{M}_\odot$) spirals, we find no evidence to suggest that a galaxy's size (i.e. effective radius a_e) is dependent on the environment. This result suggests that internal drivers are responsible for any potential size evolution inherent to these galaxies. However, for intermediate-/low-mass spirals ($M_* < 10^{10}\,\mathrm{M}_\odot$) we do find some evidence for a possible environmental effect, with the mean galaxy size ($\overline{a}_\mathrm{e}$) being $\sim$ 15–20 per cent larger in the field than in the cluster. This result is driven by a population of low-mass, large-a_e field spirals (observed to contain extended stellar discs) that are largely absent from the cluster environments. This difference implies that the fragile extended stellar discs of these spiral galaxies may not survive the environmental conditions in the cluster.

We expand on this result by investigating the effect of the environment on the structure of galactic discs in spiral and S0 galaxies. Using V-band radial surface brightness $\mu(r)$ profiles, we identify break features in the stellar disc (down-bending break – *truncation*; up-bending break – *antitruncation*) and evaluate their dependence on the galaxy environment. For both spiral and S0 galaxies, we find no evidence to suggest an environmental dependence on the frequency of these break features. We also find no evidence to suggest an environmental dependence on the scalelength h of pure exponential discs, or the break strength T (outer-to-inner scalelength ratio) of broken exponential discs. These results indicate that the stellar distribution in the outer regions of spiral/S0 galaxies is not significantly influenced by the galaxy environment.

In our structural analyses, one interesting observation was that truncated $\mu(r)$ profiles (down-bending breaks) are very rare in S0s; whereas in spiral galaxies they are commonplace. We expand on this result by comparing the structural properties of the disc (scalelength h, break strength T, break surface brightness μ_brk) in spiral and S0 galaxies. In these comparisons, we find no evidence to suggest that the scalelength h of pure exponential discs or the break surface brightness μ_brk of broken exponentials is dependent on the galaxy morphology. However, we do find some evidence to suggest that the break strength T is smaller (weaker) in S0s compared to spiral galaxies. This result suggests that some process inherent to the morphological transformation of spiral galaxies into S0s *does* affect the structure of the stellar disc causing a weakening of $\mu(r)$ breaks and may even eliminate truncations from S0 galaxies. In additional structural comparisons, we also find that the fraction of

exponential bulges is the same ($\sim$ 20 per cent) in both spiral and S0 galaxies, suggesting that major mergers are not driving this transformation.

Finally, we complement our structural analyses with an assessment of whether the excess light in the outer regions of antitruncated (up-bending) $\mu(r)$ profiles is caused by an outer exponential disc or an extended spheroidal component: we use bulge–disc decomposition in order to achieve this. For spiral galaxies, in the vast majority of cases, evidence indicates that the excess light at large radii is related to an outer shallow disc. We thus conclude that in the majority of spiral galaxies, antitruncated outer stellar discs cannot be explained by bulge light and thus remain a pure disc phenomenon. However, for S0s, bulge light can have a significant effect in the outer regions of the $\mu(r)$ profile. In approximately half of S0 antitruncations, the excess light at large radii can be entirely accounted for by light from an extended spheroidal component. These results suggest that as a galaxy evolves from a spiral into an S0, the galaxy naturally evolves into a more bulge-dominated system. We suggest a fading stellar disc (e.g. caused by gas stripping and the termination of star formation) is consistent with this result.

In conclusion, our environmental studies indicate that the environment has little direct affect on the size and structure of a galaxy's stellar distribution. This result implies that physical processes directly affecting the structure of the stellar distribution (e.g. mergers or harassment), are not driving the observed morphology–density relation. With respect to both our environmental and morphological studies, we can conclude that more subtle processes acting on the gaseous component of a galaxy (e.g. ram-pressure stripping) are more likely to play an important role in the origin of the morphology–density relation and the transformation of spirals into S0s.

Acknowledgements

First and foremost, I wish to thank my Ph.D supervisors, Alfonso and Meghan, for all their scientific and personal support over the last four years. Their guidance and encouragement has been instrumental in the production of this thesis and I consider myself extremely fortunate to have benefited from their experience and expertise. Additional thanks must also go to Carlos Hoyos, for his vital assistance with the computational analyses – as well as for some entertaining discussions. I also wish to thank the entire STAGES collaboration for the production of an amazing and easy to use data set – you saved me many months of tedious ground work! Finally, a special thank you goes to my family and friends (especially PTB) for their unwavering understanding and support during my Ph.D studies, for putting up with my high stress levels over the last few months of writing and for helping me not to lose perspective of what I was trying to achieve.

Published work

The majority of the work contained within this thesis has already been presented in several published works: Chapter 3 (Paper i), Chapter 4 (Paper ii) and Chapter 6: Section 6.2 (Paper iii). The work presented in Chapter 5 and Chapter 6: Section 6.3 will feature a forthcoming paper (Paper iv).

i) **Maltby D. T.**, Aragón-Salamanca A., Gray M. E., Barden M., Häußler B., Wolf C., Peng C. Y., Jahnke K., McIntosh D. H., Böhm A., van Kampen E., 2010, MNRAS, 402, 282: *'The environmental dependence of the stellar-mass–size relation in STAGES galaxies'.*

ii) **Maltby D. T.**, Gray M. E., Aragón-Salamanca A., Wolf C., Bell E. F., Jogee S., Häußler B., Barazza F. D, Böhm A., Jahnke K., 2012a, MNRAS, 419, 669: *'The environmental dependence of the structure of outer galactic discs in STAGES spiral galaxies'.*

iii) **Maltby D. T.**, Hoyos C., Gray M. E., Aragón-Salamanca A., Wolf C., 2012b, MNRAS, 420, 2475: *'Antitruncated stellar light profiles in the outer regions of STAGES spiral galaxies: bulge or disc related?'*

iv) **Maltby D. T.**, Aragón-Salamanca A., Gray M. E., Hoyos C., Wolf C., Jogee S., Böhm A., 2012c, MNRAS, submitted: *'The environmental dependence of the structure of galactic discs in STAGES S0 galaxies: implications for S0 formation'.*

The vast majority of the work presented in this thesis was carried out by the author, with advice from the paper coauthors listed above. Where the material presented is the result of more collaborative work, this is mentioned in the relevant chapter.

Chapter 1

Introduction

The notion that there might be *'island universes'* or galaxies outside our own Milky Way has its roots back in the mid-eighteenth century. However, it was only in the 1920s that this hypothesis was eventually confirmed and that the field of extra-galactic astronomy was born. Prior to this, any observed galaxies were simply regarded as 'nebulae of an unknown nature' and it was hotly debated as to whether these systems were internal or external to our Galaxy.

The matter was finally solved in 1923 when Edwin Hubble made the seminal discovery that so-called 'spiral nebulae' are indeed external to the Milky Way (Hubble 1925a,b). Using Cepheid variable stars, he was able to determine that the distances to some galaxies (e.g. the Andromeda 'nebula') were $> 200\,\mathrm{kpc}$, placing them well outside our own Galactic system. Consequently, he was able to definitively conclude that spiral nebulae were extra-galactic in nature and galaxies in their own right.

Hubble followed up this discovery with the observation that 'extra-galactic nebulae' could be grouped into different categories based on their overall appearance or morphology (Hubble 1926, 1936). The resulting classification scheme, often called 'The Hubble Sequence', remains in widespread use today (see Fig. 1.1).

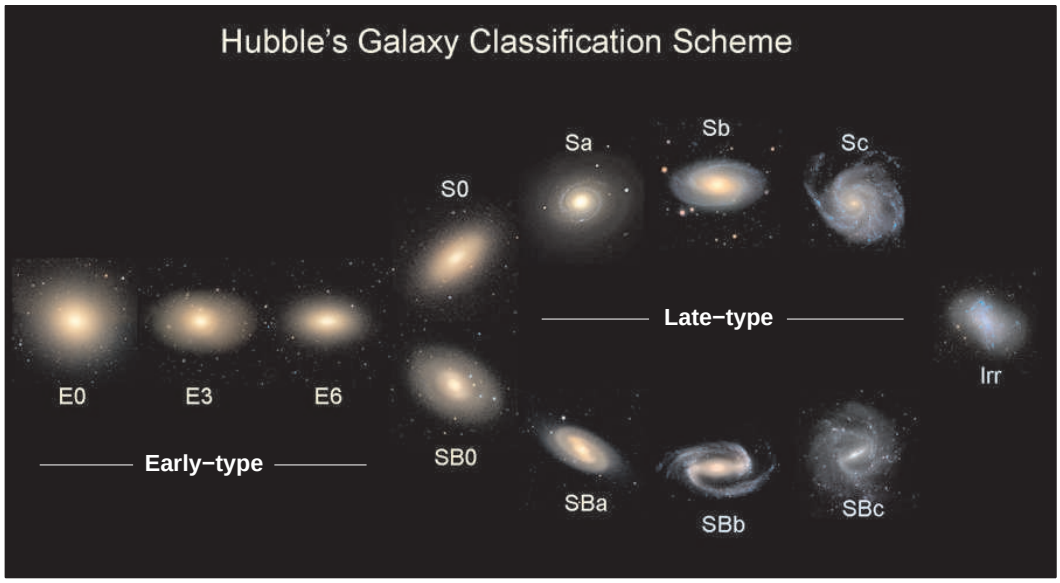

Figure 1.1. The Hubble sequence. This figure was created using galaxies from the Sloan Digital Sky Survey (SDSS; York et al. 2000) classified by the members of the GalaxyZoo project (Lintott et al. 2008; image credit – http://www.galaxyzoo.org).

The Hubble sequence divides galaxies into four main categories or Hubble types: ellipticals, lenticulars, spirals and irregulars.

1. *Elliptical galaxies (E):* smooth ellipsoidal systems with very little internal structure. The shape of the stellar distribution ranges from spheroidal (E0) to a highly flattened distribution (E6).

2. *Lenticular galaxies (S0):* a transitional class – systems with an outer smooth disc structure (no spiral arms) in addition to a central spheroidal bulge.

3. *Spiral galaxies (S/SB):* systems with an outer disc structure containing visible spiral arms and a central spheroidal bulge. The spiral class is subdivided into two parallel sequences, the normal spirals (S) and the barred spirals (SB), the latter of which exhibit an elongated 'bar-like' structure in the central region. The parallel spiral sequences (Sa–Sc/SBa–SBc) represent a decrease in the prominence of the central bulge and an opening up of the spiral arm structure. Later extensions to these spiral sequences include the additional Sd class, which contain a very small nucleus and irregular spiral arms (de Vaucouleurs 1959a).

4. *Irregular galaxies (Irr):* unordered systems with no obvious structure.

Hubble referred to the elliptical and lenticular classes as *'early-types'* and the spiral and irregular classes as *'late-types'*, a terminology still in widespread use today. This nomenclature suggests that Hubble may have originally suspected the Hubble sequence to represent an evolutionary sequence. However, Hubble (1926) states very clearly that these terms are simply intended to convey an increase in structural complexity and are not intended to have temporal connotations. We now know that evolutionary paths of this nature are almost certainly incorrect; however, the exact evolutionary path followed by galaxies remains largely uncertain.

Through the subsequent study of other galaxy properties, it is now well established that there exist many correlations between the Hubble-type morphology and properties such as colour and spectral type (Humason 1936; Holmberg 1958; de Vaucouleurs 1961; Roberts & Haynes 1994). These correlations show that the optical colours (e.g. $U - R$) of early-type galaxies (E/S0) are predominantly redder than those of late-type galaxies (spirals), although there are many exceptions e.g. blue ellipticals (Schawinski et al. 2009) and dusty red spirals (van den Bergh 1976; Wolf et al. 2009; Masters et al. 2010). Through the advent of modern photometric surveys, e.g. the Sloan Digital Sky Survey (SDSS; York et al. 2000), these correlations have now been studied using many thousands of galaxies and resulted in the discovery of an intrinsic colour bimodality in the local galaxy population (Strateva et al. 2001; Kauffmann et al. 2003; Balogh et al. 2004).

Strateva et al. (2001) initially reported this colour bimodality using data from SDSS (see Fig 1.2). Using visual morphologies and spectral classifications for a subset of galaxies, they were also able to establish that the two distinct peaks in the bimodality correspond roughly to early-type (E, S0 and Sa) and late-type galaxies (Sb, Sc and Irr), as expected. These two populations are now commonly known as *'the red sequence'* and *'the blue cloud'*, respectively (e.g. Bell et al. 2004).

The light we detect from a galaxy is the integrated light of its stellar population (although possibly modified by the effects of dust). Therefore, a galaxy's optical colour is directly related to the composition of its stellar component. For the bulk of the stellar population (i.e. main sequence stars), the most luminous stars are the

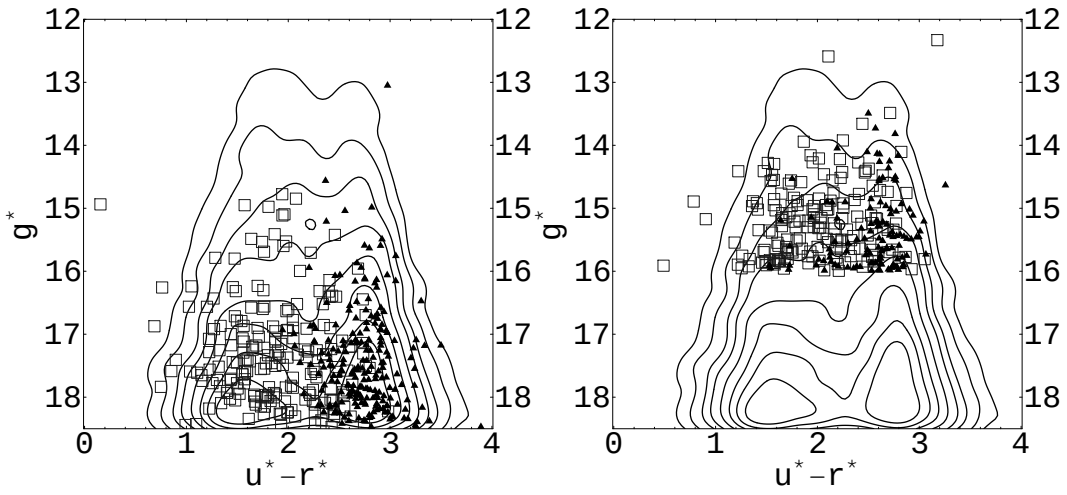

Figure 1.2. The colour bimodality of the local galaxy population (Strateva et al. 2001). The colour bimodality from SDSS (contours) compared to a subsample of early- (triangles) and late-type (squares) galaxies classified spectroscopically (left-hand panel) and by visual inspection (right-hand panel).

hot, blue, massive but short-lived OB stars. Due to their extremely high luminosity, a relatively small number of OB stars can completely overwhelm the total light produced by fainter stars in the stellar population. Consequently, a galaxy may have a blue optical colour even if the majority of its stellar population is comprised of fainter redder stars (Ellis et al. 2001). If a galaxy has a blue optical colour (i.e. late-types), this really indicates the presence of young massive OB stars and is a clear signature of on-going or recent star formation. In contrast, low-mass redder stars generally contribute relatively little to the light output of a galaxy; and therefore, if a galaxy has a red optical colour (i.e. early-types) this indicates not only the absence of young OB stars but also the presence of luminous evolved red giant stars. Consequently, red optical colours are a signature of an old, passive (non star-forming) stellar population (although dust effects can be a complicating factor, e.g. dusty red spirals; Wolf et al. 2009).

Spectroscopy has reinforced these theories through the identification of characteristic spectral features in galaxy spectra which relate to the stellar spectral types and their effect on the interstellar medium. For example, the presence of OB stars is commonly indicated by the emission lines produced from their ionisation of interstellar gas (e.g. [O II], Hα), the strength of which can also be used to estimate a galaxy's star-formation rate (SFR). The use of spectroscopy, along with radio/submillimetre imaging, has also enabled the detection of cold gas in galaxies (the raw material for star formation). Unsurprisingly, the amount of cold gas in a galaxy is also dependent on morphology, with early-type galaxies having less cold gas (and consequently less star formation) than late-types galaxies (see e.g. Roberts & Haynes 1994).

When one considers all these correlations with morphology, it becomes clear that there are two distinct galaxy populations in the Universe: old red passively evolving galaxies with early-type (E/S0) morphologies, and blue star-forming galaxies with late-type (spiral) morphologies. This bimodality raises the fundamental question;

> *'What evolutionary path leads some galaxies to become old red passive ellipticals/lenticulars as opposed to young blue star-forming spirals?'*

One way in which we can try and explore this issue is to compare galaxy properties between different galaxy populations (e.g. different redshift ranges or galaxy environments) and search for characteristic differences that could shed light on their evolution.

1.1 The galaxy environment

It has long been known that galaxies are not distributed randomly throughout the Universe. Instead, most galaxies are actually found in gravitationally bound groups or clusters (Hubble & Humason 1931; Shapley 1933; Abell 1965). This fact, coupled with observations of apparently interacting galaxies, has given rise to the idea that galaxies may be influenced by their local surroundings (i.e. the galaxy environment). Galaxy environment can be defined in many different ways; however, it generally relates to the local density of galaxies. Therefore, the range of galaxy environments span from the high-densities of cluster cores to the low-densities of the general field (i.e. galaxies in relative isolation).

In order to understand the origin of the galaxy environment, we must first understand how galaxies assemble their mass and how structures form in the Universe. Our current theories of structure formation are largely based on the well-established principle of hierarchical assembly.

1.1.1 Hierarchical assembly

The light we detect from a galaxy originates from either its stellar or gaseous component. However, these components account for only a very small fraction of a galaxy's overall mass. It is now widely accepted that the vast majority of mass in a galaxy ($\sim$ 90 per cent), and indeed the Universe as a whole, is comprised of weakly interacting non-baryonic dark matter (see Spergel et al. 2007, for current determinations). This dark matter extends well beyond the visible extent of the galaxy and dominates the gravitational interactions in the Universe.

In current theories of structure formation (e.g. Davis et al. 1985), the dark matter density distribution in the very early Universe contained small-amplitude Gaussian fluctuations with the highest peaks in this density distribution being the first to collapse under their own gravity. Over time, these small collapsing dark matter haloes accrete more material from the surrounding Universe and grow in mass. At the same time, stars begin to form as gas is accreted and a galaxy is born in the centre of the halo. Under the influence of gravity, the dark matter haloes then begin to continually merge with each other, forming ever larger haloes or structures (Lacey & Cole 1993; see Fig. 1.3). This growth in structure through merging is known as *'hierarchical assembly'*. In this model, it is the dark matter halos that are merging *not* the galaxies embedded within them. Therefore, over time, groups and clusters of galaxies are built up as their individual dark matter halos merge and form ever larger structures.

As a direct result of this model, the largest gravitationally collapsed structures in the Universe today (i.e. high-density galaxy clusters) are expected to have older, more evolved galaxy populations than lower-density environments (i.e. galaxy groups and the general field; De Lucia et al. 2006). Consequently, these models predict that correlations should exist between the properties of galaxies and the galaxy environment. It is now well established that such correlations do exist between

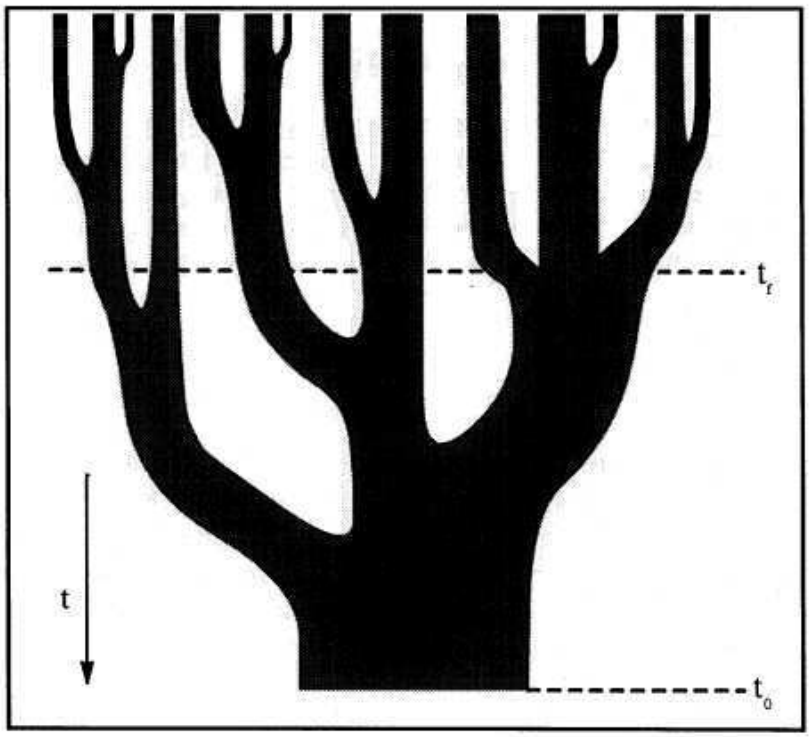

Figure 1.3. A schematic representation of the growth of dark matter haloes by hierarchical assembly (Lacey & Cole 1993). In this figure, known as a 'merger tree', time increases from top to bottom and the width of the branches represent the mass of a halo, and its progenitors at any given time t.

galaxy properties such as morphology, colour and star-formation rate (SFR), and the environment in which they are found. We shall review these correlations in the following sections.

1.1.2 The morphology–density relation

It has long been known that there exists a contrast between the morphologies of galaxy populations in low- and high-density environments (Hubble & Humason 1931; Abell 1965; Oemler 1974). Galaxies in high-density cluster cores are predominantly of early-type (E/S0) morphology, while galaxies in the low-density field are mainly late-type (spiral) galaxies. However, Dressler (1980) was the first to quantify this relationship as a function of the local galaxy density ($z \sim 0$) and establish the correlation now known as the *morphology–density relation* (see Fig. 1.4). This correlation clearly shows that the fraction of elliptical and S0 galaxies increases smoothly with increasing galaxy density from the outskirts of the cluster environment to the denser cluster core. A corresponding decrease in the late-type (spiral + irregular) fraction with increasing galaxy density is also observed.

Subsequent studies at higher redshift ($z \sim 0.5$) have revealed significant evolution in the morphology–density relation over cosmic time (Dressler et al. 1997). At higher redshifts $z \sim 0.5$, the fraction of ellipticals in the cluster environment is similar to that found in the local Universe. However, at $z \sim 0.5$ the fraction of S0s in the cluster environment is significantly lower than observed in the local Universe, while the fraction of cluster spirals is proportionally higher. This result suggests that the

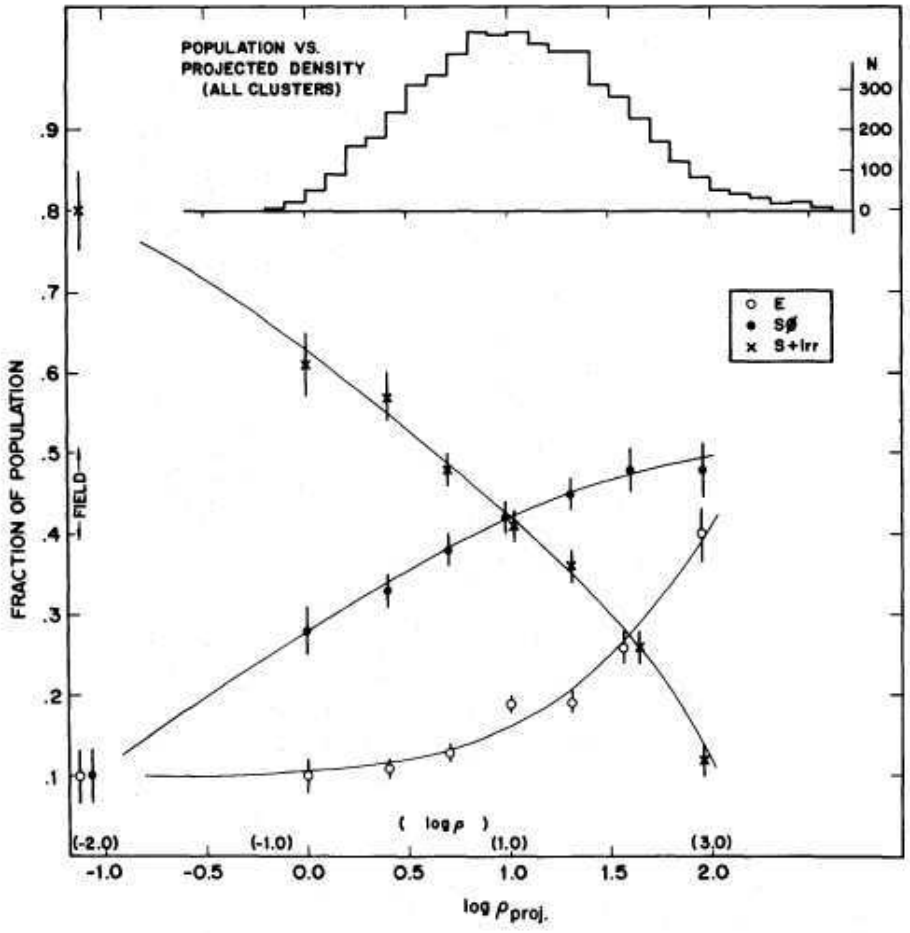

Figure 1.4. The morphology–density relation (Dressler 1980). The observed fraction of elliptical (E), S0 and spiral+irregular (S+Irr) galaxies as a function of the log of projected galaxy density $\rho_{\rm proj.}$ (in galaxies Mpc^{-2}) from a sample of 55 rich clusters ($z \sim 0$). The fraction of elliptical and S0 galaxies increases smoothly from low to high densities, while the fraction of spiral+irregular galaxies decreases.

progenitors of low-z S0 galaxies are predominantly spiral galaxies. Therefore, it seems plausible that blue star-forming spiral galaxies can fall into the gravitational well of a cluster, have their star formation extinguished by the cluster environment, and then eventually evolve into the S0s we see in the Universe today.

1.1.3 Other correlations with environment

In addition to morphology, there are several other galaxy properties that also show strong correlations with the galaxy environment, e.g. colour, star-formation rate (SFR) and the fraction of active galactic nuclei (AGN).

(i) *Galaxy colours.* The photometric colours of galaxies show a distinct correlation with the galaxy environment (e.g. Kodama et al. 2001; Blanton et al. 2005; Baldry et al. 2006). In the comparison of optical colours (e.g. V-I), galaxies in high-density regions tend to be redder than analogous galaxies (i.e. galaxies of similar luminosity) in lower density environments (see Fig. 1.5). In addition to this,

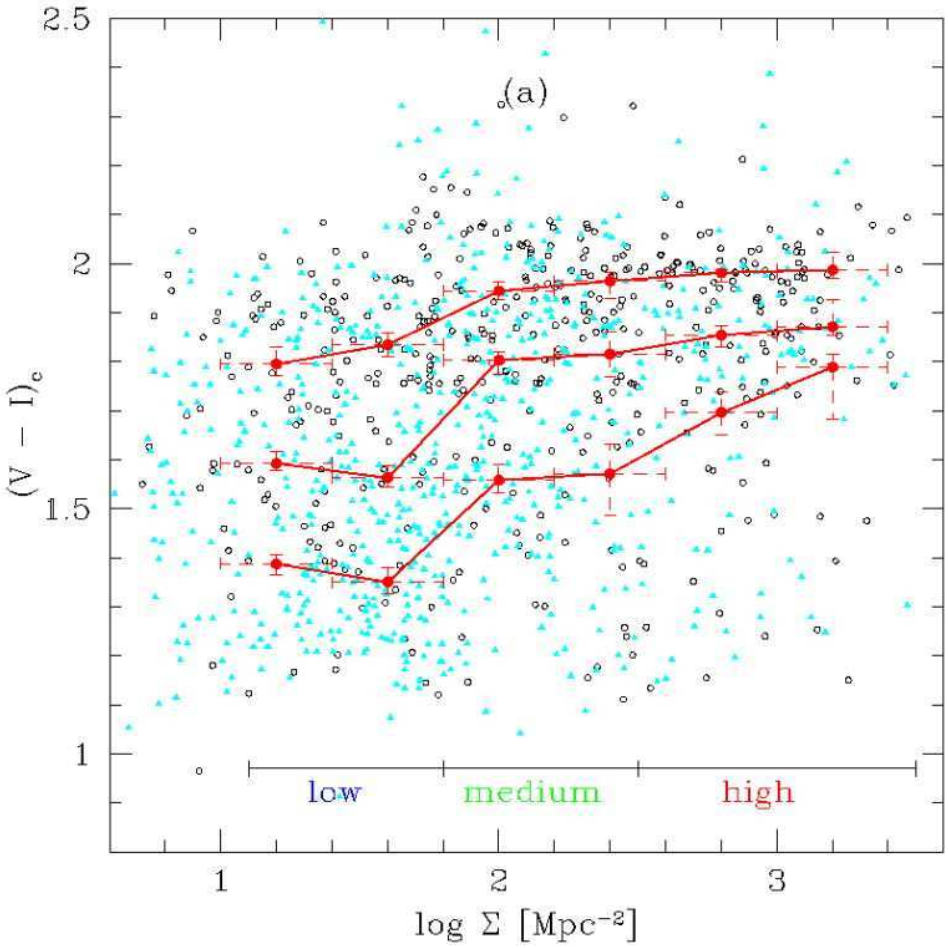

Figure 1.5. Galaxy colour as a function of environment (Kodama et al. 2001). The correlation between colour (V- I) and local galaxy density Σ for a rich cluster (A851, $z = 0.41$). The three red lines represent the 25th, 50th and 75th percentile colours. The open circles and filled triangles show galaxies brighter and fainter than $I = 21.4$, respectively. In this data, an abrupt transition in colour is observed at $\log \Sigma \sim 2$. Note: the Σ scale was miscalculated in Kodama et al. (2001) and the subject of a later erratum (Kodama et al. 2003).

some studies (e.g. Kodama et al. 2001) also report an abrupt transition in colour at some characteristic density (see Fig. 1.5), implying a critical density at which the colours of in-falling galaxies are more strongly affected by the cluster environment. However, in other studies that use more general measures of the galaxy environment (e.g. halo mass), this critical density is not observed (Weinmann et al. 2006).

(ii) *Star-formation rate.* Recent observations have also reported that the star-formation rate (SFR) of galaxies is strongly correlated with the galaxy environment (e.g. Lewis et al. 2002; Gómez et al. 2003). Using optical tracers of SFR (e.g. Hα emission), it has been shown that galaxies in high-density environments have lower SFRs than those in lower density environments (see Fig. 1.6). This trend is particularly noticeable when you consider strongly star-forming galaxies (i.e. those in the 75th percentile of the SFR distribution). In addition to this, an abrupt transition in SFR at some characteristic density is sometimes observed (e.g. Gómez et al. 2003; see Fig. 1.6), implying a critical density at which the star formation of in-falling galaxies is more strongly effected by the cluster environment (c.f. to the critical

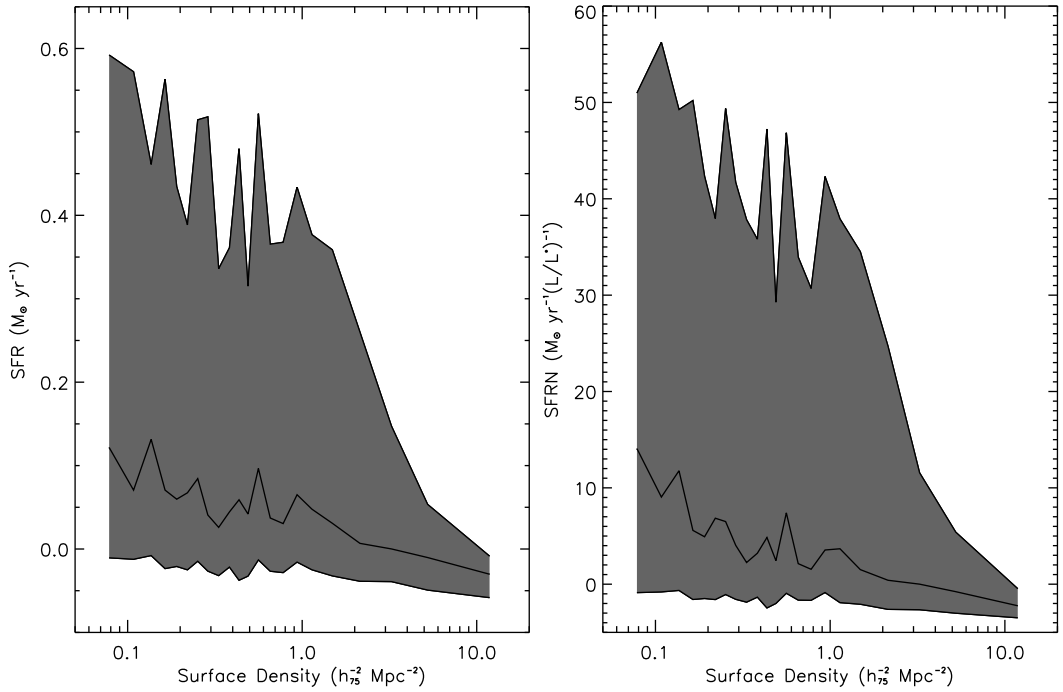

Figure 1.6. Galaxy star formation as a function of environment (Gómez et al. 2003). Left-hand panel: the distribution of star-formation rate (SFR) as a function of the projected local surface density of galaxies from SDSS. Right-hand panel: a similar distribution for the luminosity normalised SFR (SFRN). In both cases, the shaded area represents the observed distribution, with the upper and lower limits being the 75th and 25th percentiles, respectively. The embedded solid line is the median SFR. In this data, an abrupt transition in the SFR distribution is observed at a surface density $\sim 1\,\mathrm{h}_{75}^{-2}\,\mathrm{Mpc}^{-2}$.

density observed by Kodama et al. 2001 using galaxy colour). However, in other studies that use more general measures of the galaxy environment (e.g. halo mass), this critical density is not observed (Weinmann et al. 2006).

An important consideration in these relations is that the optical signatures of SFR can be obscured in galaxies that have large amounts of interstellar dust (e.g. dusty red spirals; Wolf et al. 2009). Using infrared data, Wolf et al. (2009) probed this obscured star formation and found that the SFR of star-forming galaxies in the high-density cluster environment is clearly lower than in the low-density field. They also found that the SFR of blue galaxies alone is similar in both the field and cluster environments, suggesting dusty red spirals represent a key intermediate stage in galaxy evolution.

(iii) *AGN fraction.* There is also a potential relationship between the fraction of galaxies hosting AGN and the local galaxy density. Using [O III] emission as an indicator of AGN activity, Kauffmann et al. (2004) find that twice as many galaxies host AGN in low-density environments compared to high-density environments.

It is not really surprising that we observe these density correlations given the well-established morphology–density relation and the observed correlations between galaxy properties and Hubble type. However, through studying different galaxy properties as a function of environment we can assess which galaxy properties are more susceptible to environmental influences and hence determine potential evolutionary paths for galaxies in-falling to the cluster environment. Considering all the

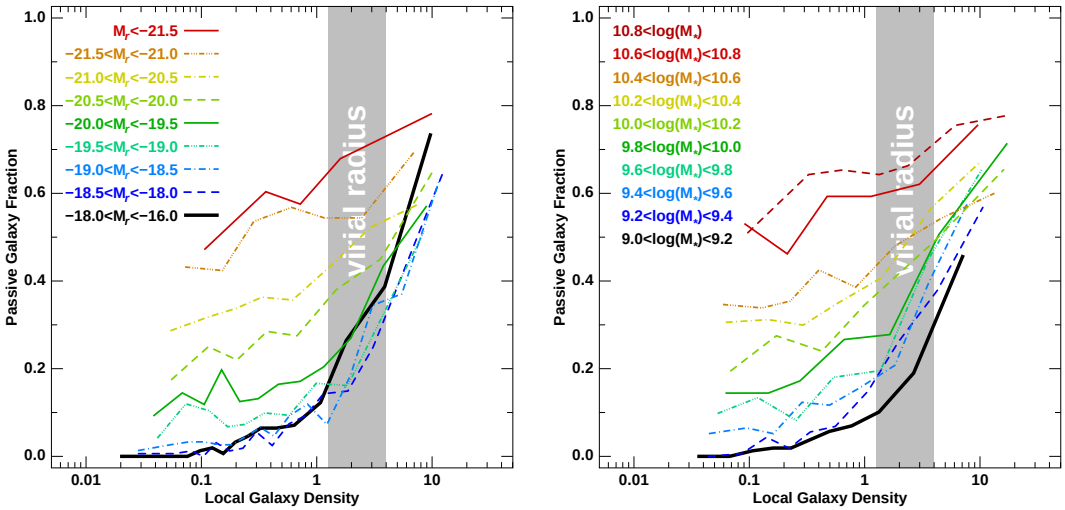

Figure 1.7. The robustness of different mass galaxies to the effect of the galaxy environment (Haines et al. 2007). The fraction of passively evolving galaxies as a function of the local galaxy density in SDSS for different luminosity (left-hand panel) and stellar mass ranges (right-hand panel).

observed correlations with environment, it is clear that there is a trend to a more passive (non star-forming) and spheroidal galaxy population in dense environments. This observation suggests that blue star-forming spiral galaxies falling into the gravitational well of a cluster, somehow have their star formation extinguished by the cluster environment and eventually evolve into the S0s we see in the Universe today.

In addition to these environmental correlations, it has also become apparent that a galaxy's luminosity (and hence stellar mass) is a critical factor in governing how susceptible a galaxy is to environmental influences (Haines et al. 2006, 2007). Using data from SDSS, Haines et al. (2007) find that the correlation between the fraction of passive (non star-forming) galaxies and the local galaxy density is a strong function of luminosity and stellar mass (see Fig. 1.7). For luminous high-mass galaxies, the variation in the passive galaxy fraction from low- to high-density environments is much less extreme than for fainter low-mass galaxies. This result suggests that low-mass galaxies are far more susceptible to the effects of the galaxy environment than high-mass galaxies (e.g. less able to withstand any effect that could diminish their gas supply and suppress star formation).

1.1.4 Galaxy evolution: 'nature' versus 'nurture'

The fact that a galaxy's morphology, colour and star-formation rate is closely related to the local density of galaxies suggests the local environment is of key importance in the formation and of evolution galaxies. The observed correlations (see Sections 1.1.2 and 1.1.3) show a clear trend to a more passive and spheroidal population in dense environments. However, despite this evidence it remains uncertain as to whether the galaxy environment has any direct effect on the individual galaxies concerned.

In hierarchical models of galaxy formation (e.g. De Lucia et al. 2006), galaxies in the highest-density environments (i.e. cluster cores) formed earlier than analogous galaxies in lower-density environments (see Section 1.1.1). Therefore, it is natural to expect cluster galaxies to have older and more evolved stellar populations than analogous galaxies in the field. Consequently, it is possible that secular evolution

can account for the observed density correlations and that the environment itself has little or no direct effect on individual galaxies. However, at the same time, galaxies that formed in the high-density environments will also have had more time to experience the external influence of their local environment. Any such influences would also act on any in-falling galaxies as they are accreted into larger haloes. This raises the fundamental problem of '*nature*' versus '*nurture*' in our understanding of galaxy evolution:

1. *Nature:* galaxies are essentially unaffected by their local environment and the origin of the observed density correlations is due to cluster galaxies being older and more evolved than analogous galaxies in the field. Galaxies evolve secularly, with a galaxy's mass being key in determining the effect of internal processes (e.g. AGN feedback) on the observed properties of the galaxy.

2. *Nurture:* galaxies are directly affected by their local environment, resulting in their observed properties, e.g. gas content, star-formation rate, colour and morphology.

In reality, the nature–nurture hypotheses are not mutually exclusive and a mixture of both scenarios may be responsible for the observed density correlations. This fact has led some authors to suggest that the nature–nurture debate is ill posed (e.g. De Lucia et al. 2012). However, nonetheless, the role of the galaxy environment in determining the properties of galaxies remains one of the most fundamental and yet still unanswered aspects in our understanding of galaxy evolution.

1.1.5 Outstanding questions

At the current time, there are several key outstanding problems in our understanding of galaxy evolution and the role of the galaxy environment:

(i) *How does star formation get suppressed in the cluster environment?* Correlations of star-formation rate with galaxy density suggest that star formation is suppressed in high-density environments. The removal of the raw material for star formation (i.e. cold gas) from a galaxy is the most likely explanation. However, whether this is due to an internal process (e.g. AGN activity; Croton et al. 2006) or external influences (i.e. the cluster environment) is still uncertain. An additional complication is that our current models of galaxy formation predict this cold gas supply to be continually replenished by accretion from an outer hot gas reservoir (e.g. Fall & Efstathiou 1980), thus leading to sustained star formation in the galactic disc. If old stellar populations are to evolve, this process must also be interrupted.

(ii) *How do spiral galaxies transform into S0s?* The suppression of star formation by the cluster environment is one potential mechanism by which a spiral galaxy could begin its transformation into an S0. However, the existence of S0 galaxies in the general field implies that either cluster processes are not responsible, or that S0s can form via alternative processes in different environments. Consequently, understanding the processes that can quench star formation and how they relate to the galaxy environment remains a topic of extensive study.

(iii) *What drives the morphology–density relation?* Understanding the origin of the morphology–density relation is key to our understanding of the role of the galaxy environment in galaxy evolution. However, at the present time we are still largely uncertain about what physical processes can bring about changes in stellar

structure (e.g. disc-to-spheroid transformations), how these are related to changes in star formation, and how these processes are related to the galaxy environment.

Disentangling the relative importance of both internal and external influences in galaxy evolution is vital to understanding these problems. However, this is very challenging and remains a topic of considerable effort by the scientific community. The matter is further complicated by the fact that changes in star formation are not necessarily related to changes in morphology. The processes that bring about these changes may well act on different timescales and in different regimes. In the following section, we shall review some of these potential environmental processes and explore how they can bring about changes in morphology and star formation in a galaxy.

1.2 Environmental processes

Many potential processes have been suggested in order to try and account for the observed correlations between the properties of galaxies and their local environment. However, the exact mechanisms driving these correlations remain elusive. Certain physical processes inherent to galaxy evolution and related to the galaxy environment may contribute, e.g. by terminating star formation through gas stripping or by disrupting the stellar distribution. However, direct evidence for these processes is still lacking and their relative importance in galaxy evolution remains uncertain.

The numerous potential processes and related varying terminology can be somewhat confusing. However, several useful reviews are now available (e.g. Treu et al. 2003; Boselli & Gavazzi 2006; Poggianti 2006). Following the distinctions laid out by Treu et al. (2003), we separate these potential environmental processes into three broad categories: those related to galaxy-galaxy interactions, those related to galaxy-cluster gravitational interactions, and finally those that refer to an interaction between a galaxy and the intracluster medium (ICM). We expand on each of these categories in the following sections.

1.2.1 Galaxy-galaxy interactions

These processes refer to the gravitational interactions between two or more galaxies.

(a) *Strong interactions – mergers:* low-speed interactions between galaxies resulting in a merging of their stellar distributions (Icke 1985; Bekki 1998). Mergers are most efficient when galaxies are at relatively low velocities; therefore, mergers are thought to be more prevalent in low-density environments (i.e galaxy groups) than in high-density cluster cores. There are two main schemes for classifying mergers: one based on the mass ratio of the merging galaxies;

  (i) *Major mergers:* the merger between two galaxies of similar mass. These dramatic events often lead to fundamental structural changes in the stellar distribution of the remnant galaxy (i.e. turning disc galaxies into ellipticals; e.g. González-García & Balcells 2005).

  (ii) *Minor mergers:* the merging of a large mass galaxy with a small companion (also called *satellite accretion*). These events can result in a smooth stellar envelope or thick outer disc forming around the more massive galaxy (Naab et al. 2007). These events may be prevalent in both the field and cluster environments.

and another scheme based on the amount of available gas in the merging galaxies.

(i) *'Dry' mergers:* the merging of gas poor galaxies (e.g. van Dokkum 2005; Bell et al. 2006). These events result in little triggered star formation and may lead to a subsequent expansion of the stellar distribution (also called *'dissipationless'* merging).

(ii) *'Wet' mergers:* the merging of gas rich galaxies resulting in triggered star formation as the gaseous components are driven into the central regions of the remnant galaxy (Mihos & Hernquist 1996; Barton et al. 2000).

(b) *Tidal interactions:* multiple interactions at either low or high velocities.

(i) *Low-speed tidal interactions:* low-speed galaxy encounters that do not result in a merger event. Such encounters could cause the *'tidal stripping'* of stellar and gaseous material from interacting galaxies. These events are expected to be more prevalent at high-densities but may play an important role in low-density environments (i.e. galaxy groups).

(ii) *High-speed tidal interactions – galaxy harassment:* multiple high-speed encounters between galaxies in the cluster environment (Moore et al. 1996). Such interactions could lead to the tidal stripping of gas and stellar material from the 'harassed' galaxy and/or disrupt the structure of the stellar distribution (i.e. gradually turn a disc galaxy into a spheroid).

1.2.2 Galaxy-cluster gravitational interactions

These interactions occur between an in-falling cluster galaxy and the gravitational potential of the cluster.

(a) *Tidal compression of galactic gas:* the tidal compression of a galaxy's gas due to gravitational interactions with the cluster potential (Byrd & Valtonen 1990; Henriksen & Byrd 1996). This process can trigger star formation and lead to an increase in the star-formation rate.

(b) *Tidal truncation of the outer galactic regions:* the tidal truncation (stripping) of the outer regions of a galaxy's dark matter halo due to the gravitational potential of the cluster (Merritt 1983, 1984). These tidal interactions can lead to structural changes in the in-falling galaxy's mass profile. However, if the outer hot gas reservoir is also affected (see Section 1.1.5), this process can also lead to a quenching of star formation (i.e. *strangulation*, see Section 1.2.4).

1.2.3 Galaxy-ICM interactions

These interactions occur between an in-falling cluster galaxy and the gaseous component of the cluster – the intracluster medium (ICM).

(a) *Ram-pressure stripping:* the removal of cold gas from a galaxy's interstellar medium (ISM) due to the pressure exerted by the intracluster medium (Gunn & Gott 1972). The removal of the galactic gas supply leads to suppressed star formation in the affected galaxy. Ram-pressure stripping is expected to be most prevalent in very dense environments (e.g. cluster cores).

(b) *ICM pressure:* the compression of interstellar gas clouds due to the pressure exerted by the intracluster medium (Dressler & Gunn 1983; Evrard 1991). This process can trigger star formation and lead to a temporary increase in the star-formation rate.

(c) *Turbulent and viscous stripping:* various transport processes in the intracluster medium (ICM) that can lead to the stripping of a galaxy's interstellar medium (e.g. Nulsen 1982). The removal of the galactic gas supply leads to suppressed star formation in the affected galaxy.

(d) *Thermal evaporation:* the thermal evaporation (heating) of a galaxy's interstellar medium (ISM) by interactions with the hot intracluster medium (Cowie & Songaila 1977). The removal of the galactic gas supply leads to suppressed star formation in the affected galaxy.

1.2.4 Potential environmental effects

In the previous sections, we have explored some of the many potential processes by which a galaxy can be influenced by its local environment. However, regardless of the exact physical mechanism responsible, these environmental processes can either affect the galaxy's stellar distribution (morphology), cold gas component, or outer extended hot gas reservoir. As a consequence, these processes can lead to three broad effects on a subject galaxy:

(i) *Morphological transformation:* mainly the disruption of the structure of the stellar distribution caused by galaxy-galaxy interactions (e.g. mergers or harassment). These events could also be the origin of intracluster light as interacting galaxies lose stars to the intracluster medium. However, some morphological transformations are possible without disrupting the stellar distribution. If star formation is suppressed in the stellar disc (e.g. by gas stripping), then the disc will gradually fade and the bulge-to-disc ratio will change. This can significantly affect the observed morphology (see e.g. Poggianti 2006).

(ii) *Triggered/suppressed star formation:* the compression/stripping of a galaxy's cold gas component leading to a rapid triggering/termination of star formation – timescales $\sim 10^7$ yrs.

(iii) *Gradual decline in star formation – strangulation:* the removal of a galaxy's outer hot gas reservoir (Larson et al. 1980; see Section 1.1.5) leading to the slow decrease in the star-formation rate as the galaxy depletes its remaining cold gas supply (also known as *starvation* or *suffocation*) – timescales $> 1\,\mathrm{Gyr}$.

However, these effects can also be induced from internal processes (e.g. AGN activity; Croton et al. 2006). Consequently, disentangling the effects of internal and external influences on galaxy evolution is an extremely challenging and daunting task. Ultimately, several unrelated processes may work together to bring about the above effects and explain the observed environmental correlations (see Sections 1.1.2 and 1.1.3). As an added complication, these processes may work on very different timescales and be more/less effective in different galaxy environments and for galaxies of different mass. Galaxies may undergo some physical changes in low-density environments (i.e. galaxy groups) and then complete their morphological transformations as the group itself in-falls to the cluster environment (i.e. pre-processing).

The time-lag between processes acting on a galaxy and the visual signatures of the effects they induce is also a complication.

Considering all the above issues, it is clear that galaxy evolution is undoubtedly a very complex process. However, through studying different galaxy properties (both in structure and star formation) as a function of the galaxy environment, both for different galaxy morphologies and stellar masses ranges, we can try and unravel the role of the galaxy environment in galaxy evolution.

1.3 The size and structure of galaxies and the galaxy environment

In this thesis, we use observational data to explore the effect of the galaxy environment on the size and structure of a galaxy's stellar distribution. Therefore, we are essentially exploring whether or not the galaxy environment can cause strong effects that can disrupt the stellar distribution (e.g. through galaxy-galaxy interactions). Other more subtle processes, acting on the gaseous component and causing a triggering/termination of star formation (e.g. ram-pressure stripping) are not directly probed by this work, although these processes could still have an indirect effect on the galaxy morphology.

1.3.1 The size of the stellar distribution

Several scaling relations are known to exist for galaxies in the Universe. The most famous are the relations between the luminosity of a galaxy and the velocity of its component stars (Faber & Jackson 1976; Tully & Fisher 1977):

(i) *The Faber–Jackson relation:* for spheroidal (elliptical) galaxies, the central stellar velocity dispersion σ_0 increases with increasing galaxy luminosity L roughly as

$$L \propto \sigma_{\rm o}^{\alpha} \qquad \alpha \sim 4. \tag{1.1}$$

(ii) *The Tully–Fisher relation:* for disc (spiral/S0) galaxies, the maximum rotational velocity $v_{\rm max}$ increases with increasing galaxy luminosity L roughly as

$$L \propto v_{\rm max}^{\alpha} \qquad \alpha \sim 4. \tag{1.2}$$

For both spheroidal and disc galaxies, the velocities v of the stellar population are directly governed by the total mass $M_{\rm tot}$ of the galaxy (i.e. $M_{\rm tot}(r) = rv^2/G$). Consequently, these relations indicate that the more luminous a galaxy is, the greater its total mass $M_{\rm tot}$. More importantly, if we assume the surface brightness of a given galaxy type is roughly constant ($L \propto r^2$), these relations imply that for that galaxy type, the mass-to-light ratio (M/L) is well-defined. If galaxies contained no dark matter, one would expect a well-defined M/L, since a galaxy's luminosity L is directly related to the mass of its stellar component M_* (note: $M/L \nsim$ constant since a galaxy's luminosity will also depend on the specific properties of the stellar population, especially age). However, since the majority of a galaxy's mass is comprised of dark matter (see Section 1.1.1), these relations are surprising. Somehow the amount of stellar mass in a galaxy is related to the mass of its dark matter halo.

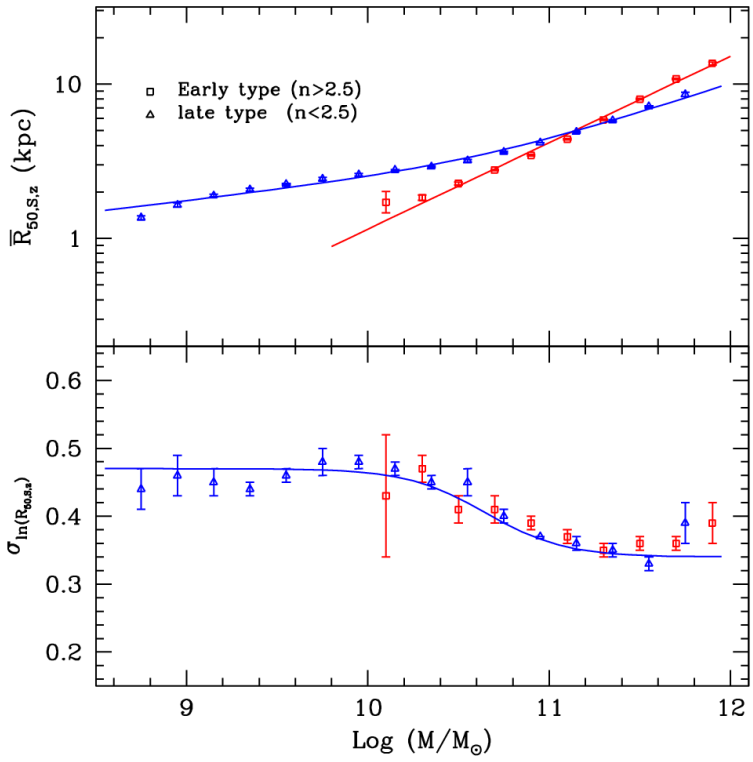

Figure 1.8. The stellar-mass–size relation generated using 140 000 galaxies from SDSS (Shen et al. 2003). The median (top) and dispersion (bottom) of the distribution of half-light radius in the z-band ($\overline{R}_{50,\mathrm{S},z}$) as a function of stellar mass. The half-light radii were determined from Sérsic fits and the relations shown are for early- (squares) and late-type (triangles) galaxies as defined by their Sérsic index n (see Section 1.3.2).

Another well-established scaling relation is the Kormendy relation – the relationship between the luminosity L (and hence stellar mass M_*) of a galaxy and the physical size of its stellar distribution (Kormendy 1977; Shen et al. 2003; see Fig. 1.8). This relation shows that the brighter (and hence more massive) a galaxy is, the greater its physical size (as measured by the half-light or effective radius r_e – the radius within which half of a galaxy's total light is emitted). For stellar mass M_*, this relationship is known as the *stellar-mass–size relation*.

Various physical processes could potentially effect the physical size of a galaxy (e.g. 'dry' merging or minor mergers, see Section 1.2.1) and the rate of these processes may be related to the galaxy environment. Therefore, comparisons of the stellar-mass–size relation between galaxies in the field and cluster environments can be used to assess whether or not the galaxy environment affects the physical size of galaxies, and hence aid in determining the importance of these processes in driving the morphology–density relation. We shall return to this problem in Chapter 3.

1.3.2 The structure of the stellar distribution

Since the work of Patterson (1940), de Vaucouleurs (1959b) and Freeman (1970), we have known that the light profiles of disc galaxies are comprised of two main structural components: an inner component dominated by a bulge (spheroidal component); and an outer component consisting of an exponentially declining stellar disc (see Fig. 1.9).

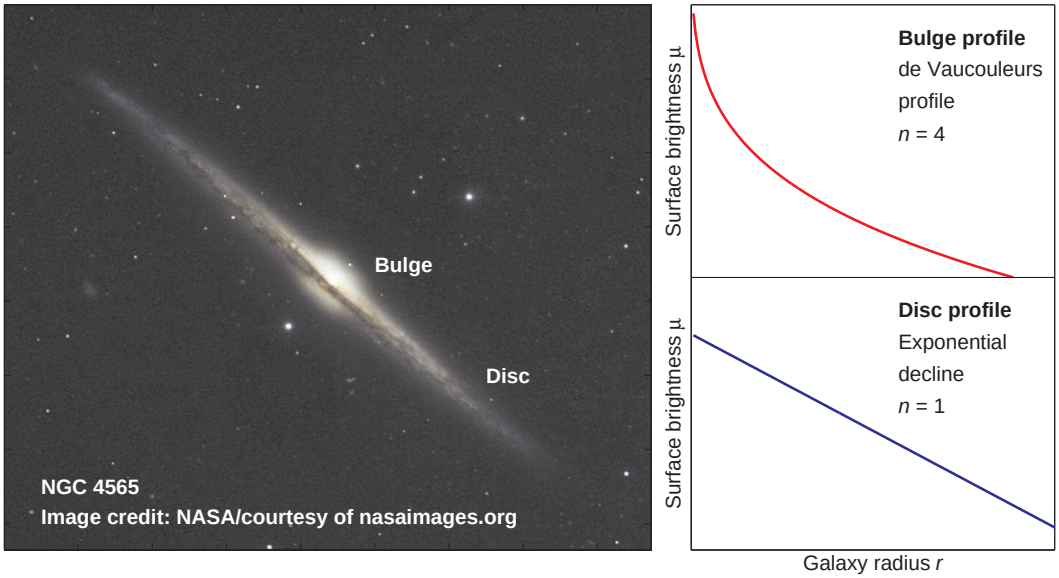

Figure 1.9. The structure of a typical disc galaxy (NGC 4565). The central bulge component follows a de Vaucouleurs ($r^{1/4}$) profile, while the outer exponential disc follows a simple exponential decline.

(i) *Bulge component:* the light profile for the bulge component generally follows a 'classical', de Vaucouleurs (1948), $r^{1/4}$ profile given by

$$\mu(r) = \mu_{\rm e} + 8.3268 \left[\left(\frac{r}{r_{\rm e}} \right)^{1/4} - 1 \right], \tag{1.3}$$

where μ is the surface brightness in mag arcsec^{-2}, r is the radius and $\mu_{\rm e}$ is the surface brightness at the effective radius $r_{\rm e}$. These profiles are thought to originate from the result of a major merger event. Bulge profiles that do not follow this general form are called '*pseudo bulges*' and are thought to form from secular processes (Kormendy 1993; Kormendy & Kennicutt 2004).

(ii) *Disc component:* the light profile for the stellar disc generally follows a simple exponential decline with some minor deviations related to substructure (e.g. spiral arms). The exponential decline is given by

$$\mu(r) = \mu_0 + 1.0857 \left(\frac{r}{h} \right), \tag{1.4}$$

where μ is the surface brightness in mag arcsec^{-2}, r is the radius, μ_0 is the central ($r = 0$) surface brightness (minus the bulge component) and h is the characteristic scalelength.

For a more general description of a galaxy's light profile, an alternative single component parameterization known as a Sérsic (1968) profile is often used. For surface brightness μ in mag arcsec^{-2}, a Sérsic profile is given by

$$\mu(r) = \mu_{\rm e} + 1.0857\kappa \left[\left(\frac{r}{r_{\rm e}} \right)^{1/n} - 1 \right], \tag{1.5}$$

where n is the Sérsic index (a concentration parameter) and the normalisation constant $\kappa = \kappa(n) \simeq 1.9992n - 0.3271$. In this general description, a disc profile has $n = 1$, and a bulge profile has $n = 4$. In reality, galaxies contain both disc and bulge components and to different extents; and therefore, the Sérsic profile (and Sérsic index) provides a useful description/measure of the concentration of the galaxy's stellar distribution. For massive galaxies (e.g. $M_* > 10^{10}\,\mathrm{M}_\odot$), the Sérsic index is broadly related to morphology with early-type (elliptical) galaxies having $n > 2.5$ and late-type (disc) galaxies having $n < 2.5$. Due to the simple and useful parameterization of the Sérsic profile, these profiles are very common in current galaxy surface brightness model-fitting codes, e.g. GALFIT (Peng et al. 2002).

The structure of galactic discs

We now know the classical picture of a galaxy (simple bulge and disc) does not hold for the majority of galaxies in the Universe. For disc galaxies in particular, this simple model has been shown to fail at the faint surface brightness in the outer regions of the stellar disc (van der Kruit 1979; Pohlen et al. 2002). Since van der Kruit (1979), we have known that the exponential decline in the outer disc does not extend out to the last measured point but can be truncated (sharply cut off) after several scalelengths. More recently, Pohlen et al. (2002) have shown that the exponential disc does not cut off completely at the truncation. They find that most profiles are actually best described by a two-slope model (broken exponential), characterised by an inner and outer exponential scalelength separated by a relatively well-defined break radius r_{brk}. Many studies have now reported (mainly using surface photometry) the existence of broken exponential discs (*truncations*) in disc galaxies in both the local (Pohlen et al. 2002, 2007; Pohlen & Trujillo 2006; Bakos et al. 2008; Erwin et al. 2008, 2012; Gutiérrez et al. 2011; Maltby et al. 2012a) and distant $z < 1$ Universe (Pérez 2004; Trujillo & Pohlen 2005; Azzollini et al. 2008).

As a direct result of these studies, a comprehensive classification scheme for disc galaxies has emerged based on break features in the outer disc component of their radial $\mu(r)$ profiles (see e.g. Pohlen & Trujillo 2006; Erwin et al. 2008). This classification scheme consists of three broad profile types (Type I, II and III):

1. Type I (no break) – the galaxy has a simple exponential profile extending out to several scalelengths (e.g. Bland-Hawthorn et al. 2005);

2. Type II (down-bending break, *truncation*) – a broken exponential with a shallow inner and steeper outer region separated by a relatively well-defined break radius r_{brk} (van der Kruit 1979; Pohlen et al. 2002);

3. Type III (up-bending break, *antitruncation*) – a broken exponential with the opposite behaviour to a Type II profile (i.e. a shallower region beyond r_{brk}; Erwin et al. 2005).

In each case, the classification refers to the outer, disc component of the galaxy $\mu(r)$ profile and does not consider the inner bulge component even if the bulge is near exponential in nature. Examples of each profile type are shown in Fig. 1.10.

Measurements independent of surface photometry (from resolved star counts) are also available on nearby galaxies for each of the three profile types. Bland-Hawthorn et al. (2005) find that NGC 300 has a simple exponential profile extending out to ~ 10 scalelengths (Type I); Ferguson et al. (2007) argue that M33 is best described

as a broken exponential with a down-bending break (Type II), and Ibata et al. (2005) report that M31 could be described as having an antitruncated disc (Type III).

Understanding the structure of galactic discs is an important aspect in understanding the formation and evolution of disc galaxies and the role of the galaxy environment. The fragile, outer regions of these galactic discs are more easily affected by interactions with other galaxies and the cluster environment, and therefore their structural characteristics must be closely related to their evolutionary history. Consequently, exploring the effect of the galaxy environment on the light distribution (surface brightness μ profile) of disc galaxies should aid in our understanding of the physical processes of galaxy evolution occurring in different galaxy environments. We shall explore this problem in Chapters 4–6 of this thesis.

1.4 Thesis overview

This thesis concerns the effect of the galaxy environment on the physical size and structure of the stellar distribution for relatively local galaxies ($z < 0.3$). Consequently, this work focuses on the exploration of whether or not the galaxy environment can cause strong effects that can disrupt a galaxy's stellar distribution, and hence drive the morphology–density relation.

In order to achieve this, we first require extensive and high-quality data on a large sample of local galaxies. We find the Space Telescope A901/2 Galaxy Evolution Survey (STAGES; Gray et al. 2009) an ideal data set within which to carry out our studies. An overall summary of the STAGES survey is contained in Chapter 2, along with a description of how we measure the galaxy environment and select our galaxy samples.

We then begin our investigations in Chapter 3, where we explore the effect of the galaxy environment on the physical size of galaxies using the stellar-mass–size relation. For different Hubble-type morphologies, we compare the stellar-mass–size relation between the environments of the general field, the cluster, and the extreme environment of the cluster core. These comparisons have allowed us to assess whether or not the galaxy environment has any effect on galaxy sizes; and therefore, assess whether processes that can cause an expansion of the stellar distribution are driving the morphology–density relation.

We then move on to explore the effect of the galaxy environment on the structure of galactic discs. In Chapter 4, we investigate the effect of the galaxy environment on the structure of radial surface brightness profiles in spiral galaxies. We then complement this work with an analogous investigation on the effect of the environment on the galactic discs of S0 galaxies (Chapter 5). The comparisons of galactic disc structure between galaxies in different environments and between galaxies of different morphology, has allowed us to assess whether the galaxy environment has any influences on stellar disc structure and shed light on potential evolutionary paths for spiral galaxies to evolve into S0s. We conclude this work with an examination of the impact of the de Vaucouleurs (1948) bulge profile on the surface brightness profile of the stellar disc in both spiral and S0 galaxies (Chapter 6).

The overall conclusions of this work, and their impact on our current theories of galaxy evolution, are discussed in Chapter 7. Throughout this thesis, we adopt a cosmology of $H_0 = 70\,\mathrm{km\,s^{-1}\,Mpc^{-1}}$, $\Omega_\Lambda = 0.7$ and $\Omega_m = 0.3$, and use AB magnitudes unless stated otherwise.

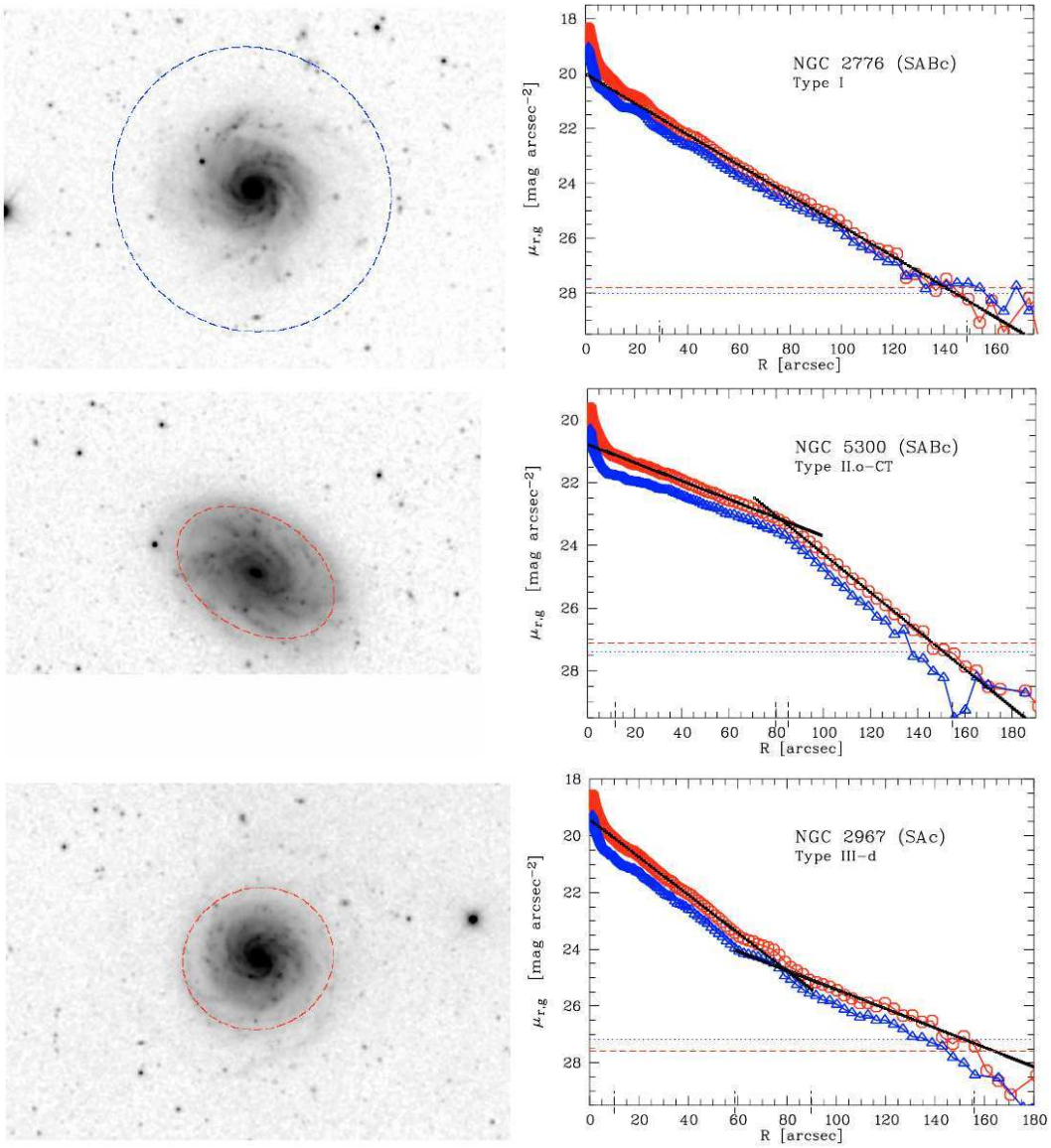

Figure 1.10. Stellar disc profile types (Pohlen & Trujillo 2006). The three main types of radial surface brightness $\mu(r)$ profile for disc galaxies: Type I – no break or pure exponential profile (top row), Type II – down-bending break or *truncation* (middle row), and Type III – up-bending break or *antitruncation* (bottom row). Left-hand panels: r'-band images. Right-hand panels: azimuthally-averaged radial $\mu(r)$ profiles in the g' (blue triangles) and r' (red circles) band.

Chapter 2

The STAGES survey

In order to explore the effect of the galaxy environment on the size and structure of galaxies, we require high-quality multiwavelength data and imaging on a large sample of local galaxies covering a wide range of environments and luminosities. Such extensive observations are most easily sourced from the rich archives available from modern surveys. For our research aims, the extensive multiwavelength data and imaging available from the Space Telescope A901/2 Galaxy Evolution Survey (STAGES; Gray et al. 2009) forms an invaluable data set within which to carry out our studies. Indeed, the work presented in this thesis is entirely based on the STAGES data and imaging published by Gray et al. (2009).

2.1 Overview

STAGES is an extensive multiwavelength survey designed to probe the physical drivers of galaxy evolution across a wide range of environments and luminosities (Gray et al. 2009). The survey targets the complex Abell(A) 901/902 multicluster system ($z \sim 0.167$), which consists of three clusters (A901a, A901b and A902) and related groups [e.g. the South-West (SW) group], all located within $0.5^\circ \times 0.5^\circ$ ($\sim 5 \times 5\,\mathrm{Mpc}^2$; see Fig. 2.1). Consequently, the survey region encompasses a wide range of galaxy environments spanning from the general field to the intermediate densities of the A901/2 cluster cores [projected cluster galaxy number density ($R < 24$) up to $\sim 1600\,\mathrm{gal\,Mpc}^{-3}$; Heiderman et al. 2009][1]. Therefore, the A901/2 system provides an ideal laboratory within which to explore the effect of the galaxy environment on the observed properties of galaxies and galaxy evolution.

The primary STAGES observations consist of an 80-tile V-band (F606W) *Hubble Space Telescope* (*HST*)/Advanced Camera for Surveys (ACS) mosaic covering the full $0.5^\circ \times 0.5^\circ$ span of the multicluster system (see Fig. 2.1). This ACS imaging is complemented by high-precision photometric redshifts and observed-/rest-frame spectral energy distributions (SEDs) from the 17-band COMBO-17 photometric redshift survey (Wolf et al. 2003), as well as extensive multiwavelength observations using the *Spitzer Space Telescope*, *Galaxy Evolution Explorer* (*GALEX*), 2 degree field (2dF), *XMM–Newton*, and the Giant Metrewave Radio Telescope (GMRT).

The main goal of the STAGES *HST*/ACS imaging was to obtain morphologies and structural parameters for all cluster galaxies down to $R = 24\,\mathrm{mag}$. To address

[1]Note: this core density is greater than in the Virgo cluster ($\sim 360\,\mathrm{gal\,Mpc}^{-3}$; Binggeli et al. 1987) but lower than in the Coma cluster ($\sim 10\,000\,\mathrm{gal\,Mpc}^{-3}$; The & White 1986). Also note that only order of magnitude comparisons are applicable between the quoted core densities. This is due to differences in the sample selections used by the respective works (i.e. magnitude limits).

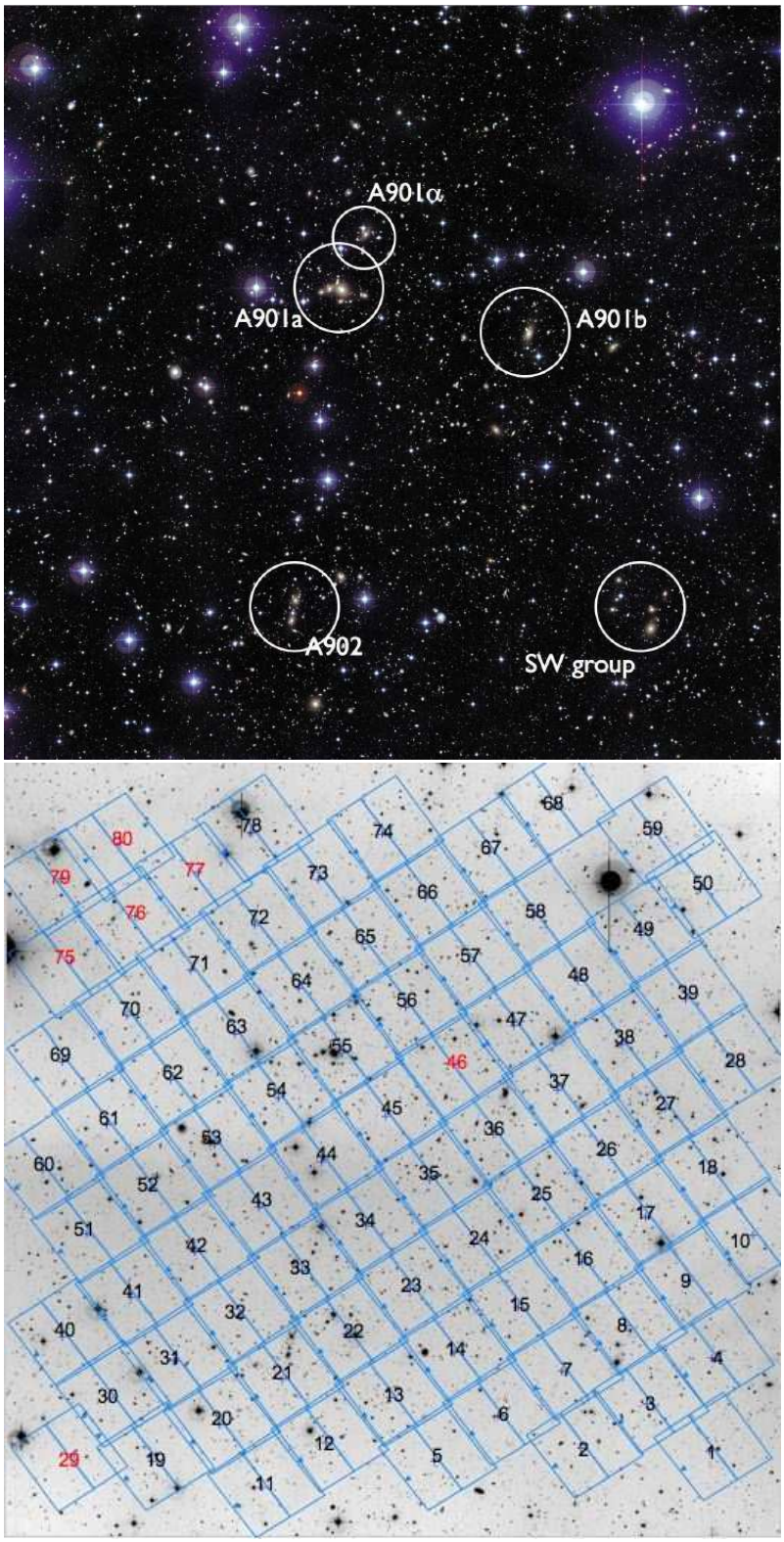

Figure 2.1. The STAGES A901/2 field. Top panel: an image of the complete A901/2 field created using colour information (RGB) from the ground-based COMBO-17 survey (Wolf et al. 2003). The cores of the three Abell clusters (A901a, A901b and A902) and the South-West (SW) group are encircled for reference (note: also encircled is A901α – some suspected in-falling substructure related to A901a). Bottom panel: a schematic showing the *HST*/ACS 80-tile mosaic. Image credit – http://www.nottingham.ac.uk/astronomy/stages.

this aim, Gray et al. (2009) have performed Sérsic profile fitting using the GALFIT code (Peng et al. 2002) on all *HST*/ACS images and also conducted simulations to quantify the completeness of the survey, all of which are publicly available[2]. Additionally, all galaxies with $R < 23.5$ and $z_{\rm phot} < 0.4$ (5090 galaxies, where R is the total Vega magnitude) were visually classified by seven members of the STAGES team into the Hubble types (E, S0, Sa, Sb, Sc, Sd, Irr) and their intermediate classes (Gray et al., in preparation). Weighted average estimates of the Hubble types, ignoring bars and degrees of asymmetry, were generated. For this classification, S0s were defined to be disc galaxies with a visible bulge but no spiral arms (smooth disc); and the spiral classification (Sa–Sd) represents a decreasing sequence in the apparent bulge-to-disc (B/D) ratio.

The COMBO-17 observations used in the STAGES data catalogue were obtained with the Wide Field Imager (WFI) at the Max Planck Gesellschaft/European Southern Observatory (ESO) 2.2-m telescope on La Silla, Chile (see Wolf et al. 2003, for further details). COMBO-17 used five broad-band filters *UBVRI* and 12 medium-band filters covering wavelengths from 350 to 930 nm to define detailed optical SEDs and high-quality photometric redshifts for objects with $R < 24$ ($\sim 15\,000$ galaxies). Generally, photometric redshifts from COMBO-17 are accurate to 1 per cent in $\delta z/(1+z)$ at $R < 21$, which has been spectroscopically confirmed. Photo-z quality degrades for progressively fainter galaxies reaching accuracies of 2 per cent for galaxies with $R \sim 22$ and 10 per cent for galaxies with $R > 24$ (Wolf et al. 2004, 2008). The galaxy evolution studies to date on the COMBO-17 data that use photo-z defined galaxy samples all restrict themselves to galaxies that are brighter than $R = 24$ to ensure that only reliable redshifts are used. Stellar-mass estimates derived from SED fitting the 17-band photometry are also available for COMBO-17 galaxies (Borch et al. 2006; Gray et al. 2009). These estimates used a template library derived from PEGASE (Fioc & Rocca-Volmerange 1997) population synthesis models and a Kroupa et al. (1993) stellar initial mass function (IMF).

2.2 Defining the galaxy environment

In this thesis, we shall explore the size and structure of galaxies across a wide range of galaxy environments spanning from the general field to the intermediate densities of the A901/2 cluster cores. In order to achieve this, we first define a large, mass-limited ($M_* > 10^9\,{\rm M}_\odot$), parent sample of field and cluster galaxies in STAGES from which all other galaxy samples used in this thesis are drawn. In the following sections, we outline our field and cluster sample selection and our definition of the galaxy environment.

2.2.1 Selection of a cluster sample

Gray et al. (2009) suggest a cluster sample for STAGES defined solely from photometric redshifts. In their sample selection, the photo-z distribution of cluster galaxies is assumed to follow a Gaussian, while the distribution of field galaxies is assumed to be consistent with the average galaxy counts $N(z, R)$ outside the cluster and to vary smoothly with redshift and magnitude. Cluster galaxies are then defined simply via a redshift interval around the known spectroscopic redshift of the cluster, $z_{\rm phot} = [0.17 - \Delta z, 0.17 + \Delta z]$, the width of which varies with

[2]http://www.nottingham.ac.uk/astronomy/stages

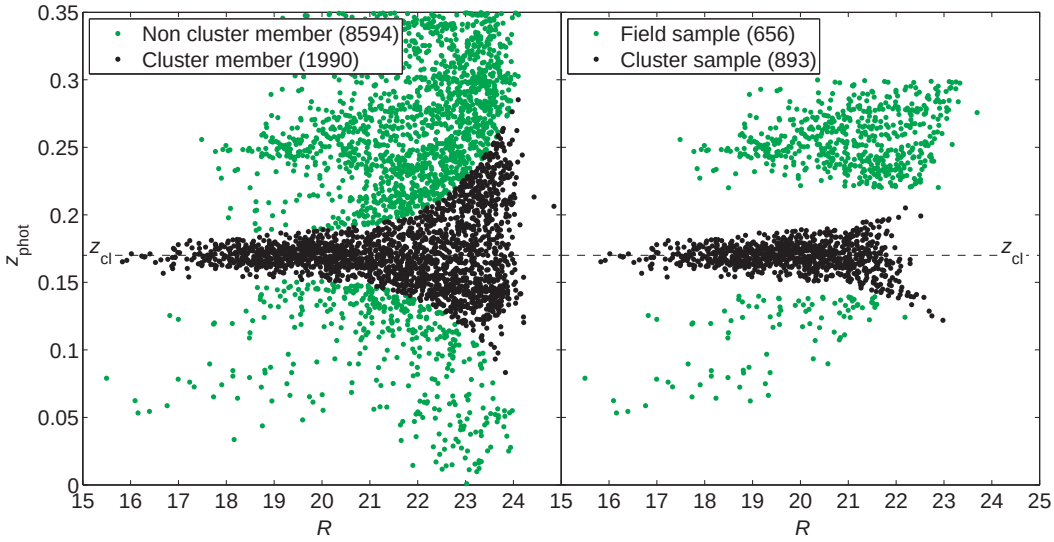

Figure 2.2. The selection of a field and cluster sample. Left-hand panel: the photometric redshift versus R-magnitude for STAGES galaxies showing the cluster selection defined by Equation 2.1 (black points). Non cluster members are shown in green. Right-hand panel: the photometric redshift versus R-magnitude for the mass-limited ($M_* > 10^9\,\mathrm{M}_\odot$) cluster (black points) and field (green points) samples, showing there is no overlap between the two samples as might be inferred from their redshift ranges. The cluster sample reaches $R \sim 23$ and the field sample reaches $R \sim 23.5$. Respective sample sizes are shown in the legends.

R-magnitude (see Fig. 2.2). The half-width Δz as a function of R-magnitude is

$$\Delta z(R) = \sqrt{0.015^2 + 0.0096525^2[1 + 10^{0.6(R_{\mathrm{tot}}-20.5)}]}. \qquad (2.1)$$

This cluster selection adopts a narrow redshift range for bright R-magnitudes due to the high precision of the COMBO-17 photometric redshifts; however, the interval increases in width towards fainter R-magnitudes to accommodate for the increase in the photo-z error. Gray et al. (2009) calculate the completeness and contamination of this cluster selection as a function of R-magnitude by using the counts of their smooth models. In these calculations, they compromise Δz so that the completeness of the cluster selection is > 90 per cent at all magnitudes (see Fig. 2.3). The completeness of this selection converges to nearly 100 per cent for bright galaxies (see Gray et al. 2009, for further details). Contamination is defined to be the fraction of field galaxies in the cluster sample *at* a given magnitude (not below) and increases rapidly for fainter galaxy samples.

In the STAGES data catalogue published by Gray et al. (2009), several useful flags are included to aid in the selection of various galaxy samples (e.g. $combo\_flag$, $stages\_flag$ and $phot\_flag$). The Gray et al. (2009) cluster selection can easily be selected from the STAGES catalogue by using the criterion $combo\_flag \geq 4$.

For our cluster sample, we first select a reliable sample of cluster galaxies from the STAGES catalogue using the following criteria:

(i) Cluster galaxies detected in COMBO-17 ($combo\_flag \geq 4$),

(ii) Galaxies with reliable COMBO-17 photometry ($phot\_flag < 8$),

(iii) *HST*-extended sources in STAGES ($stages\_flag \geq 3$).

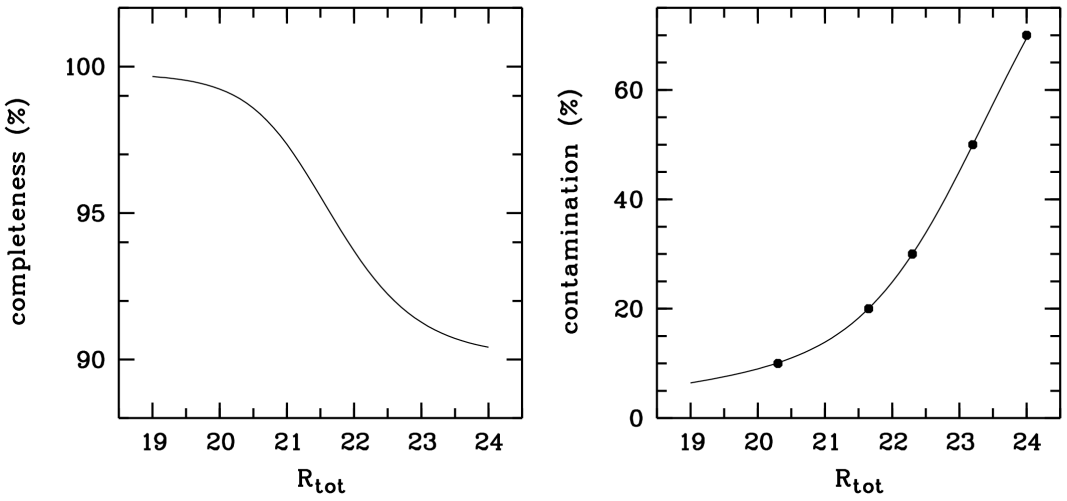

Figure 2.3. The completeness and contamination of the Gray et al. (2009) cluster selection. Left-hand panel: the completeness of the cluster selection defined by Equation 2.1 as a function of R-magnitude. Right-hand panel: the field contamination of the cluster selection as a function of R-magnitude. Contamination is defined to be the fraction of field galaxies in the cluster sample *at* a given magnitude (not below). Throughout this thesis, completeness of the cluster selection is > 90 per cent and overall contamination by the field is < 25 per cent. Figure taken from Gray et al. 2009: Fig. 14.

We then limit this cluster sample by stellar mass ($\log M_*/\mathrm{M}_\odot > 9$) and obtain a final cluster sample containing 893 galaxies. This sample reaches down to $R = 23$ and has a photo-z range at the low-mass end of $z_{\mathrm{phot}} = [0.122, 0.205]$ (see Fig. 2.2).

Extreme environments: the cluster core

In this thesis, we will also consider comparisons of the field environment with the more extreme environment of the A901/2 cluster cores. Any potential effects of the galaxy environment on the size and structure of galaxies should be more apparent in these comparisons. We select galaxies located in the cores of the STAGES A901/2 system by using a similar procedure to Wolf et al. (2009).

Wolf et al. (2009) define a sample of cluster core galaxies in STAGES by using the stellar mass surface density Σ^{M_*} of cluster member galaxies. Using a mass-limited cluster sample with $M_* > 10^9\,\mathrm{M}_\odot$, they measure the local stellar mass surface density inside a fixed aperture with radius $r \sim 1.75\,\mathrm{arcmin}$, corresponding to a radius $r = 300\,\mathrm{kpc}$ at the redshift of the cluster ($z_{\mathrm{cl}} = 0.167$). The aperture stellar mass surface density $\Sigma_r^{M_*}$ in units of $\mathrm{M}_\odot\,\mathrm{Mpc}^{-2}$ was then used to define a cluster core sample. Galaxies where

$$\log \Sigma^{M_*}_{300\,\mathrm{kpc}}(> 10^9 \mathrm{M}_\odot) > 12.5 \tag{2.2}$$

were designated to lie within the four cluster cores of the STAGES multicluster system (A901a, A901b, A902 and SW group).

By applying the same selection procedure to our mass-limited ($M_* > 10^9\,\mathrm{M}_\odot$) cluster sample (see Section 2.2.1), we obtain a cluster subsample of 203 cluster core galaxies. Fig. 2.4 shows the location of our cluster and cluster core sample galaxies in the STAGES region and illustrates the extraction of cluster core galaxies from the cluster sample.

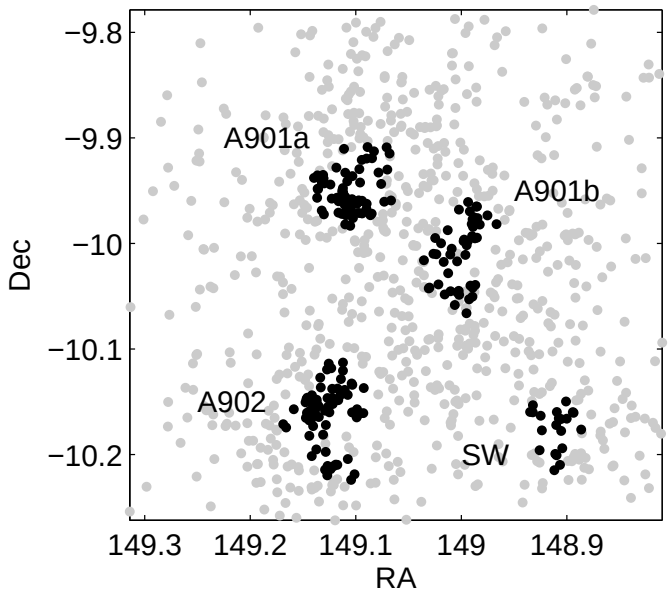

Figure 2.4. A sky map of the STAGES A901/2 field showing our mass-selected cluster sample galaxies ($M_* > 10^9\,\mathrm{M}_\odot$). Galaxies located where the aperture stellar mass surface density $\log \Sigma^{M_*}_{300\,\mathrm{kpc}}(> 10^9\,\mathrm{M}_\odot) > 12.5$ (black points) are designated to lie within the four main cores of the multicluster system (A901a, A901b, A902 and SW group).

2.2.2 Selection of a field comparison sample

For our field comparison sample, we first we select a reliable sample of galaxies from the STAGES catalogue using the following criteria:

(i) Galaxies detected in COMBO-17 ($combo\_flag \geq 3$),

(ii) Galaxies with reliable COMBO-17 photometry ($phot\_flag < 8$),

(iii) *HST*-extended sources in STAGES ($stages\_flag \geq 3$).

Our field sample is then selected from these STAGES galaxies by applying a redshift interval either side of the cluster redshift ($z_{\mathrm{cl}} = 0.167$) that avoids the cluster selection. We use a lower redshift interval at $z = [0.05, 0.14]$ and an upper redshift interval at $z = [0.22, 0.30]$, based on a similar sample selection used by Wolf et al. (2009). We then limit this sample by stellar mass ($\log M_*/\mathrm{M}_\odot > 9$) and obtain a final field sample containing 656 galaxies which reach $R = 23.5$ (see Fig. 2.2). The upper redshift interval for the field contains much more volume and hence more galaxies than the lower redshift interval.

In the data catalogue published by Gray et al. (2009), there exist two sets of derived values for galaxy properties such as magnitude and stellar mass: one based on the photo-z estimate and another assuming the galaxy is located at the known spectroscopic redshift of the cluster ($z_{\mathrm{cl}} = 0.167$). Throughout this thesis, we use the original photo-z estimates for our field samples and the fixed redshift values for our cluster samples. This practice prevents the propagation of photo-z errors into the physical values of our cluster galaxies.

Fig. 2.2 shows the redshift–magnitude diagram for our field and cluster samples and shows that there is no overlap between the field and cluster samples near $z \simeq 0.13$ as might be inferred from their photo-z ranges in the above discussion. The two

stellar-mass estimates for every galaxy help to explain why this is not the case (Wolf et al. 2009). Only at faint magnitudes ($R > 21.5$) do the photo-z ranges of the field and cluster selection overlap. At these magnitudes, estimates of stellar mass are $\log M_*/\mathrm{M}_\odot \approx 9$ in the fixed redshift set of values (galaxy forced to $z_{\mathrm{cl}} = 0.167$) and $\log M_*/\mathrm{M}_\odot \approx 8.6$ in the original estimates. Consequently, galaxies at these magnitudes only get included in the mass-limited samples of the cluster and not the field (see Wolf et al. 2009, for a full explanation).

2.2.3 Visual morphologies: the STAGES morphological catalogue

In this thesis, we obtain visual morphologies for our field and cluster samples from the STAGES morphological catalogue. Gray et al. (in preparation) produced this catalogue by obtaining visual morphologies for all galaxies with $z_{\mathrm{phot}} < 0.4$ and $R < 23.5$. These visual morphologies include the standard Hubble types (E, S0, Sa, Sb, Sc, Sd, Irr) as well as other classifications (e.g. compact objects, stars). In order to assess any selection effect or incompleteness introduced by only using galaxies with visual morphologies, we plot the stellar-mass–magnitude (M_*–R) relations for our field and cluster samples without the stellar mass cut (see Fig. 2.5).

For our cluster sample, all galaxies with $\log M_*/\mathrm{M}_\odot > 9$ have $R < 23.5$ and have visual morphologies in the STAGES morphological catalogue. Therefore, we introduce no further incompleteness to our mass-limited cluster sample by selecting only galaxies that have visual morphologies. The distribution of visual morphologies for our cluster sample and our cluster core subsample are presented in Table 2.1. One cluster member (object #4658) defined as a galaxy in COMBO-17 is subsequently reclassified as a star upon inspection of the *HST*/ACS imaging. Consequently, this object is removed from our mass-limited cluster sample ($N_{\mathrm{cl}} = 892$).

For our field sample, apart from two exceptions, all galaxies with $\log M_*/\mathrm{M}_\odot > 9$ have $R < 23.5$ and have visual morphologies in the STAGES morphological catalogue. Therefore, essentially no further incompleteness is introduced to our mass-limited field sample by selecting only galaxies that have visual morphologies. One bright high-mass galaxy (object #35364) in our mass-limited sample was not contained in the STAGES morphological catalogue due to anomalous photometric flags, but upon subsequent visual inspection this galaxy was classified as a late-type spiral (Sbc). For completeness, this spiral galaxy is retained in our field sample. A faint ($R > 23.5$) galaxy (object #5622) in our mass-limited sample is also unclassified due to the galaxy being too faint for the visual morphology classification. Consequently, this galaxy is removed from our mass-limited field sample ($N_{\mathrm{fld}} = 655$). The distribution of visual morphologies for our field sample is shown in Table 2.1.

Table 2.1. The visual morphologies for our field and cluster samples and our cluster core subsample obtained from the STAGES morphological catalogue (Gray et al., in preparation).

	Elliptical galaxy	Lenticular galaxy	Spiral galaxy	Irregular galaxy	Compact object	Star	?
Field	100	60	318	139	12	0	26
Cluster	192	216	383	86	3	1	12
Core	64	67	59	10	0	0	3

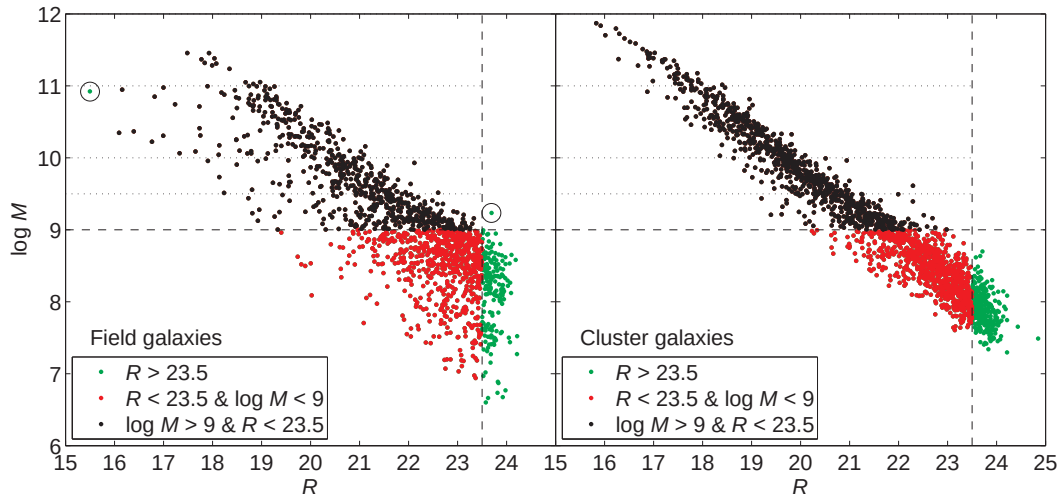

Figure 2.5. Stellar-mass–magnitude (M_*–R) relations for the field (left-hand panel) and cluster (right-hand panel) samples without the stellar mass cut. In both cases, green points: sample galaxies without visual morphologies in STAGES, red points: sample galaxies with visual morphologies in STAGES and with stellar mass $\log M_*/\mathrm{M}_\odot < 9$; black points: sample galaxies with visual morphologies in the STAGES morphological catalogue and with stellar mass $\log M_*/\mathrm{M}_\odot > 9$. Our mass-limited cluster and field samples are sample galaxies with $\log M > 9$ and $R < 23.5$, where $M = M_*/\mathrm{M}_\odot$. In the field M_*–R diagram, the two galaxies highlighted with a circle are those in our mass-limited sample without visual morphologies. For both the cluster and field samples, selecting only galaxies with visual morphologies essentially introduces no further incompleteness. The dashed lines show the stellar-mass ranges used in Table 2.3.

2.2.4 Sample completeness

The completeness of the STAGES survey is > 90 per cent for $R < 23.5$ (Gray et al. 2009) which is true for all galaxies in our field and cluster samples (see Fig. 2.2). However, based on previous COMBO-17 experience Wolf et al. (2009) estimate that at low stellar masses $M_* < 10^{9.5}\,\mathrm{M}_\odot$, the field sample could have an additional 20 per cent incompleteness. This is due to COMBO-17 photometric redshifts and stellar masses being missing for ~ 20 per cent of field galaxies with R-magnitudes corresponding to $M_* < 10^{9.5}\,\mathrm{M}_\odot$. Consequently, our field sample is > 90 per cent complete for $M_* > 10^{9.5}\,\mathrm{M}_\odot$ and > 70 per cent complete for $M_* < 10^{9.5}\,\mathrm{M}_\odot$. For our cluster sample, completeness is > 90 per cent and contamination by the field is < 25 per cent, based on the R-magnitude the cluster sample reaches (Gray et al. 2009; see Figs 2.2 and 2.3). Various properties of the final field and cluster samples and the cluster core subsample are shown in Table 2.2.

In this thesis, we sometimes consider mass-limited subsamples of the field and cluster samples and cluster core subsample in different stellar-mass ranges (e.g. $\log M_*/\mathrm{M}_\odot \in [9, 9.5]$). We expect the completeness of the cluster samples to be > 90 per cent and the contamination of the cluster samples by the field to be < 25 per cent in all cases. Various properties of the final field and cluster samples and the cluster core subsample in different stellar-mass ranges are shown in Table 2.3.

Table 2.2. Properties of the field and cluster galaxy samples and the cluster core subsample.

Property	Field sample	Cluster sample	Core subsample
$N_{\rm gal}$	655	892	203
Completeness	$> 70\,\%$	$> 90\,\%$	$> 90\,\%$
Contamination	–	$< 25\,\%$	$< 25\,\%$
$R_{\rm mean}$	20.85	19.86	19.69
$M_{B(\rm min)}$	-15.11	-15.50	-15.75
$M_{B(\rm max)}$	-21.97	-22.48	-22.48
$z_{\rm phot,mean}$	0.236	0.169	0.169
$z_{\rm phot,min}$	0.053	0.122	0.129
$z_{\rm phot,max}$	0.300	0.205	0.197

Table 2.3. Properties of the field and cluster galaxy samples and the cluster core subsample in different stellar-mass ranges.

$\log M_*/\mathrm{M}_\odot$ range	[9, 9.5]	[9.5, 10]	[10, 11]	[11, 12]
Field galaxy sample				
N_{gal}	308	163	173	11
Completeness	$> 70\,\%$	$> 90\,\%$	$> 90\,\%$	$> 90\,\%$
Contamination	–	–	–	–
R_{mean}	21.82	20.78	19.35	18.18
$M_{B(\mathrm{min})}$	−15.11	−16.90	−17.37	−20.46
$M_{B(\mathrm{max})}$	−19.82	−20.11	−21.46	−21.97
$z_{\mathrm{phot,mean}}$	0.235	0.240	0.231	0.250
$z_{\mathrm{phot,min}}$	0.062	0.064	0.053	0.234
$z_{\mathrm{phot,max}}$	0.299	0.299	0.300	0.267
Cluster galaxy sample				
N_{gal}	298	236	302	56
Completeness	$> 90\,\%$	$> 95\,\%$	$> 95\,\%$	$> 95\,\%$
Contamination	$< 25\,\%$	$< 15\,\%$	$< 10\,\%$	$< 5\,\%$
R_{mean}	21.22	20.11	18.83	17.21
$M_{B(\mathrm{min})}$	−15.50	−15.60	−18.29	−19.78
$M_{B(\mathrm{max})}$	−19.76	−20.23	−21.82	−22.48
$z_{\mathrm{phot,mean}}$	0.167	0.171	0.170	0.169
$z_{\mathrm{phot,min}}$	0.122	0.151	0.154	0.154
$z_{\mathrm{phot,max}}$	0.205	0.190	0.187	0.181
Core galaxy subsample				
N_{gal}	60	47	70	26
Completeness	$> 90\,\%$	$> 95\,\%$	$> 95\,\%$	$> 95\,\%$
Contamination	$< 25\,\%$	$< 15\,\%$	$< 10\,\%$	$< 5\,\%$
R_{mean}	21.28	20.19	19.00	16.97
$M_{B(\mathrm{min})}$	−15.75	−17.39	−18.57	−20.35
$M_{B(\mathrm{max})}$	−19.76	−19.74	−20.81	−22.48
$z_{\mathrm{phot,mean}}$	0.167	0.172	0.170	0.168
$z_{\mathrm{phot,min}}$	0.129	0.156	0.156	0.160
$z_{\mathrm{phot,max}}$	0.197	0.188	0.181	0.181

Chapter 3

The stellar-mass–size relation and the galaxy environment

In this chapter, we explore the effect of the galaxy environment on the stellar-mass–size relation for local galaxies ($z < 0.3$) using the *HST*/ACS imaging and data from the STAGES survey (see Chapter 2). Certain physical processes inherent to galaxy evolution and related to the galaxy environment (e.g. mergers, see Section 1.2), may affect the physical size of some galaxies by e.g. causing an expansion of the stellar distribution (Bell et al. 2005; van Dokkum 2005) or causing stellar disc truncations (van der Kruit 1979; Younger et al. 2007). The work presented in this chapter aims to address this hypothesis.

The majority of the work presented in this chapter has been published in the Maltby et al. (2010) paper. That paper explores the effect of the galaxy environment on the stellar-mass–size relation for different Hubble-type morphologies: elliptical, lenticular and spiral galaxies. However, in this chapter we also present the stellar-mass–size relations for the general galaxy population independent of morphology. In this work, all the statistical analyses are my own work but the necessary measurements of stellar mass M_*, galaxy size r_e and photometric redshift z are drawn from the STAGES data catalogue published by Gray et al. (2009).

3.1 Introduction

Recent observations have found that massive galaxies at high redshift ($z > 1$) are much more compact than galaxies of the same stellar mass in the local Universe (Daddi et al. 2005; Trujillo et al. 2006a; Longhetti et al. 2007; Cimatti et al. 2008; van Dokkum et al. 2008). The extreme rarity of these compact high-mass objects in the local Universe (Shen et al. 2003; Cimatti et al. 2008; Trujillo et al. 2009) implies a strong size evolution in massive galaxies. Various studies have characterized this size evolution for massive galaxies between $z \sim 1.5$ and $z = 0$ (Trujillo et al. 2007; Rettura et al. 2010; van der Wel et al. 2008) and out to higher redshifts $z \sim 3$ (Trujillo et al. 2006b; Toft et al. 2007; Zirm et al. 2007; Buitrago et al. 2008; Franx et al. 2008; van Dokkum et al. 2008). The observed size evolution is especially strong for high-mass galaxies ($M_* > 10^{10}\,\mathrm{M}_\odot$; Franx et al. 2008) with spheroidal morphologies (Trujillo et al. 2007). Trujillo et al. (2007) find that, for massive galaxies at a given stellar mass, disc-like objects were a factor of 2 smaller at $z \sim 1.5$ than their counterparts at $z = 0$, while spheroid-like galaxies were are a factor of 4 smaller at $z \sim 1.5$ compared to analogous spheroids in the local Universe. This observed

size evolution is stronger than but in qualitative agreement with hierarchical semi-analytical model predictions (e.g. Khochfar & Silk 2006).

Systematic uncertainties (e.g. errors in photometric redshifts and mass measurements) could potentially have hampered previous studies of size evolution. However, van der Wel et al. (2008) find, using dynamical masses and spectroscopic redshifts, that these systematic effects are too small to account for the observed size evolution.

Several physical processes have been suggested to account for the observed size evolution, e.g. mergers and AGN feedback.

(i) *Merger processes.* One potential process is dissipationless or 'dry' merging (without star formation; Bell et al. 2005; van Dokkum 2005). Due to the reduced amounts of available gas, 'dry' mergers are efficient in increasing the physical size of the stellar distribution but inefficient at causing new star formation. Another possible process is satellite or smooth envelope accretion (Naab et al. 2007), where accreted stars from minor/major mergers form an envelope around the compact remnant, the size of which increases smoothly with decreasing redshift. If this is the case, we might expect to find the compact core hidden within early-type galaxies in the local Universe. As we expect the merger rate to depend on environment, both these processes are environment dependent and may cause a growth in size over time. However, mergers also cause an increase in the stellar mass. Therefore, these processes could potentially only cause an evolution parallel to the mass–size relation as opposed to the observed size evolution at fixed stellar mass. Simple arguments based on the virial theorem suggest that for equal-mass mergers the radius increases linearly with mass, while for minor mergers the radius can increase as the square of the mass (Naab et al. 2009). Considering this expected evolution with respect to the local mass–size relation (Shen et al. 2003; see Fig. 1.8) shows that mergers could only cause evolution parallel to the mass–size relation for high-mass ($M_* > 10^{11}$) early-type galaxies (see e.g. van Dokkum et al. 2008). Consequently, merger events are a valid scenario for explaining the size evolution of galaxies.

(ii) *AGN feedback.* An alternative environmental-independent process originally proposed by Fan et al. (2008). They argue that for massive spheroidal galaxies ($M_* > 2 \times 10^{10}\,\mathrm{M}_\odot$), the observed size evolution is directly related to the rapid mass loss driven by AGN feedback, where the amount of cold gas removed from the central regions of the galaxy can be enough to drive a large increase in the galaxy size by a factor > 3. Lower mass galaxies would also experience a weaker but non-negligible size evolution mainly due to the mass loss powered by stellar winds and supernova explosions, which is in qualitative agreement with observations (Franx et al. 2008).

Hierarchical models of galaxy evolution predict that early-type galaxies of similar stellar mass in the cluster environment are older than those in the field due to e.g. accelerated galaxy evolution in dense environments (De Lucia et al. 2004). If clusters are regions of accelerated evolution one should expect an earlier growth in size for early-type cluster galaxies and a difference between galaxy sizes in the field and cluster environments. For late-type galaxies, disc truncations (van der Kruit 1979) may occur on top of this accelerated evolution and may also depend on environment.

Both early- and late-type galaxies follow stellar-mass–size relations (Shen et al. 2003; Barden et al. 2005; McIntosh et al. 2005; Graham & Worley 2008) with the physical size increasing as a function of stellar mass (see Section 1.3.1). Presently, the few studies that have explored the environmental dependence of the stellar-mass–size relation have been largely limited to small samples of massive ($M_* > 10^{10}\,\mathrm{M}_\odot$), early-type galaxies (Cimatti et al. 2008; Rettura et al. 2010). Recently, Cimatti

et al. (2008) found a potential trend using a small sample of 48 field and cluster, massive early-type galaxies from the $z = 1.237$ RDCS 1252.9-2927 cluster and the Great Observatories Origins Deep Survey (GOODS; Giavalisco et al. 2004) South Field. They find a hint that at fixed redshift $z \approx 1$, massive cluster early-type galaxies are preferentially located within the $z \sim 0$ mass–size relation compared to their counterparts in lower density environments. However, Rettura et al. (2010) come to a different conclusion and find no environmental dependence of the mass–size relation using a small sample of 45 field and cluster, massive early-type galaxies drawn from the same fields and redshift range as Cimatti et al. (2008); they conclude that early-type galaxies must undergo a similar size evolution in both environments in order to account for the typical sizes of early-type galaxies at lower redshifts.

For late-type galaxies, recent works (Guo et al. 2009; Weinmann et al. 2009) have compared the sizes of satellite and central, early- and late-type group galaxies from the Sloan Digital Sky Survey (SDSS; York et al. 2000). At fixed stellar mass, satellite galaxies lie in larger groups/clusters (i.e. denser environments) than central galaxies of similar stellar mass. Both Guo et al. (2009) and Weinmann et al. (2009) find no difference between the radii of satellite and central early-type galaxies; however, at low-masses ($M_* < 10^{10.75}\,\mathrm{M}_\odot$), late-type satellites have moderately smaller radii than similar mass late-type central galaxies. Similar results have also been reported by Kauffmann et al. (2004) and van den Bosch et al. (2008).

The aim of this study is to investigate whether the stellar-mass–size relation for different Hubble-type morphologies is affected by the galaxy environment by using larger, more statistically viable field and cluster samples than used in previous works.

The structure of this chapter is as follows. In Section 3.2, we give a brief description of our sample selection, describe the determination of our stellar masses (Section 3.2.1) and detail the estimation of our galaxy sizes (Section 3.2.2). Then in Section 3.3, we present our observed stellar-mass–size relations in different galaxy environments and for different Hubble-type morphologies. We provide a discussion of our results in Section 3.4 and finally draw our conclusions in Section 3.5.

3.2 Data and sample selection

For this study, we draw our galaxy samples from STAGES (Gray et al. 2009) using the field and cluster selection defined in Chapter 2 (Section 2.2). This selection results in a large, mass-limited ($M_* > 10^9\,\mathrm{M}_\odot$), visually classified sample of ~ 1500 galaxies from both the field and cluster environments. This sample is comprised of 655 field galaxies and 892 cluster galaxies, 203 of which are from the cluster core.

3.2.1 Measuring stellar mass

The stellar masses listed in the STAGES data catalogue and used in this work were originally estimated by Borch et al. (2006) for galaxies in COMBO-17. These estimates were derived from the SED fitting of the 17-band photometry using a template library derived from PEGASE (Fioc & Rocca-Volmerange 1997) population synthesis models and a Kroupa et al. (1993) stellar initial mass function (IMF). Random errors in stellar mass are estimated to be ~ 0.1 dex on a galaxy–galaxy basis in the majority of cases. Systematic errors (for the given population synthesis model and IMF) are argued to be ~ 0.1 dex for galaxies without ongoing or recent major starbursts; however, for galaxies with strong starbursts, the stellar mass could be overestimated by up to ~ 0.5 dex (see Borch et al. 2006, for further details).

The robustness of these stellar masses to aperture effects on the COMBO-17 SEDs was estimated by Wolf et al. (2009) using a few dozen galaxies. They find that the stellar masses of elliptical/S0 galaxies are reliable everywhere, but the stellar masses of spiral galaxies are only reliable for $\log M_*/\mathrm{M}_\odot < 11$. For spiral galaxies with $\log M_*/\mathrm{M}_\odot > 11$, the total observed $B-R$ colours were bluer than the aperture colours by ~ 0.3 mag, leading to an overestimation of the stellar mass by up to 0.5 dex. Consequently, in STAGES most spirals with $\log M_*/\mathrm{M}_\odot > 11$ actually have M_* just below $10^{11}\,\mathrm{M}_\odot$ (see Wolf et al. 2009, for further details).

3.2.2 Measuring galaxy size

For our measurement of galaxy size, we use the effective radius along the semimajor axis a_e of the galaxy's 2D surface brightness distribution. Historically, work in this field has used the circularized effective radius $r_\mathrm{e} = a_\mathrm{e}\sqrt{q}$, where q is the axial ratio of the galaxy (ratio of semiminor to semimajor effective radius), as the estimate of the galaxy size. However, the use of circularized quantities has no effect on the significance of the results of this work or our overall conclusions. Therefore, we choose to use the more physically meaningful a_e as our measurement of galaxy size.

Gray et al. (2009) use the data pipeline Galaxy Analysis over Large Areas: Parameter Assessment by GALFITting Objects from SExtractor (GALAPAGOS; Barden et al. 2012) to perform the extraction and Sérsic model fitting of source galaxies from the *HST*/ACS V-band imaging. This data pipeline uses the GALFIT code (Peng et al. 2002) to fit Sérsic (1968) radial surface brightness models to each ACS image.

GALFIT is a 2D fitting algorithm that determines a best-fitting model for the observed galaxy surface brightness distribution. 2D Sérsic (1968) $r^{1/n}$ models are convolved with the point spread function (PSF) of the original ACS (F606W) images and compared to the original surface brightness distribution. The best-fitting model is obtained by minimising the χ^2 of the fit using a Levenberg–Marquardt algorithm (Press et al. 1997). GALFIT determines several structural parameters for the galaxy including the effective radius along the semimajor axis a_e (in image pixels), axial ratio q and the Sérsic index n (a concentration parameter, see Section 1.3.2)[1].

We use simulations of the STAGES data set in order to determine the reliability of the GALFIT structural parameters. Gray et al. (2009) simulated over 10 million galaxy images with a range of properties analogous to the real STAGES data and subjected this data set to the same data pipeline. Using a similar approach to that described by Häussler et al. (2007), we determine the error in our GALFIT structural parameters by comparing the input and output structural parameters for a simulated sample selected by output magnitude and Sérsic index to match that of our galaxy samples. In this work, we use galaxy samples of different morphologies, environments and stellar mass ranges. For each sample, we obtain the R-magnitude range and use it to select an analogous sample from the simulations. The mean error in the GALFIT semimajor axis effective radius as determined from simulations is

$$\delta a_{\mathrm{e(galfit)}} = \frac{|a_{\mathrm{e(sim)}} - a_{\mathrm{e(galfit)}}|}{a_{\mathrm{e(sim)}}}, \tag{3.1}$$

and was found to increase slightly with decreasing stellar mass and be < 10 per cent in all cases (see Table 3.1).

[1]Note: for computational efficiency, in Gray et al. (2009) n is restricted to the range $0.2 < n < 8$. Consequently, galaxies with $n = 0.2$ or $n = 8$ represent constrained, unreliable GALFIT models.

Table 3.1. The R-magnitude range (Vega), mean error in GALFIT galaxy size as determined by simulations ($\mathrm{Size_{galfit}}$) and total error in galaxy size for the different morphologies, environments and stellar mass ranges used in this work.

$\log M_*/\mathrm{M}_\odot$ range	Field				Cluster	
	R range	$\mathrm{Size_{galfit}}$ error	Distance error	Total size error	R range	$\mathrm{Size_{galfit}}$ (Total size) error
All galaxies						
[9, 9.5]	18.7–23.3	8 %	17 %	18 % (±0.5 kpc)	19.2–23.0	7 % (±0.2 kpc)
[9.5, 10]	17.9–22.6	6 %	11 %	12 % (±0.4 kpc)	18.6–22.3	6 % (±0.2 kpc)
[10, 11.5]	15.5–21.1	5 %	7 %	8 % (±0.4 kpc)	16.3–20.1	5 % (±0.2 kpc)
Elliptical galaxies (E)						
[9, 9.5]	19.3–23.3	8 %	19 %	20 % (±0.3 kpc)	19.9–22.7	6 % (±0.1 kpc)
[9.5, 10]	20.3–22.0	5 %	15 %	15 % (±0.3 kpc)	19.6–22.3	6 % (±0.1 kpc)
[10, 11.5]	16.8–21.1	5 %	5 %	7 % (±0.3 kpc)	16.3–19.9	5 % (±0.2 kpc)
Lenticular galaxies (S0)						
[9, 9.5]	18.8–22.6	6 %	20 %	20 % (±0.4 kpc)	20.6–22.1	6 % (±0.1 kpc)
[9.5, 10]	18.8–21.9	5 %	14 %	14 % (±0.4 kpc)	19.7–21.0	5 % (±0.1 kpc)
[10, 11]	18.1–21.0	5 %	5 %	7 % (±0.2 kpc)	17.6–19.9	5 % (±0.2 kpc)
Spiral galaxies (Sp)						
[9, 9.5]	18.7–23.3	8 %	15 %	17 % (±0.5 kpc)	19.6–22.2	6 % (±0.2 kpc)
[9.5, 10]	17.9–22.6	6 %	10 %	11 % (±0.4 kpc)	18.6–20.9	5 % (±0.2 kpc)
[10, 11]	15.5–21.1	5 %	8 %	9 % (±0.4 kpc)	16.9–20.1	5 % (±0.3 kpc)

The semimajor axis effective radii a_e were transformed into intrinsic linear scales using the fixed cluster redshift ($z_{cl} = 0.167$) for our cluster galaxies and the original COMBO-17 photo-z estimate for our field galaxies. Therefore, the photo-z errors only propagate into the physical sizes of our field galaxies and not our cluster galaxies. Fixing the redshift of the cluster sample has little effect on the a_e distribution of our cluster galaxies ($\langle \Delta a_e \rangle < 0.12\,\mathrm{kpc}$; < 4 per cent) but eliminates the main source of a_e uncertainty (photo-z errors). However, not all cluster galaxies would be located at the central redshift of the cluster ($z_{cl} = 0.167$). From spectroscopy, we know that the STAGES multicluster system is at a distance of $\sim 600\,\mathrm{Mpc}$ but has a maximum '*apparent depth*' of 20 Mpc along the line of sight[2]. This introduces a maximum error of $\Delta a_e < 0.06\,\mathrm{kpc}$ (< 2 per cent) in the a_e of cluster galaxies associated with fixing the cluster sample at the cluster redshift. For our field galaxies, the mean error in a_e associated with the photo-z error (i.e. error in distance to galaxy) was calculated for each morphology and stellar mass range. The distance error is larger for lower stellar masses (see Table 3.1) and is < 20 per cent in all cases. We return to the effect of this error in Section 3.4.1. The total mean error in our galaxy sizes is < 20 per cent for our field sample and < 10 per cent for our cluster sample for all morphologies and stellar mass ranges used in this work.

3.2.3 Reliability of structural parameters

We remove all high-mass ($\log M_*/\mathrm{M}_\odot > 11$) spiral galaxies from our galaxy samples (one field and 14 cluster, five of which are from the cluster core) due to the unreliable nature of their measured stellar masses (Wolf et al. 2009; see Section 3.2.1).

We also remove galaxies with poor GALFIT model fits (i.e. those with Sérsic index $n \leq 0.2$ or $n \geq 6$) due to the potential unreliable nature of their structural parameters. Galaxies with $n = 0.2$ or $n = 8$ are unreliable due to constraints in the GALFIT fitting process (see Section 3.2.2). However, a visual inspection of the ACS images revealed that galaxies with $n \geq 6$ (mainly low surface brightness objects) also have potentially unreliable structural parameters (i.e. incorrect a_e) and the removal of these galaxies from our samples also removes many outliers from our stellar-mass–size relations. This Sérsic index cut removes 25 galaxies (~ 4 per cent) from the field sample (11 E, 1 S0, 10 Sp and 3 Irr) and 45 galaxies (~ 5 per cent) from the cluster sample (20 E, 13 S0, 10 Sp, 1 Irr and 1 compact object), eight galaxies of which are from the cluster core subsample (6 E, 1 S0 and 1 Sp). Some authors consider high Sérsic indices ($n > 6$) intrinsic for galaxies (e.g. Caon et al. 1993; Graham et al. 1996); however, this Sérsic cut only affects the significance of our results for high-mass ellipticals where it removes some of the brightest cluster galaxies (BCGs) that were biasing our results. Otherwise, this Sérsic cut has no effect on the overall significance of the results of this work or our conclusions. The five BCGs[3] in the STAGES multicluster system are also poorly fitted by GALFIT due to large amounts of intracluster light. However, two BCGs are removed by the Sérsic data cut and the remainder (three BCGs) are all high-mass ($\log M_*/\mathrm{M}_\odot > 11.5$) ellipticals which are not considered in the comparison of our stellar-mass–size relations (see Section 3.3).

[2]Note: this 'apparent depth' is due to the fingers-of-god effect on the redshifts – an elongation of the cluster in redshift space along the line of sight. This effect is caused by a Doppler shift associated with the peculiar velocities of galaxies in the cluster.

[3]Five BCGs are associated with the STAGES field: one for each of the clusters, A901a/b and the SW group (see Fig. 2.1), and two for the A902 cluster (possibly due to the superposition of multiple groups along the line of sight; Rhodes et al., in preparation).

This leaves a final sample of 629 field galaxies and 833 cluster galaxies, 190 of which are from the cluster core (see Table. 3.2).

Table 3.2. The visual morphologies for our final field and cluster samples and our cluster core subsample obtained from the STAGES morphological catalogue (Gray et al., in preparation).

	Elliptical galaxy	Lenticular galaxy	Spiral galaxy	Irregular galaxy	Compact object	Star	?
Field	89	59	307	136	12	0	26
Cluster	172	203	359	85	2	0	12
Core	58	66	53	10	0	0	3

3.3 The stellar-mass–size relation in STAGES

In this section, we discuss the stellar-mass–size relations for our sample of field and cluster galaxies and our cluster subsample of cluster core galaxies (independent of the galaxy morphology). We compare the stellar-mass–size relations between the environments of the field and cluster, and the field and cluster core (see Fig. 3.1).

In order to assess the effect of the galaxy environment on galaxy size $a_{\rm e}$, we split the field and cluster samples and the cluster core subsample into three stellar mass bins; $\log M_*/{\rm M}_\odot \in [9, 9.5], [9.5, 10]$ and $[10, 11.5]$. In our comparisons, we do not consider $\log M_*/{\rm M}_\odot > 11.5$ (consisting of five cluster core ellipticals) because there are no analogous field galaxies with $M_* > 10^{11.5}\,{\rm M}_\odot$ to compare to these cluster galaxies. We then calculate the mean semimajor axis effective radius $\overline{a}_{\rm e}$ with associated 1σ uncertainty in the mean for each stellar mass bin and environment (see Table 3.3). The values of $\overline{a}_{\rm e}$ with 1σ error bars are overplotted on our stellar-mass–size relations (see Fig. 3.1).

For high-mass ($\log M_*/{\rm M}_\odot > 10$) galaxies, we find no significant difference between the value of $\overline{a}_{\rm e}$ for the field and cluster/core samples. However, at lower stellar masses ($\log M_*/{\rm M}_\odot < 10$), we find that $\overline{a}_{\rm e}$ is significantly smaller in the cluster/core than in the field.

In order to test the significance of these results, we construct $a_{\rm e}$ cumulative distribution functions (CDFs; see Fig. 3.2) for our mass-selected galaxy subsamples and perform Kolmogorov–Smirnov (K–S) tests between corresponding mass-selected subsamples from the field and the cluster environments. We also perform analogous K–S tests in a comparison of the field and cluster core environments. These K–S tests are used in order to obtain the probability that the field and cluster $p_{\rm (field/cluster)}$, and the field and cluster core $p_{\rm (field/core)}$ samples are *not* drawn from the same continuous $a_{\rm e}$ distributions. The results for each stellar mass bin are shown in Table 3.3.

In this study, we only consider an environmental effect on the stellar-mass–size relation to be significant if K–S tests yield a 2σ level probability ($p \geq 0.95$) for $p_{\rm (field/cluster)}$ or $p_{\rm (field/core)}$. For high-mass galaxies ($\log M_*/{\rm M}_\odot \in [10, 11.5]$), $p_{\rm (field/cluster)}$ is below the 2σ level, while $p_{\rm (field/core)}$ is at the 2σ level. However, for intermediate-/low-mass galaxies ($\log M_*/{\rm M}_\odot \in [9, 9.5], [9.5, 10]$), both $p_{\rm (field/cluster)}$ and $p_{\rm (field/core)}$ are above the 3σ level. These high-significance results imply that at stellar masses $M_* < 10^{10}\,{\rm M}_\odot$, our field and cluster samples are *not* drawn from the

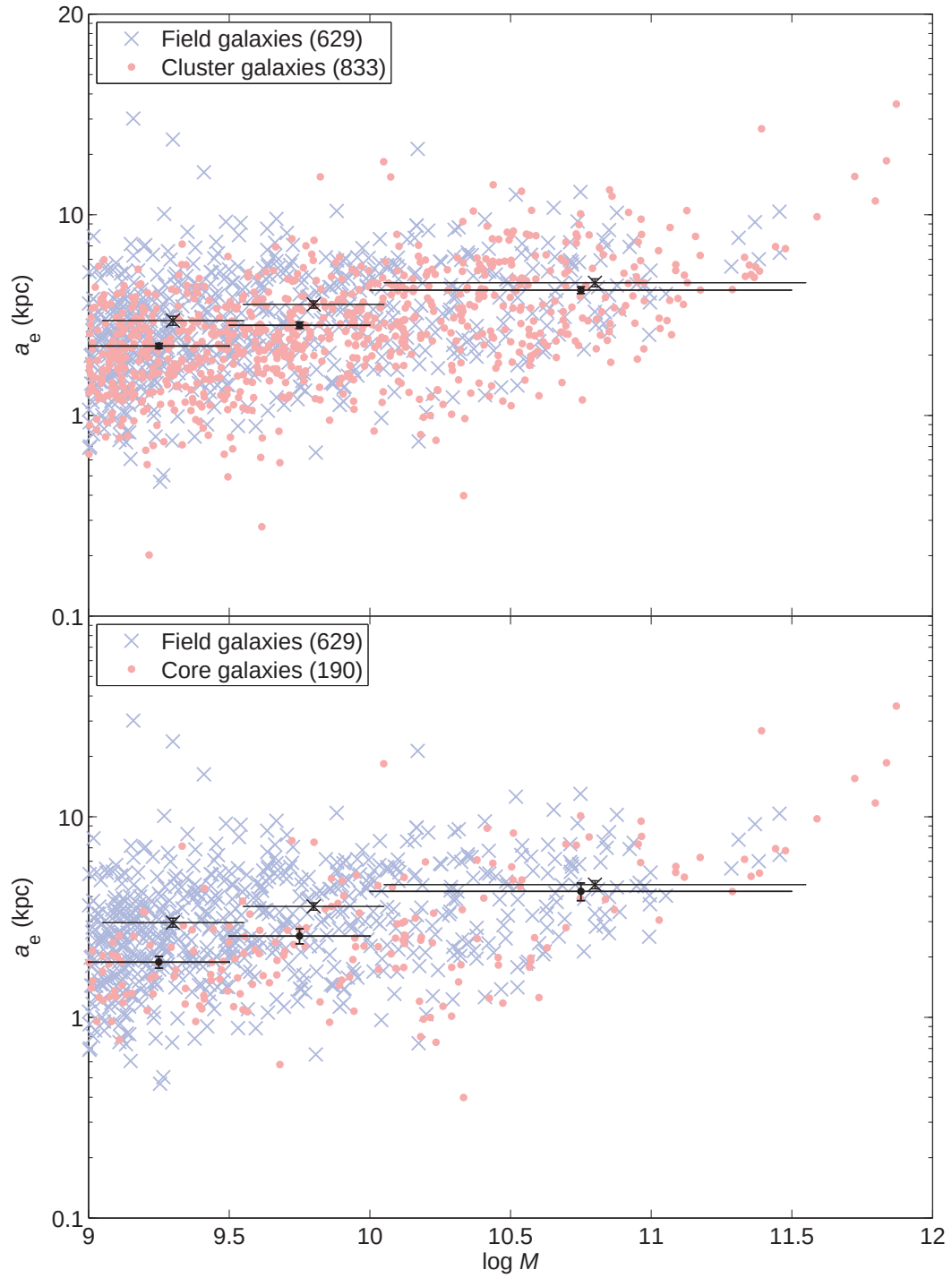

Figure 3.1. The stellar-mass–size relation in different environments. Top: a comparison of the stellar-mass–size relation in the field (blue crosses) and cluster (red points) environment. Bottom: a comparison of the stellar-mass-size relation in the field (blue crosses) and cluster *core* (red points) environment. For each stellar mass bin (represented by the x-axis error bars), we overplot on the observed distributions the mean semimajor axis effective radius $\overline{a}_e$ in the field and cluster/core. The a_e error bars are the uncertainty (1σ) in the mean. For display purposes, the field $\overline{a}_e$ values are displaced in stellar mass by +0.05 dex. The mean relative size error is < 20 per cent and uncertainties in the stellar mass are ~ 0.1 dex. Respective sample sizes are shown in the legends and $M = M_*/\mathrm{M}_\odot$.

Table 3.3. The environmental dependence of the stellar-mass–size relation. The mean semimajor axis effective radii $\overline{a}_{\rm e}$ ($\pm 1\sigma$) of galaxies in different stellar mass ranges for the field, cluster and cluster core environments, and the K–S test results: the probability that the field and cluster $p_{\rm (field/cluster)}$, and field and cluster core $p_{\rm (field/core)}$ samples are *not* drawn from the same continuous $a_{\rm e}$ distributions. We find some evidence for an environmental effect on $\overline{a}_{\rm e}$ and environmental dependence of the stellar-mass–size relation at intermediate/low masses ($M_* < 10^{10}\,{\rm M}_\odot$).

$\log M_*/{\rm M}_\odot$ range	Field $\overline{a}_{\rm e}$ (kpc)	Cluster $\overline{a}_{\rm e}$ (kpc)	Core $\overline{a}_{\rm e}$ (kpc)	$p_{\rm (field/cluster)}$	$p_{\rm (field/core)}$
[9, 9.5]	2.97 ($\pm$0.15)	2.22 ($\pm$0.07)	1.89 ($\pm$0.13)	0.999 925	0.999 997
[9.5, 10]	3.57 ($\pm$0.15)	2.82 ($\pm$0.10)	2.54 ($\pm$0.22)	0.999 995	0.999 266
[10, 11.5]	4.59 ($\pm$0.21)	4.21 ($\pm$0.16)	4.25 ($\pm$0.43)	0.879 762	0.958 101

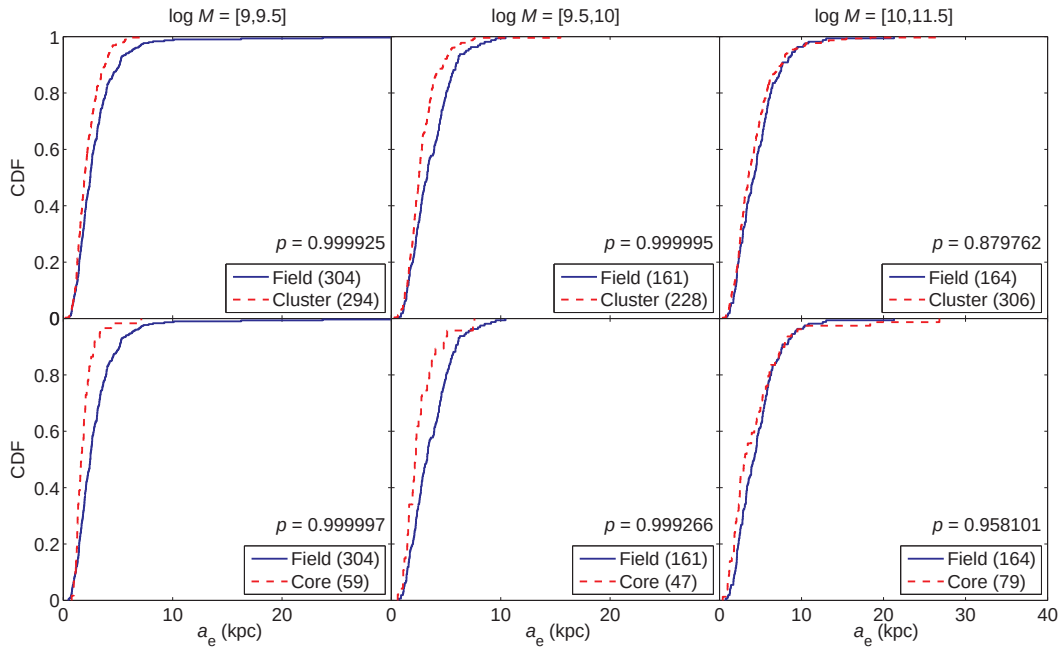

Figure 3.2. The a_e CDFs in different environments. Top row: a comparison of the a_e CDFs in the field (blue line) and cluster (red dashed line) for different stellar mass ranges. Bottom row: a similar comparison between the field (blue line) and cluster *core* (red dashed line). The probability p that compared samples are *not* drawn from the same continuous a_e distributions is shown in the bottom right of each plot. Respective sample sizes are shown in the legends and $M = M_*/\mathrm{M}_\odot$.

same continuous a_e distributions. Consequently, these results suggest that at stellar masses $M_* < 10^{10}\,\mathrm{M}_\odot$ the stellar-mass–size relation is dependent on the galaxy environment with galaxy sizes being significantly smaller in the cluster/core than in the field.

However, it is important to remember that early-type galaxies (e.g. ellipticals) tend to have more compact light distributions compared to late-type galaxies (e.g. spirals; see Section 1.3.2). Consequently, at fixed stellar mass early-type galaxies tend to have smaller a_e compared to late-type galaxies. Since early-type galaxies are expected to be more prevalent in the cluster environment (Dressler 1980), it is possible that the morphological mix of our field and cluster/core samples is causing a bias in our results. The distribution of visual morphologies for the different environments and stellar mass ranges used in this study are presented in Fig. 3.3.

For all stellar masses ($10^9 < M_* < 10^{11.5}\,\mathrm{M}_\odot$), the fraction of early-types (ellipticals and S0s) is considerably higher in the cluster than the field. Additionally, for stellar masses $M_* > 10^{10}\,\mathrm{M}_\odot$ the fraction of late-types (spirals) is considerably higher in the field than the core. Consequently, it seems that the morphological mix of our field and cluster/core samples could be the origin of the high significance we observe for an effect of the environment on the stellar-mass–size relation.

Therefore, in order to perform a fair comparison of our stellar-mass–size relations in different environments it is necessary to separate our galaxy samples by morphology. We limit our analysis to the main Hubble types (elliptical, S0 and spiral) and obtain a sample of 455 field galaxies (89 E, 59 S0, 307 Sp) and 734 cluster galaxies (172 E, 203 S0, 359 Sp), 177 of which are from the cluster core (58 E, 66 S0, 53 Sp). Irregular galaxies and other objects are not considered any further in this study.

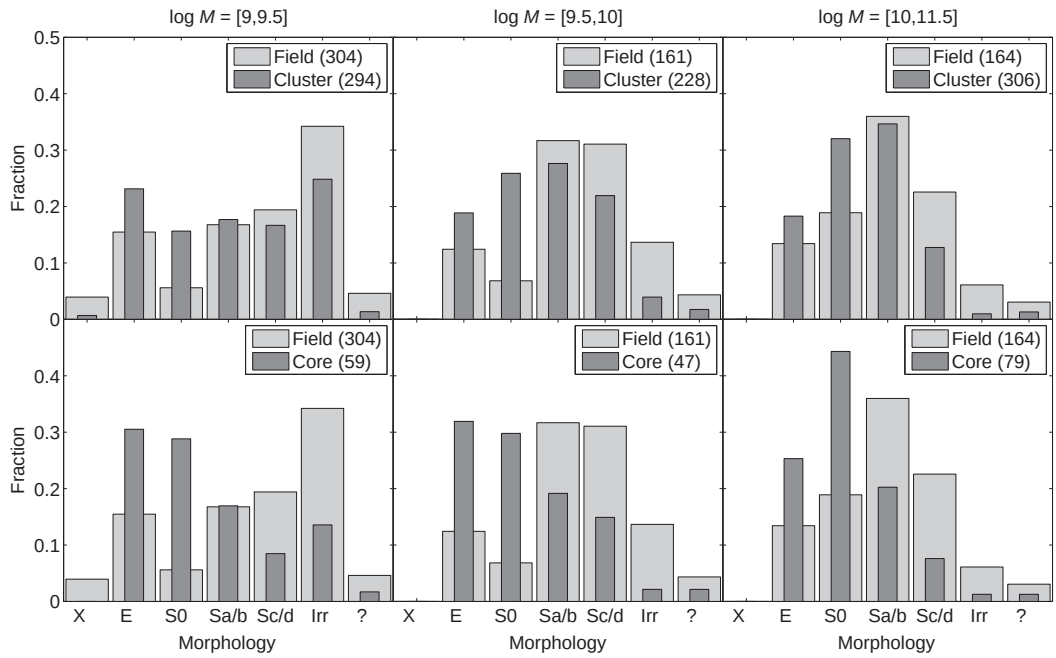

Figure 3.3. The distribution of visual morphologies for different environments and stellar mass ranges. Top row: a comparison of the morphology distribution in the field (light grey) and cluster (dark grey) environment for different stellar mass ranges. Bottom row: a similar comparison between the field (light grey) and cluster *core* (dark grey). The morphology label 'X' represents the Compact objects category. Respective sample sizes are shown in the legends and $M = M_*/\mathrm{M}_\odot$.

3.3.1 The stellar-mass–size relation by Hubble-type morphology

In this section, we discuss the stellar-mass–size relations for different Hubble-type morphologies in different galaxy environments. For the three main Hubble types (ellipticals, S0s and spirals), we compare the stellar-mass–size relations between the field and cluster, and the field and cluster core (see Fig. 3.4).

For each Hubble type, the field and cluster samples and cluster core subsample are split into three stellar mass ($\log M_*/\mathrm{M}_\odot$) bins. The two low-mass bins, $[9, 9.5]$ and $[9.5, 10]$, are the same for all Hubble types but the high-mass bin varies. We use a high-mass bin of $[10, 11]$ for spiral and lenticular galaxies but extended it to $[10, 11.5]$ for elliptical galaxies. For spiral galaxies, we do not consider $\log M_*/\mathrm{M}_\odot > 11$ due to unreliable stellar masses (Wolf et al. 2009; see Section 3.2.1). For lenticular galaxies, we do not consider $\log M_*/\mathrm{M}_\odot > 11$ due to there being no field lenticulars with $M_* > 10^{11}\mathrm{M}_\odot$ to compare to cluster lenticulars. We remove 10 cluster S0s, five of which are from the cluster core, with $M_* > 10^{11}\mathrm{M}_\odot$ from our stellar-mass–size relations. For elliptical galaxies, we do not consider $\log M_*/\mathrm{M}_\odot > 11.5$ due to there being no field ellipticals with $M_* > 10^{11.5}\mathrm{M}_\odot$ to compare to cluster ellipticals. We remove five cluster ellipticals (including three BCGs), all from the cluster core, with $M_* > 10^{11.5}\mathrm{M}_\odot$ from our stellar-mass–size relations.

For each Hubble type and environment, we calculate the mean semimajor axis effective radius $\overline{a}_\mathrm{e}$ with associated 1σ uncertainty in the mean for each stellar mass bin (see Table 3.4). The values of $\overline{a}_\mathrm{e}$ with 1σ error bars are overplotted on our stellar-mass–size relations (see Fig. 3.4). For elliptical and lenticular galaxies, we find no significant difference between the values of $\overline{a}_\mathrm{e}$ for the field and cluster/core samples

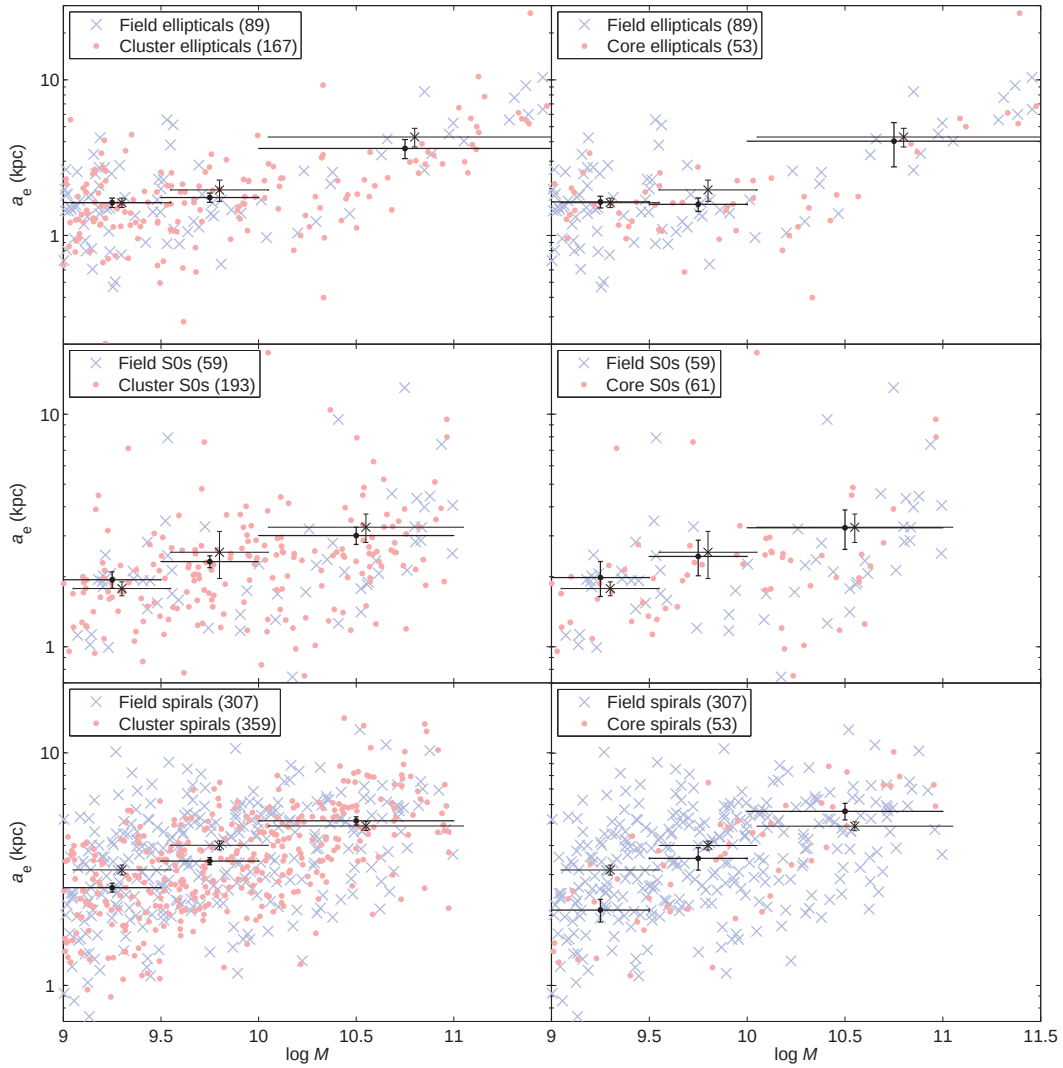

Figure 3.4. The stellar-mass–size relations for, top row: elliptical galaxies, middle row: lenticular galaxies (S0) and bottom row: spiral galaxies. Left-hand panels: a comparison of the stellar-mass–size relation in the environments of the field (blue crosses) and the cluster (red points). Right-hand panels: a comparison of the stellar-mass–size relation in the environments of the field (blue crosses) and the cluster *core* (red points). For each stellar mass bin (represented by the x-axis error bars), we overplot on the observed distributions the mean semimajor axis effective radius $\overline{a}_e$ in the field and the cluster/core. The $\overline{a}_e$ error bars are the uncertainty (1σ) in the mean. For display purposes, the field $\overline{a}_e$ values are displaced in stellar mass by +0.05 dex. There are no spiral or lenticular galaxies with $\log M > 11$ as these have explicitly been removed from our stellar-mass–size relations (see Section 3.3.1). We observe no significant difference between the stellar-mass–size relations in each environment for each morphological type, except for intermediate-/low-mass spirals. For stellar masses $\log M < 10$, we find that the cluster spirals have values of $\overline{a}_e$ significantly smaller than the $\overline{a}_e$ for field spirals of the same mass. We also find that low-mass spirals ($\log M < 9.5$) in the core have $\overline{a}_e$ significantly smaller than similar galaxies in the field. The mean relative size error is < 20 per cent and uncertainties in the stellar mass are ~ 0.1 dex. Respective sample sizes are shown in the legends and $M = M_*/\mathrm{M}_\odot$.

Table 3.4. The environmental dependence of the stellar-mass–size relation for different Hubble types. The mean semimajor axis effective radii $\overline{a}_{\rm e}$ ($\pm 1\sigma$) of our elliptical, lenticular and spiral galaxies in different stellar mass ranges for the field, cluster and cluster core environments, and the K–S test results for elliptical, lenticular and spiral galaxies: the probability that the field and cluster $p_{\rm (field/cluster)}$, and field and cluster core $p_{\rm (field/core)}$ samples are *not* drawn from the same continuous $a_{\rm e}$ distributions. We find no environmental effect on $\overline{a}_{\rm e}$ or environmental dependence of the stellar-mass–size relation for all morphological types, except for intermediate-/low-mass spirals ($M_* < 10^{10}\,{\rm M}_\odot$).

$\log M_*/{\rm M}_\odot$ range	Field $\overline{a}_{\rm e}$ (kpc)	Cluster $\overline{a}_{\rm e}$ (kpc)	Core $\overline{a}_{\rm e}$ (kpc)	$p_{\rm (field/cluster)}$	$p_{\rm (field/core)}$
Elliptical galaxies (E)					
[9, 9.5]	1.62 ($\pm$0.11)	1.63 ($\pm$0.11)	1.64 ($\pm$0.14)	0.745	0.578
[9.5, 10]	1.96 ($\pm$0.31)	1.75 ($\pm$0.12)	1.58 ($\pm$0.16)	0.554	0.159
[10, 11.5]	4.29 ($\pm$0.59)	3.62 ($\pm$0.51)	4.03 ($\pm$1.28)	0.825	0.830
Lenticular galaxies (S0)					
[9, 9.5]	1.78 ($\pm$0.12)	1.94 ($\pm$0.16)	1.99 ($\pm$0.34)	0.688	0.613
[9.5, 10]	2.55 ($\pm$0.59)	2.33 ($\pm$0.14)	2.45 ($\pm$0.43)	0.405	0.268
[10, 11]	3.27 ($\pm$0.46)	3.01 ($\pm$0.25)	3.25 ($\pm$0.63)	0.136	0.255
Spiral galaxies (Sp)					
[9, 9.5]	3.14 ($\pm$0.16)	2.63 ($\pm$0.12)	2.11 ($\pm$0.24)	0.775	0.967
[9.5, 10]	4.00 ($\pm$0.18)	3.42 ($\pm$0.12)	3.52 ($\pm$0.39)	0.998	0.566
[10, 11]	4.85 ($\pm$0.21)	5.10 ($\pm$0.21)	5.61 ($\pm$0.46)	0.084	0.733

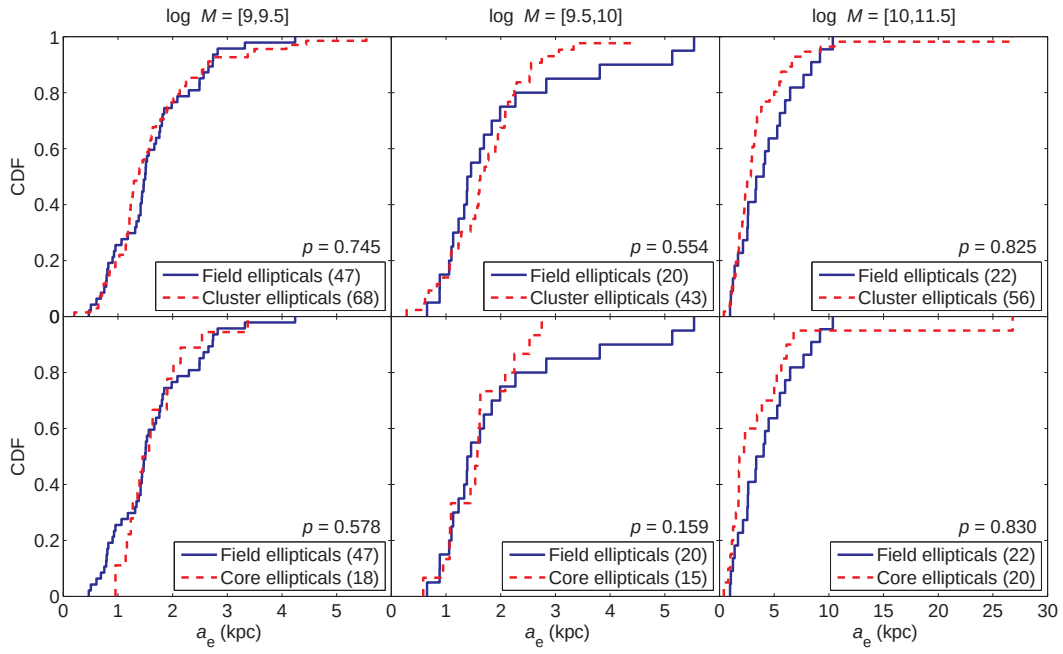

Figure 3.5. The $a_{\rm e}$ CDFs for our elliptical galaxies. Top row: a comparison of the CDFs for elliptical galaxies in the field (blue line) and the cluster (red dashed line) for different stellar mass ranges. Bottom row: a similar comparison for elliptical galaxies in the field (blue line) and cluster *core* (red dashed line). The probability p that compared samples are *not* drawn from the same continuous $a_{\rm e}$ distributions is shown in the bottom right of each plot. Respective sample sizes are shown in the legends and $M = M_*/{\rm M}_\odot$. We find no significant difference between the CDFs in each environment and no evidence to suggest our elliptical galaxies are *not* drawn from the same continuous $a_{\rm e}$ distributions.

in all mass bins. For high-mass spirals ($\log M_*/{\rm M}_\odot > 10$), we find no significant difference between the value of $\overline{a}_{\rm e}$ for the field and cluster samples; however, we find that core spirals have $\overline{a}_{\rm e}$ slightly larger than field spirals. For lower stellar masses ($\log M_*/{\rm M}_\odot < 10$), we find that cluster spirals have values of $\overline{a}_{\rm e}$ significantly smaller than the $\overline{a}_{\rm e}$ for field spirals of the same mass. We also find that low-mass spirals ($\log M_*/{\rm M}_\odot < 9.5$) in the core have $\overline{a}_{\rm e}$ significantly smaller than similar galaxies in the field (see Table 3.4). Using the median $a_{\rm e}$ instead of the mean $a_{\rm e}$ only removes the difference in average size between the low-mass ($\log M_*/{\rm M}_\odot < 9.5$) spirals of the cluster and the field. Otherwise, these results are robust to the use of median $a_{\rm e}$.

In order to test the significance of these results, for each Hubble type and environment we construct $a_{\rm e}$ CDFs (see Figs 3.5–3.7) and perform K–S tests between corresponding mass-selected subsamples from the field and the cluster, and field and cluster core. The results per mass bin for each Hubble type are shown in Table 3.4.

For elliptical and lenticular galaxies, the probability that the field and cluster $p_{\rm (field/cluster)}$, and the field and cluster core $p_{\rm (field/core)}$ samples are *not* drawn from the same continuous $a_{\rm e}$ distributions is below the 2σ level in all mass bins. Therefore, we find no evidence to suggest an environmental dependence on the stellar-mass–size relation for these galaxies. This result is in qualitative agreement with the work of Rettura et al. (2010) who came to the same conclusion at higher redshift ($z \sim 1$) using a much smaller sample of 45 cluster and field early-type galaxies.

For high-mass spiral galaxies ($\log M_*/{\rm M}_\odot \in [10, 11]$), both the probabilities $p_{\rm (field/cluster)}$ and $p_{\rm (field/core)}$ are below the 2σ level. Therefore, we find no evidence to

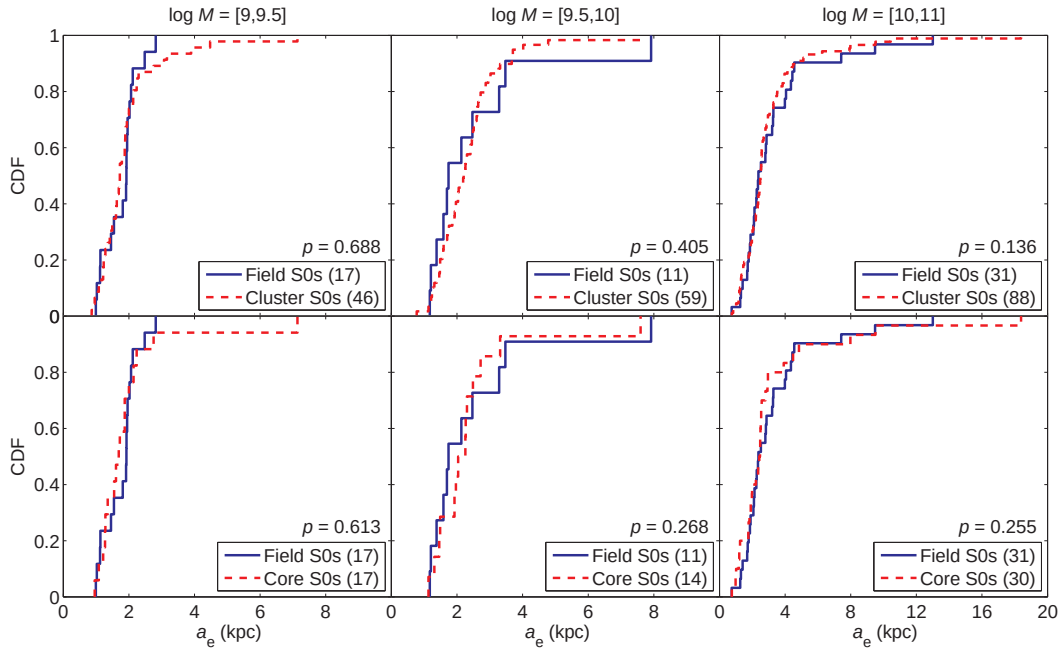

Figure 3.6. The a_e CDFs for our S0 galaxies. Top row: a comparison of the CDFs for S0 galaxies in the field (blue line) and the cluster (red dashed line) for different stellar mass ranges. Bottom row: a similar comparison for S0 galaxies in the field (blue line) and cluster *core* (red dashed line). The probability p that compared samples are *not* drawn from the same continuous a_e distributions is shown in the bottom right of each plot. Respective sample sizes are shown in the legends and $M = M_*/\mathrm{M}_\odot$. We find no significant difference between the CDFs in each environment and no evidence to suggest our S0 galaxies are *not* drawn from the same continuous a_e distributions.

suggest an environmental dependence on the stellar-mass–size relation for high-mass spirals. However, for intermediate- and low-mass spirals we find evidence for a potential environmental dependence on the stellar-mass–size relation. For intermediate-mass spirals ($\log M_*/\mathrm{M}_\odot \in [9.5, 10]$), the probability $p_{(\mathrm{field/core})}$ is below the 1σ level; however, we find a significant probability (at the 3σ level) for $p_{(\mathrm{field/cluster})}$. This is in agreement with the difference seen between $\overline{a}_e$ for intermediate-mass spirals in the field and cluster environments (see Fig. 3.4) where we find a larger $\overline{a}_e$ for field spirals. For low-mass spirals ($\log M_*/\mathrm{M}_\odot \in [9, 9.5]$), the probability $p_{(\mathrm{field/cluster})}$ is below the 2σ level; however, $p_{(\mathrm{field/core})}$ is at the 2σ level. Again, this is in agreement with the difference seen between $\overline{a}_e$ for low-mass spirals in the field and core environments (see Fig. 3.4) where we find a larger $\overline{a}_e$ for field spirals. Therefore, there appears to be a population of large-a_e, intermediate-/low-mass spirals in the field that is largely absent from the cluster and cluster core environments.

3.4 Discussion

The main result of this work is the lack of any environmental dependence for the majority of the galaxy types studied. The significance observed for intermediate-/low-mass spirals is inconclusive and requires further verification by similar studies in other fields. In this section, we discuss some of the considerations for the reliability of our results and for establishing the stellar-mass–size relation at low stellar masses.

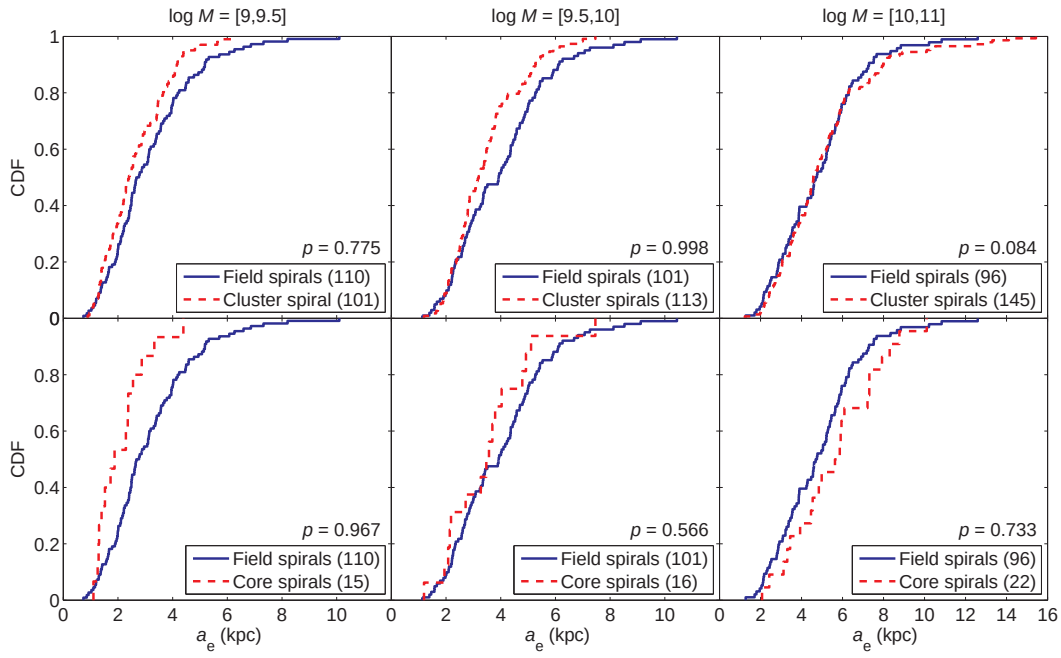

Figure 3.7. The $a_{\rm e}$ CDFs for our spiral galaxies. Top row: a comparison of the CDFs for spiral galaxies in the field (blue line) and the cluster (red dashed line) for different stellar mass ranges. Bottom row: a similar comparison for spiral galaxies in the field (blue line) and cluster *core* (red dashed line). The probability p that compared samples are *not* drawn from the same continuous $a_{\rm e}$ distributions is shown in the bottom right of each plot. Respective sample sizes are shown in the legends and $M = M_*/{\rm M}_\odot$. We find no significant difference between the CDFs in each environment except for intermediate-mass spirals ($\log M \in [9.5, 10]$) in the comparison of the field and cluster, and for low-mass spirals ($\log M \in [9, 9.5]$) in the comparison of the field and cluster *core*. The high probability p ($> 2\sigma$ level) in these comparisons suggests that the respective samples are *not* drawn from the same continuous $a_{\rm e}$ distributions.

The majority of our field galaxies have redshift $z \sim 0.24$ while our cluster galaxies have $z = 0.167$. Using the fits of Buitrago et al. (2008), we evaluated the expected size evolution between the mean redshifts of our field and cluster samples to be ~ 10 per cent (~ 5 per cent for discs and ~ 10 per cent for spheroids). Presently, size evolution has only been characterized for the most massive galaxies ($M_* > 10^{11}\,{\rm M}_\odot$; Trujillo et al. 2007; Buitrago et al. 2008). Consequently, these fits do not hold for our galaxy samples (mostly with $M_* < 10^{11}\,{\rm M}_\odot$), but we use them to give an idea of the degree of expected evolution. Therefore, neglecting any environmental effects, on average our field galaxies are expected to be ~ 10 per cent smaller than our cluster galaxies. However, we observe the opposite trend for our spiral galaxies at intermediate/low stellar masses.

The evidence we find for an environmental dependence on the stellar-mass–size relation for intermediate-/low-mass spirals does not however appear in a consistent way. The significance of $p_{\rm (field/cluster)}$ is at the 3σ level for intermediate masses ($\log M_*/{\rm M}_\odot \in [9.5, 10]$), but only just above the 1σ level for low masses ($\log M_*/{\rm M}_\odot \in [9, 9.5]$). Either the significance at intermediate masses is not robust and there is no environmental dependence or the significance at low masses is being masked by some effects (e.g. photometric redshift errors or contaminations). We explore the impact of these effects on our results in the following sections.

3.4.1 The effect of photometric redshift errors

In the determination of our physical galaxy sizes $a_{\rm e}$, we have used the cluster redshift ($z_{\rm cl} = 0.167$) for our cluster samples but used the original COMBO-17 redshift estimates for our field sample. Therefore, the errors in the COMBO-17 photometric redshifts (δz) propagate into the physical size measurements of our field galaxies. The relative error in $a_{\rm e}$ associated with this photo-z error is

$$\frac{\delta a_{\rm e}}{a_{\rm e}} = \frac{\max|D(z) - D(z \pm \delta z)|}{D(z)}, \tag{3.2}$$

where D is the distance to the galaxy. The relative error $\delta a_{\rm e}/a_{\rm e}$ (i.e. the error in the distance to the galaxy δD) is related to both the R-magnitude and stellar mass of our field galaxies (see Fig. 3.8). The errors can reach up to ~ 50 per cent for individual galaxies and generally increase towards fainter R-magnitudes and with decreasing stellar mass. We therefore need to be careful that large $\delta a_{\rm e}/a_{\rm e}$ galaxies are not affecting our analysis, especially at intermediate/low stellar masses where we find a difference in $\overline{a}_{\rm e}$ between the field and cluster/core spirals.

The individual photo-z errors (δz) from COMBO-17 are estimated errors based on the shape of the redshift probability distribution function (zPDF) for a galaxy. Consequently, they can sometimes underestimate the true error when the zPDF is based on an incomplete set of comparison templates (i.e. the real galaxy spectrum is an unusual one). When the zPDF is wide and the estimated error is large, it really means that redshift ambiguities are present and that the measured photometric redshift is potentially unreliable. In order to assess the effect of large $\delta a_{\rm e}/a_{\rm e}$ galaxies on our stellar-mass–size relations and analysis, we remove all galaxies from our field sample with $\delta a_{\rm e}/a_{\rm e} > 10$ per cent (see Figs 3.8 and 3.9).

For elliptical galaxies, there was no effect on the level of significance of the K–S test results, $p_{\rm (field/cluster)}$ and $p_{\rm (field/core)}$, in each mass bin. In no cases did the level of significance go above the 2σ level. Therefore, our conclusion that there is no evidence to suggest an environmental dependence on the stellar-mass–size relation for elliptical galaxies is robust with respect to large $\delta a_{\rm e}/a_{\rm e}$ galaxies.

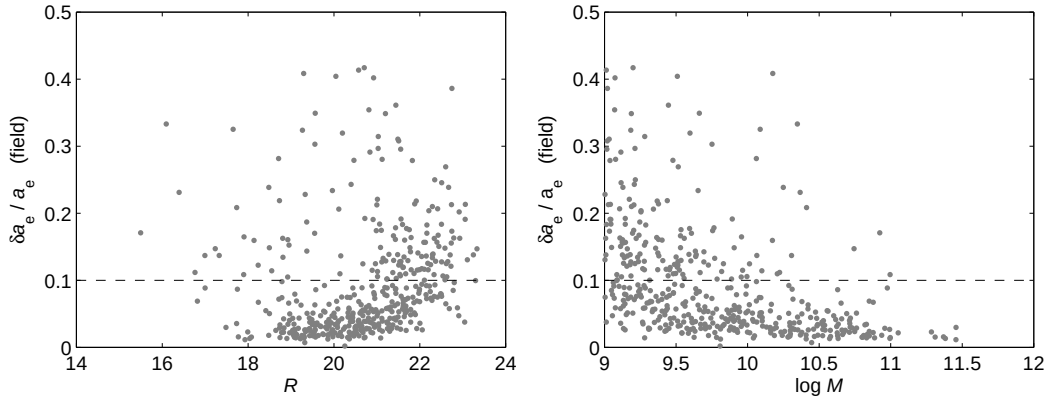

Figure 3.8. Left-hand panel: the relative error in the physical size $a_{\rm e}$ associated with the photo-z error $\delta a_{\rm e}/a_{\rm e}$ (i.e. error in distance to galaxy) for our field sample versus R-band magnitude (Vega) showing that the error increases towards fainter magnitudes due to the increasing photo-z error. Right-hand panel: $\delta a_{\rm e}/a_{\rm e}$ for our field sample versus stellar mass showing that the error increases with decreasing stellar mass ($M = M_*/{\rm M}_\odot$). To test the robustness of our results, we discard all high error objects (> 10 per cent; above dashed line) from our field sample and assess the effect on our K–S test results.

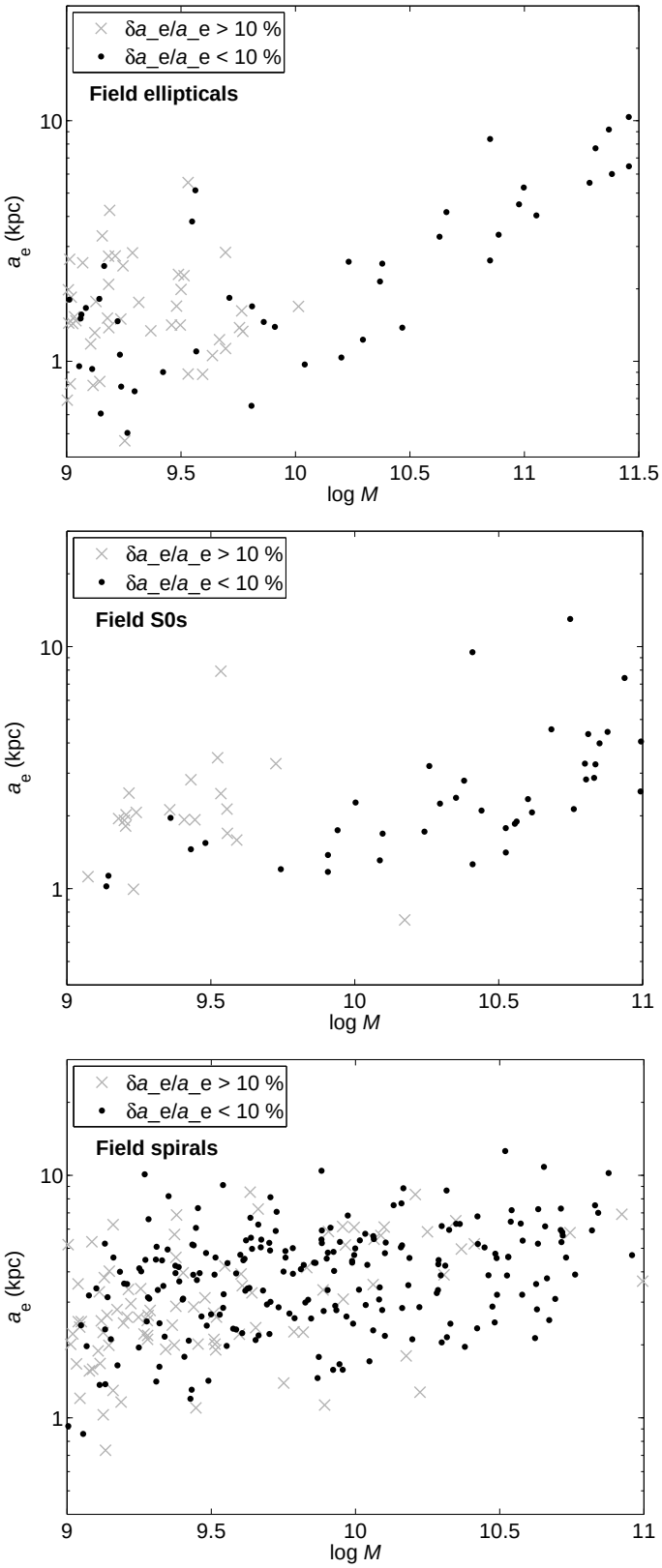

Figure 3.9. Testing the effects of large $\delta a_{\rm e}/a_{\rm e}$ (distance) errors. The stellar-mass–size relations for our field samples showing galaxies with a relative error $\delta a_{\rm e}/a_{\rm e} > 10$ per cent (grey) and $\delta a_{\rm e}/a_{\rm e} < 10$ per cent (black) for elliptical (top), lenticular (centre) and spiral (bottom) galaxies.

For lenticular galaxies, there was no effect on the level of significance of the K–S test results for high and low masses ($\log M_*/\mathrm{M}_\odot \in [9, 9.5], [10, 11]$) with $p_{(\mathrm{field/cluster})}$ and $p_{(\mathrm{field/core})}$ remaining below the 2σ significance level. However, at intermediate masses ($\log M_*/\mathrm{M}_\odot \in [9.5, 10]$) both $p_{(\mathrm{field/cluster})}$ and $p_{(\mathrm{field/core})}$ increase in significance to the 2σ level. In this case, the removal of the large $\delta a_\mathrm{e}/a_\mathrm{e}$ galaxies has introduced a selection effect (see Fig. 3.9) causing a bias towards smaller sizes and also dramatically reduced the number of field lenticulars in this mass bin. Therefore, we do not trust the high significance in this case and our conclusion that there is no evidence to suggest an environmental dependence on the stellar-mass–size relation for these galaxies is robust with respect to large $\delta a_\mathrm{e}/a_\mathrm{e}$ galaxies.

For high-mass spirals ($\log M_*/\mathrm{M}_\odot \in [10, 11]$), the significance is also robust with respect to the removal of the large $\delta a_\mathrm{e}/a_\mathrm{e}$ galaxies and is below the 2σ level for both $p_{(\mathrm{field/cluster})}$ and $p_{(\mathrm{field/core})}$. For intermediate-mass spirals ($\log M_*/\mathrm{M}_\odot \in [9.5, 10]$), the high significance of $p_{(\mathrm{field/cluster})}$ increases to above the 3σ level; however, $p_{(\mathrm{field/core})}$ remains below the 2σ level, possibly due to low number statistics. For low-mass spirals ($\log M_*/\mathrm{M}_\odot \in [9, 9.5]$), the high significance of $p_{(\mathrm{field/core})}$ remains at the 2σ level, and the significance of $p_{(\mathrm{field/cluster})}$ increases from below the 2σ level to the 3σ level, indicating that large $\delta a_\mathrm{e}/a_\mathrm{e}$ errors could be masking the effect in this region. Therefore, our conclusion that the field and cluster/core samples are potentially *not* drawn from the same continuous a_e distributions at intermediate/low masses is robust with respect to large $\delta a_\mathrm{e}/a_\mathrm{e}$ errors.

3.4.2 The effect of a photometric redshift bias

At present, photometric redshifts on the STAGES (A901/2) field have only been assessed for quality by comparison to spectroscopic redshifts at bright magnitudes. Wolf et al. (2004) find for a sample of 404 bright galaxies with $R < 20$ and $z \in [0, 0.3]$, 351 of which were from the A901/2 field, that 77 per cent had photo-z deviations of $|\delta_z/(1+z)| < 0.01$, and only 1 per cent had deviations $|\delta_z/(1+z)| > 0.04$ from the true redshift.

There are currently no spectroscopic redshifts on the A901/2 field for comparison at faint magnitudes. However, a faint spectroscopic data set does exist on the COMBO-17 *Chandra* Deep Field-South (CDFS) from the VIMOS Very Large Telescope (VLT) Deep Survey (VVDS; Le Fèvre et al. 2004). Hildebrandt et al. (2008) use a sample of 420 high-quality spectroscopic redshifts that are reasonably complete to $R_\mathrm{aperture} < 23$ and find a 1σ scatter of 0.018 in $\delta z/(1+z)$ and also a mean bias of -0.011.

The mean redshift bias is dependent on errors in the photometric calibration. In COMBO-17 the photometric calibration has slight variations from field to field and therefore the photo-z bias measured on the CDFS cannot be assumed to hold for the A901/2 field. However, we need to be careful that any environmental effect on the stellar-mass–size relation between the field and cluster/core samples is not due to a redshift bias on our field sample causing biased galaxy a_e. In order to address this, we use the bias for the CDFS field as an order of magnitude estimate for any potential redshift bias on the A901/2 field. We then assess the degree of uncertainty caused by a $\pm$ redshift bias on our field sample, and evaluate its propagation into our results. We do not consider the result valid if the redshift bias introduces any significance at the 2σ level due to the uncertain nature of the bias. However, we test to see if the bias causes our high significance results (i.e. intermediate-/low-mass spirals) to drop below the 2σ level.

For intermediate-mass spirals ($\log M_*/\mathrm{M}_\odot \in [9.5, 10]$), $p_{(\mathrm{field/cluster})}$ is only robust to a positive redshift bias. However, after the removal of large $\delta a_\mathrm{e}/a_\mathrm{e}$ galaxies the level of significance is completely robust to a $\pm$ redshift bias and is always above the 3σ level. For low-mass spirals ($\log M_*/\mathrm{M}_\odot \in [9, 9.5]$), the level of significance for $p_{(\mathrm{field/core})}$ is only robust to a positive redshift bias. However, after the removal of large $\delta a_\mathrm{e}/a_\mathrm{e}$ galaxies the level of significance is completely robust to a $\pm$ redshift bias and is always above the 3σ level. For $p_{(\mathrm{field/cluster})}$ after the removal of large $\delta a_\mathrm{e}/a_\mathrm{e}$ galaxies the significance is completely robust to a $\pm$ redshift bias and is always above the 2σ level.

3.4.3 The effect of contaminations

Contamination of our cluster samples by the field could also have potentially masked an environmental dependence on the stellar-mass–size relation for low-mass spirals. In order to address this issue, we use Monte Carlo simulations to evaluate the effect of these contaminations on the $\overline{a}_\mathrm{e}$ in each stellar mass bin for our spiral galaxies.

For each environment and stellar mass bin, we assume the true a_e distribution follows a Gaussian with the same mean and standard deviation as the corresponding subsample in the actual data. Using Monte Carlo simulations, we then sample the respective a_e distributions in order to obtain a simulated sample of field and 'pure' cluster galaxies in each stellar mass bin. The respective sample sizes are matched to that of the actual data. We then perform K–S tests between the corresponding subsamples from the field and cluster distributions and obtain the probability $p_{(\mathrm{field/cluster})}$ in each stellar mass bin. The pure cluster samples were then contaminated by galaxies sampled from the field distribution, with a fraction corresponding to the expected contamination level given in Table 2.3. Analogous K–S tests are then performed between the field and contaminated cluster samples. We perform 100 000 iterations of this Monte Carlo simulation process.

For high-mass spirals ($M_* > 10^{10}\,\mathrm{M}_\odot$), the contamination of the cluster samples by the field has no effect on the fraction of iterations in which $p_{(\mathrm{field/cluster})}$ is above the 2σ level (< 20 per cent). For lower mass spirals ($M_* < 10^{10}\,\mathrm{M}_\odot$), the contamination of the cluster samples by the field causes the fraction of iterations in which $p_{(\mathrm{field/cluster})}$ is above the 2σ level to decrease substantially from ~ 80 per cent to ~ 60 per cent. Therefore, in ~ 20 per cent of cases the contaminations have caused $p_{(\mathrm{field/cluster})}$ to fall below the 2σ level. This implies that the contamination of the cluster sample by the field (up to 25 per cent) could potentially be masking an environmental dependence at lower stellar masses.

For each iteration, we also obtain $\Delta\overline{a}_\mathrm{e}$ between the pure and contaminated cluster samples in each stellar mass bin in order to assess if any potential bias in $\overline{a}_\mathrm{e}$ is caused by the contamination by the field (see Fig. 3.10). We then correct for this bias and evaluate its effect on our real K–S tests to assess if the contamination is potentially masking an environmental dependence for spiral galaxies at low stellar masses. For high and intermediate masses ($\log M_*/\mathrm{M}_\odot \in [9.5, 10], [10, 11]$), this bias has no effect on the significance of the K–S tests. However, we do observe a change in significance at low stellar masses ($\log M_*/\mathrm{M}_\odot \in [9, 9.5]$), where we find that a mean $\overline{a}_\mathrm{e}$ bias of $+0.13$ kpc is expected on the cluster sample (see Fig. 3.10). Correcting for this bias causes the significance of $p_{(\mathrm{field/cluster})}$ to increase from 0.775 to above the 2σ level (0.965). This indicates that the 25 per cent contamination of the cluster sample by the field is potentially masking an environmental dependence at low stellar masses.

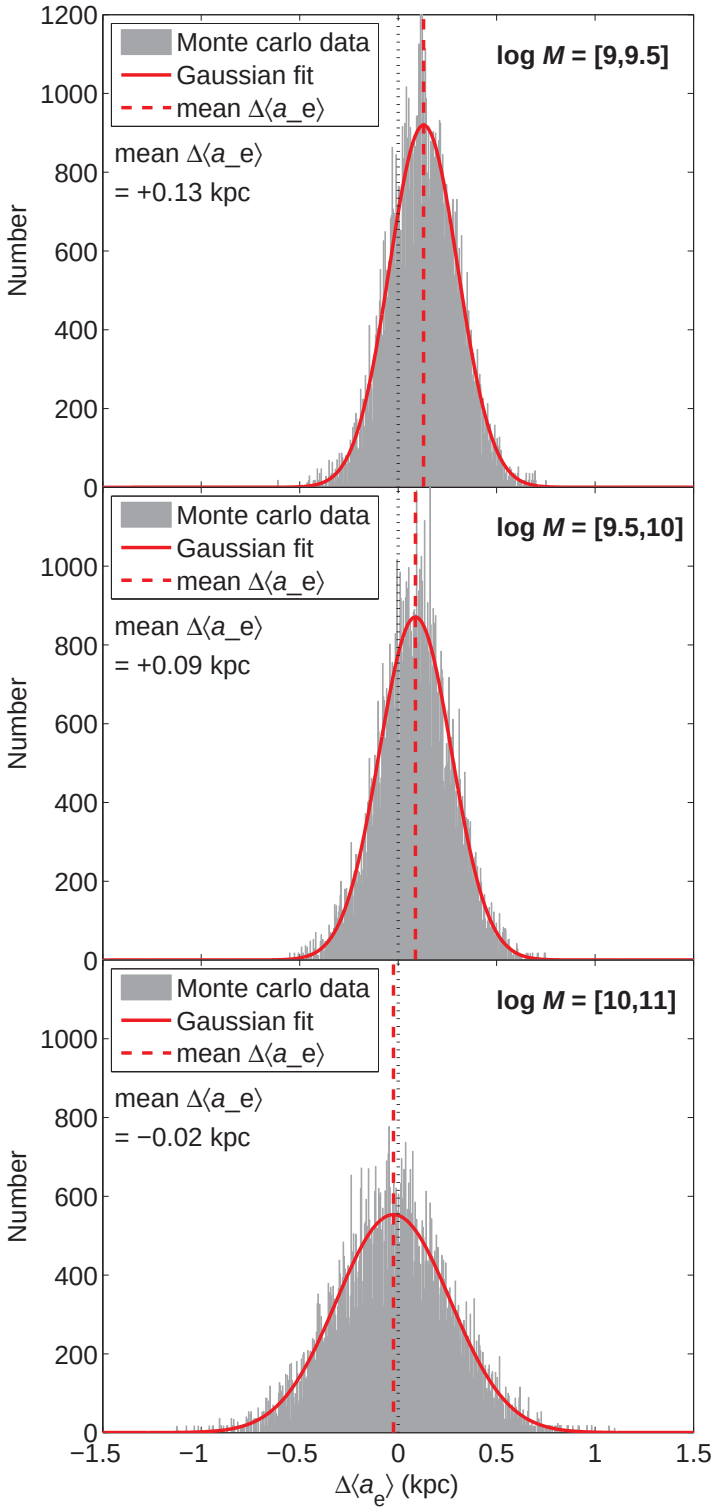

Figure 3.10. The effect of field contaminations on the mean galaxy size $\overline{a}_{\rm e}$ in the cluster environment. The distributions of $\Delta\overline{a}_{\rm e}$ ($\overline{a}_{\rm e:contaminated} - \overline{a}_{\rm e:pure}$) from the Monte Carlo simulations for high-mass, $\log M_*/{\rm M}_\odot \in [10, 11]$ (top); intermediate-mass, $\log M_*/{\rm M}_\odot \in [9.5, 10]$ (centre); and low-mass, $\log M_*/{\rm M}_\odot \in [9, 9.5]$ (bottom) spiral galaxies. We fit a Gaussian to each distribution (red line) and obtain the mean bias in $\overline{a}_{\rm e}$ caused by the field contaminations (red dashed line). The mean bias increases towards lower stellar masses reaching $+0.14\,$kpc at low stellar masses ($M_* < 10^{9.5}\,{\rm M}_\odot$).

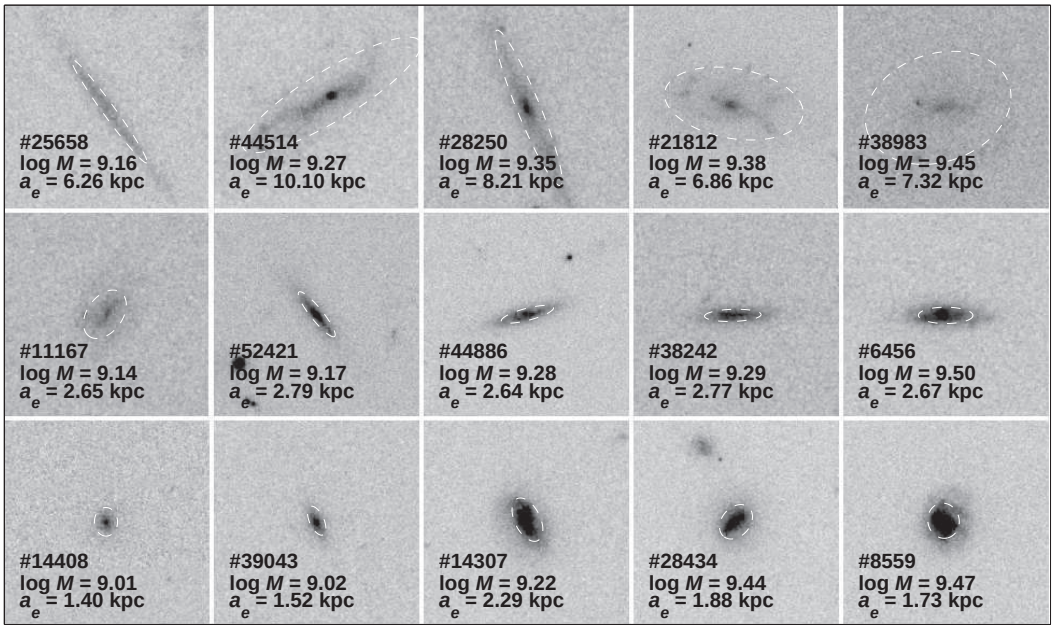

Figure 3.11. Low-mass, $\log M_*/\mathrm{M}_\odot \in [9, 9.5]$ spiral galaxies from different environments. Top row: a selection of large-a_e ($a_\mathrm{e} > 6\,\mathrm{kpc}$), low-mass spiral galaxies from the field environment. Middle row: median-a_e field spirals of similar stellar mass. Bottom row: median-a_e cluster core spiral galaxies of similar stellar mass. The a_e isophote is over-plotted on each image to give an assessment of the physical size of the galaxy. The large-a_e field spirals show the presence of an extended disc that is absent from the cluster core spirals. We hypothesize that the extended disc of these large-a_e spirals may not survive the environmental conditions of the cluster core. Image size $20 \times 20\,\mathrm{kpc}^2$.

3.4.4 Visual inspection

In order to further validate our results, we examined the ACS images of low-mass ($\log M_*/\mathrm{M}_\odot \in [9, 9.5]$), large-$a_\mathrm{e}$ ($a_\mathrm{e} > 6\,\mathrm{kpc}$) field spirals and compared them to the ACS images of median-a_e field and cluster core spirals of similar stellar mass. The semimajor axis effective radius a_e isophote (calculated using the ellipticity and position angle from the STAGES GALFIT model; Gray et al. 2009) was over-plotted on each ACS image in order to assess the physical size of the galaxy. Fig. 3.11 shows a selection of these comparisons across the low-mass range. We find that our large-a_e field spirals appear to have extended discs that are not present in the cluster core spirals. We inspected the ACS images for all 15 low-mass cluster core spirals and find that these extended discs are absent from all but one of the low-mass spirals in the cluster core. The exception could well be a field contaminate (we expect a 25 per cent contamination of the cluster sample by the field; see Section 2.2.4) or could be just arriving in the core of the cluster. In Fig. 3.11, a couple of the large-a_e spiral fits (e.g. #21812 and #38983) are potentially unreliable with the effective radius appearing to be overestimated. However, the fact that no similar potentially unreliable fits are observed in the cluster core suggests that the field sample is drawn from a different parent population for low-mass spirals. We hypothesize that the extended discs present in the low-mass, large-a_e field spirals do not survive the environmental conditions of the cluster core.

3.5 Conclusions

In this chapter, we have presented the stellar-mass–size relations for local galaxies ($z < 0.3$) in three different environments: the field, cluster and cluster core, using *HST*/ACS imaging and data from STAGES. We use a large sample of field and cluster galaxies and a cluster subsample of cluster core galaxies, and determine the significance of an environmental dependence on the stellar-mass–size relation.

Independent of morphology, the stellar-mass–size relation exhibits a significant dependence on the galaxy environment, especially at stellar masses $M_* < 10^{10}\,\mathrm{M}_\odot$ where galaxy sizes are significantly smaller in the cluster/core than in the field. However, the concentration of a galaxy's light profile (and hence its physical size) is not independent of morphology. Early-type galaxies tend to have more compact light distributions compared to late-type galaxies and are more prevalent in the cluster environment than in the field (Dressler 1980). Consequently, it appears that the morphological mix of our field and cluster/core samples could be the origin of the high significance observed. We conclude that in order to perform a fair comparison of the stellar-mass–size relation in different environments, it is necessary to separate our galaxy samples by morphology. We therefore determine the significance of an environmental dependence on the stellar-mass–size relation independently for the three main Hubble types: elliptical, lenticular and spiral galaxies.

For elliptical and lenticular galaxies, significance of an environmental dependence on the stellar-mass–size relation is below the 2σ level for all mass bins, $\log M_*/\mathrm{M}_\odot \in [9, 9.5], [9.5, 10], [10, 11.5]/[10, 11]$. These results have been shown to be completely robust to galaxies with high photo-z errors and to the effect of a potential photo-z bias on the A901/2 field. We conclude that there is no evidence to suggest a significant dependence on the environment of the stellar-mass–size relations for elliptical and lenticular galaxies. This implies that elliptical and lenticular galaxies have undergone a similar size evolution in these environments. This result is in qualitative agreement with the work of Rettura et al. (2010) who came to the same conclusion at higher redshift ($z \sim 1$) using a much smaller sample of 45 cluster and field massive ($M_* > 5 \times 10^{10}\,\mathrm{M}_\odot$) early-type galaxies.

Size evolution is observed to be stronger for early-type galaxies than late-type galaxies (Trujillo et al. 2007). Therefore, if the environment was the principal driver of size evolution, one would expect the environmental dependence of the stellar-mass–size relation to be strongest for elliptical and lenticular galaxies. The fact that we find no such dependence suggests internal drivers [e.g. active galactic nuclei (AGN) feedback; Fan et al. 2008] are governing their size evolution.

For spiral galaxies, we also find no evidence to suggest an environmental dependence on the stellar-mass–size relation for high masses ($\log M_*/\mathrm{M}_\odot > 10$), with the significance of an environmental dependence below the 2σ level. However, we find a significant environmental dependence (at the 2σ level) at intermediate/low stellar masses ($\log M_*/\mathrm{M}_\odot < 10$). We also find the mean a_e for low-mass spirals to be larger in the field than the cluster/core due to a population of large-a_e spirals in the field that are largely absent from the cluster/core environments. Inspection of the ACS images of low-mass spirals has shown that large-a_e spirals in the field contain extended discs that are largely absent from the cluster and cluster core. We hypothesize that the observed fragile discs of these low-mass field spirals may not survive the conditions of the cluster environments. The significance of these results have been shown to be completely robust to large photo-z errors and a potential photo-z

bias on the A901/2 field. This result is in qualitative agreement with the work of Guo et al. (2009) and Weinmann et al. (2009), who find that at fixed mass, low-mass late-type satellite galaxies (in larger groups/clusters) are smaller than similar mass late-type central galaxies (in smaller groups, i.e. the field).

Size evolution is observed to be stronger for more massive galaxies (Franx et al. 2008). Therefore, if the environment was the principal driver behind the size evolution of spiral galaxies, one would expect the environmental dependence of the stellar-mass–size relation to be stronger for high-mass spirals. However, the fact that we find no such dependence suggests that internal drivers are governing their size evolution. For low-mass spirals, we do observe a significant effect of the environment on the stellar-mass–size relation suggesting that the environment probably has an effect on the size evolution at intermediate/low masses.

However, these results are for one survey field (STAGES), and one multicluster complex of intermediate galaxy density at low redshift ($z \sim 0.167$). Therefore, it is important to investigate whether we see the trends observed in the STAGES A901/2 field in other survey fields across a wide range of redshift and cluster mass. Exploring the effect of the environment on galaxy sizes at higher redshifts is of key importance. In the relatively local Universe (e.g. STAGES), size evolution may already have ceased in both the field and cluster environments, even if the environment is the principal driver. However, in the more distant Universe size growth may still be occurring in the field and cluster environments and at different rates. Probing denser, more massive cluster environments (e.g. the Coma cluster) is also important because some environmental drivers may only be significant in very high density environments. The comparison of high redshift studies with those from the local Universe across a wide range of environments will then allow for galaxy size evolution to be characterized as a function of environment and provide the body of evidence needed to assess whether the galaxy environment really does play a role in galaxy size evolution.

In order to assess the potential mechanisms responsible for size evolution, in the following chapters we extend our studies to explore the environmental dependence of galaxy radial surface brightness $\mu(r)$ profiles in STAGES galaxies. By looking at galaxy $\mu(r)$ profiles, we can assess whether spiral/lenticular galaxies have discs that are truncated or antitruncated, which will affect the effective radius, and may also be dependent on the environment (see Chapters 4 and 5). Other related studies considering the $\mu(r)$ profiles of elliptical galaxies (e.g. Häussler et al., in preparation), may also be able to determine whether early-type galaxies have compact cores or cusps. If compact cores are identified, it would be evidence for smooth envelope accretion (minor/major mergers) having an effect on the size evolution of galaxies.

Chapter 4

The structure of galactic discs and the galaxy environment: spiral galaxies

In this chapter, we explore the effect of the galaxy environment on the structure of galactic discs in *spiral* galaxies using the *HST*/ACS imaging and data from the STAGES survey (see Chapter 2). The structure of the outer regions of galactic discs is important to our understanding of the formation and evolution of spiral galaxies. These faint, outer regions are more easily affected by interactions with other galaxies and the cluster environment, and therefore their structural characteristics must be closely related to their evolutionary history. Certain physical processes inherent to galaxy evolution and related to the galaxy environment (e.g. ram-pressure stripping, mergers and harassment, see Section 1.2) could have an effect on the galactic disc and hence also affect the light distribution (surface brightness μ profile) of a galaxy. Consequently, the light profiles of spiral galaxies may show some dependence on the galaxy environment. The work presented in this chapter aims to address this hypothesis.

The majority of the work presented in this chapter has been published in the Maltby et al. (2012a) paper. This paper explores the effect of the galaxy environment on the shape of V-band radial $\mu(r)$ profiles for relatively local spiral galaxies ($z < 0.3$). In this work, all the profile fitting and statistical analyses are my own work. However, the measurements of stellar mass M_*, photometric redshift z, colour (B-V) and effective radius r_e used throughout this work, as well as the critical estimates of the sky background (see Section 4.3.2), are drawn from the STAGES data catalogue published by Gray et al. (2009).

4.1 Introduction

The light profiles of spiral galaxies consist of two principal components: an inner, bulge-dominated component; and an outer exponentially declining stellar disc with some minor deviations related to spiral arms (de Vaucouleurs 1959b; Freeman 1970; see Section 1.3.2). However, since van der Kruit (1979) we have known that this 'classical' picture fails for the majority of spiral galaxies in the Universe, particularly at the faint surface brightness μ of the outer stellar disc. We now know that most disc profiles are actually best described by a two-slope model (broken exponential), characterised by an inner and outer exponential scalelength separated by a relatively well-defined break radius r_brk (Pohlen et al. 2002). Many studies have now reported (mainly using surface photometry) the existence of broken exponential stellar discs, or *truncations*, in spiral galaxies in both the local (Pohlen et al. 2002, 2007; Pohlen

& Trujillo 2006; Bakos et al. 2008; Erwin et al. 2008; Gutiérrez et al. 2011) and distant $z < 1$ Universe (Pérez 2004; Trujillo & Pohlen 2005; Azzollini et al. 2008). Broken exponential stellar discs have also been reported through the use of resolved star counts on some nearby galaxies (e.g. Ibata et al. 2005; Ferguson et al. 2007).

As a direct result of these studies, a comprehensive classification scheme for disc galaxies has emerged based on break features in the outer disc component of their radial $\mu(r)$ profiles (see e.g. Pohlen & Trujillo 2006; Erwin et al. 2008; and Section 1.3.2: Fig. 1.10). This classification scheme consists of three broad profile types (Type I, II and III): Type I (no break) – the galaxy has a simple exponential profile extending out to several scalelengths (e.g. Bland-Hawthorn et al. 2005); Type II (down-bending break, *truncation*) – the exponential is broken with a shallow inner and steeper outer exponential region separated by a relatively well-defined break radius $r_{\rm brk}$ (van der Kruit 1979; Pohlen et al. 2002); Type III (up-bending break, *antitruncation*) – a broken exponential with the opposite behaviour to a Type II profile (i.e. a shallower region beyond $r_{\rm brk}$; Erwin et al. 2005). In each case, the classification refers to the outer, disc component of the galaxy $\mu(r)$ profile and does not consider the inner varying bulge component. In some cases, the inner bulge component may be near exponential in nature (i.e. pseudo bulges; Kormendy & Kennicutt 2004); however, this classification scheme only considers the disc component and is fairly insensitive to the nature of the inner (bulge) profile.

At present, the physical origins of the different profile types are not well understood. Some models suggest that Type II profiles (truncations) could be the consequence of a radial star formation threshold in disc column density (e.g. Kennicutt 1989; Elmegreen & Parravano 1994; Schaye 2004). This theory may account for a sharp truncation (cut off), but does not explain observations of extended outer exponential components in some galaxies (e.g. Pohlen et al. 2002). Another theory has been proposed by Debattista et al. (2006), who find down-bending breaks in simulated disc profiles solely from collisionless N-body simulations. They suggest Type II galaxies are the consequence of a resonance phenomenon and a redistribution of angular momentum that leads to an increased central density and surface brightness. Many models now incorporate both these ideas and suggest that the inner disc forms as a consequence of the star formation threshold, while the outer disc forms by the outward migration of stars from the inner disc to regions beyond the star formation threshold. This migration could be due to resonant scattering with spiral arms (Roškar et al. 2008a,b) or clump disruptions (Bournaud et al. 2007). Alternatively, another model is suggested by Foyle et al. (2008), who use simulations to show that by starting from a single exponential disc, the inner disc forms as the bulge draws mass from the inner regions. As a consequence, the inner disc profile becomes shallower, while the outer region stays almost unaffected. For Type III profiles, their discovery is still very recent (Erwin et al. 2005) and therefore much less effort has been afforded to their origin. Erwin et al. (2005) suggest that in some cases the excess light beyond the radius $r_{\rm brk}$ could actually be attributed to light from the spheroidal bulge or halo extending beyond the end of the disc; however, these cases seam to be quite rare (Maltby et al. 2012b; see Chapter 6). In general, it appears that Type III profiles are the consequence of a disturbed system and that recent minor mergers could produce up-bending stellar profiles in the remnant galaxy (Younger et al. 2007; Sil'Chenko et al. 2011).

However, all these models rely on the break in the surface brightness profile having an analogous break in the stellar mass surface density profile. Bakos et al. (2008)

used colour profiles to calculate stellar mass surface density profiles for a sample of Type II and Type III galaxies identified by Pohlen & Trujillo (2006). Interestingly, for Type II galaxies they find the stellar mass surface density profiles are almost purely exponential. Therefore, the break in the surface brightness profile is not necessarily related to a break in the stellar mass surface density profile. Consequently, the surface brightness break may not be due to the distribution of stellar mass but could be due to a radial change in the stellar population. For Type III galaxies, however, they do find an analogous break in the stellar mass surface density profile indicating these breaks could be due to the stellar mass distribution.

Investigating the frequency of profile types in different galaxy environments will provide evidence for their origin and the effect of the environment on the outer stellar disc. Presently, there have been few systematic searches for stellar disc truncations in spiral galaxies in either the local (Pohlen & Trujillo 2006; Erwin et al. 2008) or distant Universe (Trujillo & Pohlen 2005; Azzollini et al. 2008). Pohlen & Trujillo (2006) use a sample of ~ 90 face-on to intermediate inclined nearby late-type (Sb–Sdm) spiral galaxies from the Sloan Digital Sky Survey (SDSS; York et al. 2000) and find that approximately 10 per cent are Type I, 60 per cent are Type II and 30 per cent are Type III. They also report that the shape of the profiles correlate with Hubble type. In their sample, down-bending breaks are more frequent in later Hubble types, while the fraction of up-bending breaks rises towards earlier types. They also find no relation between the galaxy environment, as determined by the number of nearest neighbours, and the shape of the surface brightness profile. However, they do not reach very dense environments and low number statistics did not allow for major conclusions. Azzollini et al. (2008) recently conducted the largest systematic search for stellar disc truncations yet undertaken at intermediate redshift ($0.1 < z < 1.1$) using the Great Observatories Origins Deep Survey (GOODS; Giavalisco et al. 2004) south field. They use a sample of 505 galaxies and obtain the frequency of profile types in different redshift ranges. They find that the frequency of profile types (Type I:II:III) is 25:59:15 per cent for $0.1 < z < 0.5$, and does not vary significantly with redshift out to $z \sim 1.1$.

The aim of this study is to undertake a systematic search for broken exponentials in the field and cluster environment using the STAGES Survey (Gray et al. 2009; see Chapter 2) and to investigate whether the galaxy environment has any effect on the stellar distribution in the outer stellar disc. We investigate whether the type and strength of radial $\mu(r)$ profile breaks in the outer stellar discs of spiral galaxies is dependent on the galaxy environment. This work builds on previous studies by using larger and more statistically viable field and cluster samples and by reaching higher density environments. However, it is important to note that STAGES only covers an intermediate-density environment (see Heiderman et al. 2009) and not a high-density environment (e.g. the Coma cluster; The & White 1986). We also wish to point out that in this work we use a slightly different profile classification scheme to that used by Pohlen & Trujillo (2006) and Azzollini et al. (2008) (see Section 4.4.3). Therefore, direct comparisons of the results of this work to the previous works mentioned above cannot be made.

The structure of this chapter is as follows. In Section 4.2, we give a brief description of our sample selection. In Section 4.3, we describe the method used to obtain our radial surface brightness $\mu(r)$ profiles from the STAGES *HST*/ACS V-band imaging and then explain our profile classification scheme in Section 4.4. We present our results in Section 4.5 and finally draw our conclusions in Section 4.6.

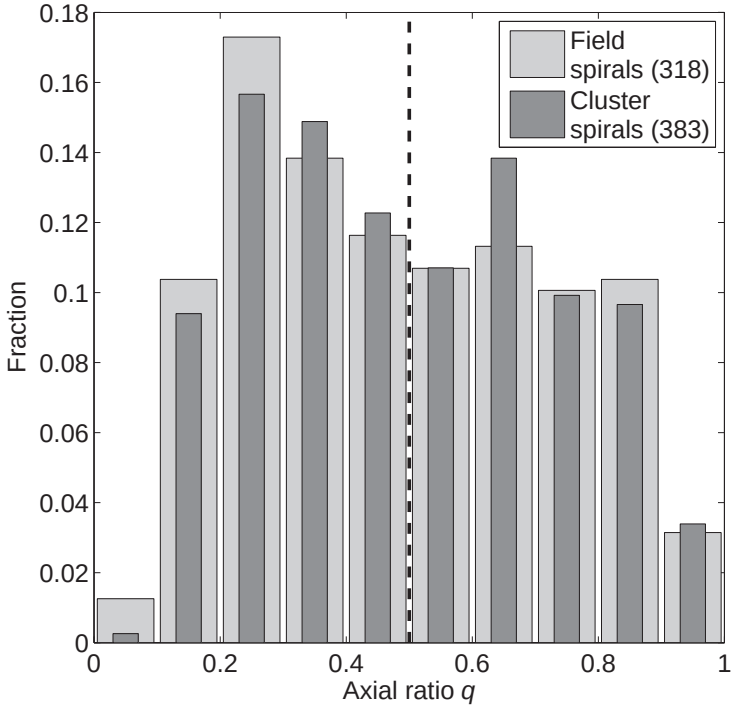

Figure 4.1. The distribution of minor-to-major axial ratio q for our field (light grey) and cluster (dark grey) spiral samples. The q cut ($q > 0.5$, represented by a black dashed line) ensures the selection of face-on to intermediately inclined spiral galaxies ($i < 60°$). Relative errors in q are < 3 per cent. Respective sample sizes are shown in the legend.

4.2 Data and sample selection

For this study, we draw our sample of spiral galaxies from STAGES (Gray et al. 2009) using the field and cluster selection defined in Chapter 2 (Section 2.2). This selection results in a large, mass-limited ($M_* > 10^9\,\mathrm{M}_\odot$), visually classified (Sa–Sdm) sample of $\sim$ 700 spiral galaxies from both the field and cluster environments (318 field spirals and 383 cluster spirals, see Chapter 2: Table 2.1).

The field and cluster samples are then restricted by galaxy inclination i to select face-on to intermediately inclined spiral galaxies by using the axial ratio q of the galaxy as determined by the STAGES GALFIT models (Gray et al. 2009). The minor-to-major axial ratio q ($q = b/a = 1 - e$, where a and b are the semimajor and semiminor axes, respectively, and e is the ellipticity) is restricted to correspond to an inclination i of less than 60° ($q > 0.5$ or $e < 0.5$). This cut is necessary to minimise the influence of dust on our surface brightness $\mu(r)$ profiles and also allows reliable information on features like bars, rings and spiral structure. The distribution of axial ratio q for our field and cluster samples showing the axial ratio q cut is presented in Fig. 4.1. This cut removes $\sim$ 50 per cent of spiral galaxies from both our field and cluster samples. The final field sample contains 145 spirals reaching down to $R \sim 23$, and the final cluster sample contains 182 spirals reaching down to $R \sim 22$ (see Fig. 4.2). Some relevant properties of the final field and cluster spiral samples are shown in Table. 4.1. The morphological mix (Sa, Sb, Sc, Sd)[1] of the final field and cluster samples are shown in Fig. 4.3.

[1]In this study, intermediate spiral classes are grouped to the earlier Hubble type (e.g. Sab → Sa).

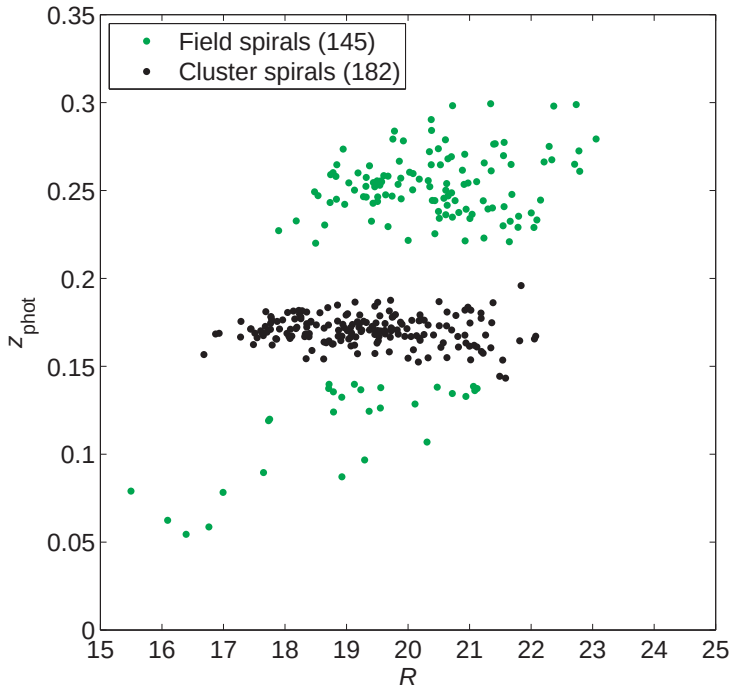

Figure 4.2. The photometric redshift $z_{\rm phot}$ versus total R-band magnitude (Vega) for the final field (green points) and cluster (black points) spiral galaxy samples. The field sample reaches $R \sim 23$ and the cluster sample reaches $R \sim 22$. Respective sample sizes are shown in the legend.

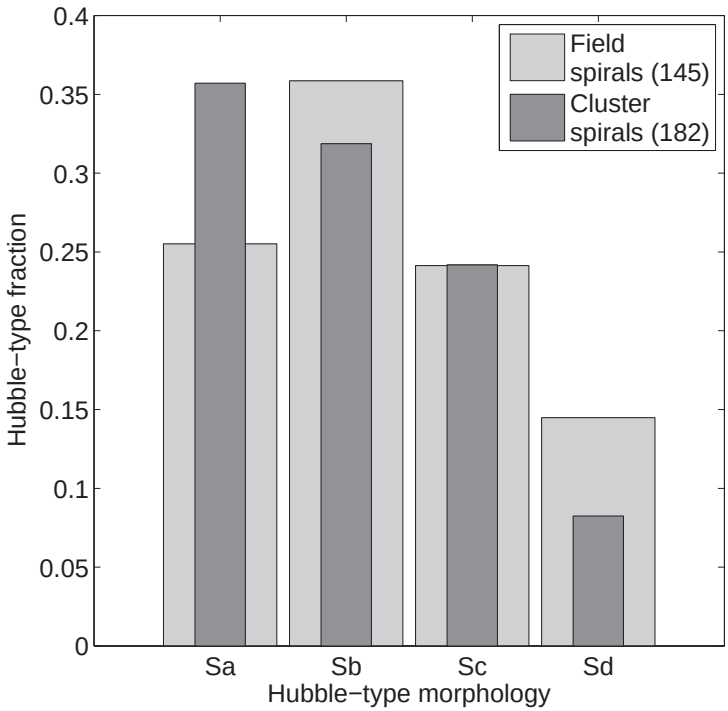

Figure 4.3. The distribution of Hubble-type morphologies for the final field (light grey) and cluster (dark grey) spiral galaxy samples. Respective sample sizes are shown in the legend. A significant excess of earlier types (Sa) is observed in the cluster environment.

Table 4.1. Properties of the final field and cluster spiral galaxy samples.

Property	Field	Cluster
$N_{\rm gal}$	145	182
Completeness	$> 70\,\%$	$> 90\,\%$
Contamination	–	$< 25\,\%$
$R_{\rm mean}$	20.14	19.32
$M_{B(\rm min)}$	-15.1	-16.1
$M_{B(\rm max)}$	-21.5	-21.8
$z_{\rm phot,mean}$	0.227	0.171
$z_{\rm phot,min}$	0.055	0.143
$z_{\rm phot,max}$	0.299	0.196

4.3 Profile fitting

For each galaxy in our field and cluster sample, we use the IRAF task ellipse[2] in order to obtain azimuthally-averaged radial surface brightness $\mu(r)$ profiles from the STAGES *HST*/ACS V-band imaging. The ACS images used include the sky background, and the necessary sky subtraction is performed after profile fitting (see Section 4.3.2). For further details on the fitting method used by ellipse see Jedrzejewski (1987).

We run ellipse using bad-pixel masks that remove flagged pixels from our isophotal fits. This is necessary in order to remove sources of contamination such as background/companion galaxies and foreground stars (everything not associated with the galaxy itself; see Fig. 4.4 for an example). Gray et al. (2009) generated these bad-pixel masks for each STAGES galaxy using the data pipeline Galaxy Analysis over Large Areas: Parameter Assessment by GALFITting Objects from SExtractor (GALAPAGOS; Barden et al. 2012). GALAPAGOS performs an extraction of source galaxies from the STAGES *HST*/ACS V-band imaging and uses the GALFIT code (Peng et al. 2002) to fit Sérsic (1968) radial surface brightness models to each galaxy image. The bad-pixel masks are generated for each STAGES galaxy in order to remove sources of contamination from these surface brightness models. However, occasionally in crowded regions GALFIT performs multiobject fitting, and therefore the companion galaxies in these cases are not removed by the bad-pixel mask as they are too close to the subject galaxy. In these cases (27 field and 33 cluster galaxies, ~ 18 per cent), the companion galaxies are removed from the ACS image by subtraction of their GALFIT surface brightness model. The residuals of the companion galaxies are not expected to have any significant effect on the azimuthally-averaged radial surface brightness $\mu(r)$ profile for the subject galaxy. Isophotal fitting is only attempted when the fraction of flagged (masked) data points in the isophote is less than 0.5 and fitting is terminated if this condition is broken.

For all our ellipse isophotal fits, the galaxy centre is fixed (all isophotes have a common centre) using the centre of the galaxy determined from the GALFIT Sérsic model (Gray et al. 2009). We also use logarithmic radial sampling with steps of

[2] STSDAS package – version 2.12.2

0.03 dex (0.07 geometric sampling in ellipse terminology) and start from an initial semimajor axis of 10 pixels.

Using a similar procedure to previous works (Pohlen & Trujillo 2006; Erwin et al. 2008), we fit two different sets of ellipses to each galaxy ACS image. The first is a free-parameter fit (fixed centre, free ellipticity e and position angle PA) and tends to follow morphological features such as bars and spiral arms. Consequently, these free fits are not suitable for the characterisation of the underlying outer stellar disc studied in this work. Therefore, we use a fixed-parameter fit (fixed centre, e and PA) in order to produce our final $\mu(r)$ profiles.

The initial free-parameter fit (fixed centre, free e and PA) is used to determine the ellipticity and position angle of the outer disc component. For each sample galaxy, the ACS image was inspected with the contrast adjusted in order to get an estimate of the semimajor axis for the end of the stellar disc $a_{\mathrm{disc\,lim}}$ (where the galaxy surface brightness enters the background noise). This 'stellar disc limit' $a_{\mathrm{disc\,lim}}$ corresponds to the outer stellar disc region and is used to obtain the ellipticity and position angle of the outer stellar disc, $e_{\mathrm{disc\,lim}}$ and $\mathrm{PA}_{\mathrm{disc\,lim}}$, respectively, from the ellipse free fit e and PA radial profiles (see Fig. 4.4). Fig. 4.4 shows the fitting procedure for an example galaxy.

In some cases, the fit failed at the stellar disc limit $a_{\mathrm{disc\,lim}}$ due to ellipse error limits in the radial intensity gradient. However, adjusting this threshold allowed these fits to be forced out to $a_{\mathrm{disc\,lim}}$. In order to ensure that the ellipticity $e_{\mathrm{disc\,lim}}$ and position angle $\mathrm{PA}_{\mathrm{disc\,lim}}$ of the outer stellar disc are reliable, we compared the values obtained from the ellipse fit to a manual measurement of $e_{\mathrm{disc\,lim}}$ and $\mathrm{PA}_{\mathrm{disc\,lim}}$ measured directly off the ACS image during the visual inspection. The ellipse values agreed with the visually measured values in all cases.

However, in some cases the ellipse radial e and PA profiles could be unstable at the stellar disc limit $a_{\mathrm{disc\,lim}}$. In these cases, seven field ($\sim$ 5 per cent) and 13 cluster galaxies ($\sim$ 7 per cent), we use the last reliable e and PA obtained from the ellipse profiles as our estimate of e and PA for the outer stellar disc.

In some other cases, the free fit failed completely at $a_{\mathrm{disc\,lim}}$. Subsequent inspection of the ACS image sometimes revealed structure at $a_{\mathrm{disc\,lim}}$ that was clearly intrinsic to the subject galaxy (i.e. an axisymmetric stellar disc or spiral arms). In these cases, 27 field ($\sim$ 19 per cent) and 24 cluster galaxies ($\sim$ 13 per cent), we use the estimate of $e_{\mathrm{disc\,lim}}$ and $\mathrm{PA}_{\mathrm{disc\,lim}}$ measured directly off the ACS image as our estimate of e and PA for the outer stellar disc. Unfortunately, in a few cases the ACS image was too noisy for a reliable manual measurement of $e_{\mathrm{disc\,lim}}$ and $\mathrm{PA}_{\mathrm{disc\,lim}}$. In these cases, seven field ($\sim$ 5 per cent) and four cluster galaxies ($\sim$ 2 per cent), we use the value of the e and PA determined by GALFIT in the STAGES Sérsic models (Gray et al. 2009) as our estimate of e and PA for the outer stellar disc.

A fixed-parameter fit (fixed centre, e and PA), using the e and PA of the outer stellar disc obtained from the free fit, is then used to produce our final surface brightness profiles (see Fig. 4.4). The fixed fits are forced to extend out well into the sky background (semimajor axis of 600 pixels). During the fixed-fitting process we also perform four iterations of a 3σ rejection applied to deviant points below and above the average to smooth some of the bumps in the surface brightness profiles that are due to non-axisymmetric features, i.e. not part of the stellar disc (e.g. star-forming regions and supernovae). The final profile fits then undergo a sky subtraction and surface brightness calibration in order to produce the final surface brightness $\mu(r)$ profiles which will be discussed in the following sections.

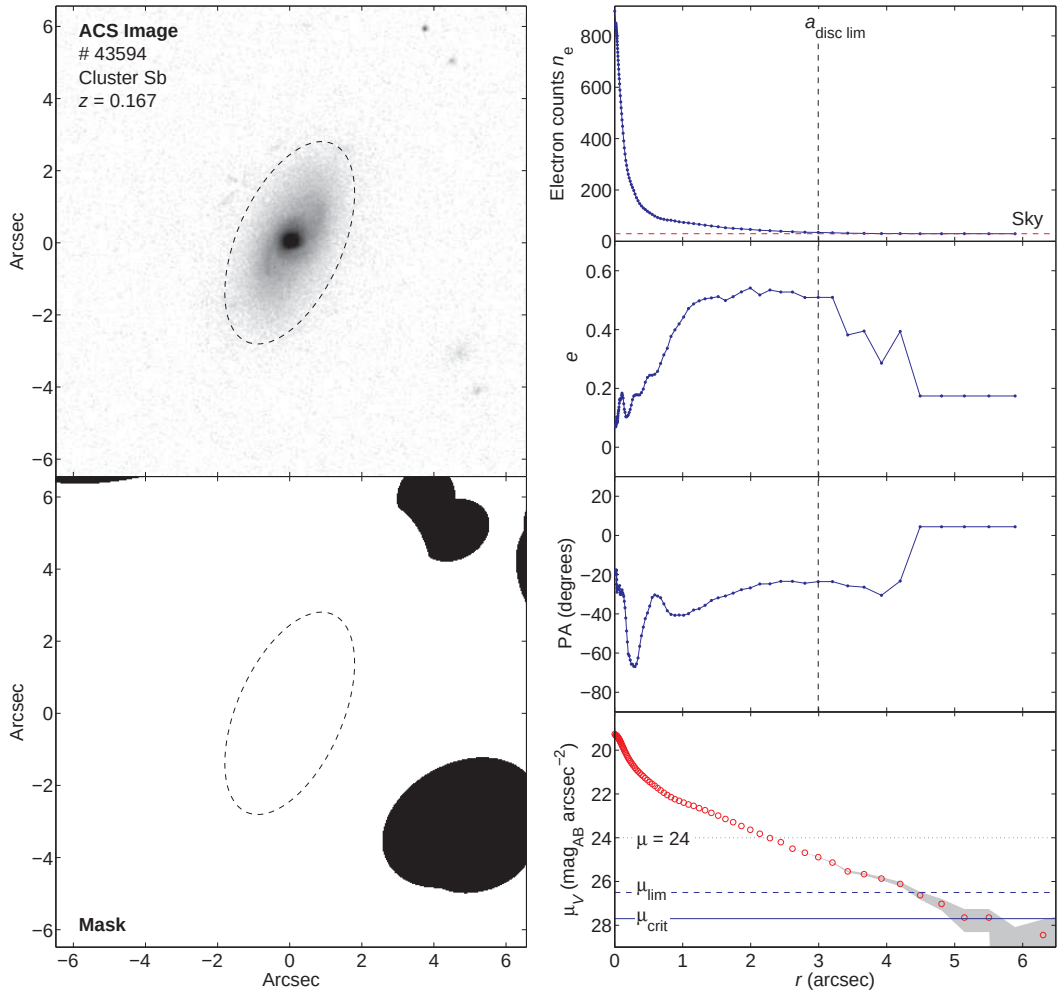

Figure 4.4. Example profile fit. Left-hand column: ACS image (top) and bad-pixel mask (bottom) showing the visually-determined stellar disc limit $a_{\rm disc\,lim}$ (black dashed line). The ACS image is shown with a logarithmic grey-scale. Right-hand column, top panel: the azimuthally-averaged radial electron count $n_{\rm e}$ profile from the free-parameter fit showing the GALAPAGOS sky background (red dashed line) and the stellar disc limit $a_{\rm disc\,lim}$ (black dashed line). Right-hand column, second and third panels: the ellipticity e and position angle PA radial profiles from the free fit showing the position of the stellar disc limit $a_{\rm disc\,lim}$ (black dashed line) used to obtain the e and PA of the outer stellar disc. PA is measured east of north. Right-hand column, bottom panel: the final azimuthally-averaged radial surface brightness $\mu(r)$ profile from the fixed-parameter fit. The error in the surface brightness (grey shaded area) is due to oversubtracting and undersubtracting the sky background by $\pm1\sigma$. The limiting surface brightness $\mu_{\rm lim}$ (blue dashed line) and critical surface brightness $\mu_{\rm crit}$ (blue solid line) represent the limit to which we trust profile breaks and the $\mu(r)$ profile, respectively.

4.3.1 Photometric calibration

The STAGES *HST*/ACS V-band images have pixel values in units of electrons $n_{\rm e}$. These can be converted into AB magnitudes per pixel using the following expression:

$$m_{\rm AB} = -2.5\log_{10}\left(\frac{\rm PHOTFLAM \times n_e}{\rm EXPTIME}\right) + zpt_{\rm AB}, \tag{4.1}$$

where the AB zero-point

$$zpt_{\rm AB} = {\rm PHOTZPT} - 5\log_{10}({\rm PHOTPLAM}) + 18.6921. \tag{4.2}$$

The following FITS header keywords are used in this conversion (ACS Data Handbook v5.0; Pavlovsky et al. 2006):

- PHOTFLAM $= 7.766405 \times 10^{-20}\,{\rm erg\,cm^{-2}\,\AA^{-1}\,electron^{-1}}$,
- PHOTPLAM $= 5.919369 \times 10^{3}\,$Å,
- PHOTZPT $= -21.10$.

The effective exposure time EXPTIME (after ACS subpixel drizzling) varies for each sample galaxy and is between 700 and 770 s. The AB magnitude for each pixel $m_{\rm AB}$ can then be converted into a surface brightness μ using the ACS pixel scale (0.03 arcsec):

$$\mu = m_{\rm AB} + 2.5\log_{10}({\rm pixel\,scale^2}). \tag{4.3}$$

This gives a surface brightness μ per pixel in ${\rm mag_{AB}\,arcsec^{-2}}$ in the V band. For our spiral galaxies, the azimuthally-averaged radial flux profiles are converted into $\mu(r)$ profiles using this calibration. However, several corrections are also required in order to correct the surface brightness μ for Galactic extinction, individual galaxy inclination i and surface brightness dimming.

(i) *Galactic extinction.* The STAGES field is affected by reddening due to substantial foreground dust (Galactic extinction; see Gray et al. 2009), and an extinction correction $A_{\rm extinction}$ of -0.18 mag in the V band is required.

(ii) *Inclination of galaxy.* The surface brightness μ of a spiral galaxy increases with its inclination i to the line of sight. We correct for galaxy inclination using the surface brightness correction $A_i = -2.5\log_{10}(1-e)$, where e is the ellipticity of the outer isophote (Freeman 1970). We use the ellipticity determined for the fixed fit $e_{\rm disc\,lim}$ (outer isophote) to correct for galaxy inclination i. We do not attempt to correct the surface brightness for internal extinction (dust effects). However, since the galaxies studied here are all reasonably face-on ($\langle q\rangle = 0.7$, $\langle i\rangle = 45^\circ$), and as we are dealing with the outer parts of the galactic disc, dust is expected to have very little effect on the surface brightness correction and no effect on the presence or strength of truncations/antitruncations in the stellar disc.

(iii) *Surface brightness dimming.* We correct the surface brightness $\mu(r)$ profiles of our field galaxies so they are at the redshift of the cluster ($z_{\rm cl} = 0.167$). This allows a fair comparison between galaxies across the redshift range of our sample. All cluster member galaxies are assumed to be at the cluster spectroscopic redshift. Surface brightness $\mu \propto (1+z)^{-4}$ for bolometric luminosity (with μ in ${\rm flux\,arcsec^{-2}}$). However, for observations taken using a physical filter (width $\Delta\lambda_{\rm filter}$), the effective filter width $\Delta\lambda_{\rm eff}$ is dependent on z; $\Delta\lambda_{\rm eff} = \Delta\lambda_{\rm filter}/(1+z)$. Consequently, the

actual μ corresponding to light emitted from within the filters wavelength range is $(1+z)$ times brighter than observed (i.e. $\mu \propto (1+z)^{-3}$). Therefore, since STAGES uses the V-band (F606W) filter, we correct the μ of our field galaxies by multiplying the galaxy flux (in electrons $n_{\rm e}$) by $(1+z_{\rm gal})^3/(1+z_{\rm cl})^3$, where $z_{\rm gal}$ is the photometric redshift of the field galaxy from COMBO-17. This leads to a surface brightness correction A_z for our field galaxies, where

$$A_z = -2.5\log_{10}\left(\frac{(1+z_{\rm gal})^3}{(1+z_{\rm cl})^3}\right). \tag{4.4}$$

Therefore, the final surface brightness $\mu_{\rm corrected}$ corrected for Galactic extinction, galaxy inclination i and surface brightness dimming is given by

$$\mu_{\rm corrected} = \mu_{\rm measured} + A_{\rm extinction} + A_i + A_z. \tag{4.5}$$

4.3.2 Sky subtraction

During the GALFIT Sérsic model fitting performed by the GALAPAGOS pipeline (Gray et al. 2009), the sky level is calculated individually for each source galaxy by evaluating a flux growth curve and using the full science frame. In this study, for each sample galaxy we use the sky level determined by GALAPAGOS for our sky subtraction. Fig. 4.4 includes the free-fit radial intensity profile (in electron counts $n_{\rm e}$) for an example galaxy showing the sky background determined by GALAPAGOS.

The error in the GALAPAGOS sky level was estimated using observed 'dark' patches of sky located in some of the STAGES ACS tiles (tiles 01, 10, 31 and 60; see Gray et al. 2009). Each patch (measuring 100×100 pixels) was visually inspected to ensure it was clear of any V-band sources. The distribution of electron counts $n_{\rm e}$ (pixel values) in each dark patch is Gaussian in all cases. For each ACS tile, we obtain the mean pixel value $\langle n_{\rm e}\rangle$ in each dark patch of sky and then the standard deviation in the mean pixel values $\sigma_{\langle n_{\rm e}\rangle}$ (see Table 4.2). The distribution of mean pixel values $\langle n_{\rm e}\rangle$ is approximately Gaussian for each tile. The final $\pm1\sigma$ sky error is the mean $\sigma_{\langle n_{\rm e}\rangle}$ from the four selected ACS tiles and is $\sim \pm0.18$ electron counts (see Table 4.2).

For our $\mu(r)$ profiles, the sky subtraction error due to the error in the GALAPAGOS sky background dominates over the individual errors produced by ellipse in the fitting process. At $\mu < 25\,{\rm mag\,arcsec^{-2}}$, the fit error dominates over the error in the sky subtraction but has a negligible effect on the $\mu(r)$ profile. However, at $\mu > 25\,{\rm mag\,arcsec^{-2}}$ the sky subtraction error dominates the error in the $\mu(r)$ profile. The sky subtraction error can have a significant effect on the $\mu(r)$ profile of our spiral galaxies, especially in the outer regions where the surface brightness approaches that of the sky background. However, for any particular galaxy the global sky subtraction error is approximately constant across the length of the $\mu(r)$ profile. Therefore, we can specify the error in our $\mu(r)$ profiles by generating profiles for when the sky background is oversubtracted and undersubtracted by $\pm1\sigma$ (see Fig. 4.4).

The $\pm1\sigma$ error in the sky background corresponds to a critical surface brightness limit $\mu_{\rm crit}$ below which the sky-subtracted $\mu(r)$ profile of a galaxy becomes unreliable. This critical surface brightness $\mu_{\rm crit}$ is approximately $27.7\,{\rm mag\,arcsec^{-2}}$. We also define a limiting surface brightness $\mu_{\rm lim}$, corresponding to a $\pm3\sigma$ sky error, below which identifying profile breaks becomes unreliable. The limiting surface brightness $\mu_{\rm lim}$ is approximately $26.5\,{\rm mag\,arcsec^{-2}}$.

Table 4.2. Determination of the $\pm 1\sigma$ sky error from observed dark patches of sky in the STAGES *HST*/ACS V-band imaging.

STAGES tile	$N_{\rm dark\ patches}$	$\sigma_{\langle n_{\rm e} \rangle}$ (counts)
01	24	0.119
10	28	0.131
31	23	0.340
60	30	0.111
$\pm 1\sigma$ sky error = mean $\sigma_{\langle n_{\rm e} \rangle}$		0.175

4.4 Profile classification

4.4.1 Profile inspection

For each spiral galaxy in our field and cluster sample, the azimuthally-averaged radial surface brightness profile $\mu(r)$ was visually inspected in order to identify potential profile breaks (inflection points in the exponential region of the μ profile). Due to the subjective nature of some profile classifications, this inspection was carried out by three independent assessors (DTM, AAS, MEG). Three possible cases were considered: i) no break or simple exponential profile; ii) a single broken exponential either down-bending or up-bending; and iii) cases with two profile breaks. In each case, break identification relates to the outer disc component of the galaxy $\mu(r)$ profile and does not consider the inner varying bulge component.

Our break identification is based solely on the $\mu(r)$ profiles and without direct inspection of the ACS images. We chose not to relate the $\mu(r)$ profile breaks to visually-identified structural features because we wanted a break classification method that treated all galaxies equally, in a self-consistent manner, and avoided the prejudice that image inspection could introduce. Additionally, the aims of this work are to explore the effect of the environment on the structure of the outer regions of the galactic disc, regardless of the origins of any identified structural features.

If a $\mu(r)$ profile break was identified, the radial limits of exponential regions either side of the break radius $r_{\rm brk}$ were also estimated allowing for some bumps and wiggles due to spiral substructure (e.g. spiral arms and star-forming regions). For the inner exponential, the inner boundary is manually selected to avoid the region dominated by the bulge component. For the outer exponential, the outer boundary is generally taken to be where the $\mu(r)$ profile reaches the critical surface brightness $\mu_{\rm crit}$ (1σ above the sky background) but may be at higher μ depending on the nature of the profile. A small manually selected transition region (non-exponential) is allowed between the exponential regions either side of the break. The break radius $r_{\rm brk}$ is defined as the mean radius of the radial limits for this transition region.

Due to the subjective nature of some galaxy profile classifications, the number of galaxies with either no, one or two breaks varied subtly between the different assessors. To account for this, in what follows we perform parallel analyses on the breaks identified by each assessor and compare the final results.

4.4.2 Defining the outer stellar disc

In this study, we wish to consider the effect of the galaxy environment on the outer regions of the stellar disc for spiral galaxies. Therefore, we only wish to consider broken exponentials in the outer disc region of the $\mu(r)$ profile. Any effect of the environment should be stronger in these faint, fragile, outer regions. Fig. 4.5 shows the surface brightness at the break radius $\mu_{\rm brk}$ for galaxies with one and two breaks. In the case of one break, for each assessor there appears to be a slight difference in the distribution of $\mu_{\rm brk}$ between the field and cluster samples, with cluster breaks occurring at fainter surface brightnesses. Kolmogorov-Smirnov (K–S) tests between the respective field and cluster samples show that this environmental difference is driven by Type III (up-bending break, antitruncated) profiles with a significance at the 2σ–3σ level. We offer no interpretation of this result due to its uncertain nature. In the case of two inflection points, we consider the inner and outer breaks separately and the separation between the inner and outer break occurs at a surface brightness $\mu \sim 24\,{\rm mag\,arcsec^{-2}}$ (see Fig. 4.5). The same conclusion is reached for the break samples generated by each assessor. Inner and outer breaks may have different physical origins. Therefore, in order to ensure we are comparing intrinsically similar μ breaks in the stellar disc, we limit the breaks analysed to those with $\mu_{\rm brk} > 24\,{\rm mag\,arcsec^{-2}}$ (outer disc breaks) and to the outermost break if two inflection points are present within this range. There may be break features at a surface brightness $\mu < 24\,{\rm mag\,arcsec^{-2}}$, and these may be related to the galaxy environment. However, we focus on breaks in the outer disc as these are more likely to be susceptible to environmental effects. We acknowledge that in doing this there is some potential for missed environmental effects in the inner disc; therefore, we do include some additional tests using the inner/initial break (see Section 4.5.4).

In Section 4.3.2, we defined a limiting surface brightness $\mu_{\rm lim}$ ($\pm 3\sigma$ sky error) of $26.5\,{\rm mag\,arcsec^{-2}}$. In our analysis, we do not trust breaks at a μ fainter than the $\mu_{\rm lim}$ level as this is where identification of breaks becomes unreliable due to the deviation of the profiles generated by oversubtracting and undersubtracting the sky by $\pm 1\sigma$ (see Fig. 4.4). We therefore also restrict our analysis to profile breaks that have $\mu_{\rm brk} < 26.5\,{\rm mag\,arcsec^{-2}}$.

4.4.3 Profile types

We classify our spiral galaxies into three broad profile types: those classified to be Type $\rm I_o$, Type $\rm II_o$, or Type $\rm III_o$ depending on break features in their outer stellar disc only (o denotes 'outer', $24 < \mu < 26.5\,{\rm mag\,arcsec^{-2}}$). Our classification assumes only one break in the outer disc. If two breaks are present, the outer break is used for classification. This is only the case for four (~ 3 per cent) field galaxies. If the $\mu(r)$ profile has no break in the outer disc, then the galaxy has a simple exponential outer disc and is classified as Type $\rm I_o$. Galaxies that are pure exponentials across the length of their $\mu(r)$ profile, aside from the varying bulge component (Type I, a subset of Type $\rm I_o$), are also identified. If the $\mu(r)$ profile has a down-bending break in the outer disc ($\mu_{\rm brk} > 24\,{\rm mag\,arcsec^{-2}}$), then the galaxy has an *outer disc truncation* and is classified as Type $\rm II_o$; however, if the $\mu(r)$ profile has an up-bending break, then the galaxy has an *outer disc antitruncation* and is classified as Type $\rm III_o$. Examples of each profile type (Type I, $\rm I_o$, $\rm II_o$ and $\rm III_o$), as well as their ACS images showing the break radius $r_{\rm brk}$ isophote, are shown in Fig. 4.6. Note that this classification scheme is different to that used by previous works (e.g. Pohlen & Trujillo 2006).

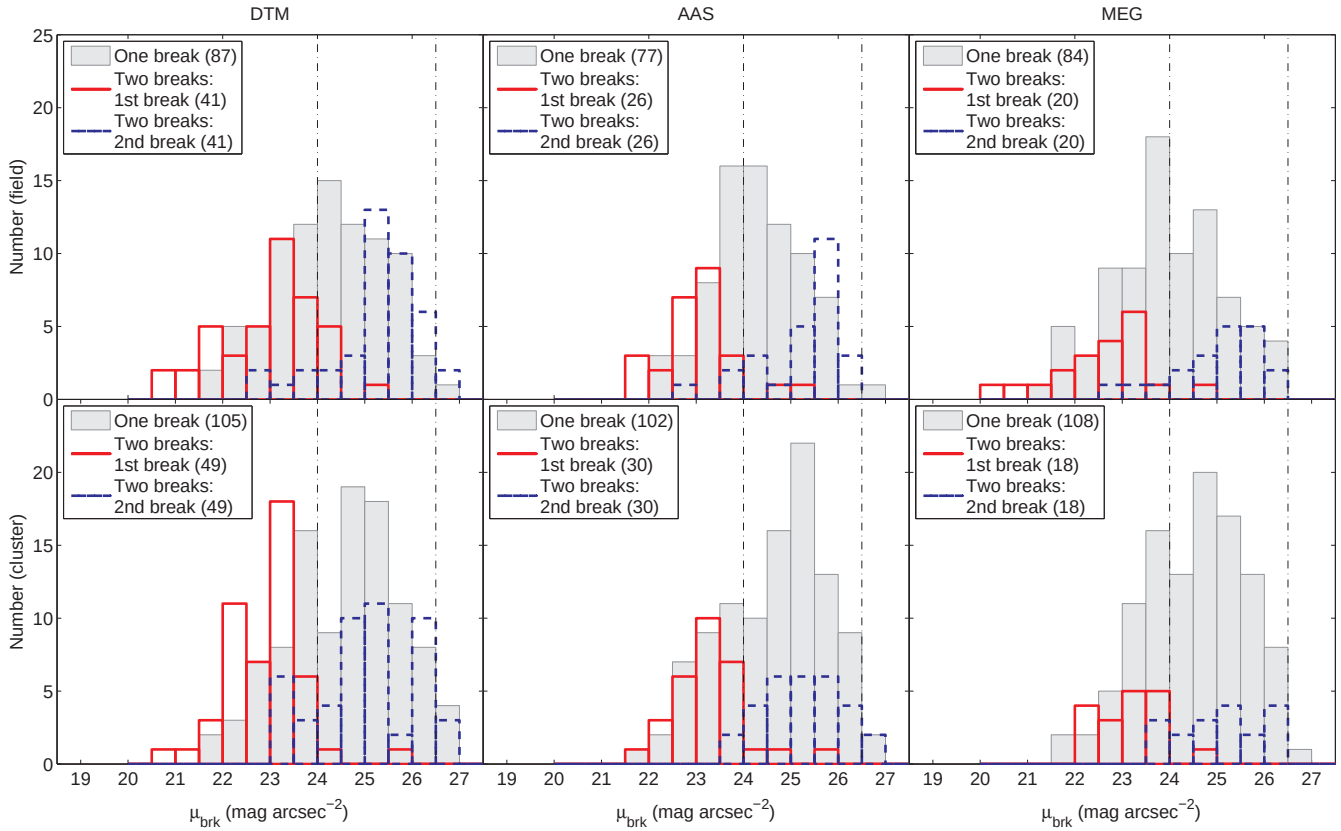

Figure 4.5. The distribution of break surface brightness $\mu_{\rm brk}$. The surface brightness at the break radius $\mu_{\rm brk}$ for field (top row) and cluster (bottom row) galaxies as determined by DTM (left-hand column), AAS (centre column) and MEG (right-hand column). The distributions show galaxies with one break (grey shaded area), and both the inner (red line) and outer break (blue dashed line) of galaxies with two breaks. For the case of two breaks, the separation between the inner and outer break occurs at a surface brightness μ of $\sim 24\,{\rm mag\,arcsec^{-2}}$. The position of the break surface brightness cut $24 < \mu_{\rm brk} < 26.5\,{\rm mag\,arcsec^{-2}}$ used to create our final break samples is shown (black dashed lines). Respective sample sizes are shown in the legends. Contamination of the cluster sample by the field is < 25 per cent.

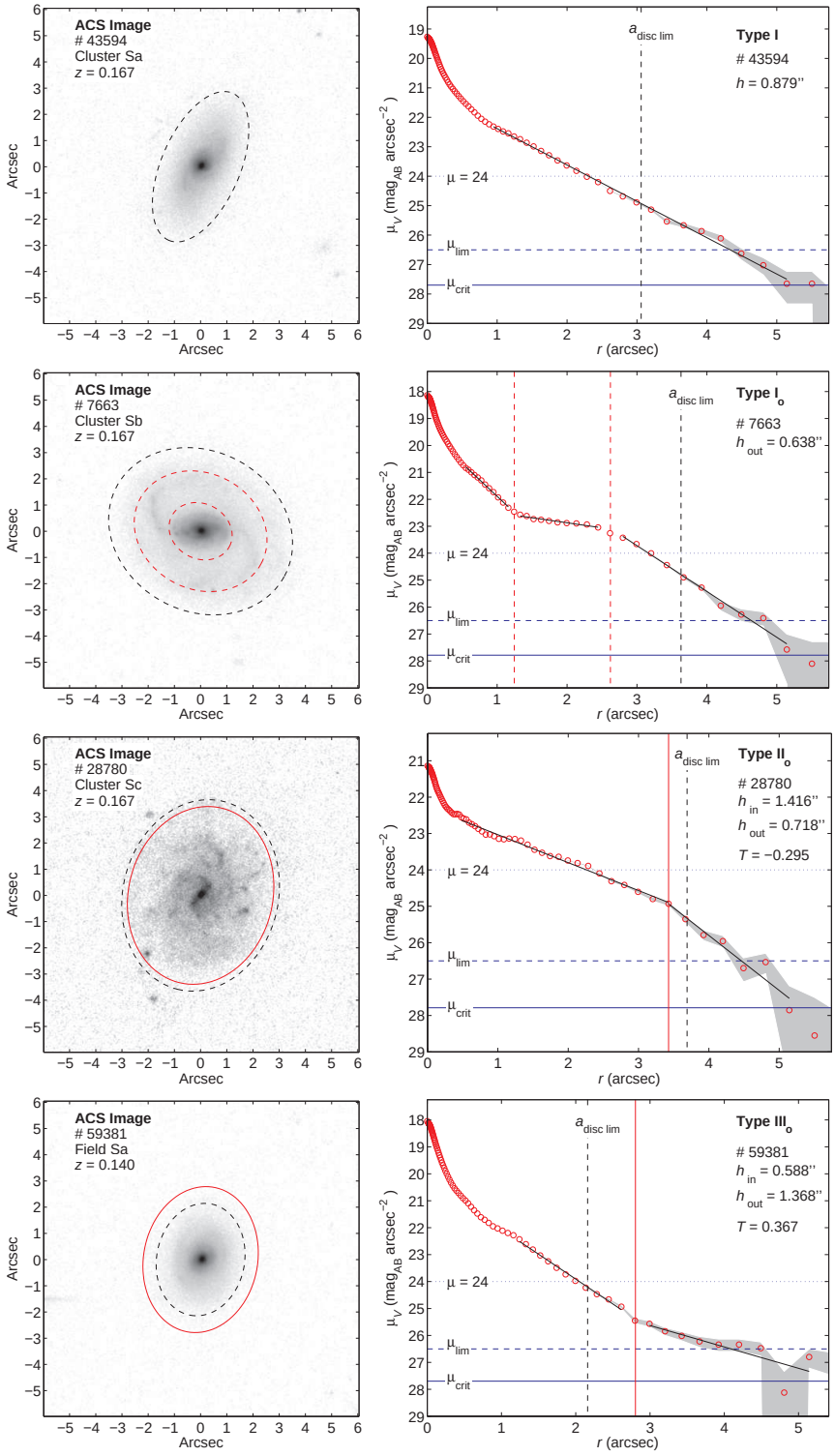

Figure 4.6. Examples of each class of profile (DTM classification). Top to bottom: Type I, Type I_o, Type II_o and Type III_o. Left-hand panels: ACS V-band images. Right-hand panels: azimuthally-averaged V-band radial surface brightness $\mu(r)$ profiles. We overplot the break radii in the outer stellar disc, $24 < \mu < 26.5\,\mathrm{mag\,arcsec^{-2}}$ (red solid lines). Also shown are break radii with $\mu_{\mathrm{brk}} < 24\,\mathrm{mag\,arcsec^{-2}}$ (red dashed lines), which are not considered in this study, and the stellar disc limit $a_{\mathrm{disc\,lim}}$ (black dashed line). The inner and outer scalelength, h_{in} and h_{out}, respectively, and the break strength T are also shown for reference. The ACS images are in a logarithmic grey-scale.

4.4.4 Measuring scalelength and break strength

In the following section, we obtain our exponential fits using a linear least-squares fit to the original $\mu(r)$ profile between the radial limits identified during the visual inspection (see Section 4.4.1).

For spiral galaxies with no $\mu(r)$ profile break in the outer stellar disc (Type $\mathrm{I_o}$ – including all Type I), we obtain the disc scalelength h using a simple exponential fit $[h = 1.086 \times \Delta r/\Delta\mu_{\mathrm{fit}}(r)]$ across the length of the disc component. For these galaxies, the mean random error in scalelength due to the exponential fitting routine is < 10 per cent. The mean systematic error in the scalelength due to the error in the sky subtraction $\pm 1\sigma$ (see Section 4.3.2) is also < 10 per cent. In the case of bulge-less spiral galaxies with pure exponential discs (i.e. Type I Sd galaxies), the disc scalelength h was also confirmed to be compatible with the GALFIT effective radius r_{e} ($r_{\mathrm{e}} \sim 1.7h$), as expected.

For spiral galaxies where a $\mu(r)$ profile break was identified in the outer disc (Type $\mathrm{II_o/III_o}$), we obtain the scalelength h of exponential fits either side of the break radius r_{brk}, and therefore obtain an inner and outer exponential fit for the stellar disc. The inner exponential disc extends from a radius of $r_{\mathrm{in,min}}$ to $r_{\mathrm{in,max}}$ and has a scalelength h_{in} given by

$$h_{\mathrm{in}} = 1.086 \times \frac{r_{\mathrm{in,max}} - r_{\mathrm{in,min}}}{\mu_{\mathrm{fit}}(r_{\mathrm{in,max}}) - \mu_{\mathrm{fit}}(r_{\mathrm{in,min}})}, \tag{4.6}$$

where μ_{fit} is the surface brightness from the exponential fit. Similarly, the outer exponential disc extends from a radius of $r_{\mathrm{out,min}}$ to $r_{\mathrm{out,max}}$ and has a scalelength h_{out} given by

$$h_{\mathrm{out}} = 1.086 \times \frac{r_{\mathrm{out,max}} - r_{\mathrm{out,min}}}{\mu_{\mathrm{fit}}(r_{\mathrm{out,max}}) - \mu_{\mathrm{fit}}(r_{\mathrm{out,min}})}. \tag{4.7}$$

For these galaxies, the mean random error in scalelength due to the exponential fitting routine is < 10 per cent for h_{in} and < 20 per cent for h_{out}.

In order to measure the strength of our Type $\mathrm{II_o/III_o}$ profile breaks, we define a break strength T as the logarithm of the outer-to-inner scalelength ratio[3]:

$$T = \log_{10} h_{\mathrm{out}}/h_{\mathrm{in}}. \tag{4.8}$$

A Type $\mathrm{I/I_o}$ galaxy (pure exponential) has no break, and therefore has a break strength of $T = 0$. A Type $\mathrm{II_o}$ galaxy (down-bending break, outer disc truncation) has a smaller outer scalelength h_{out} with respect to its inner scalelength h_{in}, and therefore has a negative break strength ($T < 0$). Similarly, a Type $\mathrm{III_o}$ galaxy (up-bending break, outer disc antitruncation) has a larger outer scalelength h_{out} with respect to its inner scalelength h_{in}, and therefore has a positive break strength ($T > 0$). For our spiral galaxies, the mean random error in T due to the exponential fitting routine is $\sim \pm 0.1$ (< 20 per cent). In order to assess the effect of the sky subtraction error (see Section 4.3.2) on our break strength T measurements, we plot break strength T against outer scalelength h_{out} for our Type $\mathrm{II_o/III_o}$ spiral galaxies (as classified by DTM) with error bars in T due to the sky subtraction error $\pm 1\sigma$ (see Fig. 4.7). The mean systematic error in T due to the sky subtraction error is also $\sim \pm 0.1$.

[3]Note: a logarithm is used to define the break strength T due to the wide range of values encountered in our measurements of outer-to-inner scalelength ratio ($h_{\mathrm{out}}/h_{\mathrm{in}}$).

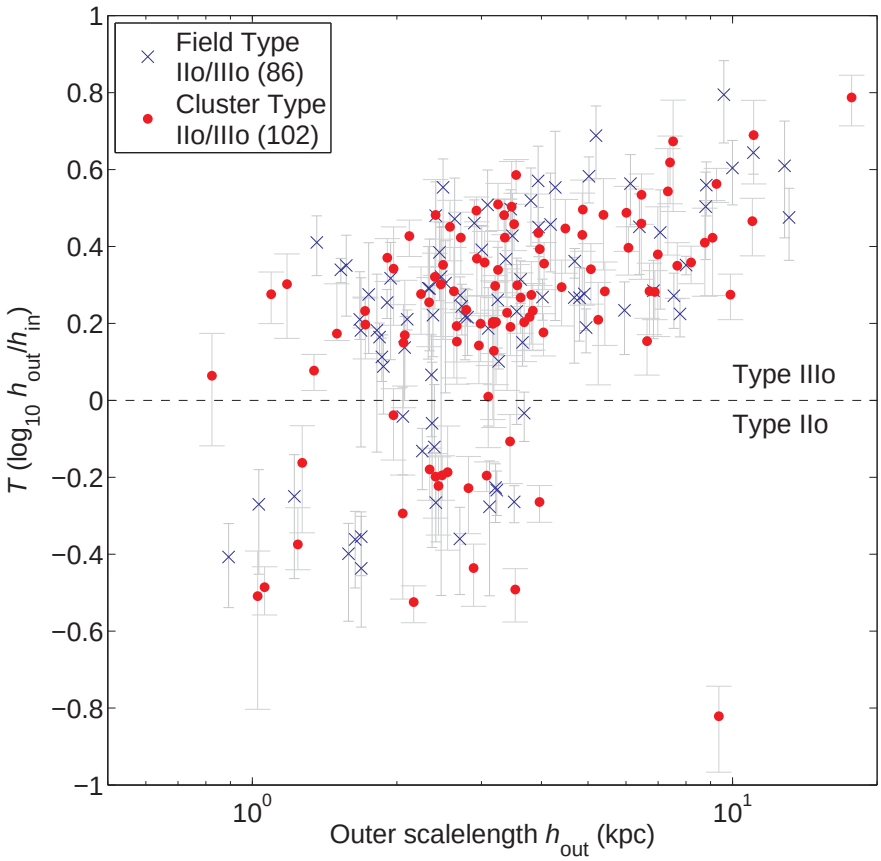

Figure 4.7. A comparison of break strength T and outer scalelength $h_{\rm out}$ for our Type $\rm II_o/III_o$ galaxies in the field (blue crosses) and cluster (red points) environment (DTM classification). An outlying cluster galaxy located at $h_{\rm out} = 453.2\,$kpc, $T = 2.382$ is not shown for clarity (object #60598; an unusual outer μ profile make T and $h_{\rm out}$ potentially uncertain for this galaxy, however this fact has no effect on our results or our conclusions). The T error bars represent the error from the sky subtraction ($\pm 1\sigma$) on a galaxy–galaxy basis. The mean error in T is ± 0.1. Respective sample sizes are shown in the legend.

We present a selection of our $\mu(r)$ profiles with fitted exponential regions and overplotted break radii for spiral galaxies from both the field and cluster environments in Figs 4.8 and 4.9, respectively.

Non-linear exponential fits

In the outer regions of the surface brightness $\mu(r)$ profile, negative sky-subtracted flux can occur. Surface brightness cannot be defined for a negative flux. Therefore, these points are absent from our linear exponential fits to surface brightness. However, this could potentially lead to a slight measurement bias and a larger outer scalelength $h_{\rm out}$ for some profiles. In order to address this issue, we repeated all measurements of scalelength ($h_{\rm in}$ and $h_{\rm out}$) and break strength T using a non-linear least-squares exponential fit to the flux radial profile (retaining negative fluxes). We then compared these results to those from the linear fits to surface brightness in order to assess if any measurement bias was present. The results from both fitting methods were in very good agreement and no bias was observed. Therefore, we use the linear fits to surface brightness in our analysis.

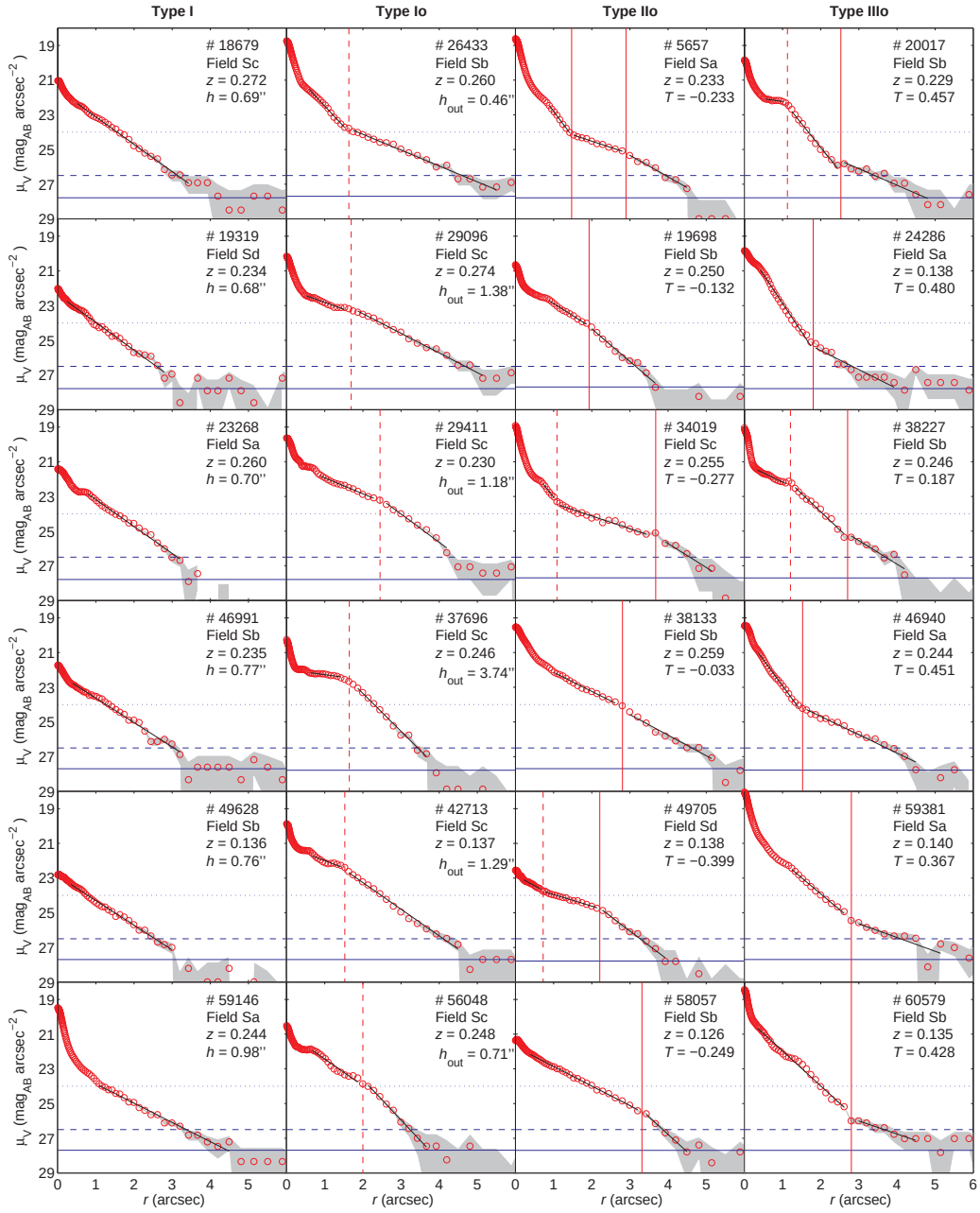

Figure 4.8. Example azimuthally-averaged radial surface brightness $\mu(r)$ profiles for different profile types in the field environment (DTM classification). First column: Type I profiles (pure exponential profiles). Second column: Type $\mathrm{I_o}$ profiles which have a simple exponential region in the outer disc ($24 < \mu_V < 26.5\,\mathrm{mag\,arcsec^{-2}}$, region between blue dashed and dotted lines). Third column: Type $\mathrm{II_o}$ profiles (down-bending break in outer disc, *outer disc truncations*). Forth column: Type $\mathrm{III_o}$ profiles (up-bending break in outer disc, *outer disc antitruncations*). The error in the $\mu(r)$ profiles is for an oversubtraction and undersubtraction of the sky by $\pm1\sigma$. The critical surface brightness μ_{crit} ($\pm1\sigma$ sky error, blue solid line) and limiting surface brightness μ_{lim} ($\pm3\sigma$ sky error, blue dashed line) are shown on the profiles. The position of outer disc profile breaks ($24 < \mu_{\mathrm{brk}} < 26.5\,\mathrm{mag\,arcsec^{-2}}$) are overplotted as red solid lines, breaks with $\mu_{\mathrm{brk}} < 24\,\mathrm{mag\,arcsec^{-2}}$ are represented by red dashed lines. The least-square exponential fits to exponential regions are overplotted on the relevant sections of the $\mu(r)$ profiles. The Hubble type, redshift z, scalelength h, and break strength T of the galaxies are also shown for reference.

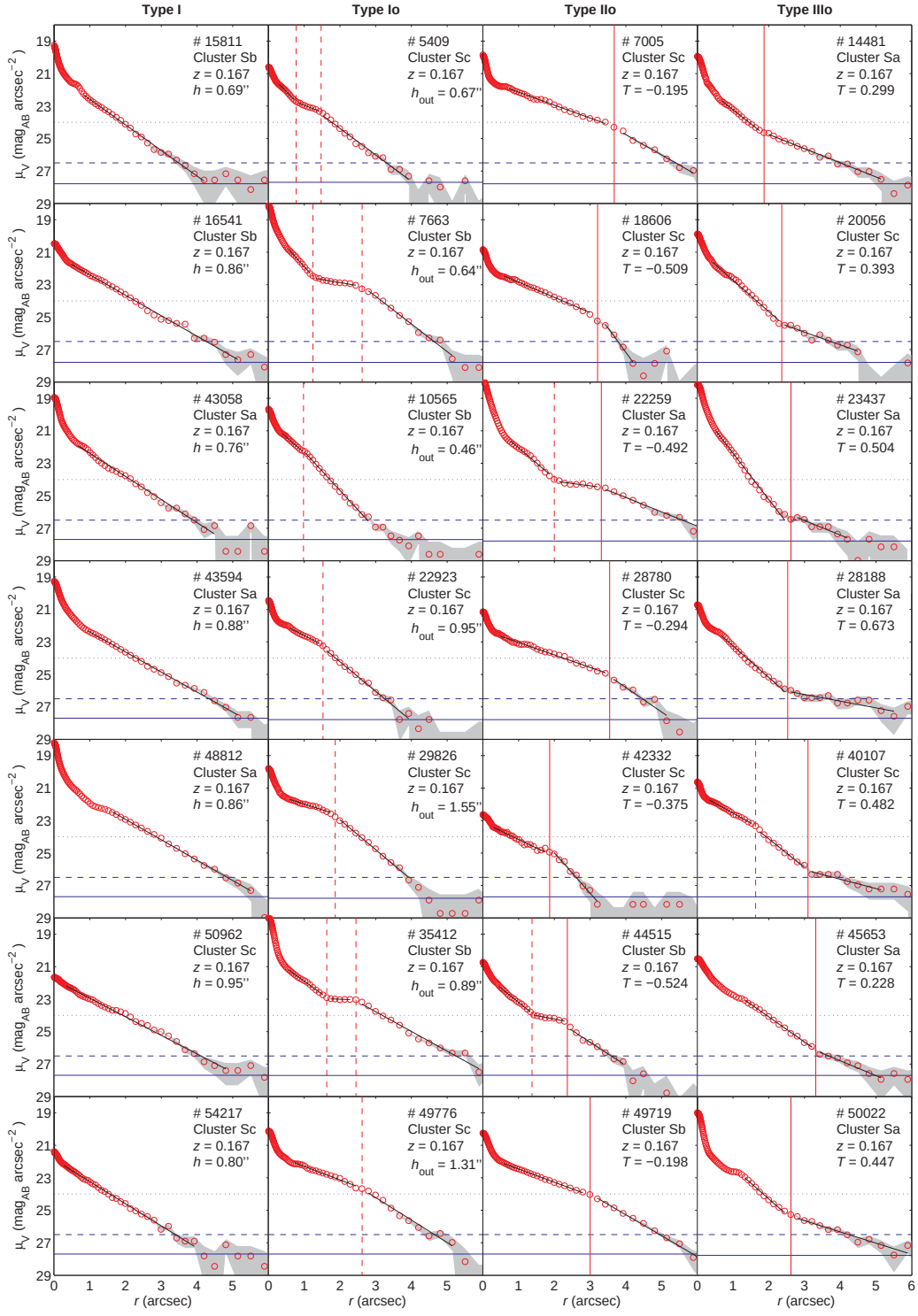

Figure 4.9. Example azimuthally-averaged radial surface brightness $\mu(r)$ profiles for different profile types in the cluster environment (DTM classification). Figure same as Fig. 4.8 but for the cluster environment.

4.5 Results

The frequencies of profile classifications by each assessor (DTM, AAS, MEG) for spiral galaxies in the field and cluster environments are shown in Table 4.3. In each case, the profile classification is based on $\mu(r)$ breaks in the outer stellar disc ($24 < \mu < 26.5\,\mathrm{mag\,arcsec^{-2}}$). The uncertainty in the frequency/fraction of profile types δf_i ($f_i = N_i/N_{\mathrm{total}}$) is calculated using

$$\left(\frac{\delta f_i}{f_i}\right)^2 = \left(\frac{\delta N_i}{N_i}\right)^2 + \left(\frac{\delta N_{\mathrm{total}}}{N_{\mathrm{total}}}\right)^2 - \frac{2\sqrt{N_i N_{\mathrm{total}}}}{N_i N_{\mathrm{total}}}, \tag{4.9}$$

where $\delta N_i = \sqrt{N_i}$ and $\delta N_{\mathrm{total}} = \sqrt{N_{\mathrm{total}}}$. This is simply the uncertainty in a fraction for correlated numerator/denominator variables[4].

Due to the subjective nature of some profile classifications, the frequency obtained for each profile type varies subtly between the different assessors. The agreement between the three assessors is generally good for the outer disc profile types (Type $\mathrm{I_o}$, $\mathrm{II_o}$ and $\mathrm{III_o}$). This agreement is very good in the cluster, but slightly weaker in the field due to most of the galaxies being at higher redshift and therefore having poorer quality profiles. There is less agreement between the three assessors for the frequency of Type I profiles (pure exponentials) due to the subjective nature of the classification of weak profile breaks across the length of the $\mu(r)$ profile and inner profile breaks near the bulge component.

The frequencies of profile types in the outer stellar disc (Type $\mathrm{I_o}$, $\mathrm{II_o}$ and $\mathrm{III_o}$) are approximately the same in the field and cluster environment. For both field and cluster spirals, $\sim$ 50 per cent have a simple exponential profile in the outer stellar disc (Type $\mathrm{I_o}$), $\sim$ 10 per cent exhibit a down-bending break (outer disc truncation, Type $\mathrm{II_o}$) and $\sim$ 40 per cent exhibit an up-bending break (outer disc antitruncation, Type $\mathrm{III_o}$). The frequency of Type I profiles is also the same in the field and cluster for each assessor and is $\sim 20 \pm 10$ per cent. We stress that due to our profile classification being based on breaks with $\mu_{\mathrm{brk}} > 24\,\mathrm{mag\,arcsec^{-2}}$, our profile-type fractions do not necessarily need to agree with those of previous works (e.g. Pohlen & Trujillo 2006). For our cluster galaxies, we also investigated the frequency of outer disc profile types as a function of stellar mass surface density (range 10^{10}–$10^{13}\,\mathrm{M_\odot\,Mpc^{-2}}$; see Section 2.2.1, for details of how this was measured). However, no significant differences were observed. These results suggest that the profile type in the outer disc of spiral galaxies is not affected by the environment from the field to the intermediate densities of the A901/2 clusters.

In this work, we define the outer disc to be $24 < \mu < 26.5\,\mathrm{mag\,arcsec^{-2}}$ (see Section 4.4.2). Our outer disc profile types are based on this somewhat arbitrary but justified definition. Independently and uniformly adjusting the upper and lower μ limits for the outer disc by $+0.5\,\mathrm{mag\,arcsec^{-2}}$ affects our profile-type fractions by < 10 per cent. In each case, there remains no significant differences between the fractions in the field and cluster environment.

The majority of our field sample have redshift $z \sim 0.23$, while the cluster galaxies have $z \sim 0.167$. However, evolutionary effects are not expected to have an impact

[4]Note: this error estimation is not accurate for small values of N_i or N_{total}, where it underestimates the true error in the population proportion. The correct method for determining such errors is described by Cameron (2011). However, in this work, Equation 4.9 provides a valid approximation in the majority of cases and any in depth determinations would be unlikely to have any significant effect on our observed trends or conclusions.

Table 4.3. The frequency of profile types in the field and cluster environments for the three independent assessors (DTM, AAS, MEG). Type I is a subsample of Type I_o and percentage errors are calculated using Equation 4.9.

Assessor	Type I	Outer disc profile types			Unclassified
		Type I_o	Type II_o	Type III_o	
Field galaxies					
DTM	17 ($12 \pm 2\,\%$)	59 ($41 \pm 2\,\%$)	18 ($12 \pm 2\,\%$)	68 ($47 \pm 2\,\%$)	0
AAS	42 ($29 \pm 3\,\%$)	76 ($52 \pm 2\,\%$)	14 ($10 \pm 2\,\%$)	55 ($38 \pm 2\,\%$)	0
MEG	38 ($26 \pm 3\,\%$)	86 ($59 \pm 2\,\%$)	16 ($11 \pm 2\,\%$)	40 ($28 \pm 3\,\%$)	3 ($2 \pm 2\,\%$)
Cluster galaxies					
DTM	28 ($15 \pm 2\,\%$)	80 ($44 \pm 2\,\%$)	19 ($10 \pm 2\,\%$)	83 ($46 \pm 2\,\%$)	0
AAS	48 ($26 \pm 2\,\%$)	83 ($46 \pm 2\,\%$)	23 ($13 \pm 2\,\%$)	74 ($41 \pm 2\,\%$)	2 ($1 \pm 1\,\%$)
MEG	48 ($26 \pm 2\,\%$)	88 ($48 \pm 2\,\%$)	17 ($9 \pm 2\,\%$)	69 ($38 \pm 2\,\%$)	8 ($4 \pm 2\,\%$)

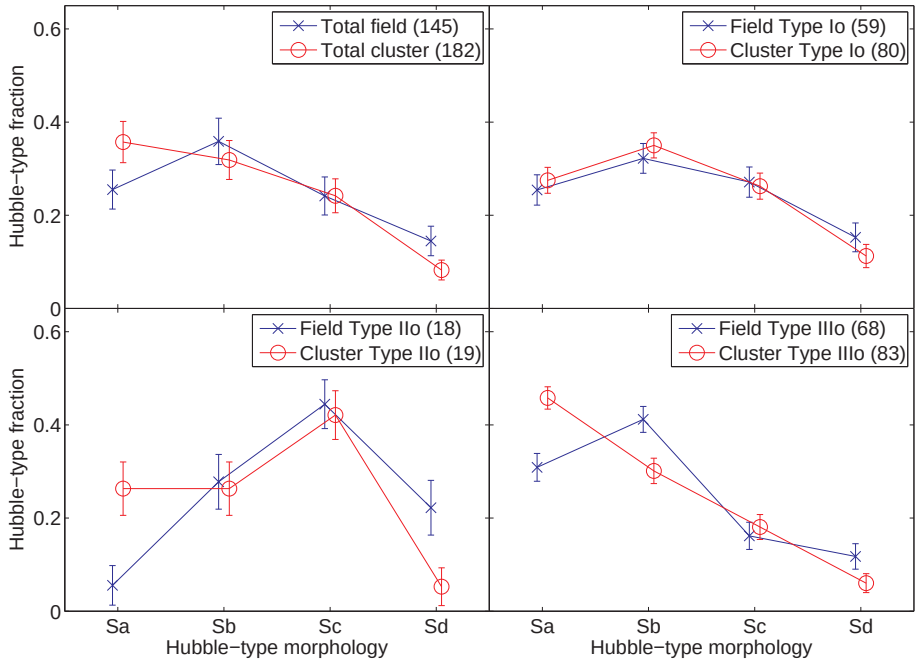

Figure 4.10. The morphological mix for outer disc profile types (DTM classification). The fraction of each Hubble type in the field (crosses) and cluster (circles) environment for the total spiral galaxy sample (top left), Type I_o galaxies (top right), Type II_o galaxies (bottom left) and Type III_o galaxies (bottom right). Respective sample sizes are shown in the legends, and the errors in the Hubble-type fraction were calculated using Equation 4.9. Contamination of the cluster sample by the field is < 25 per cent. We observe no significant difference between the morphological mix in the field and cluster for each profile type.

on the results of this work. The break strength T of our field galaxies shows no correlation with redshift, and evolutionary effects on the scalelength h between the mean redshifts of our field and cluster samples is only ~ 5 per cent (based on the fits of Buitrago et al. 2008, for the expected size evolution of massive disc galaxies).

4.5.1 Morphology

For each outer disc profile type (Type I_o, II_o and III_o), we compare the morphological mix (Sa, Sb, Sc, Sd) in the field and cluster environment to that of the total spiral galaxy sample (see Fig. 4.10). We also considered whether or not the spiral galaxies exhibited a central bar.

The morphological mix of the total galaxy sample is approximately the same in the field and cluster, with perhaps a slight excess of Sa galaxies in the cluster environment (Sa galaxies are visually defined to have a high B/D; see Section 2.1). This excess is dominated by barred Sa galaxies. For each outer disc profile type (Type I_o, II_o and III_o), the morphological mix is also approximately the same in the field and cluster environment. However, there is a potential slight excess of Sa galaxies in the cluster for both Type II_o and III_o galaxies. In both cases, the excess is dominated by barred Sa galaxies. Except for the slight excess of barred Sa galaxies in the cluster, the morphological mix for barred and unbarred galaxies is the same in the field and cluster for each profile type.

The morphological mix of Type I_o galaxies is comparable to that of the total galaxy sample. This implies that Type I_o galaxies are equally probable for all

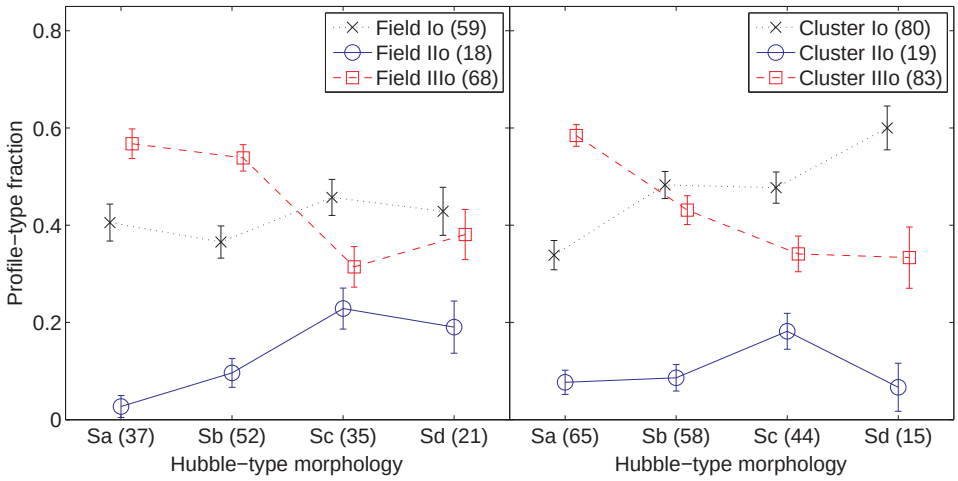

Figure 4.11. The fraction of outer disc profile types, Type I_o (crosses), Type II_o (circles) and Type III_o (squares) for different spiral Hubble-type morphologies in the field (left-hand panel) and cluster (right-hand panel) environment (DTM classification). The sample size for each profile type is shown in the legends and the sample size for each Hubble type is shown on the x-axis. The errors in the profile type fraction were calculated using Equation 4.9. Contamination of the cluster sample by the field is < 25 per cent. We observe similar trends for both field and cluster galaxies. The fraction of Type I_o is approximately constant with Hubble type, perhaps rising slightly towards later Hubble types in the cluster. However, the fraction of Type II_o galaxies (truncations) increases slightly towards later Hubble types, while the fraction of Type III_o galaxies (antitruncations) decreases.

morphological types. For Type II_o galaxies, the morphological mix fractions are affected by low number statistics. However, there is a clear trend with the Hubble-type fraction (Sa–Sc) rising towards later Hubble types. For Type III_o galaxies, the morphological mix is also comparable to that of the total galaxy sample. There is also a clear trend with the Hubble-type fraction (Sa–Sd) decreasing towards later Hubble types.

We conclude that outer disc truncations (Type II_o) are more prevalent in later Hubble types, while outer disc antitruncations (Type III_o) are more prevalent in early Hubble types. However, there is no evidence to suggest the morphological mix for the different outer disc profile types is affected by the galaxy environment.

We also compare the frequency of outer disc profile types (Type I_o, II_o and III_o) for different Hubble-type morphologies (Sa, Sb, Sc, Sd) in both the field and cluster environment (see Fig. 4.11). For Type I_o galaxies, we observe no clear correlation between the frequency of profile type and the Hubble type in both the field and cluster environment. The frequency of Type I_o galaxies is approximately the same for each Hubble-type morphology, perhaps raising slightly towards later Hubble types in the cluster environment. For Type II_o and Type III_o galaxies, a weak trend is observed between the frequency of profile type and the Hubble type in both the field and cluster environments. The frequency of Type II_o galaxies increases slightly towards later Hubble types, while the frequency of Type III_o galaxies decreases. For Sd galaxies, low number statistics could be masking the continuation of these trends. These results are in qualitative agreement with the work of Pohlen & Trujillo (2006) who find a clear correlation between the frequency of profile type and Hubble type using a sample of ~ 90 nearby galaxies from SDSS (classification based on μ breaks across the entire stellar disc so direct comparisons cannot be made). We conclude

that there is no significant difference between the frequency of outer disc profile types for different Hubble-type morphologies in the field and cluster environments.

4.5.2 Pure exponential outer discs (Type $\mathrm{I_o}$)

For spiral galaxies where no outer disc $\mu(r)$ break was identified (Type $\mathrm{I_o}$ galaxies, which include all Type I galaxies), we compare the outer scalelength h_{out} distributions in the field and cluster environments to see if there is any evidence for an environmental dependence on outer scalelength h_{out} (see Fig. 4.12). We use the fixed cluster redshift ($z_{\mathrm{cl}} = 0.167$) to determine the intrinsic outer scalelengths of our cluster Type $\mathrm{I_o}$ galaxies and the original COMBO-17 photometric redshift estimate for our field Type $\mathrm{I_o}$ galaxies. Therefore, photo-z errors only propagate into the intrinsic scalelengths of our field galaxies and not our cluster galaxies. The mean error in h_{out} associated with the photo-z error is < 10 per cent (i.e. distance to galaxy error, see Section 3.4.1).

In our $\mu(r)$ profiles, the error in the GALAPAGOS sky (see Section 4.3.2) can have a significant effect on the scalelength h and break strength T, especially in the outer regions where the surface brightness μ approaches the critical surface brightness μ_{crit} ($27.7\,\mathrm{mag\,arcsec^{-2}}$). However, for any particular galaxy the sky subtraction error can be taken to be approximately constant across the length of the $\mu(r)$ profile. Therefore, we can account for this error by performing parallel analyses for when the sky background is oversubtracted and undersubtracted by $\pm 1\sigma$. The mean error in h_{out} due to the sky subtraction error is $\sim \pm 0.3\,\mathrm{kpc}$ (< 10 per cent) for our Type $\mathrm{I_o}$ galaxies. Random errors in h_{out} due to the exponential fitting routine are also typically < 10 per cent (see Section 4.4.4). We also perform parallel analyses on the Type $\mathrm{I_o}$ samples generated by the three assessors (DTM, AAS, MEG) in order to account for the subjective nature of the profile classifications and compare the final results.

In all cases (all parallel analyses), we observe no clear difference between the distributions of outer disc scalelength h_{out} for our Type $\mathrm{I_o}$ spiral galaxies in the field and cluster environments (see Fig. 4.12).

In order to test the significance of these results, we construct outer disc scalelength h_{out} cumulative distribution functions (CDFs; see Fig. 4.12) for our Type $\mathrm{I_o}$ galaxy samples and perform K–S tests between corresponding samples from the field and cluster environments. These K–S tests are used in order to obtain the probability that the field and cluster Type $\mathrm{I_o}$ samples are *not* drawn from the same continuous h_{out} distributions. The results of these K–S tests are shown in Table 4.4.

In this work, we only consider an environmental effect on the Type $\mathrm{I_o}$ outer scalelength h_{out} to be significant if K–S tests yield a 2σ level probability for the field and cluster Type $\mathrm{I_o}$ galaxy samples *not* being drawn from the same continuous h_{out} distributions. This probability $p_{(\mathrm{field/cluster})}$ is below the 2σ level for each assessor and for when the sky background is oversubtracted and undersubtracted by $\pm 1\sigma$. Therefore, we find no evidence to suggest that the outer disc scalelength h_{out} of Type $\mathrm{I_o}$ galaxies is dependent on the galaxy environment.

We perform the same analysis for Type I galaxies, a subsample of Type $\mathrm{I_o}$ galaxies. These galaxies have a simple exponential $\mu(r)$ profile across the length of their disc component. The K–S test results for these galaxies are shown in Table 4.4. The probability $p_{(\mathrm{field/cluster})}$ is below the 2σ level in each case. Therefore, we also find no evidence to suggest that the scalelength h of Type I galaxies is dependent on the galaxy environment.

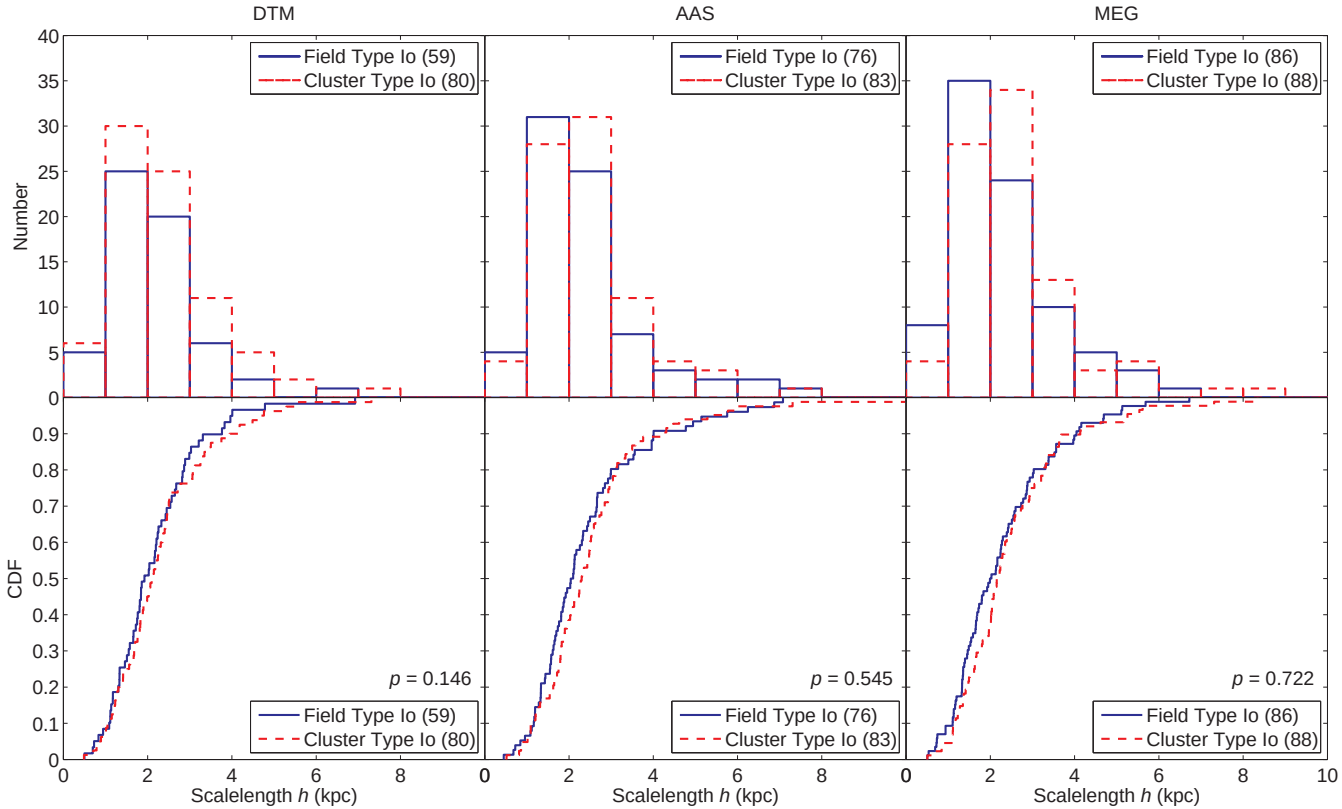

Figure 4.12. Comparing outer disc scalelength $h_{\rm out}$ distributions in different environments. Top row: outer disc scalelength $h_{\rm out}$ distributions for Type $\rm I_o$ galaxies in the field (blue line) and cluster (red dashed line) environment as classified by DTM (left-hand panel), AAS (centre panel) and MEG (right-hand panel). Bottom row: the corresponding outer scalelength $h_{\rm out}$ CDFs showing the probability p that compared samples are *not* drawn from the same continuous $h_{\rm out}$ distributions in the bottom right of each plot. Respective sample sizes are shown in the legends. Random errors in scalelength are typically < 10 per cent. Systematic errors in scalelength due to the error in the sky subtraction are also typically < 10 per cent. Contamination of the cluster sample by the field is < 25 per cent. We find no significant difference between the CDFs in each environment and no evidence to suggest that the outer scalelength $h_{\rm out}$ of our Type $\rm I_o$ galaxies are *not* drawn from the same continuous $h_{\rm out}$ distributions.

4.5.3 Broken exponential outer discs (Type $\mathrm{II_o/III_o}$)

For our Type $\mathrm{II_o}$ and $\mathrm{III_o}$ spiral galaxies, we compare the distribution of break strength T in the field and cluster environments to see if there is any evidence for an environmental dependence on break strength T in the outer disc (see Fig. 4.13). We perform similar parallel analyses and statistical tests as for our Type $\mathrm{I_o}$ galaxies. The mean error in T due to the sky subtraction error is ± 0.1 and random errors in T due to the exponential fitting routine are also typically ± 0.1 (see Section 4.4.4). The results of the K–S tests are shown in Table 4.4.

In all cases (all assessor samples and sky versions), we observe no clear difference between the T distributions in the field and cluster environments. The probability $p_{(\mathrm{field/cluster})}$ is below the 2σ level in each case. Therefore, we find no evidence to suggest that the break strength T of our Type $\mathrm{II_o/III_o}$ galaxies is dependent on the galaxy environment, and this result is robust to the error in the sky background and the subjective nature of the profile classifications.

We explore this result by splitting the combined field and cluster Type $\mathrm{II_o/III_o}$ galaxy sample into two subsamples about the median stellar mass $M_{*,\mathrm{mdn}}$ ($10^{10}\,\mathrm{M_\odot}$). Similar statistical tests are then used to determine the significance of an environmental dependence independently for high-mass ($M_* > M_{*,\mathrm{mdn}}$) and low-mass ($M_* < M_{*,\mathrm{mdn}}$) Type $\mathrm{II_o/III_o}$ galaxies. A similar test was also performed using $B-V$ colour instead of stellar mass, where B and V were obtained from the STAGES data catalogue (Gray et al. 2009) and $(B-V)_{\mathrm{mdn}} = 0.70\,\mathrm{mag}$. In all cases (all assessor samples and sky versions), the significance of an environmental dependence on break strength T remains below the 2σ level. Therefore, we conclude that there is no evidence to suggest an environmental dependence on break strength T is dependent on either the stellar mass or the $B-V$ colour of Type $\mathrm{II_o/III_o}$ galaxies.

Another test performed was a comparison of the break radius r_{brk} (in units of the GALFIT effective radius) in the field and cluster environments for both our Type $\mathrm{II_o}$ ($T < 0$) and Type $\mathrm{III_o}$ ($T > 0$) galaxies separately. In both cases, no significant difference ($< 2\sigma$) was observed between the break radius in the field and cluster environments. However, there is a slight indication that Type $\mathrm{II_o}$ breaks occur at smaller break radii than Type $\mathrm{III_o}$ breaks.

We also plot the break strength T of our Type $\mathrm{II_o/III_o}$ galaxies against the effective radius r_{e} determined by the STAGES GALFIT Sérsic models (Gray et al. 2009) (see Fig. 4.14). The size–break-strength distribution is the same for both field and cluster galaxies. However, we note that at small effective radii ($r_{\mathrm{e}} < r_{\mathrm{e,mdn}}$) there is an absence of Type $\mathrm{II_o}$ galaxies (outer disc truncations, $T < 0$) in both the field and cluster environments. $r_{\mathrm{e,mdn}}$ (3.58 kpc; DTM classification) is the median effective radius of the combined field and cluster Type $\mathrm{II_o/III_o}$ galaxy sample. In contrast, there is an abundance of Type $\mathrm{III_o}$ galaxies (outer disc antitruncations, $T > 0$) reaching down to $r_{\mathrm{e}} \sim 1\,\mathrm{kpc}$. A comparison of the break strength T distributions for large-r_{e} ($r_{\mathrm{e}} > r_{\mathrm{e,mdn}}$) and small-$r_{\mathrm{e}}$ ($r_{\mathrm{e}} < r_{\mathrm{e,mdn}}$) galaxies shows a clear difference in the two distributions (see Fig. 4.14).

In order to test the significance of this result, we construct break strength T CDFs (see Fig. 4.14), for large- and small-r_{e} Type $\mathrm{II_o/III_o}$ galaxies and perform K–S tests between the large- and small-r_{e} galaxy samples to obtain the probability the different samples are *not* drawn from the same continuous break strength T distributions. Similar parallel analyses are also performed as in previous tests.

In all cases (all assessor samples and sky versions), the probability that the large- and small-r_{e} galaxy samples $p_{(\mathrm{large}\text{-}r_{\mathrm{e}}/\mathrm{small}\text{-}r_{\mathrm{e}})}$ are being drawn from different

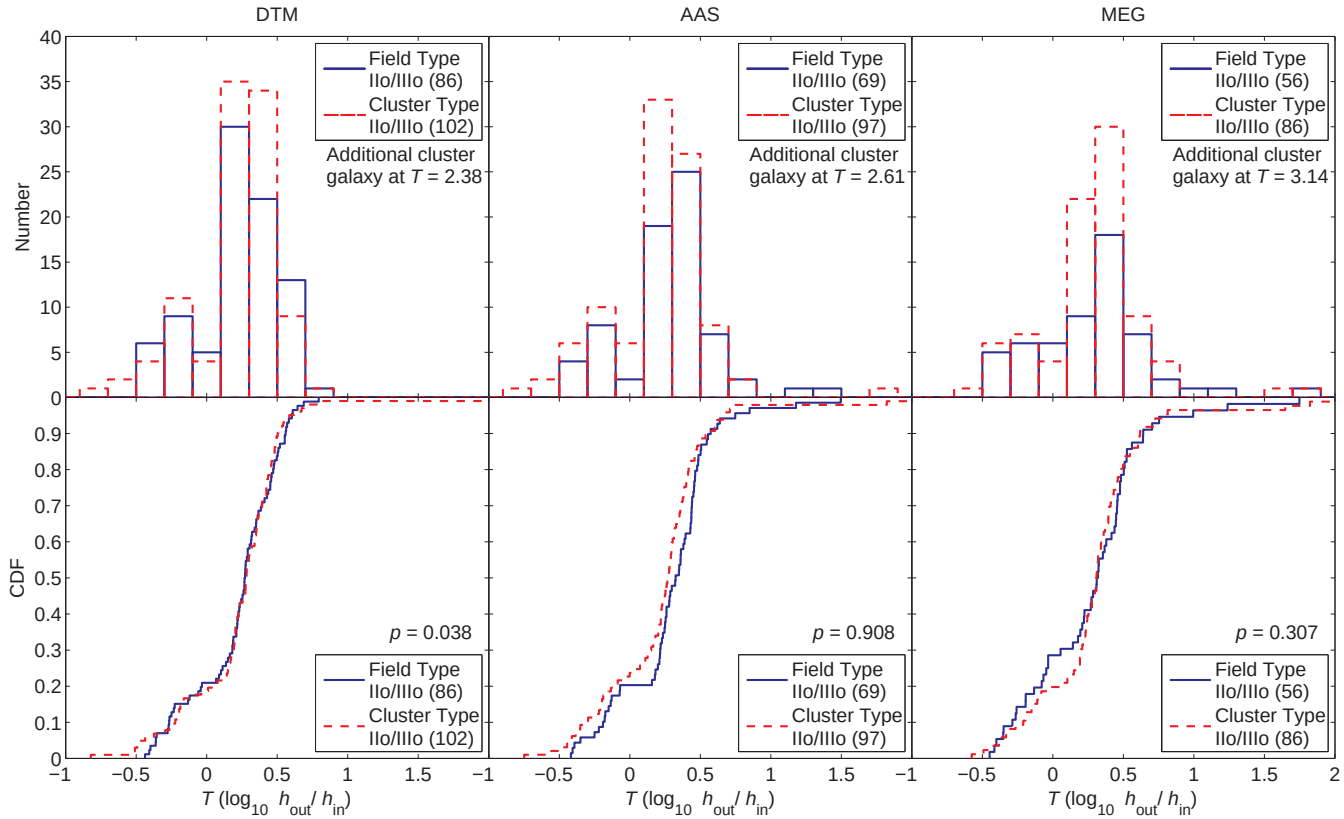

Figure 4.13. Comparing break strength T ($\log_{10} h_{\rm out}/h_{\rm in}$) distributions in different environments. Top row: break strength T distributions for Type $\rm II_o/III_o$ galaxies in the field (blue line) and cluster (red dashed line) environment as classified by DTM (left-hand column), AAS (centre column) and MEG (right-hand column). Bottom row: the corresponding break strength T CDFs showing the probability p that compared samples are *not* drawn from the same continuous T distributions in the bottom right of each plot. Respective sample sizes are shown in the legends. Random errors in break strength T are typically < 0.1. Systematic errors in break strength due to the error in the sky subtraction are also $\sim \pm 0.1$. Contamination of the cluster sample by the field is < 25 per cent. We find no significant difference between the CDFs in each environment and no evidence to suggest that the break strength T of our Type $\rm II_o/III_o$ galaxies are *not* drawn from the same continuous $h_{\rm out}$ distributions.

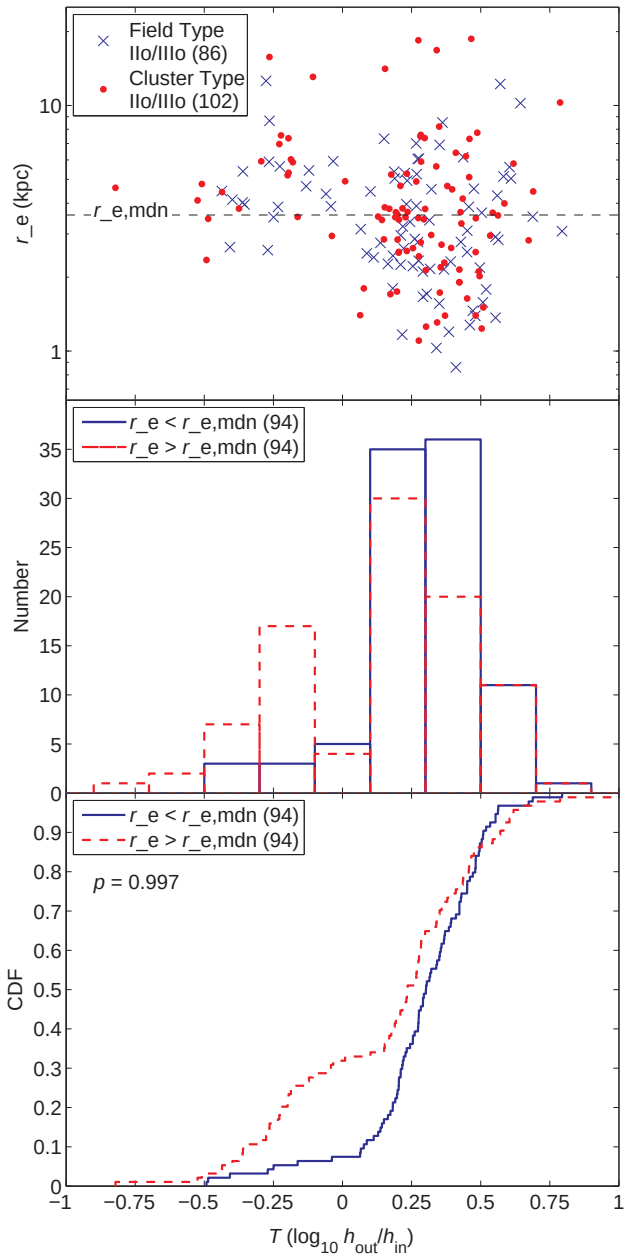

Figure 4.14. A plot of the break strength T ($\log_{10} h_{\rm out}/h_{\rm in}$) against the physical size $r_{\rm e}$ for our Type $\rm II_o/III_o$ galaxies (DTM classification). Top panel: the effective radius $r_{\rm e}$–break-strength T distributions for our field (blue crosses) and cluster (red points) Type $\rm II_o/III_o$ galaxies, showing the position of the median effective radius $r_{\rm e,mdn}$ (3.58 kpc) of the combined field and cluster sample (black dashed line). An outlying cluster galaxy, located at $T = 2.382$, $r_{\rm e} = 4.442$ kpc is not shown for clarity. Middle panel: a comparison of the distribution of break strength T for small-$r_{\rm e}$, $r_{\rm e} < r_{\rm e,mdn}$ (blue line) and large-$r_{\rm e}$, $r_{\rm e} > r_{\rm e,mdn}$ (red dashed line) Type $\rm II_o/III_o$ galaxies. Bottom panel: a comparison of the break strength T CDFs for small-$r_{\rm e}$ (blue line) and large-$r_{\rm e}$ (red dashed line) Type $\rm II_o/III_o$ galaxies. The probability p that the small-$r_{\rm e}$ and large-$r_{\rm e}$ Type $\rm II_o/III_o$ samples are *not* drawn from the same continuous break strength T distributions is shown in the top left of the plot. Respective sample sizes are shown in the legends. We find a significant difference between the CDFs of the small-$r_{\rm e}$ and large-$r_{\rm e}$ Type $\rm II_o/III_o$ samples with a high probability (at the 3σ level) that the samples are *not* drawn from the same continuous break strength T distributions.

Table 4.4. The K–S test results for Type I, Type I_o, and Type II_o/III_o galaxies as classified by DTM, AAS and MEG. K–S tests give the probability $p_{(\mathrm{field/cluster})}$ that the respective field and cluster samples are *not* drawn from the same continuous h distributions for Type I and Type I_o galaxies, and T distributions for Type II_o/III_o galaxies. Results are also shown for when the sky is oversubtracted and undersubtracted by $\pm 1\sigma$. We find no environmental dependence on either the scalelength h of Type I and Type I_o galaxies or the break strength T of Type II_o/III_o galaxies.

	$p_{(\mathrm{field/cluster})}$		
Sky subtraction	Under (-1σ)	Nominal	Over ($+1\sigma$)
Type I (h)			
DTM	0.078	0.101	0.167
AAS	0.825	0.761	0.865
MEG	0.952	0.919	0.921
Type I_o (h)			
DTM	0.096	0.146	0.186
AAS	0.545	0.545	0.859
MEG	0.797	0.722	0.386
Type II_o/III_o (T)			
DTM	0.165	0.038	0.122
AAS	0.797	0.908	0.795
MEG	0.180	0.307	0.563

continuous break strength T distributions is at the 3σ level. Therefore, we find some evidence to suggest that the break strength T of Type II_o/III_o galaxies is dependent on the galaxy's effective radius r_e, with outer disc truncations (Type II_o) being absent from small galaxies ($r_e < r_{e,mdn}$). Interestingly, this trend disappears when using breaks classified across the entire length of the disc component (i.e. Type II/III). This implies that only truncations in the *outer* galactic regions ($\mu > 24\,\mathrm{mag\,arcsec^{-2}}$) are rare in small galaxies (not truncations in general). At present, our current understanding of the nature of stellar disc truncations (see Section 4.1) is not sufficient to provide a satisfactory interpretation of this result. Therefore, this result is left open for future observations/studies to provide a suitable explanation.

4.5.4 Inner/initial disc breaks

The focus of this study is on the effect of the environment on the structure of the outer regions of galactic discs. By examining only breaks in the outer disc ($\mu > 24\,\mathrm{mag\,arcsec^{-2}}$), we have tailored our analysis to allow for the assessment of an environmental effect on the outer regions of the galactic disc, where the environment is most likely to have an effect. However, we acknowledge that there is some potential for missed environmental effects in breaks at a higher surface brightness ($\mu < 24\,\mathrm{mag\,arcsec^{-2}}$). Therefore, in order to test whether we could have missed any environmental effect in the inner disc, we repeated our analysis using the inner/initial

break for profile classification. However, we find no correlations of the frequency of profile type with the galaxy environment. We also find no significant effect of the environment on either the scalelength h of Type I galaxies (pure exponentials), or the break strength T of inner/initial breaks.

4.6 Conclusions

We present an analysis of V-band radial surface brightness $\mu(r)$ profiles for spiral galaxies from the field and cluster environments using *HST*/ACS imaging and data from STAGES. Using a large, mass-limited ($M_* > 10^9\,\mathrm{M}_\odot$), visually-classified sample of ~ 330 field and cluster spiral galaxies, we assess the effect of the galaxy environment on the $\mu(r)$ profile in the outer stellar disc ($\mu > 24\,\mathrm{mag\,arcsec}^{-2}$).

We classify our spiral galaxies according to $\mu(r)$ break features in their outer disc. If the galaxy has no break in this μ range, then the galaxy has a simple exponential profile in the outer disc and is classified as Type $\mathrm{I_o}$. Galaxies that have a simple exponential profile across the length of their disc component (Type I, a subset of Type $\mathrm{I_o}$) are also identified. However, if the galaxy exhibits a broken exponential in the outer disc, it is classified as either Type $\mathrm{II_o}$ for a down-bending break (outer disc truncation) or Type $\mathrm{III_o}$ for an up-bending break (outer disc antitruncation).

The frequency of outer disc profile types (Type $\mathrm{I_o}$, $\mathrm{II_o}$ and $\mathrm{III_o}$) is approximately the same in both the field and cluster environment. For both field and cluster spirals, ~ 50 per cent have a simple exponential profile in the outer stellar disc (Type $\mathrm{I_o}$), ~ 10 per cent exhibit a down-bending break (outer disc truncation, Type $\mathrm{II_o}$) and ~ 40 per cent exhibit an up-bending break (outer disc antitruncation, Type $\mathrm{III_o}$). These results imply that the shape of the outer disc $\mu(r)$ profile is not dependent on the galaxy environment. These results agree for break classifications performed by three independent assessors. However, we stress that due to our profile classification being based on breaks with $\mu_{\mathrm{brk}} > 24\,\mathrm{mag\,arcsec}^{-2}$, our profile type fractions do not necessarily need to agree with those of previous works (e.g. Pohlen & Trujillo 2006).

We also find that the morphological mix (Sa, Sb, Sc, Sd) of the different outer disc profile types is approximately the same in the field and cluster environment. However, we do find a dependence of the shape of the $\mu(r)$ profile in the outer stellar disc on the Hubble type. Outer disc truncations are slightly more frequent in later Hubble types, while the outer disc antitruncations are slightly more frequent in earlier Hubble types. The same dependence is observed in both the field and the cluster environments. This result is in qualitative agreement with that of Pohlen & Trujillo (2006), who find a similar correlation using galaxies from SDSS (classification based on entire disc component so direct comparisons cannot be made).

For spiral galaxies with a pure exponential outer stellar disc (Type $\mathrm{I_o}$, ~ 50 per cent), we find no evidence to suggest an environmental dependence on the outer disc scalelength h_{out}. We also find no evidence for an environmental dependence on the scalelength h for galaxies that have a pure exponential profile across the length of their disc component (Type I, a subset of Type $\mathrm{I_o}$). For galaxies with a broken exponential in their outer stellar disc, either down-bending (Type $\mathrm{II_o}$, outer disc truncation, ~ 10 per cent) or up-bending (Type $\mathrm{III_o}$, outer disc antitruncation, ~ 40 per cent), we measure the break strength T as the outer-to-inner scalelength ratio $\log_{10} h_{\mathrm{out}}/h_{\mathrm{in}}$. We also find no evidence to suggest an environmental dependence on this break strength T. We conclude that there is no evidence to suggest the stellar distribution in the outer stellar disc is affected by the galaxy environment for

these galaxies. These results have been shown to be robust to the sky subtraction error and to agree for break classifications performed by three independent assessors. This work is in qualitative agreement with the work of Pohlen & Trujillo (2006), who come to a similar conclusion for a sample of ~ 90 spiral galaxies from SDSS (classification based on entire disc component).

We also find that for galaxies with small effective radii ($r_e < 3\,\mathrm{kpc}$), Type $\mathrm{II_o}$ profiles (outer disc truncations) are rare in both the field and cluster environments. In contrast, Type $\mathrm{III_o}$ (outer disc antitruncations) are commonplace.

Our results suggest that the galaxy environment has no effect on the stellar distribution in the outer stellar disc of spiral galaxies from the field to the intermediate densities of the A901/2 clusters. This implies that the origin of broken exponentials is related to an internal mechanism (e.g. star formation threshold, resonance phenomenon) or minor mergers. Our results are consistent with previous work carried out on the effect of the galaxy environment on disc features in the STAGES survey. Marinova et al. (2009) find that the optical fraction of bars among disc galaxies does not show evidence for any strong variation between the field and the A901/2 clusters, suggesting that the mass redistribution associated with bar formation within galactic discs is not a strong function of environment from the field to intermediate densities. However, it is important to note that STAGES only covers an intermediate-density environment (see Heiderman et al. 2009) and not a high-density environment (e.g. the Coma cluster; The & White 1986). Therefore, it is important to investigate the effect of the environment on the outer disc structure at higher densities.

The results presented here are for one survey field and one multicluster complex: therefore, it is also important to investigate the environmental dependence of the outer disc structure of spiral galaxies in different surveys and across a wide redshift range. The results of such studies will enable the evolution of the outer disc to be investigated in different galaxy environments. Also, the investigation into the origin of broken exponentials will depend on multiwavelength data being used to create colour profiles and stellar mass distributions. This will allow an assessment of whether the origin of broken exponentials is due to the distribution of stellar mass or a radial change in the age of the stellar population.

Chapter 5

The structure of galactic discs and the galaxy environment: S0 galaxies

In this chapter, we explore the effect of the galaxy environment on the structure of galactic discs in *S0* galaxies using *HST*/ACS imaging and data from the STAGES survey (see Chapter 2). This work is analogous to the companion study presented in Chapter 4, which explores the effect of the galaxy environment on the structure of galactic discs in STAGES *spiral* galaxies.

In Chapter 4, we concluded that there was no evidence to suggest the galactic discs of our spiral galaxies were affected by the galaxy environment (see Section 4.6). However, environmental processes inherent to galaxy evolution (e.g. ram-pressure stripping, mergers and harassment, see Section 1.2) may act on such timescales that any observed signatures are only apparent after the spiral galaxies have evolved into S0s. Consequently, the light profiles of S0 galaxies may exhibit some dependence on the galaxy environment, even if spiral galaxies do not. Additionally, comparisons of galactic disc structure between spiral and S0 galaxies may aid in our understanding of the evolutionary paths between these morphologies. The work presented in this chapter aims to explore these hypotheses.

The majority of the work described in this chapter is to be presented in the Maltby et al. (2012c) paper. This paper explores the effect of the galaxy environment on the shape of V-band radial surface brightness $\mu(r)$ profiles for relatively local S0 galaxies ($z < 0.3$) and also compares the galactic disc structure in these S0s with the spiral galaxies from Chapter 4. In this work, all the profile fitting and statistical analyses are my own work. However, the photometric redshifts z and critical estimates of the sky background (see Section 5.3.1) used throughout this study, are drawn from the STAGES data catalogue published by Gray et al. (2009).

5.1 Introduction

The light profiles of S0 galaxies exhibit smooth exponentially declining stellar discs. Consequently, S0s can be classified according to break features in the disc component of their radial surface brightness $\mu(r)$ profiles (see Sections 1.3.2 and 4.1). The three profile types: Type I (no break, pure exponential); Type II (down-bending break, *truncation*); and Type III (up-bending break, *antitruncation*) apply equally to both spiral and S0 galaxies. For a review of the structure of galactic discs (applicable to both spiral and S0 galaxies), including the current theories on their origin, see Chapter 4 (Section 4.1).

Investigating the frequency of profile types for different morphologies and in regions of different galaxy density, is a useful tool for exploring galaxy evolution and the role of the galaxy environment. However, presently there have only been a few systematic searches for broken exponentials in stellar discs (e.g. Pohlen & Trujillo 2006; Azzollini et al. 2008; Erwin et al. 2008, 2012; Gutiérrez et al. 2011; and Chapter 4) and these rarely span the full range of disc morphologies (S0–Sdm). Pohlen & Trujillo (2006) use a local sample of ~ 90 late-type spirals (Sb–Sdm) and find the distribution of profile types I:II:III is approximately 10:60:30 per cent. However, Erwin et al. (2008) use a local sample of 66 early-type disc galaxies (S0–Sb) and find a distribution of approximately 30:40:25 per cent (the remaining ~ 5 per cent contained both Type II and Type III features). The differences in the profile-type fractions between these two authors can easily be attributed to the morphological range of their respective samples. This is because the shape of spiral galaxy $\mu(r)$ profiles is dependent on the spiral morphology, with Type II profiles being more frequent in later Hubble types, and Type III profiles being more frequent in earlier Hubble types (e.g. Pohlen & Trujillo 2006; and Chapter 4: Fig. 4.11). Consequently, the Hubble-type morphology is a very important consideration when investigating the effect of the galaxy environment on the structure of galactic discs.

Presently, there has been very little effort afforded to the effect of the galaxy environment on the structure of galactic discs in S0 galaxies. However, recently Erwin et al. (2012) have discovered an intriguing environmental dependence on the shape of S0 $\mu(r)$ profiles in the Virgo cluster. Using a sample of ~ 70 field and cluster S0 galaxies, they find that the distribution of profile types I:II:III is 25:25:50 per cent in the field, while in the cluster the distribution is 50:0:50 per cent. Thus their cluster S0s show a complete lack of Type II profiles. The origin of this result is uncertain and requires further verification by studies in other survey fields.

The aim of this study is to perform a systematic search for broken exponential stellar discs in field and cluster S0 galaxies using the STAGES survey (Gray et al. 2009; see Chapter 2) and to investigate whether the galaxy environment affects the stellar distribution in S0 galactic discs. Our work builds on previous studies by using larger and more statistically viable field and cluster samples and by being one of only a few studies to probe the high-density environments (see Erwin et al. 2012, for another example).

The structure of this chapter is as follows. In Section 5.2, we give a brief description of our S0 sample selection. In Section 5.3, we describe the method used to obtain our radial surface brightness $\mu(r)$ profiles from the STAGES *HST*/ACS V-band imaging and explain our profile classification scheme in Section 5.4. Our profile fitting and classification procedure is similar to that described in Chapter 4 for spiral galaxies (Sections 4.3 and 4.4); however, there are some key differences which are emphasised in these sections. We present our results for S0 galaxies in Section 5.5, and then compare these results with those for STAGES spiral galaxies (from Chapter 4) in Section 5.6. Finally, we draw our conclusions in Section 5.7.

5.2 Data and sample selection

In this chapter, we draw our sample of S0 galaxies from the STAGES survey (Gray et al. 2009) using the field and cluster selection defined in Chapter 2 (Section 2.2). This sample selection results in a large, mass-limited ($M_* > 10^9\,\mathrm{M}_\odot$), visually classified (S0) sample of 276 S0 galaxies from both the field and cluster environments

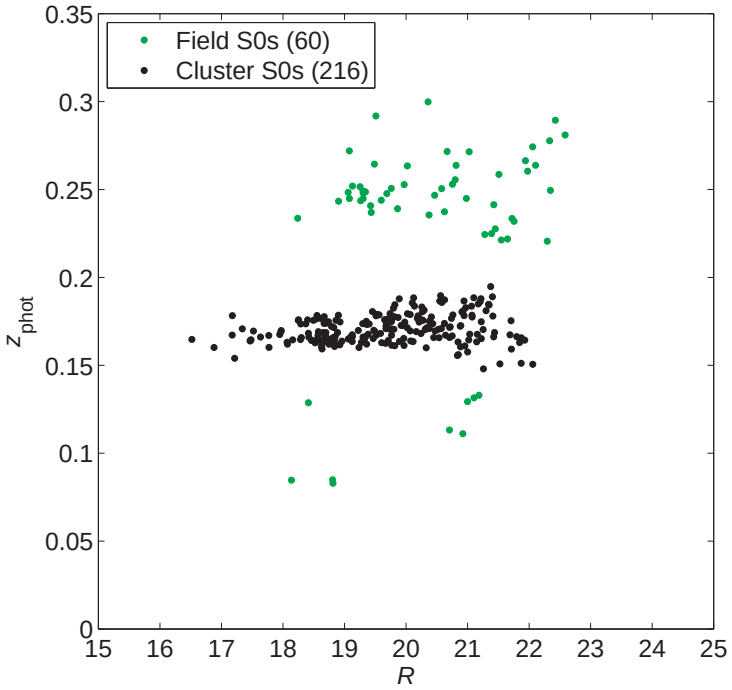

Figure 5.1. The photometric redshift $z_{\rm phot}$ versus total R-band magnitude (Vega) for the field (green points) and cluster (black points) S0 galaxy samples. The field sample reaches $R \sim 23$ and the cluster sample reaches $R \sim 22$. Respective sample sizes are shown in the legend.

(see Chapter 2: Table 2.1)[1]. This sample consists of 60 field S0s reaching down to $R \sim 23$ and 216 cluster S0s reaching down to $R \sim 22$ (see Fig. 5.1). Some relevant properties of the field and cluster S0 samples are shown in Table 5.1.

In the majority of studies that use surface photometry to explore broken exponential stellar discs, the disc galaxy samples are limited by galaxy inclination i to be face-on to intermediately inclined (e.g. Pohlen & Trujillo 2006; Erwin et al. 2012; and Chapter 4). In general, the minor-to-major axial ratio q ($q = b/a = 1-e$, where a and b are the semimajor and semiminor axes, respectively, and e is the ellipticity) is restricted to correspond to an inclination i of less than 60° ($q > 0.5$ or $e < 0.5$). The purpose of this inclination i cut is to minimise the influence of dust on the galaxy surface brightness $\mu(r)$ profiles. This is particularly important in the case of spiral galaxies, but less of an issue in S0 galaxies.

The axial ratio q for our S0 galaxies is determined from the STAGES GALFIT models (Gray et al. 2009) and the axial ratio q distributions for our field and cluster S0 samples are shown in Fig. 5.2. The suggested inclination cut of $q > 0.5$ would remove 40 per cent of our field S0s and 36 per cent of our cluster S0s. Unfortunately, this would have a drastic effect on the number of galaxies in our field S0 sample and the quality of our field property distributions and subsequent results. Therefore, in order to maintain our field sample size, we do not limit our S0 samples by galaxy inclination i in this study. However, the application of such an inclination i cut ($i < 60°$, $q > 0.5$) has no effect on the overall significance of our results or our conclusions.

[1]Note: in STAGES, the S0 classification is based on the presence of a featureless (smooth) disc and is independent of the apparent bulge-to-disc ratio B/D (see Section 2.1).

Table 5.1. Properties of the field and cluster S0 galaxy samples.

Property	Field	Cluster
$N_{\rm gal}$	60	216
Completeness	$> 70\,\%$	$> 90\,\%$
Contamination	–	$< 25\,\%$
$R_{\rm mean}$	20.44	19.71
$M_{B(\rm min)}$	-16.54	-16.45
$M_{B(\rm max)}$	-21.19	-21.78
$z_{\rm phot,mean}$	0.230	0.171
$z_{\rm phot,min}$	0.083	0.148
$z_{\rm phot,max}$	0.300	0.195

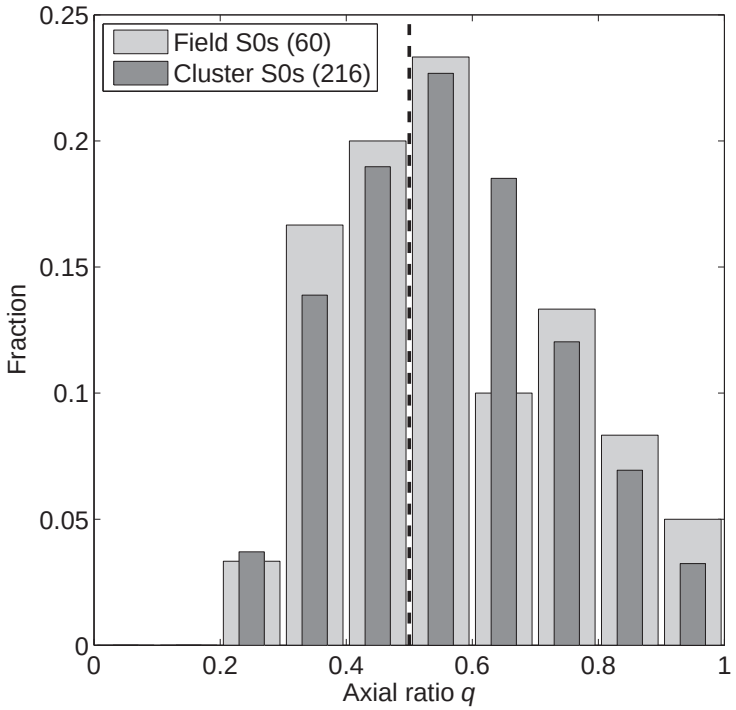

Figure 5.2. The distribution of minor-to-major axial ratio q for our field (light grey) and cluster (dark grey) S0 galaxies. The q cut used by previous works ($q > 0.5$, represented by a black dashed line) is shown for reference. Relative errors in q are < 3 per cent. Respective sample sizes are shown in the legend.

5.3 Profile fitting

For each galaxy in our field and cluster sample, we obtain the azimuthally-averaged radial surface brightness $\mu(r)$ profile from the STAGES *HST*/ACS V-band imaging. We achieve this using a similar method to that described in Chapter 4 (Section 4.3), but with the addition of some extra bad-pixel masking[2]. This extra masking was required in order to remove some low surface brightness objects not detected by the GALAPAGOS pipeline, and therefore not removed by the Gray et al. (2009) bad-pixel masks. The subtraction of unmasked companion galaxies was necessary for three field S0s (~ 5 per cent) and 27 cluster S0s (~ 10 per cent), and additional masking was also performed to remove the corresponding residuals in some of these cases.

The resultant $\mu(r)$ profiles are then corrected for Galactic foreground extinction, individual galaxy inclination i and surface brightness dimming (the μ profiles of our field galaxies, $0.05 < z_{\rm phot} < 0.30$, are corrected to the cluster redshift $z_{\rm cl} = 0.167$). For full details of the fitting procedure (performed on a different sample of galaxies), sky subtraction and subsequent photometric calibration, see Chapter 4 (Section 4.3).

5.3.1 Sky subtraction

For each S0 $\mu(r)$, we use the sky level determined by GALAPAGOS ($sky_{\rm gal}$) for our sky subtraction (Gray et al. 2009). The $\pm1\sigma$ error in this sky subtraction is ±0.18 counts (see Section 4.3.2). The sky subtraction error can have a significant effect on the $\mu(r)$ profile of our S0s, especially in the outer regions where the surface brightness μ approaches that of the sky background. However, for any particular galaxy the global sky subtraction error is approximately constant across the length of the $\mu(r)$ profile. Therefore, we can specify the error in our S0 $\mu(r)$ profiles by generating profiles for when the sky background is oversubtracted and undersubtracted by $\pm1\sigma$.

The 1σ error in the sky background corresponds to a critical surface brightness $\mu_{\rm crit}$ below which the sky-subtracted $\mu(r)$ profile of a galaxy becomes unreliable ($\mu_{\rm crit} \sim 27.7\,{\rm mag\,arcsec^{-2}}$). We also define a limiting surface brightness $\mu_{\rm lim}$, which corresponds to a 3σ sky error and below which the identification of profile breaks becomes unreliable ($\mu_{\rm lim} \sim 26.5\,{\rm mag\,arcsec^{-2}}$).

Reliability of the GALAPAGOS sky background

An initial inspection of our S0 $\mu(r)$ profiles revealed two key observations: i) many cases exhibiting significant curvature throughout the $\mu(r)$ profile; and ii) a distinct lack of truncations (Type II features). We wanted to ensure that these observations were not just the manifestation of a sky subtraction problem, causing the sky to be either oversubtracted or undersubtracted in our $\mu(r)$ profiles. Therefore, we assess the reliability of our sky subtraction by the comparison of our GALAPAGOS sky values $sky_{\rm gal}$ with an additional rough estimate for the sky background $sky_{\rm est}$.

For each S0 galaxy, we obtain this sky estimate $sky_{\rm est}$ by using pixels obtained from the four corners of the galaxy ACS image (postage stamp). The sizes of these ACS postage stamps are variable and were designed to optimally contain the galaxy during the STAGES GALFIT model fits (see Gray et al. 2009, for full details)[3].

[2]Note: due to the smoothness of S0s, the failure of the free-fits at the stellar disc limit $a_{\rm disc\,lim}$ (where the galaxy μ enters the background noise) was far less common than in our spiral galaxies.

[3]Note: the size of the postage stamps are a multiple ($2.5\times$) of the Kron (1980) radius, and therefore by definition contain ≥ 95 per cent of the subject galaxy's light (Barden et al. 2012).

Consequently, in sampling the corners of the postage stamp we have a reasonable expectation of probing the actual sky background. These corner pixels were selected using quarter-circle wedges of side equal to 5 per cent of the smallest image dimension. We then apply our bad pixel masks to ensure only 'dark' pixels are used and obtain the mean pixel value $\langle n_{\rm e} \rangle$ in each wedge. The corner-to-corner rms in these mean pixel values $\sigma_{\langle n_{\rm e} \rangle}$ is then calculated in order to determine if there is any large-scale variation in the sky level across the galaxy image. In the vast majority of cases ($>$ 90 per cent), $\sigma_{\langle n_{\rm e} \rangle} < 1$ count (count $\equiv$ ACS pixel values). Finally, we obtain our sky estimate $sky_{\rm est}$ by calculating the weighted mean of $\langle n_{\rm e} \rangle$ from the four corners of the image:

$$sky_{\rm est} = \sum_{i=1}^{4} w_i \langle n_{\rm e} \rangle_i. \tag{5.1}$$

The weight factor w_i is necessary due to the bad pixel masking and is given by

$$w_i = \frac{N_{i:\rm total} - N_{i:\rm masked}}{\sum_{i=1}^{4} N_{i:\rm total} - N_{i:\rm masked}}, \tag{5.2}$$

where $N_{i:\rm masked}$ is the number of flagged pixels and $N_{i:\rm total}$ is the total number of pixels in the respective corner wedge.

In the vast majority of cases ($>$ 90 per cent), the agreement between the GALAPAGOS sky level $sky_{\rm gal}$ and our rough sky estimate $sky_{\rm est}$ was very good ($|\Delta sky| < 0.5$ counts, where $\Delta sky = sky_{\rm est} - sky_{\rm gal}$). However, we need to ensure that any difference in these two sky values (Δsky), or indeed any variation in the sky level across the ACS image ($\sigma_{\langle n_{\rm e} \rangle}$), will not lead to a significant oversubtraction or undersubtraction of the sky in our S0 $\mu(r)$ profiles and e.g. cause general curvature in the outer regions.

To address this issue, we compare Δsky and $\sigma_{\langle n_{\rm e} \rangle}$ with the final mean surface brightness reached by the galaxy $\mu(r)$ profile $\mu_{r \to \infty}$ (see Fig. 5.3). The difference between $\mu_{r \to \infty}$ and $\mu_{\rm crit}$ (1σ above the sky) is a measure of the quality of the sky subtraction. Ideally $\mu_{r \to \infty} > \mu_{\rm crit}$, but this is not always the case due to measurement errors in the sky background. In reality, the sky subtraction is only suspect if $\mu_{r \to \infty}$ approaches the $\mu_{\rm lim}$ level (3σ above the sky). In the few cases where $\mu_{r \to \infty} < \mu_{\rm lim}$, projection effects or nearby stars are known to have affected the measured $\mu(r)$ and are flagged in our analysis. If a large potential sky error (large Δsky) or a large sky variation (large $\sigma_{\langle n_{\rm e} \rangle}$) were causing a significant error in our sky subtraction, one would expect a correlation between $\mu_{r \to \infty}$ and either Δsky or $\sigma_{\langle n_{\rm e} \rangle}$, respectively. However, no such correlations are observed (see Fig. 5.3). These results suggest that cases where $\mu_{r \to \infty}$ approaches the $\mu_{\rm lim}$ level are not the consequence of a small measurement error in our GALAPAGOS sky background or small variations in the sky level across the ACS image. Therefore, we conclude that our GALAPAGOS sky values are robust and that any small sky errors are not likely to effect the outcome of this study.

To further validate this result, we perform the same tests using the sample of spiral galaxies from Chapter 4, where no sky subtraction problems were suspected. Reassuringly, the distributions of $\mu_{r \to \infty}$ with Δsky and $\sigma_{\langle n_{\rm e} \rangle}$ for these spiral galaxies are essentially the same as for our S0s (see Fig. 5.3). Therefore, we can conclude that the GALAPAGOS sky values are adequate for this study, and that the general curvature and lack of truncations observed in our S0 $\mu(r)$ profiles appear *not* to be a manifestation of a sky subtraction error and are a real feature of our S0 galaxies.

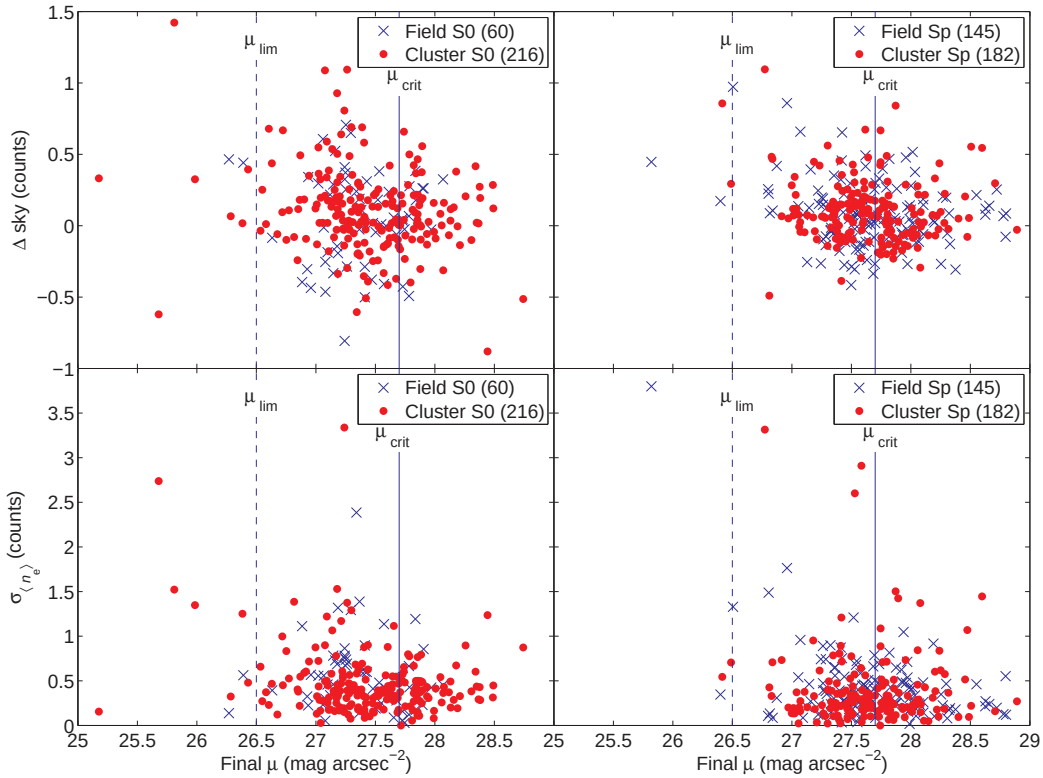

Figure 5.3. An evaluation of the sky subtraction for our S0 galaxies. Left-hand panels: a plot of the final surface brightness reached by the isophotal fit $\mu(r \rightarrow \infty)$ against the difference in our two sky values Δsky (top) and the corner-to-corner rms in the mean sky value for each galaxy image $\sigma_{\langle n_e \rangle}$ (bottom). Right-hand panels: a similar evaluation for the spiral galaxies from Chapter 4. Respective sample sizes are shown in the legends.

5.4 Profile classification

5.4.1 Profile inspection

For each S0 galaxy in our field and cluster sample, the radial surface brightness $\mu(r)$ profile was visually inspected in order to identify potential profile breaks in the exponential stellar disc. Due to the subjective nature of some profile classifications, this inspection was carried out by three independent assessors (DTM, AAS, MEG). Four possible cases were considered: i) a simple exponential profile with no break; ii) a single broken exponential either down-bending or up-bending; iii) cases with two profile breaks; and iv) no discernible exponential component (i.e. general curvature throughout the μ profile)[4]. In each case, break identification relates to the disc component of the $\mu(r)$ profile and does not consider the inner bulge component.

In this study, we follow the same procedure as described in Chapter 4 (Section 4.4.1) for the identification of $\mu(r)$ profile breaks and exponential regions. Therefore, our break identification is based solely on the $\mu(r)$ profiles and without direct inspection of the ACS images. We do not trust breaks with a break surface brightness $\mu_{\rm brk} > \mu_{\rm lim}$ (26.5 mag arcsec^{-2}, 3σ above the sky), due to the increase in the $\pm 1\sigma$ sky subtraction error causing break identification to become unreliable. We therefore restrict our analysis to $\mu(r)$ profile breaks that have $\mu_{\rm brk} < 26.5\,{\rm mag\,arcsec^{-2}}$.

[4]Note: these cases are not generally observed in our spiral galaxies from Chapter 4.

The distributions of break surface brightness $\mu_{\rm brk}$ for the breaks identified by each assessor are shown in Fig. 5.4. The $\mu_{\rm brk}$ distributions for both one and two break cases are similar in each case. However, due to the subjective nature of some profile classifications, the number of S0 galaxies with either no, one, or two breaks, varies subtly between the different assessors. To account for this, in what follows we perform parallel analyses on the breaks identified by each assessor and compare the final results.

5.4.2 Profile types

We classify our S0 galaxies into four broad profile types: those classified to be Type I, Type II, or Type III depending on break features in their stellar disc; and also Type c – cases with no discernible exponential component (i.e. general curvature). If the galaxy has a single exponential $\mu(r)$ profile with no break it is classified as Type I. If the $\mu(r)$ profile has a down-bending break, then the galaxy has a stellar disc truncation and is classified as Type II. If the $\mu(r)$ profile has an up-bending break, then the galaxy has an antitruncation in the stellar disc and is classified as Type III. However, if the $\mu(r)$ profile has no significant exponential component (general curvature), then the galaxy is classified as Type c (c denotes 'curvature').

This classification scheme assumes a maximum of one $\mu(r)$ break in the stellar disc. If two breaks are present the outer break is used for classification. This is only the case for ~ 5 per cent of our field and cluster S0 galaxies (see Fig. 5.4). In this study, we wish to assess the effect of the galaxy environment on the outer regions of S0 stellar discs. Therefore, if two breaks are present the outer break is used for classification since any effect of the environment should be stronger in the outer, fainter and more fragile break. Examples of each profile type (Type I, II, III and Type c), along with their ACS images showing the break radius $r_{\rm brk}$ isophote, are presented in Fig. 5.5.

5.4.3 Measuring scalelength and break strength

Using the same method as described in Chapter 4 (Section 4.4.4), we measure the scalelength h of our Type I galaxies and the break strength T of our Type II/III galaxies (see Equation 4.8). The mean random error due to the exponential fitting routine and the mean systematic error due to the error in the sky subtraction (see Section 5.3.1), for both our h and T measurements, are shown in Table 5.2.

The majority of our field S0s have $z \sim 0.23$, while our cluster S0s have $z \sim 0.167$. However, as with our spiral galaxies, evolutionary effects on scalelength h and T are not expected to have any impact on the results of this study (see Section 4.5).

Table 5.2. The error in Type I scalelength h and Type II/III break strength T for our S0 galaxies.

Error	Type I h	Type II/III T
mean random error (from exponential fit)	$< 10\,\%$	~ 0.1 ($< 20\,\%$)
mean systematic error (from sky subtraction)	$< 10\,\%$	~ 0.1 ($< 20\,\%$)

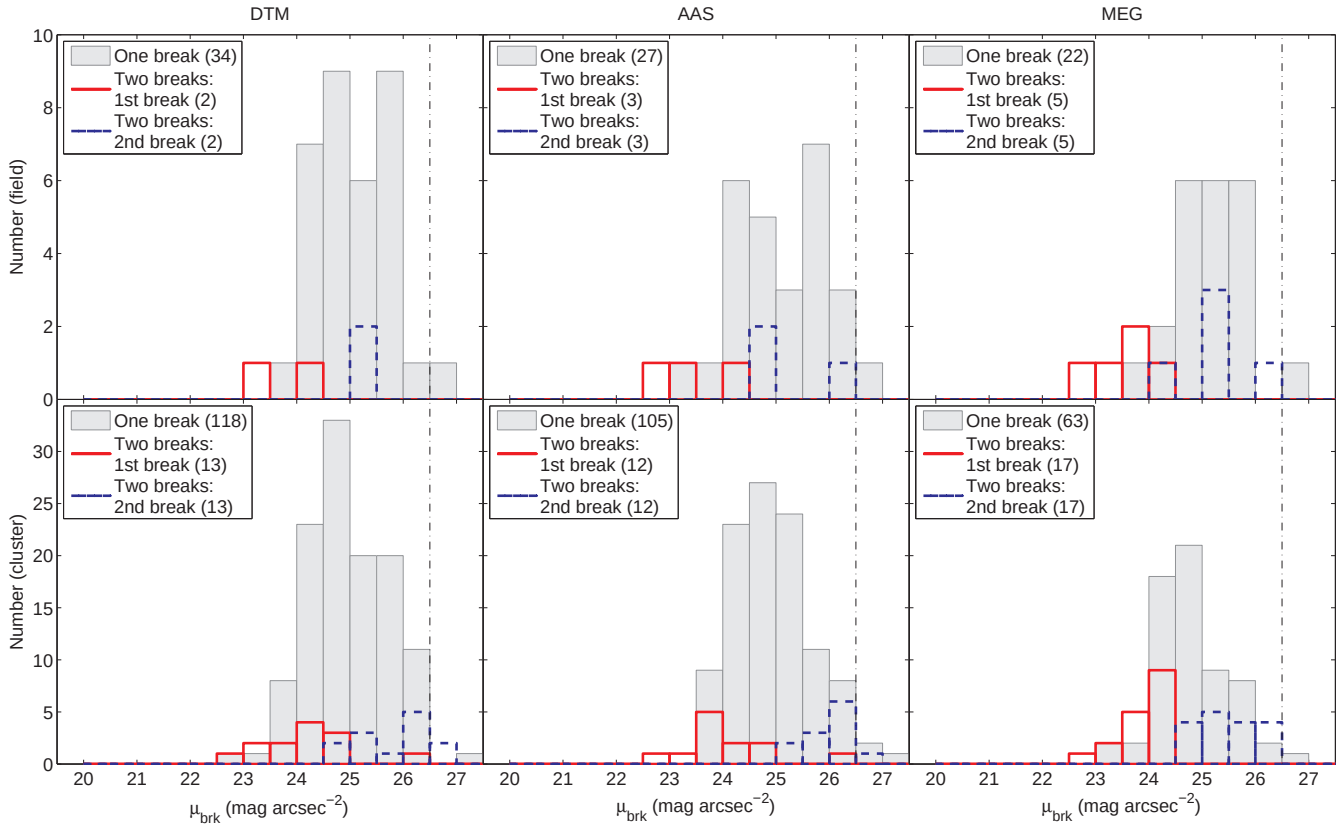

Figure 5.4. The distribution of break surface brightness $\mu_{\rm brk}$ for our S0 galaxies. The surface brightness at the break radius $\mu_{\rm brk}$ for field (top row) and cluster (bottom row) S0 galaxies as determined by DTM (left-hand column), AAS (centre column) and MEG (right-hand column). The distributions show galaxies with one break (grey shaded area), and both the inner (red line) and outer break (blue dashed line) of galaxies with two breaks. Respective sample sizes are shown in the legends. Contamination of the cluster sample by the field is < 25 per cent. Due to the subjective nature of some galaxy profile classifications, the number of galaxies with either one or two breaks varies subtly between the different assessors.

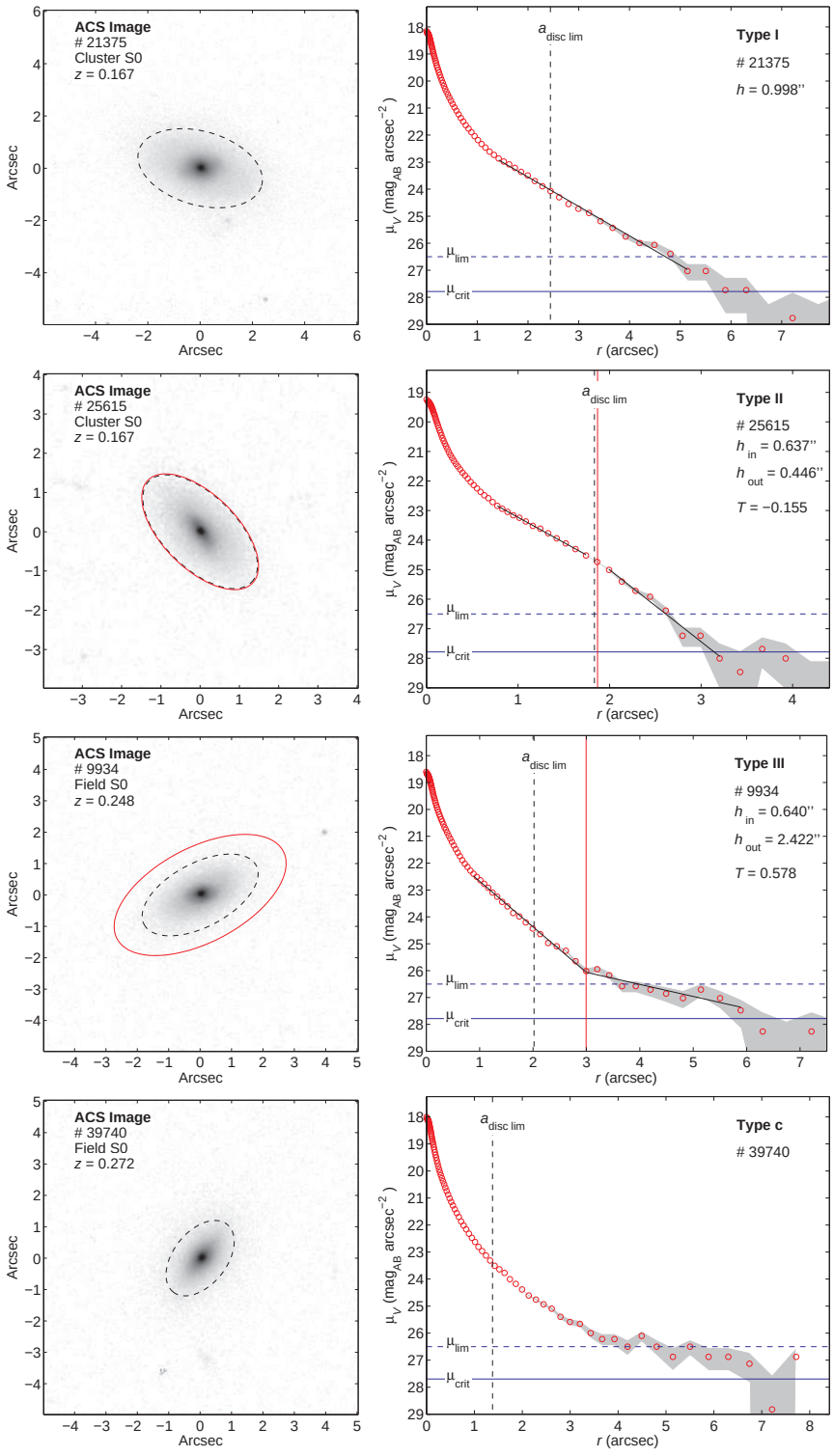

Figure 5.5. Examples of each class of S0 profile (DTM classification). Top to bottom: Type I, Type II, Type III and Type c (no discernible exponential component, i.e. general curvature). Left-hand panels: ACS V-band images. Right-hand panels: azimuthally-averaged V-band radial surface brightness $\mu(r)$ profiles. We overplot the break radii where applicable (red solid lines) and the stellar disc limit $a_{\rm disc\,lim}$ (a visual estimate of the end of the stellar disc, black dashed line). The inner and outer scalelength, $h_{\rm in}$ and $h_{\rm out}$, respectively, and the break strength T are also shown for reference. The ACS images are in a logarithmic grey-scale. Note that in our samples, Type II S0 profiles are very rare (< 5 per cent).

5.5 Results

The frequencies of the profile classifications by each assessor (DTM, AAS, MEG) for S0 galaxies in the field and cluster environments are shown in Table 5.3. These profile classifications are based on single disc breaks only and in multiple break cases the outer break is used for classification. The uncertainty in the profile-type frequencies (δf_i) is calculated using Equation 4.9 (see Chapter 4: Section 4.5).

Due to the subjective nature of some profile classifications, the frequency obtained for each profile type varies subtly between the different assessors. The agreement between the three assessors is generally very good, especially for Type I and Type II profiles. However, the agreement is slightly weaker for the frequencies of Type III and Type c (non-exponential) profiles due to the increased level of subjectivity involved in deciphering between these two profile types.

The frequencies of the profile types (Type I, II and III) are approximately the same in the field and cluster environment. For both field and cluster S0s, ~ 25 per cent have a simple exponential profile (Type I), < 5 per cent exhibit a down-bending break (truncation, Type II) and ~ 50 per cent exhibit an up-bending break (antitruncation, Type III). The frequency of profiles with no discernible exponential component (i.e. general curvature, Type c) is also approximately the same in the field and cluster environment and is ~ 20 per cent. These results suggest that the profile type of S0 galaxies is not significantly affected by the galaxy environment from the general field to the intermediate densities of the A901/2 clusters.

Previous works that use surface photometry to study the structure of galactic discs (e.g. Pohlen & Trujillo 2006; Erwin et al. 2012; and our Chapter 4), usually limit their disc galaxies by galaxy inclination i to be face-on to intermediately inclined ($i < 60^\circ$). The intention of this inclination i cut is to minimise the effects of dust on the $\mu(r)$ profiles. In this study, we make no such inclination cut (see Section 5.2). However, limiting our S0 samples by galaxy inclination ($i < 60^\circ$, $q > 0.5$) affects our profile fractions by < 5 per cent and has no effect on our conclusions.

The distinct lack of disc truncations (Type II profiles) in both our field and cluster S0s is of particular interest. Type II profiles are very common in spiral galaxies, occurring in approximately 40–60 per cent of cases (Pohlen & Trujillo 2006; Erwin et al. 2008). Therefore, it seems whatever process transforms spiral galaxies into S0s may well erase these truncations from their $\mu(r)$ profiles. This result is in partial agreement with a similar result by Erwin et al. (2012). Using a sample of ~ 70 field and cluster S0 galaxies, Erwin et al. (2012) find no Type II S0s in the cluster environment but a Type II fraction of ~ 30 per cent for their field S0s. Therefore, our Type II S0 fractions are in perfect agreement with Erwin et al. (2012) for the cluster environment, but differ significantly for the field. The origin of this disagreement is uncertain and we can offer no explanation at the present time.

An explanation for the lack of Type II profiles in our S0s can be hypothesised by considering their potential origin. Truncated $\mu(r)$ profiles (Type II) are thought to form via a radial star formation threshold and the scattering of inner disc stars to regions beyond this threshold (i.e. break radius $r_{\rm brk}$; e.g. Debattista et al. 2006). Therefore, the outer disc should be populated by old stars as these are the ones that have had enough time to make the disc migration. The discovery that the stellar mass surface density $\Sigma^{M_*}(r)$ profiles of Type II galaxies tend to be purely exponential (Bakos et al. 2008; Martínez-Serrano et al. 2009) supports this scenario and suggests that Type II $\mu(r)$ breaks are *not* related to the stellar mass distribution but due to a

Table 5.3. The frequency of profile types for S0 galaxies in the field and cluster environments and for the three independent assessors (DTM, AAS, MEG). Percentage errors are calculated using Equation 4.9.

Assessor	Disc profile types			Curvature	Unclassified
	Type I	Type II	Type III	Type c	
Field S0 galaxies					
DTM	18 ($30 \pm 4\,\%$)	1 ($2 \pm 2\,\%$)	34 ($57 \pm 3\,\%$)	5 ($8 \pm 3\,\%$)	2 ($3 \pm 2\,\%$)
AAS	18 ($30 \pm 4\,\%$)	0 (0 %)	29 ($48 \pm 3\,\%$)	13 ($22 \pm 4\,\%$)	0 (0 %)
MEG	17 ($28 \pm 4\,\%$)	0 (0 %)	26 ($43 \pm 3\,\%$)	14 ($23 \pm 4\,\%$)	3 ($5 \pm 3\,\%$)
Cluster S0 galaxies					
DTM	43 ($20 \pm 2\,\%$)	8 ($4 \pm 2\,\%$)	122 ($56 \pm 2\,\%$)	37 ($17 \pm 2\,\%$)	6 ($3 \pm 1\,\%$)
AAS	58 ($27 \pm 2\,\%$)	5 ($2 \pm 1\,\%$)	109 ($50 \pm 2\,\%$)	41 ($19 \pm 2\,\%$)	3 ($1 \pm 1\,\%$)
MEG	56 ($26 \pm 2\,\%$)	2 ($1 \pm 1\,\%$)	77 ($36 \pm 2\,\%$)	68 ($31 \pm 2\,\%$)	13 ($6 \pm 2\,\%$)

radial change in the age of the stellar population. Assuming this formation scenario, when star formation is suppressed throughout the galactic disc (e.g. via gas stripping, see Section 1.2) the age of the inner disc stellar population will gradually increase. As a result, the relative difference in stellar population age between the inner and outer disc will decrease and the mass-to-light ratio (M/L) across the $\mu(r)$ break will converge. Consequently, the $\mu(r)$ break will get weaker and may even disappear. Since spiral galaxies are thought to transform into S0s by the termination of star formation (e.g. Aragón-Salamanca et al. 2006), it seems natural to expect Type II $\mu(r)$ breaks to be weaker/rarer in S0s compared to spiral galaxies.

5.5.1 S0: pure exponential discs (Type I)

For S0s where no $\mu(r)$ break was identified in the exponential disc (Type I), we compare the scalelength h distributions in the field and cluster environments to see whether there is any evidence for an environmental dependence on the scalelength h (see Fig. 5.6). In these comparisons, our scalelengths h were transformed into intrinsic linear scales using the fixed cluster redshift ($z_{\rm cl} = 0.167$) for our cluster S0s and the COMBO-17 photo-z estimate for our field S0s. Therefore, photo-z errors only propagate into the intrinsic scalelengths of our field galaxies and not our cluster galaxies. The mean error in h associated with this photo-z error is < 10 per cent (i.e. the error in the distance to the galaxy, see Chapter 3: Section 3.4.1).

For our S0 $\mu(r)$ profiles, the error in the sky background (see Section 5.3.1) can have a significant effect on both our scalelength h and break strength T measurements, especially at large radii where the galaxy $\mu(r)$ profile approaches the critical surface brightness $\mu_{\rm crit}$ ($27.7\,{\rm mag\,arcsec^{-2}}$, 1σ above the sky). However, for any particular galaxy the sky subtraction error can be taken to be approximately constant across the length of the $\mu(r)$ profile. Therefore, we can account for this error by performing parallel analyses for when the sky background is oversubtracted and undersubtracted by $\pm1\sigma$ (±0.18 counts). The mean error in h due to the sky subtraction error is $\sim \pm0.3\,{\rm kpc}$ (< 10 per cent) for our Type I S0 galaxies. Random errors in h due to the exponential fitting routine are also typically < 10 per cent (see Section 5.4.3). We also perform parallel analyses on the Type I samples generated by the three assessors (DTM, AAS, MEG) in order to account for the subjective nature of the profile classifications and compare the final results.

In all cases (all parallel analyses), we observe no clear difference between the distributions of scalelength h for our Type I S0 galaxies in the field and cluster environments (see Fig. 5.6). In order to test the significance of these results, we construct scalelength h cumulative distribution functions (CDFs; see Fig. 5.6) for our Type I S0 galaxy samples and perform Kolmogorov–Smirnov (K–S) tests between corresponding samples from the field and cluster environments. These K–S tests are used in order to obtain the probability $p_{\rm (field/cluster)}$ that the field and cluster Type I S0 samples are *not* drawn from the same continuous h distributions. The results of these K–S tests are shown in Table 5.4.

In this study, we only consider an environmental effect on the Type I scalelength h to be significant if K–S tests yield a 2σ level probability for $p_{\rm (field/cluster)}$. However, $p_{\rm (field/cluster)}$ is below the 2σ level for each assessor and for when the sky background is oversubtracted and undersubtracted by $\pm1\sigma$ (see Table 5.4). Therefore, we find no evidence to suggest that the disc scalelength h of our Type I S0 galaxies is dependent on the galaxy environment. This result is also robust to the error in the sky subtraction and the subjective nature of the profile classifications.

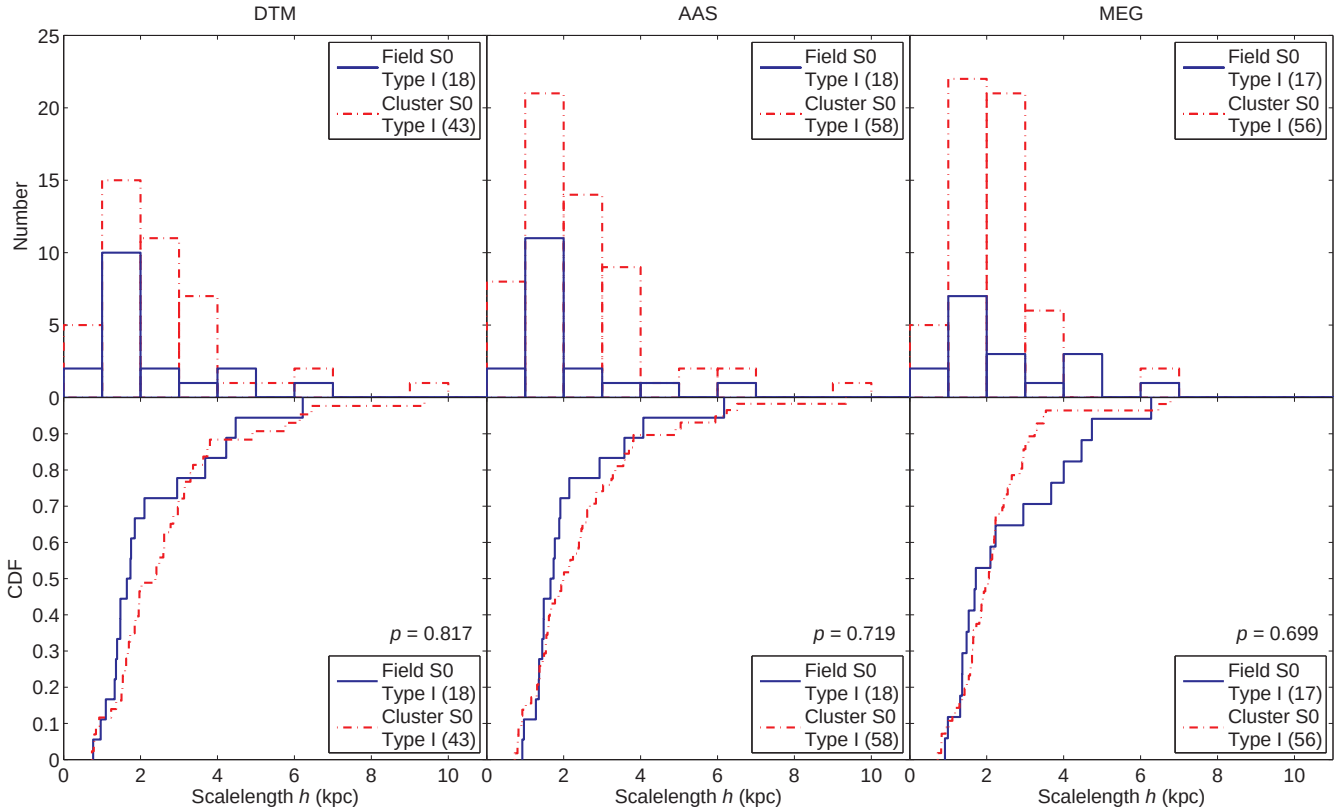

Figure 5.6. Comparing Type I disc scalelength h distributions in different environments for S0 galaxies. Top row: scalelength h distributions for S0 Type I galaxies in the field (blue line) and cluster (red dashed line) environment as classified by DTM (left-hand panel), AAS (centre panel) and MEG (right-hand panel). Bottom row: the corresponding scalelength h CDFs showing the probability p that compared samples are *not* drawn from the same continuous h distributions in the bottom right of each plot. Respective sample sizes are shown in the legends. Random errors in scalelength are typically < 10 per cent. Systematic errors in scalelength due to the error in the sky subtraction are also typically < 10 per cent. Contamination of the cluster sample by the field is < 25 per cent. We find no significant difference between the CDFs in each environment and no evidence to suggest that the scalelength h of our S0 Type I galaxies are *not* drawn from the same continuous h distributions.

5.5.2 S0: broken exponential discs (Type II/III)

For S0 galaxies where a $\mu(r)$ break was identified[5] (Type II/III galaxies), we compare the break surface brightness $\mu_{\rm brk}$ distributions in the field and cluster environments in order to see if there is any evidence for an environmental dependence on $\mu_{\rm brk}$ (see Fig. 5.7). However, since Type II profiles are very rare in our S0 galaxies (see Table 5.3) these comparisons are essentially for Type III profiles. Analogous parallel analyses and statistical tests are performed as in our Type I profile analysis (see Section 5.5.1) and the results of the K–S tests are shown in Table 5.4.

Certain physical processes inherent to galaxy evolution and dependent on the galaxy environment could potentially affect the position of $\mu(r)$ breaks (see Section 1.2). For example, tidal stripping (e.g. Faber 1973; King & Kiser 1973) could remove gas/stars from the outer regions of the stellar disc, causing star formation to cease and the outer regions to gradually fade as the stellar population ages. As a result, $\mu_{\rm brk}$ would evolve to a brighter μ in the cluster environment. However, in all cases (all assessor samples and sky versions), we observe no significant difference between the $\mu_{\rm brk}$ distributions in the field and cluster environments. The probability $p_{\rm (field/cluster)}$ is below the 2σ level in each case. Therefore, we conclude that there is no evidence to suggest that the break surface brightness $\mu_{\rm brk}$ of our S0 galaxies is dependent on the galaxy environment. This result is also robust to the error in the sky subtraction and the subjective nature of the profile classifications. However, we stress that this result may suffer from low number statistics and a larger field sample may yield different results.

We also perform analogous comparisons of the break radius $r_{\rm brk}$ distributions in the field and cluster environments for our Type II/III S0 galaxies ($r_{\rm brk}$ in units of the GALFIT effective radius). As with our $\mu_{\rm brk}$ analysis, we find no significant difference between the $r_{\rm brk}$ distributions of our Type II/III S0 galaxies in the field and cluster environments.

Type II breaks tend to be at smaller $r_{\rm brk}$ and have a brighter $\mu_{\rm brk}$ than Type III breaks. However, the mix of profile types has no effect on our $\mu_{\rm brk}/r_{\rm brk}$ comparisons since our S0 Type II/III fractions are the same in the field and cluster environments and since Type II profiles are very rare in our S0 galaxies (see Table 5.3). Similar $\mu_{\rm brk}/r_{\rm brk}$ analyses using just Type III breaks reach the same conclusions.

For our Type II/III S0 galaxies, we also compare the break strength T distributions in the field and cluster environments in order to see if there is any evidence for an environmental dependence on break strength T (see Fig. 5.8). Again, since Type II profiles are very rare in our S0 galaxies these comparisons are essentially for Type III profiles. Similar parallel analyses and statistical tests are also carried out as in our S0 Type I profile analysis (Section 5.5.1). The mean error in T due to the sky subtraction error is ± 0.1 and random errors in T due to the exponential fitting routine are also typically ± 0.1 (see Section 5.4.3). The results of the K–S tests are shown in Table 5.4.

In all cases (all assessor samples and sky versions), we observe no significant difference between the break strength T distributions in the field and cluster environments. The probability $p_{\rm (field/cluster)}$ is below the 2σ level in each case. Therefore, we find no evidence to suggest that the break strength T of our Type II/III S0 galaxies is dependent on the galaxy environment. This result is also robust to the error in the sky subtraction and the subjective nature of the profile classifications.

[5]Note: if two $\mu(r)$ breaks are identified in any one galaxy, the outer break is used in the analysis.

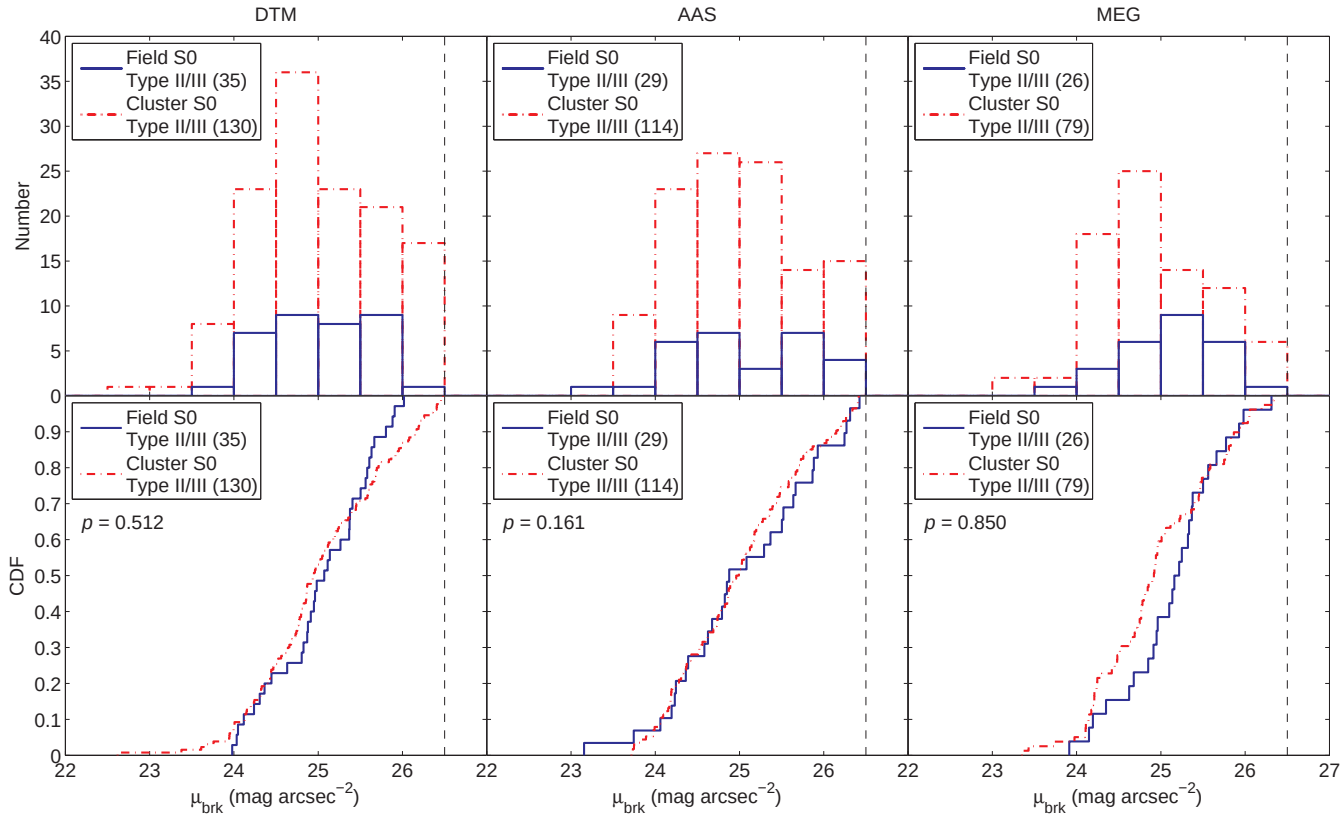

Figure 5.7. Comparing break surface brightness $\mu_{\rm brk}$ distributions in different environments for S0 galaxies. Top row: $\mu_{\rm brk}$ distributions for S0 Type II/III galaxies in the field (blue line) and cluster (red dashed line) environment as classified by DTM (left-hand column), AAS (centre column) and MEG (right-hand column). Bottom row: the corresponding $\mu_{\rm brk}$ CDFs showing the probability p that compared samples are *not* drawn from the same continuous $\mu_{\rm brk}$ distributions in the bottom right of each plot. Respective sample sizes are shown in the legends. Contamination of the cluster sample by the field is < 25 per cent. We find no significant difference between the CDFs in each environment and no evidence to suggest that the $\mu_{\rm brk}$ of our S0 Type II/III galaxies are *not* drawn from the same continuous $\mu_{\rm brk}$ distributions.

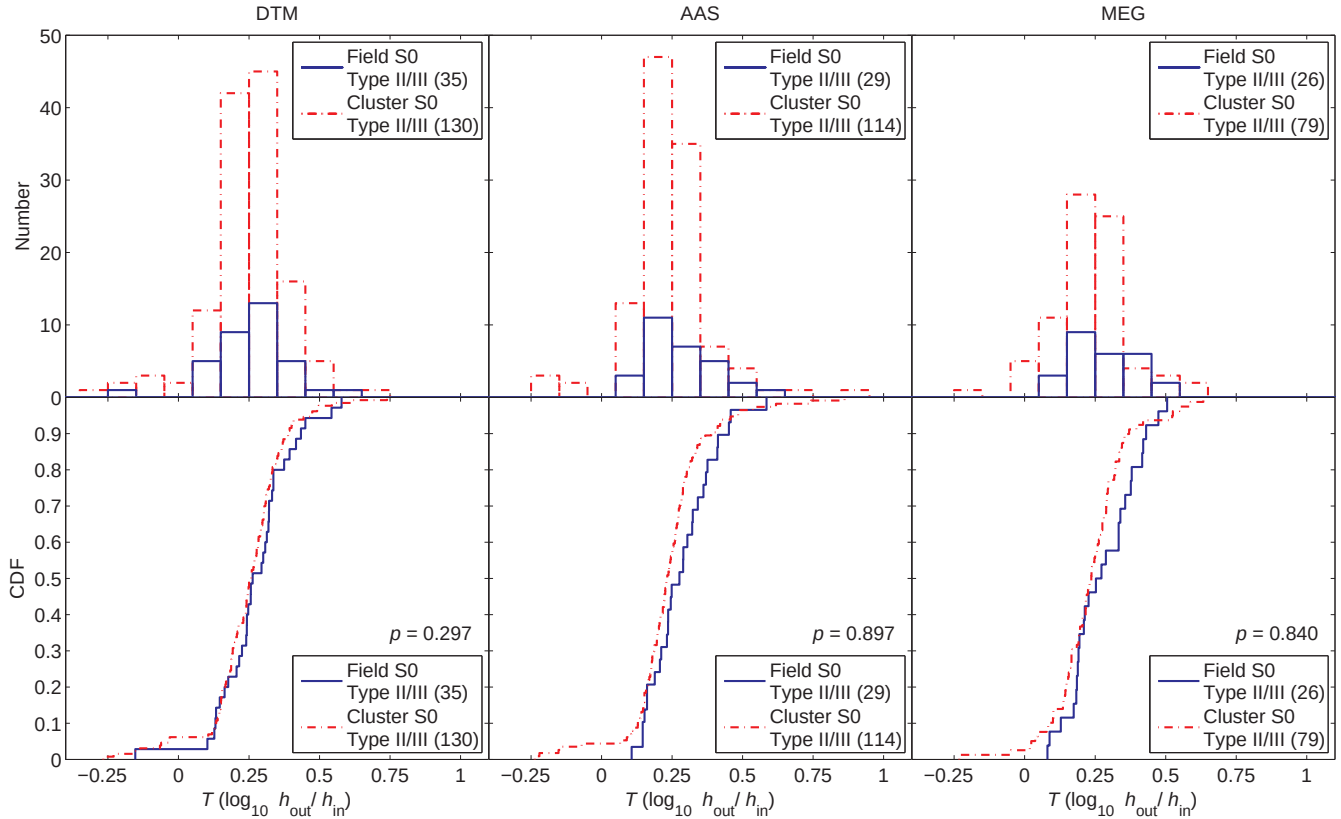

Figure 5.8. Comparing break strength T ($\log_{10} h_{\rm out}/h_{\rm in}$) distributions in different environments for S0 galaxies. Top row: T distributions for S0 Type II/III galaxies in the field (blue line) and cluster (red dashed line) environment as classified by DTM (left-hand column), AAS (centre column) and MEG (right-hand column). Bottom row: the corresponding T CDFs showing the probability p that compared samples are *not* drawn from the same continuous T distributions in the bottom right of each plot. Respective sample sizes are shown in the legends. Random errors in T are typically < 0.1. Systematic errors in T due to the error in the sky subtraction are also $\sim \pm 0.1$. Contamination of the cluster sample by the field is < 25 per cent. We find no significant difference between the CDFs in each environment and no evidence to suggest that the break strength T of our S0 Type II/III galaxies are *not* drawn from the same continuous T distributions.

Table 5.4. The K–S test results for Type I and Type II/III S0 galaxies as classified by DTM, AAS and MEG. K–S tests give the probability $p_{(\mathrm{field/cluster})}$ that the respective field and cluster samples are *not* drawn from the same continuous h distributions for Type I S0s and μ_{brk}/T distributions for Type II/III S0s. Results are also shown for when the sky is oversubtracted and undersubtracted by $\pm 1\sigma$. We find no environmental dependence on either the scalelength h of Type I profiles or the break surface brightness μ_{brk}/break strength T of Type II/III profiles for S0 galaxies.

	$p_{(\mathrm{field/cluster})}$		
Sky subtraction	Under (-1σ)	Nominal	Over ($+1\sigma$)
S0: Type I (h)			
DTM	0.811	0.817	0.822
AAS	0.755	0.719	0.804
MEG	0.589	0.699	0.621
S0: Type II/III (μ_{brk})			
DTM	0.416	0.512	0.750
AAS	0.071	0.161	0.094
MEG	0.922	0.850	0.927
S0: Type II/III (T)			
DTM	0.744	0.297	0.350
AAS	0.923	0.897	0.731
MEG	0.932	0.840	0.654

5.6 Comparing the structure of galactic discs between spiral and S0 galaxies

In this chapter, we have so far explored the effect of the galaxy environment on the structure of galactic discs in STAGES S0 galaxies. This work is analogous to the companion study presented in Chapter 4, which explores the effect of the galaxy environment on the structure of galactic discs in STAGES *spiral* galaxies. For these spiral galaxies, we found no evidence to suggest their $\mu(r)$ profiles were affected by the galaxy environment. Both the scalelength h and break strength T of our spiral galaxies showed no evidence for an environmental dependence from the general field to the intermediate galaxy densities probed by the STAGES survey (see Chapter 4, for further details). Therefore, our conclusion that there is no evidence for an effect of the galaxy environment on the structure of S0 galactic discs is in qualitative agreement with the conclusions presented in Chapter 4 for spiral galaxies.

In this section, we compare our results for S0 galaxies with those for our spiral galaxies (from Chapter 4) in order to assess the effect of galaxy morphology on the structure of galactic discs. Such comparisons of disc structure (e.g. profile type, scalelength h, break strength T, break surface brightness $\mu_{\rm brk}$) between different Hubble-type morphologies are a useful tool in exploring the evolutionary link between spiral and S0 galaxies.

5.6.1 Spiral/S0: galaxy samples

The study presented in this chapter (for S0 galaxies) and the study presented in Chapter 4 (for spiral galaxies) both use the same parent sample of morphologically classified galaxies in STAGES from which to draw their samples (see Chapter 2: Section 2.2). Both studies also perform analogous $\mu(r)$ profile fitting and break classifications. In Chapter 4, we use a large, mass-limited ($M_* > 10^9\,{\rm M}_\odot$), visually classified (Sa–Sdm) sample of 327 face-on to intermediately inclined ($i < 60^\circ$) spiral galaxies from both the field and cluster environments (145 field and 182 cluster spirals). In this chapter, our S0 sample selection is analogous to this spiral selection except for the lack of an inclination i cut (see Section 5.2). Therefore, in order to allow a fair comparison of these spiral and S0 galaxies, we need to limit our sample of S0 galaxies using the same galaxy inclination i cut used in the spiral selection ($i < 60^\circ$ or axial ratio $q > 0.5$, see Chapter 4: Section 4.2). The distribution of axial ratio q for our field and cluster S0 samples showing the axial ratio q cut is presented in Fig. 5.2. This cut removes ~ 40 per cent of field and cluster S0s from our samples. This 'matched' S0 sample contains 173 S0 galaxies (36 field and 137 cluster S0s) and is used for all our spiral/S0 comparisons.

5.6.2 Profile type (I, II and III)

Previous works (e.g. Pohlen & Trujillo 2006; Erwin et al. 2008) have found that for spiral galaxies the distribution of profile types I:II:III is approximately 20:50:30 $\pm$10 per cent. However, in this chapter we find that for S0 galaxies, ~ 25 per cent are Type I, < 5 per cent are Type II, ~ 50 per cent are Type III and ~ 20 per cent have no discernible exponential component (see Section 5.5 and Table 5.3). In comparing the profile types (disc structure) of these spiral/S0 galaxies, the most striking difference is the lack of truncations (Type II profiles) in our S0 galaxies compared to

their abundance in spiral galaxies. Therefore, it seems whatever mechanism transforms spiral galaxies into S0s may well erase these Type II features from the galaxy $\mu(r)$ profiles. Recent studies (Debattista et al. 2006; Bakos et al. 2008; Martínez-Serrano et al. 2009), suggest that Type II profiles are related to a radial change in the age of the stellar population throughout the disc, with the outer disc of Type II galaxies being populated by old stars. Therefore, the absence of Type II profiles in S0 galaxies may actually be a natural consequence of an ageing inner disc stellar population as the spirals transform into S0s (see Section 5.5, for a full explanation). Another observation is that Type III profiles seem to be slightly more frequent in S0 galaxies than in spiral galaxies. This suggests a continuation of the observed trend for spiral galaxies where Type III profiles become more frequent with progressively earlier spiral Hubble types (e.g. Pohlen & Trujillo 2006; and Chapter 4: Fig. 4.11).

5.6.3 Spiral/S0: pure exponential discs (Type I)

For spiral/S0 galaxies where no disc $\mu(r)$ break was identified (Type I), we compare the scalelength h distributions for spiral and S0 morphologies (see Fig. 5.9). These comparisons are independent of the galaxy environment (our field and cluster samples are combined) and allow for an assessment of whether the scalelength h of the stellar disc is affected by the Hubble-type morphology. Similar parallel analyses are also carried out as in previous tests.

In most cases (most parallel analyses), we observe no clear difference between the scalelength h distributions for our Type I galaxies with spiral and S0 morphologies (see Fig. 5.9). In order to test the significance of these results we construct scalelength h CDFs for our Type I galaxy samples and perform K–S tests between the corresponding spiral and S0 samples. These K–S tests are used in order to obtain the probability $p_{(\mathrm{spiral/S0})}$ that the spiral and S0 Type I samples are *not* drawn from the same continuous h distributions. The results of these K–S tests are presented in Table 5.5.

In most cases (most assessor samples and sky versions), the probability $p_{(\mathrm{spiral/S0})}$ is below the 2σ level. However, in a few cases the probability $p_{(\mathrm{spiral/S0})}$ is above the 2σ level (AAS results, see Table 5.5). As these high significance results are not robust to the subjective nature of the profile classifications, we conclude that there is no evidence to suggest that the scalelength h of our Type I galaxies is significantly affected by the Hubble-type morphology.

5.6.4 Spiral/S0: broken exponential discs (Type II/III)

For spiral/S0 galaxies where a $\mu(r)$ break was identified[6] (Type II/III), we compare both the break surface brightness μ_{brk} and break strength T distributions for our spiral and S0 galaxies.

Break surface brightness μ_{brk}

The physical processes that drive the morphology–density relation (Dressler 1980) and the transformation of spiral galaxies into S0s are not well understood (see Chapter 1). Certain mechanisms inherent to the cluster environment could be responsible, e.g. ram-pressure stripping of the interstellar medium (Gunn & Gott 1972) or tidal stripping (e.g. Faber 1973). However, the existence of S0s in the general field implies

[6]Note: if two $\mu(r)$ breaks are identified in any one galaxy, the outer break is used in the analysis.

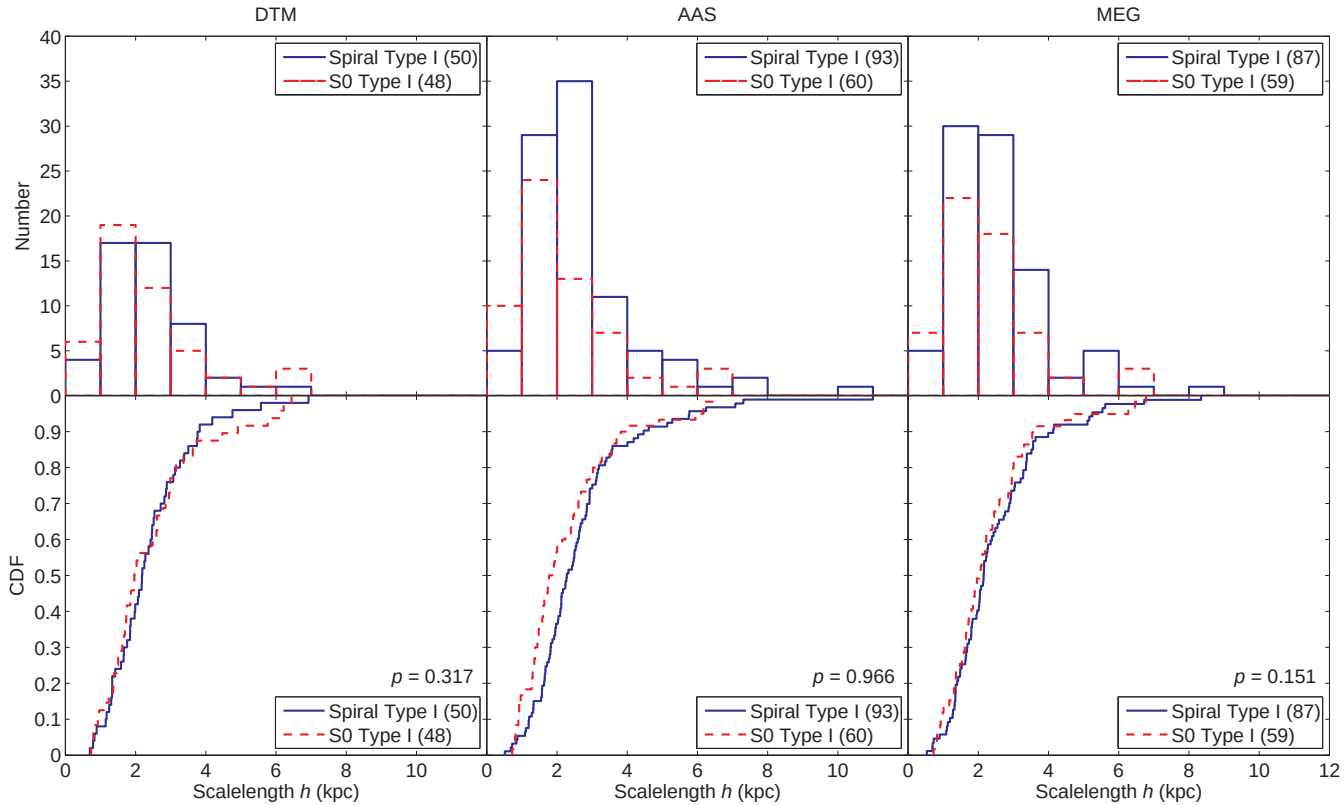

Figure 5.9. Comparing the disc scalelength h distributions for different Hubble-type morphologies. Top row: scalelength h distributions for spiral (blue line) and S0 (red dashed line) Type I galaxies as classified by DTM (left-hand panel), AAS (centre panel) and MEG (right-hand panel). Bottom row: the corresponding scalelength h CDFs showing the probability p that compared samples are *not* drawn from the same continuous h distributions in the bottom right of each plot. Respective sample sizes are shown in the legends. Random errors in scalelength h are typically < 10 per cent. Systematic errors in scalelength h due to the error in the sky subtraction are also typically < 10 per cent. We find no significant difference between the CDFs for each morphology and no evidence to suggest that the disc scalelength h of our Type I galaxies are *not* drawn from the same continuous h distributions.

that either cluster processes are not ultimately responsible, or that S0s can form via alternative processes in different environments. For example, it could be the case that cluster S0s form from in-falling spirals via the tidal stripping of interstellar gas, while field S0s are simply the faded remnants of field spirals.

For these alternative mechanisms, the processes causing star formation to be terminated and the subsequent morphological transformation would have a very different effect on the $\mu_{\rm brk}$ of any $\mu(r)$ break that was present. Therefore, the comparison of $\mu_{\rm brk}$ distributions for spiral and S0 galaxies is a useful tool in exploring the potential evolutionary links between them. If cluster S0s are the consequence of tidal stripping on in-falling spirals then one would expect the $\mu_{\rm brk}$ distribution of cluster S0s to be centred at a slightly brighter μ than that of cluster spirals. This is because tidal stripping would remove gas/stars from the outer regions of the stellar disc, causing star formation to cease and the outer regions to gradually fade as the stellar population ages. This would result in $\mu_{\rm brk}$ evolving to a brighter μ. For field S0s, if they are indeed a faded spiral remnant then one would expect the $\mu_{\rm brk}$ distribution for field S0s to be centred at a slightly fainter μ than that of field spirals. This is due to the ageing and hence fading of the stellar population across the entire stellar disc as the galaxy depletes its gas supply and ceases star formation.

Therefore, for spiral/S0 galaxies where a $\mu(r)$ break was identified (Type II/III), we compare the $\mu_{\rm brk}$ distributions between field/cluster spiral and S0 galaxies. In such comparisons it is important to remember that Type II breaks generally occur at a brighter $\mu_{\rm brk}$ than Type III breaks. For our Type II/III spirals, $\sim$ 50 per cent are Type III, while our S0s are almost exclusively ($>$ 95 per cent) Type III. Therefore, to ensure our spiral/S0 $\mu_{\rm brk}$ comparisons are fair, we only compare the $\mu_{\rm brk}$ distributions for our field/cluster spiral and S0 Type III galaxies (see Fig. 5.10). Similar parallel analyses and statistical tests (between corresponding spiral and S0 samples) are carried out as in previous tests.

For our field spiral/S0 comparison, in most cases (most assessor samples) we observe no significant difference between the $\mu_{\rm brk}$ distributions for spiral and S0 galaxies. The probability $p_{\rm (spiral/S0)}$ is below the 2σ level in most cases. For one assessor (MEG), the significance of an environmental dependence is above the 2σ level, but this may be due to low number statistics. It is interesting that for all assessors, the spiral $\mu(r)$ breaks reach to brighter $\mu_{\rm brk}$ than the S0 $\mu(r)$ breaks. This would be consistent with the hypothesis that field S0s are the faded remnants of field spirals. However, since this is very speculative we conclude that there is no evidence to suggest $\mu_{\rm brk}$ in the field is dependent on the galaxy morphology.

For our cluster spiral/S0 comparison, we also observe no significant difference between the spiral/S0 $\mu_{\rm brk}$ distributions in the majority of cases (i.e. $p_{\rm (spiral/S0)} < 2\sigma$). However, for one assessor (AAS) the significance of an environmental dependence is above the 2σ level. We also note that for all assessors, the mean $\mu_{\rm brk}$ for S0s ($24.9\,{\rm mag\,arcsec^{-2}}$) is brighter than that of spiral galaxies ($25.2\,{\rm mag\,arcsec^{-2}}$). This would be consistent with the hypothesis that cluster S0s are the consequence of tidal stripping on in-falling spirals. However, since this is very inconclusive we conclude that there is no evidence to suggest that $\mu_{\rm brk}$ in the cluster environment is dependent on the galaxy morphology.

Similar analyses were also performed using the break radius $r_{\rm brk}$ distributions ($r_{\rm brk}$ in units of the GALFIT effective radius). However, no significant differences or trends were observed for $r_{\rm brk}$ in field/cluster spiral and S0 galaxies.

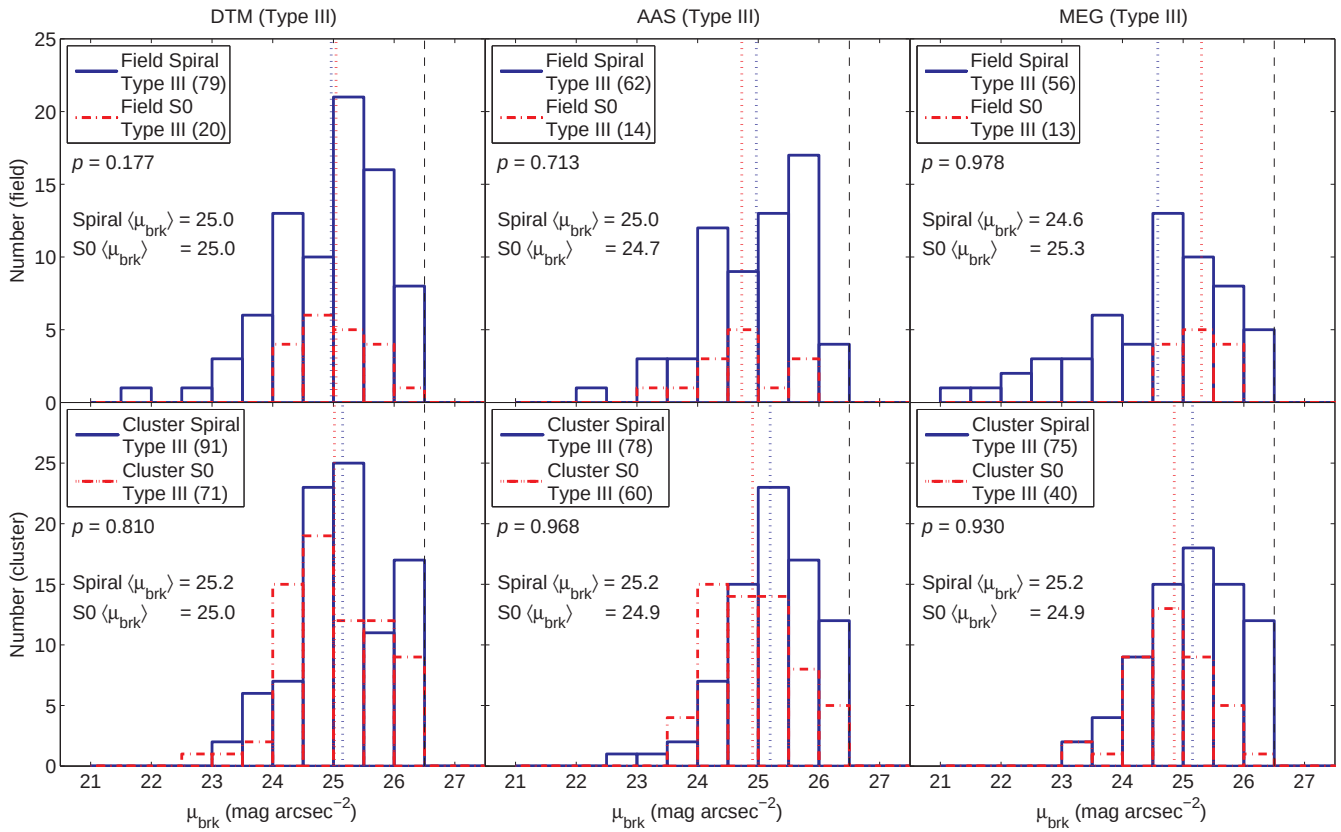

Figure 5.10. The break surface brightness $\mu_{\rm brk}$ distributions for Type III spiral and S0 galaxies in different environments. The $\mu_{\rm brk}$ distributions for field (top row) and cluster (bottom row) galaxies as determined by DTM (left-hand column), AAS (centre column) and MEG (right-hand column). The distributions show spiral galaxies (blue line) and S0 galaxies (red dashed line). The mean $\mu_{\rm brk}$ for field/cluster spirals (blue dotted line) and S0s (red dotted line) are also shown for reference. Respective sample sizes are shown in the legends. Contamination of the cluster sample by the field is < 25 per cent.

Break strength T

For our spiral galaxies, break strength T measurements were only performed on $\mu(r)$ breaks in the outer regions of the stellar disc $\mu_{\rm brk} > 24\,{\rm mag\,arcsec^{-2}}$ (the criteria used for selecting intrinsically similar outer breaks in our spiral galaxies; see Chapter 4: Section 4.4.2). Consequently, it appears that the break strength T distributions of our spiral galaxies (from Chapter 4) cannot be directly compared to the break strength T distributions of our S0 galaxies (which are not restricted by $\mu_{\rm brk}$). However, since the vast majority ($\sim$ 95 per cent) of our S0 Type II/III profiles have $\mu_{\rm brk} > 24\,{\rm mag\,arcsec^{-2}}$ anyway (see Fig. 5.7), such comparisons are actually valid.

Therefore, for spiral/S0 Type II/III galaxies[7], we compare the break strength T distributions for our spiral and S0 galaxies (see Fig. 5.11). These comparisons are independent of the galaxy environment (our field and cluster samples are combined) and allow for an assessment of whether the break strength T of the stellar disc is affected by the Hubble-type morphology. Similar parallel analyses and statistical tests are carried out as in previous tests and the results of the K–S tests are presented in Table 5.5.

In all cases (all assessor samples and sky versions), we observe a *significant difference* between the T distributions for spiral and S0 Type II/III galaxies. The probability $p_{\rm (spiral/S0)}$ is above the 3σ level in each case. Additionally, the break strength T distribution of our S0s has a much smaller variance (S0 $\sigma_T \sim 0.16$) compared to that of our spiral galaxies (spiral $\sigma_T \sim 0.4$). These results suggest that both Type II and Type III features in S0 galaxies are weaker (smaller $|T|$) than in spiral galaxies.

However, it is possible that the high significance of this result could be driven by the lack of Type II profiles in our S0 galaxies. Therefore, we repeat our analysis using the break strength T distributions for just our Type III galaxies (see Fig. 5.12). The results of the K–S tests are presented in Table 5.5. In all cases (all assessor samples and sky versions), we still observe a significant difference between the T distributions for our spiral and S0 Type III galaxies. The probability $p_{\rm (spiral/S0)}$ is above the 3σ level in each case. Also, the break strength T distribution of our Type III S0 galaxies has a much smaller variance and mean (S0 $\sigma_T \sim 0.12$, S0 $\langle T \rangle \sim 0.28$) compared to that of our spiral Type III galaxies (spiral $\sigma_T \sim 0.3$, spiral $\langle T \rangle \sim 0.4$).

Therefore, we conclude that there is some evidence to suggest that the break strength T of our Type II/III galaxies is dependent on the galaxy morphology, with $\mu(r)$ breaks in S0 galaxies being generally weaker (smaller $|T|$) than those of spiral galaxies. This result is also robust to the error in the sky subtraction and the subjective nature of the profile classifications. These results are consistent with the current theories of Type II profiles being caused by a radial variation in the age of the stellar population, with the outer disc being populated by old stars (Debattista et al. 2006; Bakos et al. 2008; Martínez-Serrano et al. 2009). In this scenario, once the galaxy has depleted its gas supply, star formation will cease in the inner disc causing it to gradually fade due to the ageing of the stellar population. This would lead to a weakening of the Type II break strength T. For Type III galaxies, further radial mixing related to the suspected minor-merger history could be responsible for the weakening of Type III features in S0 galaxies.

[7]Note: due to our spiral galaxy break strength T distributions being limited to the outer disc ($\mu_{\rm brk} > 24\,{\rm mag\,arcsec^{-2}}$), the spiral Type II/III sample used in this comparison is slightly different to that used in Section 5.6.4: Break surface brightness $\mu_{\rm brk}$.

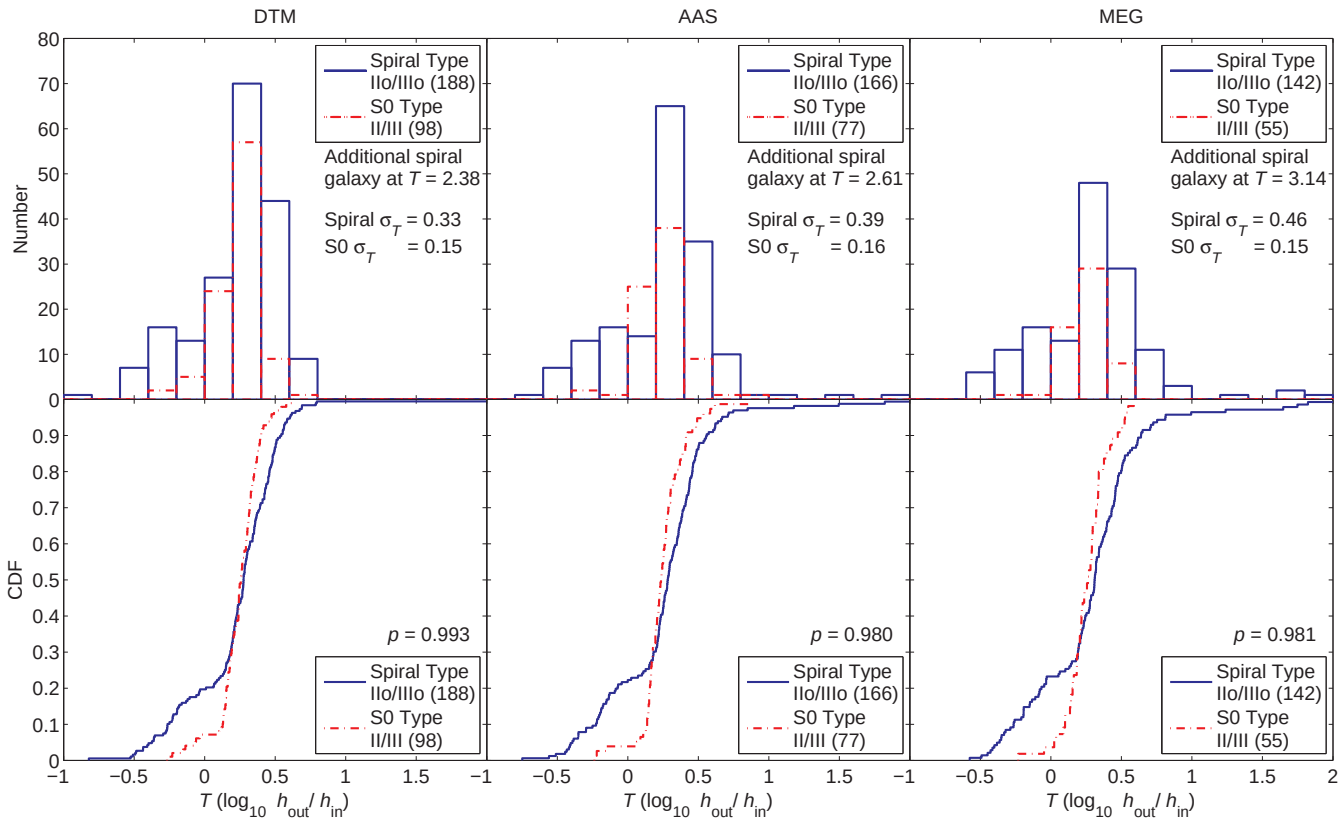

Figure 5.11. Comparing break strength T ($\log_{10} h_{\rm out}/h_{\rm in}$) distributions for spiral and S0 galaxies. Top row: break strength T distributions for spiral (blue line) and S0 (red dashed line) Type II/III galaxies as classified by DTM (left-hand column), AAS (centre column) and MEG (right-hand column). Bottom row: the corresponding break strength T CDFs showing the probability p that compared samples are *not* drawn from the same continuous T distributions in the bottom right of each plot. Respective sample sizes are shown in the legends. Random errors in T are $\sim \pm 0.1$. Systematic errors in T due to the sky subtraction error are also $\sim \pm 0.1$. Contamination of the cluster sample by the field is < 25 per cent. We find a significant ($> 3\sigma$) difference between the T CDFs for spiral and S0 galaxies.

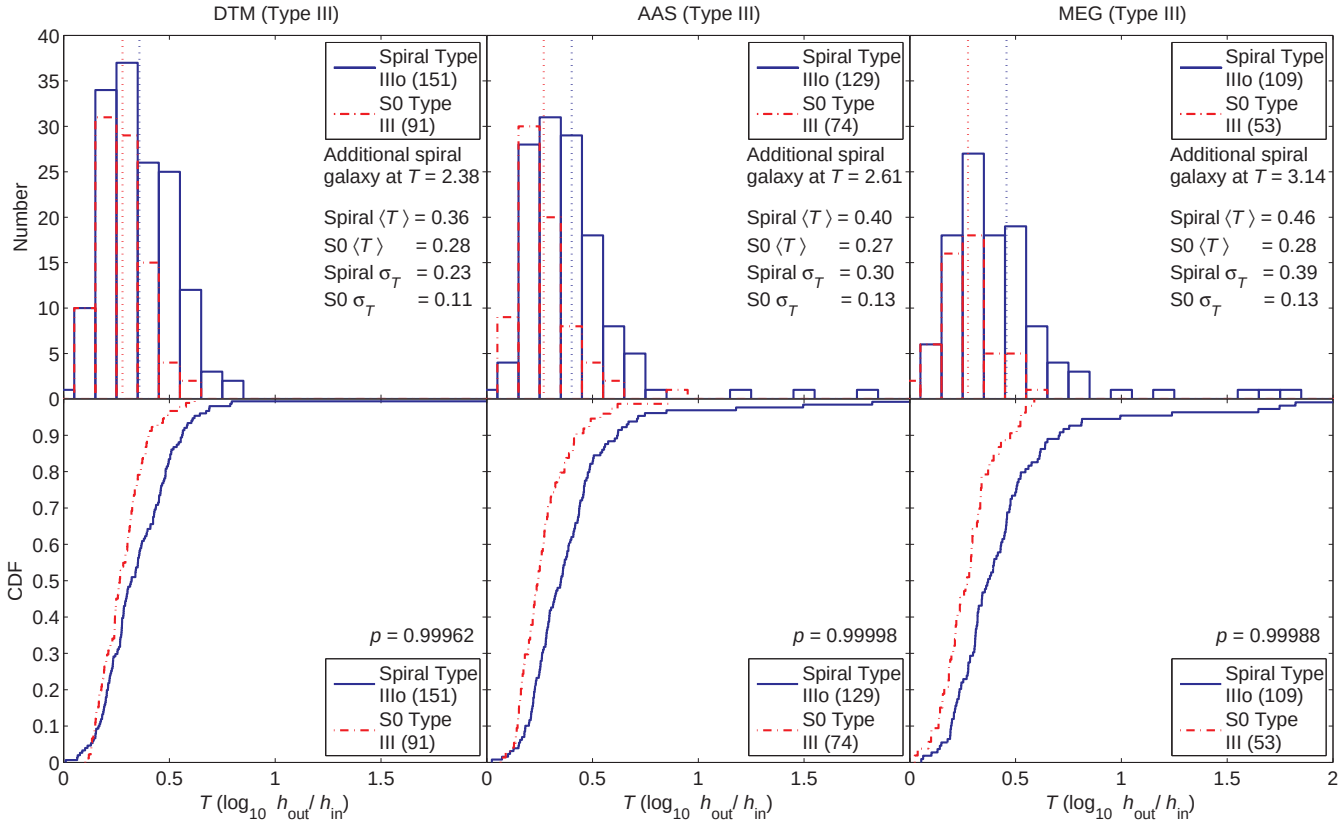

Figure 5.12. Comparing break strength T ($\log_{10} h_{\rm out}/h_{\rm in}$) distributions for Type III spiral and S0 galaxies. Figure the same as Fig. 5.11 but for Type III galaxies only. We find a significant ($> 3\sigma$) difference between the T CDFs for spiral and S0 galaxies. The mean T for spirals (blue dotted line) and S0s (red dotted line) are also shown for reference. Respective sample sizes are shown in the legends.

Table 5.5. The K–S test results for Type I, and Type II/III galaxies as classified by DTM, AAS and MEG. K–S tests give the probability $p_{(\mathrm{spiral/S0})}$ that the respective spiral and S0 samples are *not* drawn from the same continuous h distributions for Type I galaxies, and T distributions for Type II/III galaxies. Results are also shown for when the sky is oversubtracted and undersubtracted by $\pm 1\sigma$.

	$p_{(\mathrm{spiral/S0})}$		
Sky subtraction	Under (-1σ)	Nominal	Over ($+1\sigma$)
Type I (h)			
DTM	0.293	0.317	0.477
AAS	0.966	0.966	0.981
MEG	0.056	0.151	0.346
Type II/III (T)			
DTM	0.998	0.993	0.982
AAS	0.999	0.980	0.995
MEG	0.994	0.981	0.957
Type III (T)			
DTM	0.99991	0.9996	0.9997
AAS	0.999999	0.99998	0.994
MEG	0.99998	0.9999	0.983

5.6.5 Spiral/S0: bulge structure

Non-exponential bulges (mainly 'classical', de Vaucouleurs 1948, $r^{1/4}$ bulges) are thought to be the result of a major merger event (see Section 1.3.2). Therefore, if major mergers were the principal driver behind the transformation of spiral galaxies into S0s, one would expect a larger fraction of non-exponential bulges in S0s than in spiral galaxies. To address this hypothesis, we inspected the central region of the measured $\mu(r)$ profile (bulge dominated region) for each spiral/S0 galaxy in our field and cluster samples and assessed whether or not the bulge profile was exponential in nature[8]. During the bulge profile inspection, we ignored the region immediately around the galactic centre ($r < 5$ pixels) in order to account for the effect of the *HST*/ACS point spread function (PSF) on the central regions of our $\mu(r)$ profiles.

Interestingly, we find that the fraction of exponential bulges is $\sim$ 20 per cent for both our spiral and S0 galaxies and is the same in both the field and cluster environments. Therefore, the fraction of exponential/non-exponential bulges in our STAGES disc galaxies seems to be independent of both morphology and the galaxy environment (at least from the general field to the intermediate densities of the A901/2 field). Consequently, this result suggests that major mergers are not the principal driver behind the transformation of spiral galaxies into S0s and that some other cluster related process is driving the observed morphology–density relation.

[8]Note: the spiral galaxy $\mu(r)$ profiles are described in Chapter 4: Section 4.3.

5.7 Conclusions

We present an analysis of V-band radial surface brightness $\mu(r)$ profiles for S0 galaxies from the field and cluster environment using *HST*/ACS imaging and data from the STAGES survey. Using a large, mass-limited ($M_* > 10^9\,\mathrm{M}_\odot$), visually classified sample of $\sim$ 280 field and cluster S0 galaxies, we assess the effect of the galaxy environment on the shape of S0 $\mu(r)$ profiles and the structure of S0 stellar discs.

We classify our S0 galaxies according to μ break features in their $\mu(r)$ profiles and find that the frequency of profile types (Type I, II and III) is approximately the same in both the field and cluster environments. For both field and cluster S0s, $\sim$ 25 per cent have a simple exponential profile (Type I), $<$ 5 per cent exhibit a down-bending break (truncation, Type II) and $\sim$ 50 per cent exhibit an up-bending break (antitruncation, Type III). The frequency of $\mu(r)$ profiles with no discernible exponential component (i.e. general curvature, Type c) is also approximately the same in the field and cluster environments and is $\sim$ 20 per cent. These profile fractions are robust to the subjective nature of the profile classifications, agreeing for classifications performed by three independent assessors. These results imply that the shape of S0 galaxy $\mu(r)$ profiles is not dependent on the galaxy environment.

Previous works (e.g. Pohlen & Trujillo 2006; Erwin et al. 2008) have found that for spiral galaxies, $\sim 20 \pm 10$ per cent are Type I, $\sim 50 \pm 10$ per cent are Type II and $\sim 30 \pm 10$ per cent are Type III. In comparing the profile type fractions (i.e. disc structure) of these spiral galaxies with our S0s, the most striking difference is the lack of stellar disc truncations (Type II profiles) in our S0s compared to their abundance in spiral galaxies. A similar result has also been obtained for S0 galaxies in the Virgo cluster (Erwin et al. 2012). Therefore, it seems whatever mechanism transforms spiral galaxies into S0s may erase these Type II features from the galaxy $\mu(r)$ profiles. In current theories, the nature of Type II profiles is thought to be related to a radial change in the age of the stellar population throughout the disc, with the outer disc being populated by old stars (Debattista et al. 2006; Bakos et al. 2008; Martínez-Serrano et al. 2009). Consequently, as a galaxy evolves, the suppression of star formation in the inner disc (e.g. via gas stripping) would cause the age of the inner disc stellar population to increase and the M/L across the $\mu(r)$ break to converge. Therefore, the absence of Type II profiles in our S0s may actually be a natural consequence of an ageing inner disc stellar population as spiral galaxies transform into S0s.

For S0s with a pure exponential disc (Type I, $\sim$ 25 per cent), we find no evidence to suggest an environmental dependence on the disc scalelength h. For S0s with a broken exponential disc, either down-bending (Type II, truncation, $<$ 5 per cent) or up-bending (Type III, antitruncation, $\sim$ 50 per cent), we find no evidence to suggest an environmental dependence on the break surface brightness μ_{brk} or the break strength T (outer-to-inner scalelength ratio, $\log_{10} h_{\mathrm{out}}/h_{\mathrm{in}}$). These results have been shown to be robust to the error in the sky subtraction and the subjective nature of the profile classifications. Therefore, we conclude that there is no evidence to suggest that the stellar distribution in the galactic disc is affected by the galaxy environment for S0 galaxies.

Our results suggest that the galaxy environment has no effect on the stellar distribution in the galactic discs of S0 galaxies (at least from the general field to the intermediate densities of the A901/2 clusters). These results are consistent with our analogous work, presented in Chapter 4, which reaches the same conclusion but

using a sample of *spiral* galaxies from STAGES. Our results are also consistent with other studies carried out on the effect of the galaxy environment on disc features in the STAGES survey (e.g. bars; Marinova et al. 2009). However, it is important to note that STAGES only covers an intermediate-density environment (Heiderman et al. 2009) and not a high-density environment (e.g. the Coma cluster, The & White 1986). Therefore, it is important to investigate the effect of the environment on the structure of stellar discs using more extreme high-density environments.

We also compare the disc structure of our S0s with the spiral galaxies from STAGES obtained from our analogous work in Chapter 4. For spiral/S0 galaxies with a pure exponential disc (Type I), we find no evidence to suggest that the disc scalelength is dependent on the galaxy morphology. For spiral/S0 galaxies with a broken exponential disc, either down-bending (Type II, truncation) or up-bending (antitruncation, Type III), we find no evidence to suggest that the break surface brightness $\mu_{\rm brk}$ is dependent on the galaxy morphology. However, we do find some evidence (significance $> 3\sigma$) that the break strength T of spiral/S0 galaxies is dependent on the galaxy morphology. The break strength T of both Type II and Type III profiles is generally smaller (weaker) in S0s compared to spiral galaxies. The weakening of Type II breaks in S0s may be related to the ageing of the inner disc stellar population (as described above) and the weakening of Type III breaks may be related to radial mixing throughout the disc in the disturbed Type III system. In order to fully test these hypotheses, we require high-quality colour profiles, or better still stellar age profiles, on a large sample of spiral/S0 galaxies covering a wide range of stellar masses. Only then will we be able to test whether the weakening of the $\mu(r)$ break in S0 galaxies is related to a weakening of their age profile gradient.

Finally, we complement these results with a comparison of the fraction of exponential bulges in our S0s with that of the spiral galaxies studied in Chapter 4. Interestingly, we find that the fraction of exponential/non-exponential bulges is the same in both our spiral and S0 galaxies. Since non-exponential bulges are thought to be produced in major merger events, this result indicates that major merging is not the principal driver behind the transformation of spiral galaxies into S0s.

Chapter 6

Antitruncated stellar light $\mu(r)$ profiles: bulge or disc related?

In this chapter, we explore the nature of antitruncated (Type III) stellar light profiles in both spiral and S0 galaxies using the *HST*/ACS imaging from the STAGES survey (see Chapter 2). In the established classification scheme (see Section 1.3.2: Fig. 1.10), antitruncated surface brightness $\mu(r)$ profiles (Type III) have a broken exponential disc with a shallower region beyond the break radius $r_{\rm brk}$. However, the excess light at large radii is not necessarily related to an outer exponential disc and could also be associated with an extended spheroidal (bulge) component. We explore this issue by using bulge–disc (B–D) decomposition in order to determine the contribution of bulge light in the outer regions ($r > r_{\rm brk}$) of Type III galaxies.

The majority of the work presented in this chapter has been published in the Maltby et al. (2012b) paper. That paper presents a comparison of measured $\mu(r)$ profiles and analytical B–D decompositions for the Type III spiral galaxies classified in Chapter 4. However, in this chapter we also perform an analogous exploration of the nature of Type III $\mu(r)$ profiles in our S0 galaxies (from Chapter 5) and these additional results are intended for presentation in the Maltby et al. (2012c) paper. In this work, all the profile fitting and statistical analyses are my own work. However, the critical B–D decompositions carried out on the STAGES *HST*/ACS V-band imaging were performed by Carlos Hoyos (see Section 6.2.2).

6.1 Introduction

The light profiles of disc galaxies (spiral and S0) consist of two main structural components: a spheroidal bulge component; and an exponentially declining stellar disc (de Vaucouleurs 1959b; Freeman 1970; see Section 1.3.2). In this simple picture, the de Vaucouleurs ($r^{1/4}$) bulge profile dominates in the central regions, while the exponential disc dominates at larger radii. However, theoretically the $r^{1/4}$ bulge profile will always dominate again at some low surface brightness (although possibly below our detection limits). Therefore, it is plausible that for some Type III profiles (up-bending breaks) the excess light beyond the break radius $r_{\rm brk}$ could be related to light from the spheroidal bulge or halo extending beyond the end of the stellar disc. This idea was first postulated by Erwin et al. (2005), who suggest that Type III profiles can be separated into two distinct subclasses depending on whether the outer profile $r > r_{\rm brk}$ is dominated by a stellar disc (Type III-d) or a spheroidal component (Type III-s).

Erwin et al. (2005) also propose that antitruncations with a smooth gradual transition and outer isophotes that are progressively rounder than that of the main disc, suggest an inclined disc embedded within a more spheroidal outer region such as an extended bulge or halo (i.e. Type III-s). Using this 'ellipse' method, previous works (Erwin et al. 2005, 2008; Gutiérrez et al. 2011) have found that ~ 40 per cent of their Type III profiles could be described as Type III-s.

However, the ellipse method is limited for face-on discs and cases where the outer/inner disc may have different orientations or axial ratios. In these instances, B–D decomposition (e.g. Allen et al. 2006) provides a useful tool to determine the contribution of the two major structural components (bulge and disc) to the galaxy's light distribution and should provide more conclusive evidence. The aim of this work is to use B–D decomposition on a large sample of spiral/S0 galaxies with stellar disc antitruncations from the STAGES survey (Gray et al. 2009) and assess the fraction of Type III profiles that show evidence for the excess light at large radii being caused or affected by the spheroidal component. This work builds on previous studies by using an improved method for the classification of Type III-s/III-d profiles (especially for face-on discs) and by using a larger more representative sample spanning the full range of disc morphologies (S0–Sdm).

In this chapter, we perform analogous analysis on both our spiral and S0 galaxies (from Chapters 4 and 5, respectively), presenting the results for spiral galaxies in Section 6.2 and the results for S0 galaxies in Section 6.3.

6.2 Antitruncations in spiral galaxies

6.2.1 Data and sample selection

For this study, we use the spiral galaxy sample defined in Chapter 4 (Section 4.2) and obtained from the STAGES survey (Gray et al. 2009). This consists of a large, mass-limited ($M_* > 10^9\,\mathrm{M}_\odot$), visually classified (Sa–Sdm) sample of 327 face-on to intermediate inclined ($i < 60°$) spiral galaxies from both the field and cluster environments. However, two galaxies for which B–D decomposition fails are removed from this sample[1] ($N_{\rm tot} = 325$). The 182 cluster spirals are at a redshift of $z_{\rm cl} = 0.167$ and the 143 field spirals span a redshift range of $0.05 < z_{\rm phot} < 0.30$.

In Chapter 4 (Section 4.4), we analysed the surface brightness $\mu(r)$ profiles for these spiral galaxies in order to identify broken exponentials in the outer stellar disc $\mu > 24\,\mathrm{mag\,arcsec}^{-2}$ (the criteria for selecting intrinsically similar outer breaks in our spiral galaxies, see Section 4.4.2). Using the resultant profile classifications, we obtain a subsample of 78 Type III $\mu(r)$ profiles ($\mu_{\rm brk} > 24\,\mathrm{mag\,arcsec}^{-2}$) that are robust to the subjective nature of the profile classification (i.e. the classifications for the three independent assessors were in agreement). We use both this Type III subsample and the total spiral sample in this study.

6.2.2 Methodology

(i) *Bulge–disc decompositions:* for each spiral galaxy in our total sample, we perform a two-dimensional B–D decomposition based on a two-component galaxy model composed of a de Vaucouleurs ($r^{1/4}$) bulge and a single exponential disc. Decompositions were carried out on the STAGES V-band imaging using the GALFIT code (Peng et al.

[1]Note: these B–D decompositions probably failed due to the contamination from a nearby star.

2002) and the method of Hoyos et al. (2011) adapted to perform two-component fits. Several measurable properties are produced for each galaxy including position [x,y], effective radii, total magnitudes, axial ratios, position angles for the bulge and disc components and a sky-level estimation.

B–D decomposition can be sensitive to the initial conditions used to search the B–D parameter space (e.g. initial estimate for bulge-to-disc ratio B/D). Therefore, we perform two runs of the B–D decomposition with different initial conditions taken from the two extremes: one run starting from a bulge-dominated system ($B/D = 9$) and the other run starting from a disc-dominated system ($B/D = 1/9$). Comparison of these runs (hereafter Run 1 and Run 2, respectively) allows for an assessment of the uniqueness/stability of B–D decomposition on a galaxy–galaxy basis.

In the vast majority of cases ($\sim$ 85 per cent) the results were effectively the same, $\sim$ 70 per cent being exactly the same and $\sim$ 15 per cent having only minor differences that do not affect our analysis (B/D the same to within $\sim$ 10 per cent). In a few cases ($\sim$ 10 per cent), the decomposition was catastrophically unstable with Run 1/2 yielding both bulge- and disc-dominated systems. The few remaining cases ($\sim$ 5 per cent) showed moderate instabilities great enough to affect the assessment of bulge light in the outer regions of the galaxy. These stability fractions are also the same in our Type III spiral subsample. The unstable solutions are mainly driven by differences in the sky level determined during the decomposition. However, the overall conclusions of this work are not affected by these unstable solutions.

(ii) *Profile fitting:* for each spiral galaxy, we also use the IRAF task ellipse[2] in order to obtain azimuthally-averaged radial $\mu(r)$ profiles from the STAGES *HST*/ACS V-band imaging. We achieve this using a similar methodology to that described in Chapter 4 (Section 4.3) but with two minor differences:

(a) in the fixed-parameter fits (fixed centre, ellipticity e and position angle PA), we use the galaxy centre determined from our B–D decomposition. As in previous chapters, the e and PA used are for the outer stellar disc (see Section 4.3);

(b) the necessary sky subtraction is performed using the sky-level estimates generated during B–D decomposition. Note: these sky values sometimes differ slightly from those of Gray et al. (2009) used throughout Chapters 4 and 5.

Analogous fixed-parameter fits (using the same e and PA, i.e. the same isophotes) are also carried out on the disc-residual images (ACS image minus bulge-only model) resulting in a measured μ profile for the disc component $\mu_{\rm disc}(r)$. We also obtain azimuthally-averaged radial μ profiles for the decomposed B–D model using the same fixed-parameter ellipses (isophotes) as in the other profiles. This results in separate analytical radial μ profiles for both the bulge- and disc-model along the semimajor axis of the elliptical isophotes (i.e. outer stellar disc)[3].

All resultant $\mu(r)$ profiles are corrected for Galactic foreground extinction, individual galaxy inclination i and surface brightness dimming (the μ profiles of our field galaxies, $0.05 < z_{\rm phot} < 0.30$, are corrected to the redshift of the cluster $z_{\rm cl} = 0.167$). For full details of the fitting procedure, subsequent photometric calibration and an estimation of the error in the sky subtraction ($\pm$0.18 counts), see Chapter 4 (Section 4.3).

[2]STSDAS package – version 2.12.2

[3]Note: these analytical B–D model profiles were calculated by Carlos Hoyos.

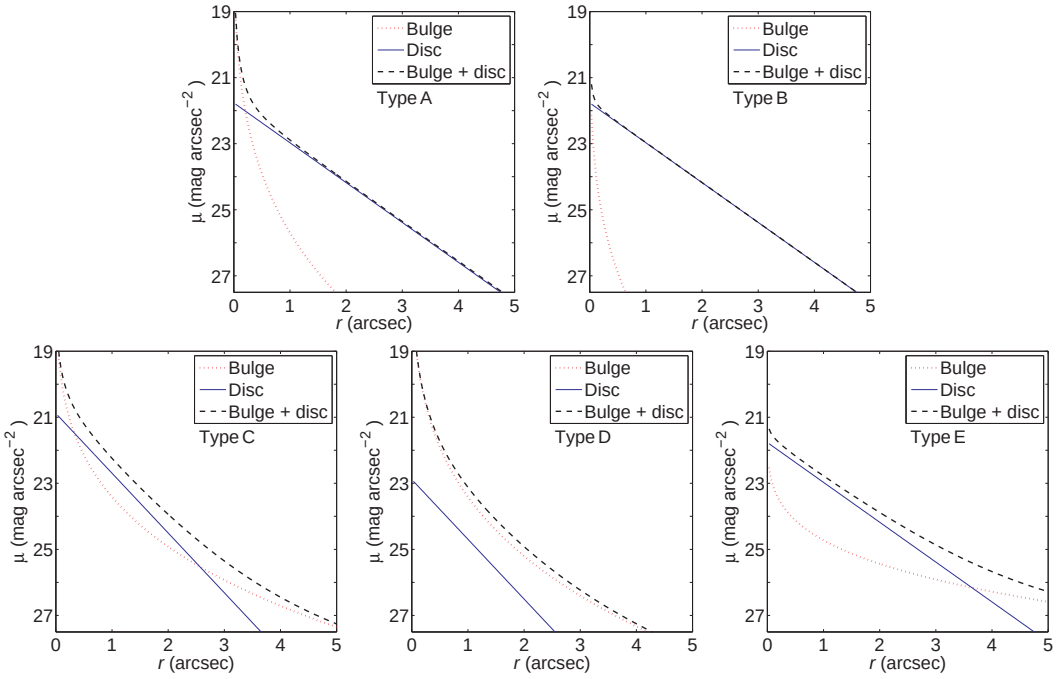

Figure 6.1. B–D profile types. Top left: Type A, 'classical' system. Top right: Type B, disc-dominated system. Bottom left: Type C, bulge-dominated at small/large radii but disc-dominated at intermediate radii. Bottom centre: Type D, bulge-dominated system. Bottom right: Type E, probable 'constrained' outer bulge (caused by an outer shallow disc).

6.2.3 Results

B–D decompositions using a de Vaucouleurs ($r^{1/4}$) bulge plus an exponential disc can be classified into four distinct profile types (e.g. Allen et al. 2006), see Fig. 6.1.

1. *Type A:* 'classical' system. The bulge profile dominates in the central regions, while the disc profile dominates at larger radii. The bulge/disc profiles cross only once.

2. *Type B:* disc-dominated system. The disc profile dominates at all radii, with a weak contribution from the bulge profile in the central region. The bulge/disc profiles never cross.

3. *Type C:* the bulge profile dominates at small/large radii, but the disc profile dominates at intermediate radii.

4. *Type D:* bulge-dominated system. The bulge profile dominates at all radii with a weak underlying disc component. The bulge/disc profiles never cross[4].

In addition to these profile types, we also observe decompositions where the disc profile dominates in the central regions, while the bulge profile dominates at larger radii (hereafter Type E). In these cases, we believe an outer antitruncated disc has incorrectly affected the bulge profile fit. Consequently, for Type E profiles B–D decomposition is not a true representation of the galaxy at large radii and in

[4]Note: capital letters are used in our B–D profile types to avoid confusion with the other classification schemes used in this thesis.

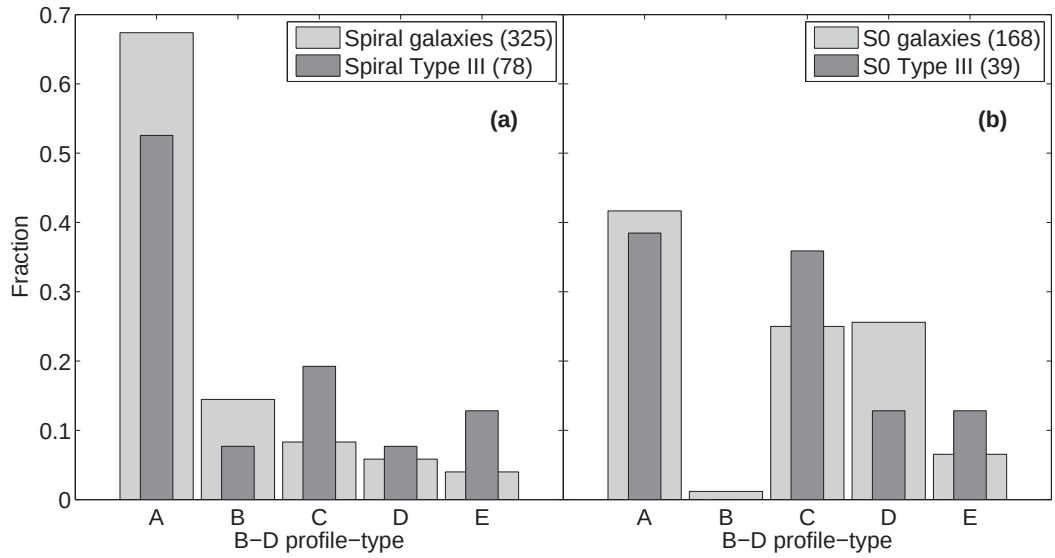

Figure 6.2. The distribution of B–D profile types. Left-hand panel: the distributions for our spiral galaxies (from Run 1). Distributions are presented for the total spiral sample (light grey) and the Type III spiral subsample (dark grey). Right-hand panel: analogous distributions for our S0 galaxies (see Section 6.3). Respective sample sizes are shown in the legends.

reality these galaxies probably have Type B compositions (or similar). Analogous constraints may also occur in some Type D profiles.

Fig. 6.2(a) shows the distribution of B–D profile types for both the total spiral sample and the Type III subsample. Comparing these distributions, we find that the fraction of Type C/E profiles is greater in the Type III subsample. This is expected from the nature of Type C/E profiles (i.e. excess light at large radii). For the total spiral sample, several other correlations between B–D profile type, Hubble-type morphology (Sa–Sd) and measured B/D are also observed. Type A/B profiles are equally probable in all Hubble types while Type C/D profiles are more common in earlier Hubble types (Sa–Sb). Also as expected, mean/median B/D decreases with progressively later Hubble types and increases for the sequence of B–D profile types B–A–C–D (increasing bulge dominance).

For each galaxy in our Type III subsample, we also compared the measured, fixed ellipse $\mu(r)$ profile with the model μ profiles from the B–D model in order to assess the contribution of bulge light in the outer regions of the galaxy ($r > r_{\rm brk}$). Fig. 6.3 shows some examples for each B–D profile type. These comparisons resulted in three possible scenarios. Bulge light in the outer profile ($r > r_{\rm brk}$) either had:

(i) *little or no contribution* ($\sim$ 70 per cent): for all Type A/B profiles the bulge contributes virtually no light at $r > r_{\rm brk}$ and in some Type C/E profiles the contribution is negligible. This can be determined by inspection of the measured disc-residual profile $\mu_{\rm disc}(r)$ and assessing if the properties of the outer profile/break ($r_{\rm brk}$, $\mu_{\rm brk}$, scalelength) have been affected with respect to the sky-subtraction error. No Type D profiles are in this category.

(ii) *minor contribution* ($\sim$ 15 per cent): approximately half of these cases are Type C profiles where the bulge profile emerges from the end of the disc and contributes some light to the outer regions of the galaxy. The remaining half are Type E

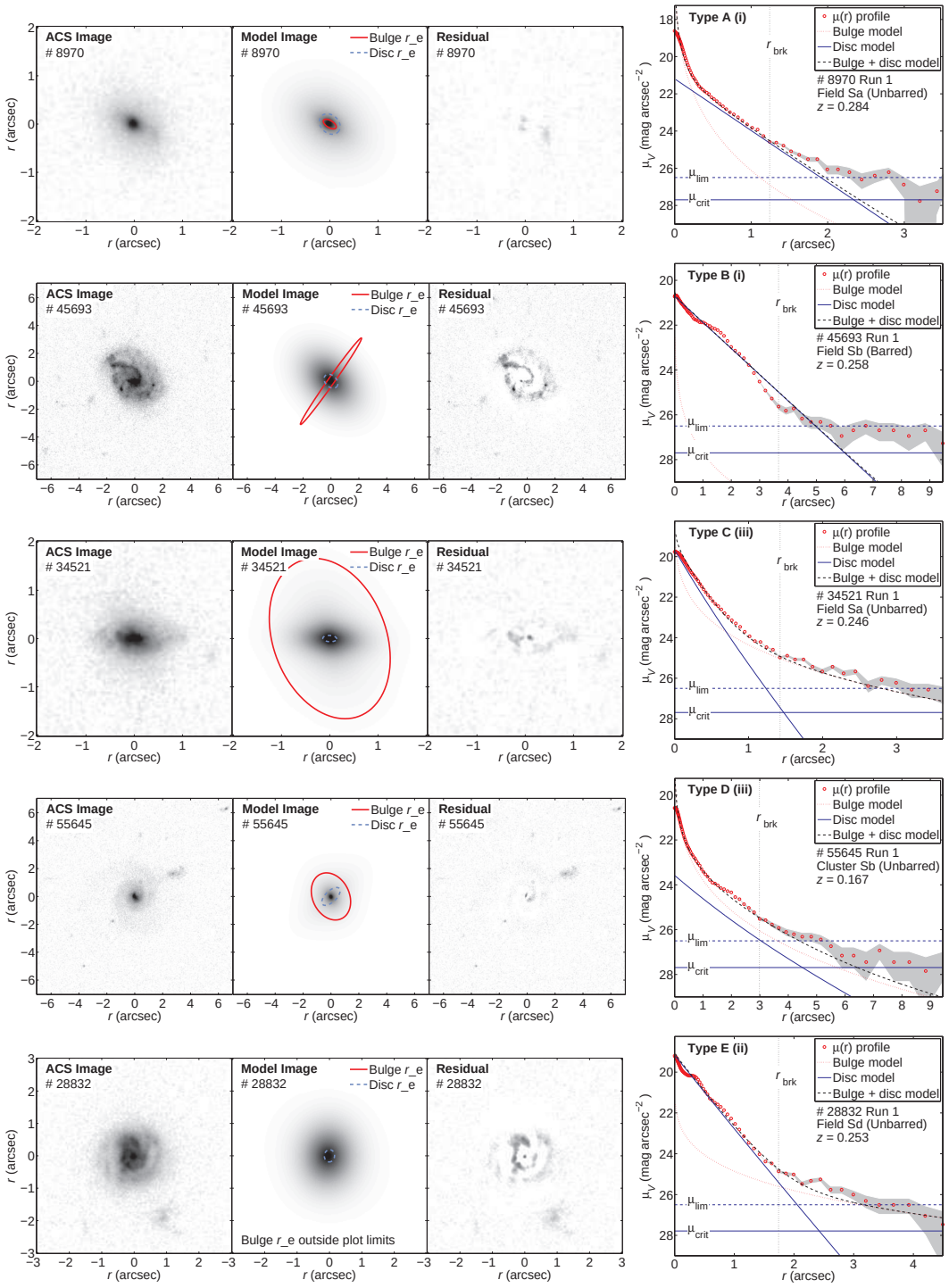

Figure 6.3. Example B–D decompositions and antitruncated $\mu(r)$ profiles. Rows, top to bottom: decompositions producing Type A, Type B, Type C, Type D and Type E profiles. The bulge (red dotted line), disc (blue line), and bulge + disc (black dashed line) profiles from B–D decomposition are overplotted on the measured $\mu(r)$ profiles (red circles). The i/ii/iii notation after the profile type indicates whether the bulge profile has a negligible, minor or major contribution outside the break radius $r > r_{\rm brk}$, respectively (see Section 6.2.3). Errors in the measured $\mu(r)$ profiles are for an oversubtraction and an undersubtraction of the sky by $\pm 1\sigma$. The $\mu_{\rm crit}/\mu_{\rm lim}$ levels represent $+1\sigma/+3\sigma$ above the sky, respectively. The model images show the effective radius isophote for both the bulge (red line) and disc (blue dashed line) models.

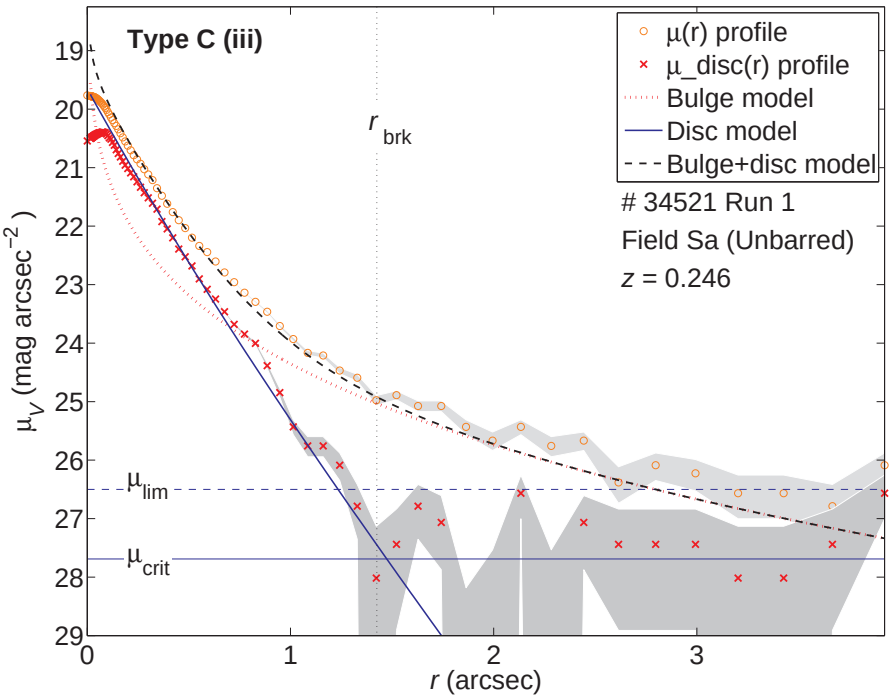

Figure 6.4. A rare/unusual example of a bulge profile causing an antitruncation in a spiral galaxy $\mu(r)$ profile (Type C example from Fig. 6.3, break radius $r_{\rm brk}$). The bulge (red dotted line), disc (blue line), and bulge + disc (black dashed line) profiles from B–D decomposition are overplotted on the measured $\mu(r)$ profile (red circles). The disc-residual $\mu_{\rm disc}(r)$ profile (measured μ profile minus bulge-only model, red crosses) shows no antitruncation (for errors, see Fig. 6.3).

profiles where the bulge appears to be constrained by an outer exponential disc. The amount contributed is enough to affect the outer profile causing $\mu_{\rm brk}$ and the outer scalelength to be different in the disc-residual profile $\mu_{\rm disc}(r)$. However, the antitruncation remains present.

(iii) *major contribution* ($\sim$ 15 per cent): the bulge contributes the majority of the light at $r > r_{\rm brk}$. Approximately half of these cases are Type D profiles where the bulge dominates at all radii. For these cases, the de Vaucouleurs profile is either interpreted as an antitruncation or being constrained by an outer shallow disc. The remaining half are all Type C profiles (with one exception which is Type E). In these latter cases the antitruncation is not observed in the disc-residual profile $\mu_{\rm disc}(r)$, see Fig. 6.4 for such an example.

These results suggest that for the majority of Type III spiral galaxies ($\sim$ 85 per cent), the excess light beyond the break radius $r_{\rm brk}$ is related to an outer shallow disc (Type III-d). However, in some of these cases ($\sim$ 15 per cent), bulge light can affect the measured properties of the disc profile (e.g. $\mu_{\rm brk}$, outer scalelength). For the remaining Type III profiles ($\sim$ 15 per cent), the excess light at $r > r_{\rm brk}$ can be attributed to the bulge profile (Type III-s). However, few of these latter cases (only three galaxies with stable decompositions, $\sim$ 5 per cent of the Type III subsample) exhibit profiles where the bulge profile extends beyond a dominant disc (Type C) and causes an antitruncation in the $\mu(r)$ profile. Therefore, we conclude that in the vast majority of cases Type III profiles in spiral galaxies are a true disc phenomenon.

6.3 Antitruncations in S0 galaxies

We complement our study on antitruncations in spiral galaxies (Section 6.2) with an analogous study exploring the nature of Type III profiles in S0 galaxies. In this work, we use the sample of STAGES S0 galaxies defined in Chapter 5 (Section 5.6.1). This consists of a large, mass-limited ($M_* > 10^9\,\mathrm{M}_\odot$), visually classified (S0) sample of 173 face-on to intermediate inclined ($i < 60°$) S0 galaxies from both the field and cluster environments. However, B–D decomposition fails for five of these galaxies[5], which are consequently removed from our S0 sample ($N_{\mathrm{tot}} = 168$). Using the disc profile classifications from Chapter 5, we also obtain a robust S0 subsample of 39 Type III $\mu(r)$ profiles (i.e. the classifications from the three independent assessors were in agreement).

For each S0 galaxy, we perform the necessary B–D decomposition using an analogous method to that used for spiral galaxies in Section 6.2.2. However, due to the smoothness of S0 stellar discs, the resultant decompositions were slightly more stable than for our spiral galaxies. In a comparison of the results from Run 1 and Run 2, ~ 90 per cent of cases were effectively the same (~ 85 per cent being exactly the same and ~ 5 per cent showing only minor differences) and in < 5 per cent of cases were the decompositions catastrophically unstable. These unstable solutions have no affect on the overall conclusions of this study. The stability fractions quoted are the same for both the total S0 sample and the Type III subsample.

The distribution of B–D profile types for both the total S0 sample and Type III subsample are presented in Fig. 6.2(b). As with our spiral galaxies, by comparing these distributions we find that the fraction of Type C/E profiles is greater in the Type III subsample as expected (see Section 6.2.3). However, a comparison of the B–D profile type distributions between our spiral and S0 galaxies shows some distinct differences. The fraction of disc-dominated B–D profile types (Type A/B) is much larger in spiral galaxies compared with S0s. Conversely, the fraction of bulge-dominated B–D profile types (Type C/D) is much larger in S0s compared with spiral galaxies. Therefore, for our galaxy samples we find that on average S0s have a higher B/D than spiral galaxies. This result is consistent with the hypothesis that spiral galaxies transform into S0s by the termination of star formation (see Section 1.1.5). The suppression of star formation in the stellar disc (e.g. by gas stripping), would cause the disc component to gradually fade and the B/D to increase. Consequently, any galaxy undergoing a spiral $\rightarrow$ S0 transformation should naturally evolve into a more bulge-dominated system.

We expand on this result by comparing the bulge PA (from B–D decomposition) with a visual estimate for the PA of the outer galactic region (i.e. PA for the outer stellar disc used in our fixed-ellipse fits, see Section 4.3). Fig. 6.5 shows these comparisons for both our spiral and S0 galaxies. For spiral galaxies, there is no obvious correlation between the PA of the bulge and the outer galactic region. This indicates that our visual estimates are *not* related to the inner bulge and are indeed probing an outer disc component. Additionally, since galactic discs are essentially axisymmetric (a consequence of rotational motion), the misalignment between the bulge and the disc also suggests a triaxial (non-axisymmetric) nature for the bulges of our spiral galaxies (see e.g. Bertola et al. 1991). In contrast, for S0 galaxies there is a significant correlation between the PA of the bulge and the outer galactic

[5]Note: these B–D decompositions probably failed due to the contamination from a nearby star or companion galaxy.

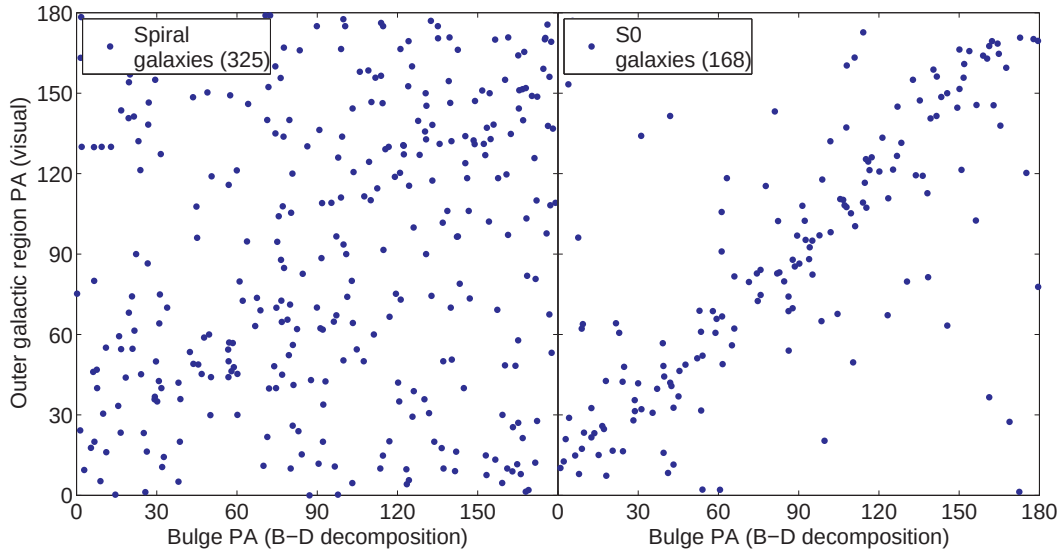

Figure 6.5. A comparison of the bulge PA (from B–D decomposition) with a visual estimate for the PA of the outer galactic regions (i.e. outer stellar disc, see Section 4.3) for both spiral galaxies (left-hand panel) and S0s (right-hand panel). Respective sample sizes are shown in the legends.

region. This alignment between the bulge and the disc component implies a bulge that is axisymmetric (oblate) in nature for many of our S0 galaxies. However, this alignment also suggests the possibility that for some of our S0s, the visual estimates could actually be probing the outer regions of the bulge component (and not the stellar disc). This result is consistent with the observation that S0s tend to have a higher B/D than spiral galaxies. Considering the high fraction of bulge-dominated B–D profiles (Type C/D) in our S0s, this is not surprising (see Fig. 6.2). However, more importantly, this result clearly indicates that light from the spheroidal (bulge) component potentially contributes a significant amount of light to the outer regions of some S0 galaxies. Consequently, bulge light may account for more Type III profiles in S0s than we observed for our spiral galaxies (see Section 6.2).

Therefore, for our Type III S0 galaxies we also compare the measured $\mu(r)$ profile with the model μ profiles from B–D decomposition in order to determine the contribution of bulge light in the outer regions of the galaxy ($r > r_{\rm brk}$). Using an analogous scheme to that presented in Section 6.2.3, we find that bulge light in the outer profile ($r > r_{\rm brk}$) either had:

(i) *little or no contribution* ($\sim$ 45 per cent): these cases are entirely comprised of Type A profiles. No Type B profiles are observed in our Type III S0 galaxies.

(ii) *minor contribution* ($\sim$ 10 per cent): the majority of these cases are Type C profiles (with one exception which is Type E).

(iii) *major contribution* ($\sim$ 45 per cent): for these cases, one quarter are Type D, one quarter are Type E, and the remaining half are Type C (where the antitruncation can be entirely accounted for by bulge light, see Fig. 6.6 for such an example).

These results suggest that for only about a half of Type III S0 galaxies ($\sim$ 55 per cent), the excess light beyond the break radius $r_{\rm brk}$ is related to an outer shallow

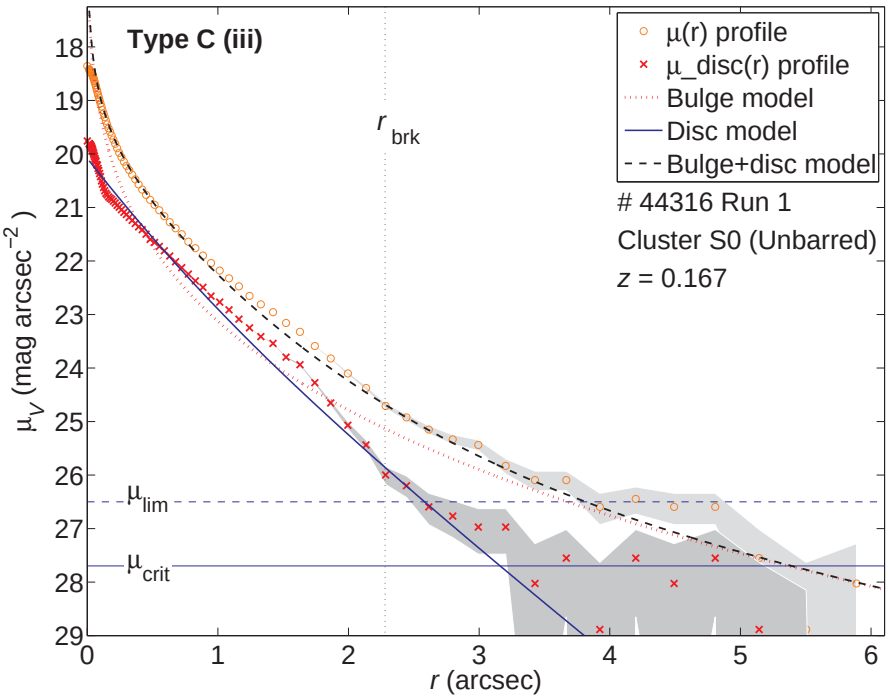

Figure 6.6. A common example of a bulge profile causing an antitruncation in an S0 $\mu(r)$ profile (break radius $r_{\rm brk}$). The bulge (red dotted line), disc (blue line), and bulge + disc (black dashed line) profiles from B–D decomposition are overplotted on the measured $\mu(r)$ profile (red circles). The disc-residual $\mu_{\rm disc}(r)$ profile (measured μ profile minus bulge-only model, red crosses) shows no antitruncation (for errors, see Fig. 6.3).

disc (Type III-d). For the remaining cases ($\sim$ 45 per cent), the excess light at $r > r_{\rm brk}$ can be attributed to the bulge profile (Type III-s). More importantly, for these latter cases a considerable fraction ($\sim$ 20 per cent of the Type III S0 subsample) exhibit profiles where the bulge profile extends beyond a dominant disc (Type C) and causes an antitruncation in the $\mu(r)$ profile. Therefore, we conclude that bulge light is an important component in the $\mu(r)$ profiles of some S0 galaxies at large radii and that antitruncations in S0s are frequently caused by either the bulge or disc component.

6.4 Conclusions

In this chapter, we have explored the nature of antitruncated (Type III) stellar light profiles in both spiral and S0 galaxies using the *HST*/ACS V-band imaging from the STAGES survey. In Type III $\mu(r)$ profiles (up-bending breaks), the excess light beyond the break radius $r_{\rm brk}$ can either be related to an outer exponential disc (Type III-d) or an extended bulge component (Type III-s). Using B–D decomposition on a large sample of Type III spiral/S0 galaxies, we assess the fraction of Type III profiles that show evidence for the excess light at large radii ($r > r_{\rm brk}$) being caused or affected by the bulge component.

(i) *Spiral galaxies:* our results suggest that for the majority of Type III spiral galaxies ($\sim$ 85 per cent), the excess light beyond the break radius $r_{\rm brk}$ is related to an outer shallow disc (Type III-d). However, it is important to note that for

some of these cases ($\sim$ 15 per cent), bulge light can affect the measured properties of the disc profile (e.g. $\mu_{\rm brk}$, outer scalelength). For the remaining Type III profiles ($\sim$ 15 per cent), the excess light at $r > r_{\rm brk}$ can be attributed to the bulge profile (Type III-s). However, few of these latter cases ($\sim$ 5 per cent of the Type III subsample) exhibit profiles where the bulge profile extends beyond a dominant disc (Type C) and causes an antitruncation in the $\mu(r)$ profile. Therefore, we conclude that in the vast majority of cases Type III profiles in spiral galaxies are indeed a true disc phenomenon.

(ii) *S0 galaxies:* our results indicate that for only about a half of Type III S0s ($\sim$ 55 per cent), the antitruncation is related to an outer shallow disc (Type III-d). For the remaining cases ($\sim$ 45 per cent), the excess light at $r > r_{\rm brk}$ can be accounted for by the bulge profile (Type III-s). More importantly, for these latter cases there are many S0s ($\sim$ 20 per cent of the Type III subsample) that exhibit Type C profiles – i.e. an antitruncated $\mu(r)$ profile caused by the bulge extending beyond a dominant disc. Therefore, we conclude that bulge light is an important component in the $\mu(r)$ profiles of many S0 galaxies at large radii and that antitruncations in S0s are commonly caused by either the bulge or disc component.

Previous works (Erwin et al. 2008; Gutiérrez et al. 2011) have used the ellipse method to classify their Type III-d/III-s profiles (see Section 6.1). The results of these works are in good agreement with their Type III profiles being $\sim$ 60 per cent Type III-d and $\sim$ 40 per cent Type III-s. In these studies, mixed samples of early-type spiral and S0 galaxies (S0–Sb) were used with S0s accounting for $\sim$ 40 per cent of the total sample. Consequently, their Type III-d/III-s fractions cannot be directly compared to those from this work. However, by assuming a similar morphological distribution, we find that our Type III profiles would have been $\sim$ 75 per cent Type III-d and $\sim$ 25 per cent Type III-s. Therefore, it appears our results are *not* consistent with those of previous works. However, consider the case where the contribution of bulge light at $r > r_{\rm brk}$ is too little to explain the antitruncation but great enough to affect the properties of the disc profile (i.e. a minor contribution). The increased contribution of bulge light to the $\mu(r)$ profile at $r_{\rm brk}$ could lead to a smoothing of the inflection and a roundening of the outer isophotes. Therefore, using the ellipse method would likely have resulted in these Type III-d profiles being classified as Type III-s. Interestingly, by applying this reasoning to our results and assuming a similar morphological distribution to previous works, we obtain fractions of $\sim$ 60/40 per cent for our Type III-d/III-s profiles, respectively (i.e. exactly the same as in previous studies). This result clearly indicates that the ellipse method potentially leads to genuine disc breaks being classified as Type III-s. Therefore, our method using B–D decomposition offers an improved, more robust way to determine whether an antitruncation is disc or spheroid related.

However, our method does have some obvious drawbacks. In a two-component B–D decomposition, an outer antitruncated disc could cause the bulge profile to be constrained and lead to an overestimation of bulge light in the outer regions of the galaxy. This naturally enhances the fraction of Type III-s profiles which therefore represents an upper limit to the fraction of genuine Type III-s profiles in our spiral/S0 Type III samples. Therefore, considering our results we can conclude that for spiral galaxies, in the vast majority of cases Type III profiles are indeed a true disc phenomenon; whereas for S0 galaxies, only about a half of Type III profiles are related to the stellar disc.

6.4.1 Implications for the formation of S0 galaxies

A comparison of the results stated for our Type III spiral and S0 galaxies provides some insight into the potential processes by which spiral galaxies transform into S0s. In the following, we highlight two key observations:

(i) *S0s generally have a higher B/D than spiral galaxies:* our B–D decompositions have shown that the fraction of bulge-dominated $\mu(r)$ profiles is larger in S0s than spiral galaxies, and that spiral galaxies have mainly disc-dominated $\mu(r)$ profiles. This result is consistent with the hypothesis that spiral galaxies transform into S0s by the termination of star formation (see Section 1.1.5). If star formation is suppressed in the stellar disc (e.g. by gas stripping), then the disc will gradually fade and the B/D will increase. Consequently, when a spiral galaxy transforms into an S0 the galaxy should naturally evolve into a more bulge-dominated system.

(ii) *Bulge light can account for more Type III profiles in S0s than spiral galaxies:* our results suggest that an extended bulge component can account for Type III features in as many as $\sim$ 45 per cent of Type III S0s, but in only $\sim$ 15 per cent of Type III spirals. This result can also be understood by the concept of a fading stellar disc as spirals transform into S0s. As the stellar disc fades, the B/D increases and consequently the tail end of the bulge profile may eventually dominate over the disc at large radii (i.e. as in Type C/D profiles, see Fig. 6.1). This process would naturally lead to an increase in the fraction of Type III-s profiles in S0 galaxies.

6.4.2 Implications for the formation of Type III profiles

Several studies have proposed potential formation scenarios for genuine antitruncated stellar discs (i.e. Type III-d profiles), mainly via satellite accretion or minor mergers (e.g. Peñarrubia et al. 2006; Younger et al. 2007). The correlations reported for spiral galaxies, where Type III profiles are more frequent in earlier Hubble types (e.g. Pohlen & Trujillo 2006; and Chapter 4: Fig. 4.11), are consistent with this scenario. However, the results of this chapter raise an important issue. For spiral galaxies, the excess of Type III profiles in early Hubble types could easily have been related to a natural increase in the number of Type III-s profiles in these galaxies (i.e. due to the increase in B/D). To address this issue, we compare the morphology distributions for both our total spiral Type III sample and our subsample of genuine disc antitruncations Type III-d (see Fig. 6.7). These comparisons clearly show that Type III-s profiles are only a significant fraction in Sa galaxies ($\sim$ 10 per cent) and that we observe the same morphology correlation using just our genuine Type III-d spiral galaxies. Therefore, our results remain consistent with the minor merger scenario for the formation of Type III profiles.

For completeness, in Fig. 6.7 we also show the fraction of Type III/III-d profiles in our S0 galaxies. However, due to the slight variations in the disc profile classification between our spiral and S0 galaxies[6], we cannot make fair comparisons between the fractions of the 'robust' Type III profiles in our total spiral and S0 samples. However, we show this result to illustrate that Type III-s profiles are a far greater component of Type III profiles in S0s ($\sim$ 45 per cent) than spiral galaxies. In con-

[6]Note: the inclusion of Type c (curvature) profiles in our S0 classification (see Section 5.4) leads to an additional constraint on the 'robust' sample of S0 Type III profiles used in this chapter (i.e. where all assessor classifications agree).

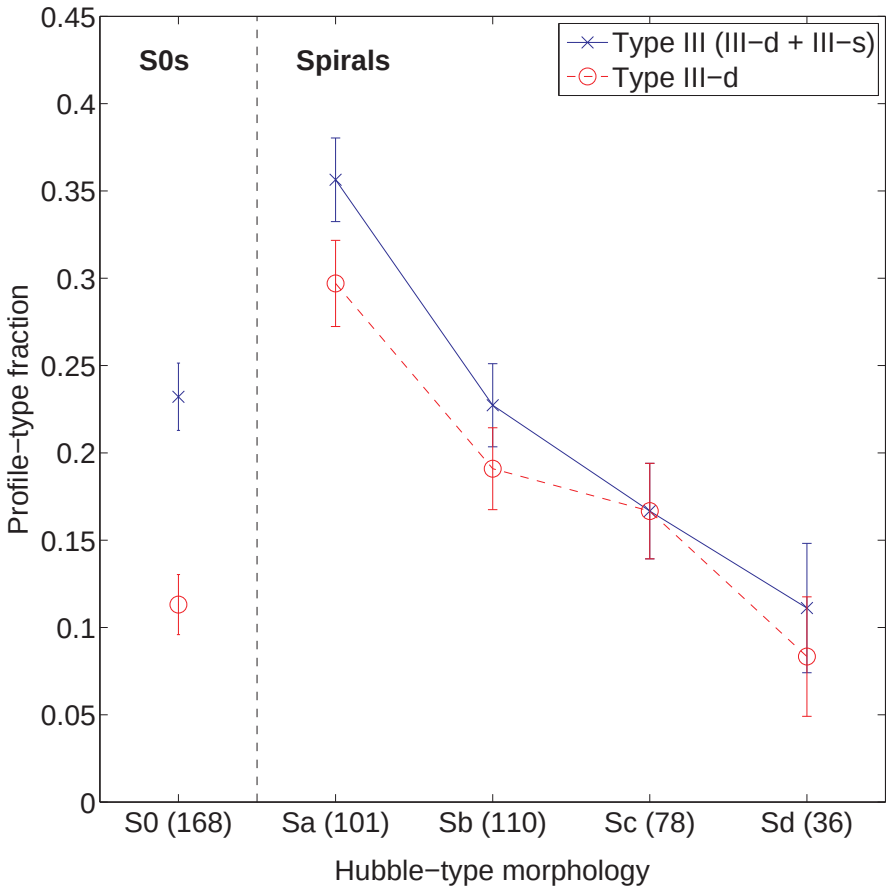

Figure 6.7. The fraction of antitruncations (Type III profiles) as a function of Hubble-type morphology (S0–Sd). The correlations shown are for all Type III profiles (blue line) and the subsample of Type III-d profiles (i.e. genuine disc antitruncations, red dashed line). The sample size for each Hubble-type is shown on the x-axis and the errors in the profile-type fractions were calculated using Equation 4.9.

clusion, we find that for spiral galaxies antitruncated stellar light profiles are indeed a true disc phenomenon. However, for S0 galaxies bulge light can be a significant component in the outer regions ($r > r_{\rm brk}$) of the galaxy, with approximately half of S0 antitruncations being caused by light from an extended bulge component.

Chapter 7

Conclusions and future work

In this thesis, we have explored the effect of the galaxy environment on the size and structure of a galaxy's stellar distribution using the *HST*/ACS V-band imaging and data from the STAGES survey (Gray et al. 2009; see Chapter 2). Certain physical processes inherent to galaxy evolution and related to the galaxy environment (e.g. ram-pressure stripping, mergers and harassment, see Section 1.2) may affect a galaxy's stellar distribution. Consequently, these environmental processes could prove to be the origin of the observed morphology–density relation (Dressler 1980; see Section 1.1.2). However, at the present time, we are still largely uncertain about what physical processes can bring about the observed changes in stellar structure (i.e. morphology) and how these processes are related to the galaxy environment. The work presented in this thesis aims to address this problem in some detail.

In addition to these environmental studies, we also use our structural analyses in order to enhance our current understanding of how spiral galaxies transform into S0s. In the following sections, we briefly highlight the key results presented in this thesis and discuss their impact on current theories of galaxy evolution. Finally, we also consider some potential directions in which this work may be extended in future studies.

7.1 The stellar distribution and the galaxy environment

7.1.1 The size of the stellar distribution

In Chapter 3, we presented the stellar-mass–size relations for elliptical, lenticular and spiral galaxies in three different environments: the field, cluster and cluster core. Using a large sample of ~ 1200 field and cluster galaxies and a subsample of cluster core galaxies, we determined the significance of an environmental dependence on the stellar-mass–size relation (i.e. galaxy sizes) for each morphological type.

For the majority of galaxies: elliptical, lenticular and high-mass ($M_* > 10^{10}\,\mathrm{M}_\odot$) spirals, we found no evidence to suggest a galaxy's physical size is influenced by the galaxy environment. However, for intermediate-/low-mass spirals ($M_* < 10^{10}\,\mathrm{M}_\odot$) we did find some evidence, significant at the 2σ level, for a potential environmental dependence on galaxy sizes: the mean effective radius a_e is ~ 15–20 per cent larger in the field than in the cluster. This is due to a population of low-mass, large-a_e field spirals that are largely absent from the cluster environments. Through a visual inspection of the V-band imaging, we found that these large-a_e field spirals contain extended stellar discs not present in their cluster counterparts. This suggests that the fragile extended stellar discs present in these spiral galaxies may not survive

the environmental conditions in the cluster. Taken together, our results suggest that internal physical processes are the main drivers governing any size evolution in galaxies, with the environment possibly playing a role affecting only the discs of intermediate-/low-mass spirals.

7.1.2 The structure of the stellar distribution

In Chapters 4 and 5, we extended our environmental studies to explore the effect of the galaxy environment on the structure of the stellar distribution in both spiral and S0 galaxies. Using a large, mass-limited ($M_* > 10^9\,\mathrm{M}_\odot$), visually classified (S0–Sd) sample of ~ 600 field and cluster galaxies, we determined the significance of an environmental dependence on the shape of a galaxy's V-band radial surface brightness $\mu(r)$ profile.

Spiral galaxies

We classified our spiral galaxies according to $\mu(r)$ break features in their outer stellar disc ($\mu > 24\,\mathrm{mag\,arcsec^{-2}}$; the criteria used for selecting intrinsically similar outer breaks in our spiral galaxies, see Section 4.4.2). If the galaxy had no break in this μ range, then the galaxy had a simple exponential profile in the outer disc and was classified as Type $\mathrm{I_o}$. Galaxies that have a simple exponential profile across the length of their disc component (Type I, a subset of Type $\mathrm{I_o}$) were also identified. However, if the galaxy exhibited a broken exponential in the outer disc, it was classified as either Type $\mathrm{II_o}$ for a down-bending break (*outer disc truncation*) or Type $\mathrm{III_o}$ for an up-bending break (*outer disc antitruncation*).

Using this classification scheme, we found that the distribution of outer disc profile types $\mathrm{I_o}$:$\mathrm{II_o}$:$\mathrm{III_o}$ is approximately 50:10:40 per cent and the same in both the field and cluster environments. This result implies that the galaxy environment has little direct effect on the shape of a galaxy's $\mu(r)$ profile in the outer stellar disc.

We expanded on this result with an assessment of whether the scalelength h or break strength T (outer-to-inner scalelength ratio, $\log h_{\mathrm{out}}/h_{\mathrm{in}}$) of our spiral galaxies is influenced by the galaxy environment. For spirals with a pure exponential outer stellar disc (Type $\mathrm{I_o}$), we found no evidence to suggest the outer disc scalelength h_{out} is dependent on the galaxy environment. We also found no evidence for an environmental dependence on the scalelength h of spirals with a pure exponential profile across the length of their disc component (Type I, a subset of Type $\mathrm{I_o}$). For galaxies with a broken exponential in their outer stellar disc, either down-bending (Type $\mathrm{II_o}$) or up-bending (Type $\mathrm{III_o}$), we also found no evidence to suggest an environmental dependence on the break strength T. Considering these results, we conclude that there is no evidence to indicate the stellar distribution in the outer stellar disc of spiral galaxies is directly affected by the galaxy environment.

S0 galaxies

We classified our S0 galaxies according to $\mu(r)$ break features in their stellar disc (note: in this case, classification is based on the entire disc component) and also found that the frequency of profile types (Type I, II and III) is approximately the same in both the field and cluster environments. For both field and cluster S0s, ~ 25 per cent had a simple exponential profile (Type I), < 5 per cent exhibited a down-bending break (Type II, *truncation*) and ~ 50 per cent exhibited an up-bending

break (Type III, *antitruncation*). For the remaining S0 galaxies ($\sim$ 20 per cent), no discernible exponential component was observed (i.e. general curvature in the μ profile).

The distinct lack of truncations (Type II profiles) in both our field and cluster S0s is of particular interest. In previous works on the disc structure of *spiral* galaxies (e.g. Pohlen & Trujillo 2006; Erwin et al. 2008), Type II profiles are very common with the distribution of profile types I:II:III being approximately 20:50:30 $\pm$10 per cent. Therefore, it seams whatever transforms spiral galaxies into S0s may erase these truncations from the $\mu(r)$ profiles. We shall return to this result in Section 7.2.

As with our spiral analyses, we expanded on our environmental comparisons by evaluating whether the scalelength h or break strength T ($\log h_{\rm out}/h_{\rm in}$) of our S0s is influenced by the galaxy environment. For S0s with a pure exponential disc (Type I), we found no evidence to indicate the disc scalelength h is dependent on the galaxy environment. For S0s with a broken exponential disc, either down-bending (Type II) or up-bending (Type III), we also found no evidence to suggest any environmental effect on the break strength T. Therefore, considering these results, we conclude that there is no evidence to suggest the stellar distribution in the stellar disc of S0 galaxies is directly affected by the galaxy environment.

7.1.3 Conclusion: implications for galaxy evolution

Taken together, the results of our environmental studies suggest that the galaxy environment has little direct effect on the size and structure of a galaxy's stellar distribution (at least from the general field to the intermediate densities probed by the STAGES survey). Consequently, our results imply that physical processes directly affecting the structure of the stellar distribution, i.e. galaxy-galaxy or galaxy-cluster gravitational interactions (e.g. mergers and harassment, see Section 1.2), are not driving the observed morphology–density relation. We conclude that more subtle processes acting on the gaseous component of a galaxy (e.g. ram-pressure stripping) are more likely to play an important role in the origin of the morphology–density relation and the transformation of spiral galaxies into S0s.

7.2 Structural analyses: implications for S0 formation

7.2.1 The structure of the stellar distribution

In Chapter 5, we complemented our environmental studies with a comparison of the stellar disc structure in our spiral and S0 galaxies. In our structural analyses, one of the most interesting observations was the lack of truncations (Type II profiles) in our S0s compared to their abundance in spiral galaxies from previous works. We expanded on this result by comparing the structural properties of the disc (scalelength h, break surface brightness $\mu_{\rm brk}$ and break strength T) in our spiral and S0 galaxies.

For spiral/S0 galaxies with a pure exponential disc (Type I), we found no evidence to suggest that the disc scalelength is dependent on the galaxy morphology. For spiral/S0 galaxies with a broken exponential disc (Type II and III), we also found no evidence to suggest that the break surface brightness $\mu_{\rm brk}$ is related to the galaxy morphology. However, we did find some evidence (significance $> 3\sigma$) that the break strength T of spiral/S0 galaxies is somehow related to the galaxy morphology. The break strength T of both Type II and Type III profiles is generally

smaller (weaker) in S0s compared to spiral galaxies. This result suggests that some process inherent to the morphological transformation of spiral galaxies into S0s can affect the structure of the stellar disc causing a weakening of $\mu(r)$ breaks and may even eliminate truncations (Type II profiles) from S0 galaxies.

In order to understand this result, we need to consider the current theory for the formation of stellar disc truncations. Truncated $\mu(r)$ profiles are thought to form via a radial star formation threshold and the radial scattering of inner disc stars to regions beyond this threshold (i.e. break radius $r_{\rm brk}$; e.g. Debattista et al. 2006). Consequently, the outer disc should be populated by old stars as these are the ones that have had enough time to make the disc migration. In this scenario, truncations (Type II profiles) are related to a radial change in the age of the stellar population throughout the disc. As a galaxy evolves, the suppression of star formation in the inner disc (e.g. via gas stripping) would cause the age of the inner disc stellar population to increase and the mass-to-light ratio (M/L) across the $\mu(r)$ break to converge. Therefore, the absence/weakening of Type II profiles in our S0s may actually be the natural consequence of the termination of star formation in the stellar disc as spiral galaxies transform into S0s.

We expanded on these structural analyses by comparing the fraction of exponential bulges observed in our spiral and S0 galaxies. Interestingly, we found that the fraction of exponential bulges is the same ($\sim$ 20 per cent) for both morphologies. Since non-exponential bulges (mainly classical, de Vaucouleurs bulges) are thought to be produced by major mergers, this result implies that major merging is not the principal driver behind the transformation of spirals into S0s.

7.2.2 The nature of stellar disc antitruncations

In Chapter 6, we explored the nature of antitruncated (Type III) stellar light profiles in both spiral and S0 galaxies. In Type III $\mu(r)$ profiles (up-bending breaks), the excess light beyond the break radius $r_{\rm brk}$ can either be related to an outer exponential disc (Type III-d) or an extended bulge component (Type III-s). Using bulge–disc (B–D) decomposition on a large sample of $\sim$ 120 Type III spiral/S0 galaxies, we assessed the fraction of Type III profiles that show evidence for the excess light at large radii ($r > r_{\rm brk}$) being caused or affected by the bulge component.

For Type III spirals, we found that in the majority of cases ($\sim$ 85 per cent), excess light beyond $r_{\rm brk}$ can be attributed to an outer shallow stellar disc (Type III-d). Therefore, we conclude that in the vast majority of cases Type III profiles in spiral galaxies are indeed a true disc phenomenon. However, for Type III S0s bulge light can have a significant effect in the outer regions of the $\mu(r)$ profile. In $\sim$ 50 per cent of Type III S0s, the excess light at large radii can be entirely accounted for by light from the bulge component (Type III-s).

We propose that these results are consistent with the hypothesis that spiral galaxies transform into S0s by the termination of star formation. The suppression of star formation in the stellar disc (e.g. by gas stripping), would cause the disc component to gradually fade and the B/D to increase. Consequently, any galaxy undergoing a spiral $\rightarrow$ S0 transformation should naturally evolve into a more bulge-dominated system. As the stellar disc fades the tail end of the bulge profile may eventually dominate over the stellar disc at large radii. Consequently, if a fading stellar disc is inherent to the morphological transformation of spirals into S0s, this would naturally lead to an increase in the fraction of antitruncations caused by the bulge component (Type III-s) in S0 galaxies.

7.3 Future work

In the final section of this thesis, we consider some of the potential directions in which this work may be extended in future studies. We consider these potential extensions with respect to several related outstanding problems:

(i) *The effect of the galaxy environment on the stellar distribution:* the results presented in this thesis suggest that the galaxy environment has little direct effect on the size and structure of a galaxy's stellar distribution. However, our results are for one survey field (STAGES), and one multicluster complex of intermediate galaxy density at low redshift ($z \sim 0.167$). Therefore, it is important to investigate whether we see the same trends observed in the STAGES A901/2 field in other survey fields across a wide range of redshift and cluster mass. Extending these studies to higher redshifts is of key importance. In the relatively local Universe, structural evolution in a galaxy's stellar distribution may already have ceased in both the field and cluster environments, even if the environment is the principal driver. However, in the more distant Universe structural changes may still be occurring in both the field and cluster environments and at different rates. Probing denser, more massive cluster environments (e.g. the Coma cluster) is also important because some environmental drivers may only be significant in very high-density environments (i.e. rich cluster cores). Ultimately, the comparison of high-redshift studies with those from the local Universe across a wide range of environments will allow for a complete assessment of whether or not the galaxy environment has any direct effect on a galaxy's stellar distribution.

(ii) *The role of the galaxy environment in galaxy evolution:* the results presented in this thesis suggest that subtle physical processes acting on the gaseous component of a galaxy (e.g. ram-pressure stripping) are likely to play an important role in driving the morphology–density relation and the transformation of spiral galaxies into S0s. With respect to this conclusion, it would be extremely interesting to expand our environmental studies to explore the effect of the galaxy environment on the structure of a galaxy's *gas* disc (e.g. using radio/submillimetre imaging). The nature of truncations/antitruncations in these gas discs as a function of the galaxy environment could yield some important evidence for the effect of ram-pressure stripping/gas compression on disc galaxies.

(iii) *S0 formation – the structure of galactic discs:* determining the true nature of truncations and antitruncations in stellar discs is vital to our understanding of the evolution of the stellar disc and how this relates to evolution in morphology. To this aim, more detailed structural analyses involving high-quality radial colour profiles (or better still, stellar-age profiles) for disc galaxies will be necessary in order to allow for important tests to be carried out on the current theories of stellar disc formation and evolution.

These are just a few potential ideas for future studies. However, in reality the scope for future work is endless. Disentangling the mysteries of galaxy evolution is an extremely challenging and daunting task and the more we learn, the more questions we have. There can be no doubt that this area of research will remain active for many years to come.

Bibliography

Abell G. O., 1965, ARA&A, 3, 1

Allen P. D., Driver S. P., Graham A. W., Cameron E., Liske J., de Propris R., 2006, MNRAS, 371, 2

Aragón-Salamanca A., Bedregal A. G., Merrifield M. R., 2006, A&A, 458, 101

Azzollini R., Trujillo I., Beckman J. E., 2008, ApJ, 684, 1026

Bakos J., Trujillo I., Pohlen M., 2008, ApJ, 683, L103

Baldry I. K., Balogh M. L., Bower R. G., Glazebrook K., Nichol R. C., Bamford S. P., Budavari T., 2006, MNRAS, 373, 469

Balogh M. L., Baldry I. K., Nichol R., Miller C., Bower R., Glazebrook K., 2004, ApJ, 615, L101

Barden M., et al., 2005, ApJ, 635, 959

Barden M., Häußler B., Peng C. Y., McIntosh D. H., Guo Y., 2012, MNRAS, 422, 449

Barton E. J., Geller M. J., Kenyon S. J., 2000, ApJ, 530, 660

Bekki K., 1998, ApJ, 502, L133

Bell E. F., et al., 2004, ApJ, 608, 752

Bell E. F., et al., 2005, ApJ, 625, 23

Bell E. F., et al., 2006, ApJ, 640, 241

Bertola F., Vietri M., Zeilinger W. W., 1991, ApJ, 374, L13

Binggeli B., Tammann G. A., Sandage A., 1987, AJ, 94, 251

Bland-Hawthorn J., Vlajić M., Freeman K. C., Draine B. T., 2005, ApJ, 629, 239

Blanton M. R., Eisenstein D., Hogg D. W., Schlegel D. J., Brinkmann J., 2005, ApJ, 629, 143

Borch A., et al., 2006, A&A, 453, 869

Boselli A., Gavazzi G., 2006, PASP, 118, 517

Bournaud F., Elmegreen B. G., Elmegreen D. M., 2007, ApJ, 670, 237

Buitrago F., Trujillo I., Conselice C. J., Bouwens R. J., Dickinson M., Yan H., 2008, ApJ, 687, L61

Byrd G., Valtonen M., 1990, ApJ, 350, 89

Cameron E., 2011, Publ. Astron. Soc. Australia, 28, 128

Caon N., Capaccioli M., D'Onofrio M., 1993, MNRAS, 265, 1013

Cimatti A., et al., 2008, A&A, 482, 21

Cowie L. L., Songaila A., 1977, Nature, 266, 501

Croton D. J., et al., 2006, MNRAS, 365, 11

Daddi E., et al., 2005, ApJ, 626, 680

Davis M., Efstathiou G., Frenk C. S., White S. D. M., 1985, ApJ, 292, 371

De Lucia G., Kauffmann G., White S. D. M., 2004, MNRAS, 349, 1101

De Lucia G., Springel V., White S. D. M., Croton D., Kauffmann G., 2006, MNRAS, 366, 499

De Lucia G., Weinmann S., Poggianti B. M., Aragón-Salamanca A., Zaritsky D., 2012, MNRAS, p. 3042

de Vaucouleurs G., 1948, Annales d'Astrophysique, 11, 247

de Vaucouleurs G., 1959a, Handbuch der Physik, 53, 275

de Vaucouleurs G., 1959b, Handbuch der Physik, 53, 311

de Vaucouleurs G., 1961, ApJS, 5, 233

Debattista V. P., Mayer L., Carollo C. M., Moore B., Wadsley J., Quinn T., 2006, ApJ, 645, 209

Dressler A., 1980, ApJ, 236, 351

Dressler A., Gunn J. E., 1983, ApJ, 270, 7

Dressler A., et al., 1997, ApJ, 490, 577

Ellis R. S., Abraham R. G., Dickinson M., 2001, ApJ, 551, 111

Elmegreen B. G., Parravano A., 1994, ApJ, 435, L121

Erwin P., Beckman J. E., Pohlen M., 2005, ApJ, 626, L81

Erwin P., Pohlen M., Beckman J. E., 2008, AJ, 135, 20

Erwin P., Gutiérrez L., Beckman J. E., 2012, ApJ, 744, L11

Evrard A. E., 1991, MNRAS, 248, 8P

Faber S. M., 1973, ApJ, 179, 423

Faber S. M., Jackson R. E., 1976, ApJ, 204, 668

Fall S. M., Efstathiou G., 1980, MNRAS, 193, 189

Fan L., Lapi A., De Zotti G., Danese L., 2008, ApJ, 689, L101

Ferguson A., Irwin M., Chapman S., Ibata R., Lewis G., Tanvir N., 2007, in de Jong, R. S., ed., Island Universes: Structure and Evolution of Disk Galaxies. Springer, Dordrecht, p. 239

Fioc M., Rocca-Volmerange B., 1997, A&A, 326, 950

Foyle K., Courteau S., Thacker R. J., 2008, MNRAS, 386, 1821

Franx M., van Dokkum P. G., Schreiber N. M. F., Wuyts S., Labbé I., Toft S., 2008, ApJ, 688, 770

Freeman K. C., 1970, ApJ, 160, 811

Giavalisco M., et al., 2004, ApJ, 600, L93

Gómez P. L., et al., 2003, ApJ, 584, 210

González-García A. C., Balcells M., 2005, MNRAS, 357, 753

Graham A., Lauer T. R., Colless M., Postman M., 1996, ApJ, 465, 534

Graham A. W., Worley C. C., 2008, MNRAS, 388, 1708

Gray M. E., et al., 2009, MNRAS, 393, 1275

Gunn J. E., Gott J. R. I., 1972, ApJ, 176, 1

Guo Y., et al., 2009, MNRAS, 398, 1129

Gutiérrez L., Erwin P., Aladro R., Beckman J. E., 2011, AJ, 142, 145

Haines C. P., La Barbera F., Mercurio A., Merluzzi P., Busarello G., 2006, ApJ, 647, L21

Haines C. P., Gargiulo A., La Barbera F., Mercurio A., Merluzzi P., Busarello G., 2007, MNRAS, 381, 7

Häussler B., et al., 2007, ApJS, 172, 615

Heiderman A., et al., 2009, ApJ, 705, 1433

Henriksen M., Byrd G., 1996, ApJ, 459, 82

Hildebrandt H., Wolf C., Benítez N., 2008, A&A, 480, 703

Holmberg E., 1958, Meddelanden fran Lunds Astronomiska Observatorium Serie II, 136, 1

Hoyos C., et al., 2011, MNRAS, p. 1914

Hubble E. P., 1925a, Popular Astronomy, 33, 252

Hubble E. P., 1925b, ApJ, 62, 409

Hubble E. P., 1926, ApJ, 64, 321

Hubble E. P., 1936, Realm of the Nebulae. Yale Univ. Press, New Haven

Hubble E., Humason M. L., 1931, ApJ, 74, 43

Humason M. L., 1936, ApJ, 83, 10

Ibata R., Chapman S., Ferguson A. M. N., Lewis G., Irwin M., Tanvir N., 2005, ApJ, 634, 287

Icke V., 1985, A&A, 144, 115

Jedrzejewski R. I., 1987, MNRAS, 226, 747

Kauffmann G., et al., 2003, MNRAS, 341, 33

Kauffmann G., White S. D. M., Heckman T. M., Ménard B., Brinchmann J., Charlot S., Tremonti C., Brinkmann J., 2004, MNRAS, 353, 713

Kennicutt Jr. R. C., 1989, ApJ, 344, 685

Khochfar S., Silk J., 2006, ApJ, 648, L21

King I. R., Kiser J., 1973, ApJ, 181, 27

Kodama T., Smail I., Nakata F., Okamura S., Bower R. G., 2001, ApJ, 562, L9

Kodama T., Smail I., Nakata F., Okamura S., Bower R. G., 2003, ApJ, 591, L169

Kormendy J., 1977, ApJ, 218, 333

Kormendy J., 1993, in Dejonghe H., Habing H. J., eds, Galactic Bulges Vol. 153 of IAU Symposium. p. 209

Kormendy J., Kennicutt Jr. R. C., 2004, ARA&A, 42, 603

Kron R. G., 1980, ApJS, 43, 305

Kroupa P., Tout C. A., Gilmore G., 1993, MNRAS, 262, 545

Lacey C., Cole S., 1993, MNRAS, 262, 627

Larson R. B., Tinsley B. M., Caldwell C. N., 1980, ApJ, 237, 692

Le Fèvre O., et al., 2004, A&A, 428, 1043

Lewis I., et al., 2002, MNRAS, 334, 673

Lintott C. J., et al., 2008, MNRAS, 389, 1179

Longhetti M., et al., 2007, MNRAS, 374, 614

Maltby D. T., et al., 2010, MNRAS, 402, 282

Maltby D. T., et al., 2012a, MNRAS, 419, 669

Maltby D. T., Hoyos C., Gray M. E., Aragón-Salamanca A., Wolf C., 2012b, MNRAS, 420, 2475

Maltby D. T., Aragón-Salamanca A., Gray M. E., Hoyos C., Wolf C., Jogee S., Boehm A., 2012c, MNRAS, *submitted*

Marinova I., et al., 2009, ApJ, 698, 1639

Martínez-Serrano F. J., Serna A., Doménech-Moral M., Domínguez-Tenreiro R., 2009, ApJ, 705, L133

Masters K. L., et al., 2010, MNRAS, 405, 783

McIntosh D. H., et al., 2005, ApJ, 632, 191

Merritt D., 1983, ApJ, 264, 24

Merritt D., 1984, ApJ, 276, 26

Mihos J. C., Hernquist L., 1996, ApJ, 464, 641

Moore B., Katz N., Lake G., Dressler A., Oemler A., 1996, Nature, 379, 613

Naab T., Johansson P. H., Ostriker J. P., Efstathiou G., 2007, ApJ, 658, 710

Naab T., Johansson P. H., Ostriker J. P., 2009, ApJ, 699, L178

Nulsen P. E. J., 1982, MNRAS, 198, 1007

Oemler Jr. A., 1974, ApJ, 194, 1

Patterson F. S., 1940, Harvard College Observatory Bulletin, 914, 9

Pavlovsky C., Koekemoer A., Mack J., 2006, ACS Data Handbook, Version 5.0. STScI, Baltimore

Peñarrubia J., McConnachie A., Babul A., 2006, ApJ, 650, L33

Peng C. Y., Ho L. C., Impey C. D., Rix H.-W., 2002, AJ, 124, 266

Pérez I., 2004, A&A, 427, L17

Poggianti B. M., 2006, in Del Toro Iniesta J. C., Alfaro E. J., Gorgas J. G., Salvador-Sole E., Butcher H., eds, The Many Scales in the Universe: JENAM 2004 Astrophysics Reviews p. 71

Pohlen M., Dettmar R., Lütticke R., Aronica G., 2002, A&A, 392, 807

Pohlen M., Trujillo I., 2006, A&A, 454, 759

Pohlen M., Zaroubi S., Peletier R. F., Dettmar R., 2007, MNRAS, 378, 594

Press W. H., Teukolsky S. A., Vetterling W. T., Flannery B., 1997, Numerical Recipes in C. Cambridge Univ. Press, Cambridge

Rettura A., et al., 2010, ApJ, 709, 512

Roberts M. S., Haynes M. P., 1994, ARA&A, 32, 115

Roškar R., Debattista V. P., Stinson G. S., Quinn T. R., Kaufmann T., Wadsley J., 2008a, ApJ, 675, L65

Roškar R., Debattista V. P., Quinn T. R., Stinson G. S., Wadsley J., 2008b, ApJ, 684, L79

Schawinski K., et al., 2009, MNRAS, 396, 818

Schaye J., 2004, ApJ, 609, 667

Sérsic J. L., 1968, Atlas de galaxias australes. Cordoba, Argentina: Observatorio Astronomico, 1968

Shapley H., 1933, Proceedings of the National Academy of Science, 19, 591

Shen S., Mo H. J., White S. D. M., Blanton M. R., Kauffmann G., Voges W., Brinkmann J., Csabai I., 2003, MNRAS, 343, 978

Sil'Chenko O. K., Chilingarian I. V., Sotnikova N. Y., Afanasiev V. L., 2011, MNRAS, 414, 3645

Spergel D. N., et al., 2007, ApJS, 170, 377

Strateva I., et al., 2001, AJ, 122, 1861

The L. S., White S. D. M., 1986, AJ, 92, 1248

Toft S., et al., 2007, ApJ, 671, 285

Treu T., Ellis R. S., Kneib J.-P., Dressler A., Smail I., Czoske O., Oemler A., Natarajan P., 2003, ApJ, 591, 53

Trujillo I., Pohlen M., 2005, ApJ, 630, L17

Trujillo I., et al., 2006a, ApJ, 650, 18

Trujillo I., et al., 2006b, MNRAS, 373, L36

Trujillo I., Conselice C. J., Bundy K., Cooper M. C., Eisenhardt P., Ellis R. S., 2007, MNRAS, 382, 109

Trujillo I., Cenarro A. J., de Lorenzo-Cáceres A., Vazdekis A., de la Rosa I. G., Cava A., 2009, ApJ, 692, L118

Tully R. B., Fisher J. R., 1977, A&A, 54, 661

van den Bergh S., 1976, ApJ, 206, 883

van den Bosch F. C., Pasquali A., Yang X., Mo H. J., Weinmann S., McIntosh D. H., Aquino D., 2008, preprint (arXiv)

van der Kruit P. C., 1979, A&AS, 38, 15

van der Wel A., Holden B. P., Zirm A. W., Franx M., Rettura A., Illingworth G. D., Ford H. C., 2008, ApJ, 688, 48

van Dokkum P. G., 2005, AJ, 130, 2647

van Dokkum P. G., et al., 2008, ApJ, 677, L5

Weinmann S. M., Kauffmann G., van den Bosch F. C., Pasquali A., McIntosh D. H., Mo H., Yang X., Guo Y., 2009, MNRAS, 394, 1213

Weinmann S. M., van den Bosch F. C., Yang X., Mo H. J., 2006, MNRAS, 366, 2

Wolf C., Meisenheimer K., Rix H.-W., Borch A., Dye S., Kleinheinrich M., 2003, A&A, 401, 73

Wolf C., et al., 2004, A&A, 421, 913

Wolf C., Hildebrandt H., Taylor E. N., Meisenheimer K., 2008, A&A, 492, 933

Wolf C., et al., 2009, MNRAS, 393, 1302

York D. G., et al., 2000, AJ, 120, 1579

Younger J. D., Cox T. J., Seth A. C., Hernquist L., 2007, ApJ, 670, 269

Zirm A. W., et al., 2007, ApJ, 656, 66